Title
SPECTROSCOPIC AND KINETIC STUDIES OF CHEMILUNINESCENCE FROM THE REACTIONS OF EXCITED MERCURY ATOMS (3P1) WITH HALOGEN MOLECULES

Author
Gundel, Lara Avery.

Publication Date
1975

SPECTROSCOPIC AND KINETIC STUDIES OF CHEMILUNINESCENCE FROM THE REACTIONS OF EXCITED MERCURY ATOMS ($^3P_1$) WITH HALOGEN MOLECULES

Lara Avery Gundel
(Ph. D. thesis)

January 1975

Prepared for the U. S. Energy Research and
Development Administration under Contract W-7405-ENG-48

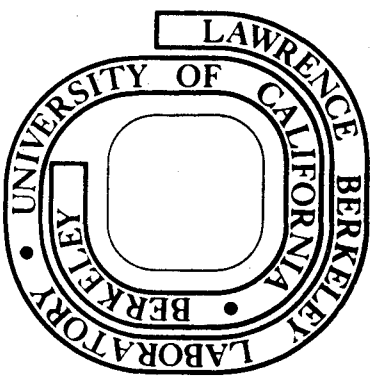

DISCLAIMER

To the Seeds of Liberation

Table of Contents

SPECTROSCOPIC AND KINETIC STUDIES OF CHEMILUNINESCENCE FROM THE REACTIONS OF EXCITED MERCURY ATOMS ($^3P_1$) WITH HALOGEN MOLECULES

Lara Avery Gundel

Inorganic Materials Research Division, Lawrence Berkeley Laboratory and Department of Chemistry; University of California, Berkeley, California

ABSTRACT

The reactions of excited mercury atoms ($^3P_1$) with Cl_2, Br_2, I_2 and ICl(XY) have been studied in a quartz flow system which was irradiated with a concentric bank of low pressure mercury lamps. Visible chemiluminescence was observed which corresponds to $HgX(B^2\Sigma^+ \rightarrow X^2\Sigma^+)$ emission. It has been shown by kinetic studies that the excited mercurous halides are formed primarily in the bimolecular reaction:

$$Hg(^3P_1) + XY(^1\Sigma_g^+) \rightarrow HgX(B^2\Sigma^+) + Y(^2P) \quad . \qquad (1)$$

The rate constant for the reaction of $Hg(^3P_1)$ with chlorine has been estimated to fall in the range $0.3\text{-}1.9\times10^{-10}$ cm^3/molecule-sec. Approximate corrections for radiation imprisonment and absorption of the incident light have been applied to obtain this estimate.

The chemiluminescent emission spectrum which accompanies the reaction of $Hg(^3P_1)$ with Cl_2 has been compared to that obtained when 200 Torr of helium is added to the irradiated flow system, and vibrational distributions have been computed for each case. Franck-Condon factors were calculated using Morse potential functions for the

B state of HgCl and two smoothly connected quasi-Morse functions for the ground state, for several choices of relative equilibrium internuclear separation. A partial sum-rule approach for Franck-Condon factors was employed to extract the vibrational distribution from the measured intensities of red shaded bands. $HgCl(B^2\Sigma^+)$ has maximum population in $v'=14$ when no helium is present. The average fraction of reaction energy invested in vibration, $\langle f_{vib} \rangle$, is 0.53. With 200 Torr of helium the $HgCl(B^2\Sigma^+)$ is almost completely relaxed to a Boltzmann distribution. Surprisal analysis of the distribution of the available reaction energy shows that $HgCl(B^2\Sigma^+)$ is formed in reaction (1) with a vibrational temperature of $\sim -2600°K$.

It was not possible to extract vibrational distributions for $HgX(B^2\Sigma^+)$ formed in the reaction of $Hg(^3P_1)$ with Br_2, I_2 or ICl. For ICl both $HgCl(B^2\Sigma^+)$ and $HgI(B^2\Sigma^+)$ were observed but contamination due to I_2 prevented an estimate of the relative rates of formation of the two possible excited species. The reactions of $Hg(^1P_1)$ + Cl_2 and $SnCl_4$ do not give any chemiluminescent products between 2500 and 6000Å.

The results of these studies have been discussed in relation to the electron transfer model which applies to the reactions of alkali and alkaline earth metals with halogens. The large rate constant for reaction and large fraction of available energy invested in product vibration are consistent with the model.

I. INTRODUCTION

In the last decade the dynamics of simple chemical reactions have been fruitfully investigated in molecular beam experiments,[1] in chemiluminescence studies,[2] and by interpretation of quenching processes involving electronically excited species.[3-6] The simplest reactions for which an understanding of molecular dynamics is unfolding are bimolecular atom transfer reactions, conveniently represented by

$$A + BC \rightarrow AB + C \ . \qquad (1)$$

The first reactions to be studied under conditions which enabled monitoring of the angular distributions of the products of single collisions were the exothermic reactions of alkali metals with hydrogen halides,[7] made possible by the discovery of differential surface ionization detection of the alkali species. The observed large cross sections for reaction between alkali metals and halogens[8] revived interest in the simple electron transfer model first proposed by McGee[9] to explain the results of diffusion flame studies with alkali atoms and dimers.[10] The essential idea is that the easily ionizable alkali atom tosses its almost free electron at the halogen molecule, a species with high electron affinity. The resulting Coulombic attraction between the newly formed ion pair accelerates the reaction rate. Attempts have been made[11] to construct potential hypersurfaces which include this non adiabatic crossing phenomenon and also reproduce the forward peaking and high internal excitation of the product molecules

which have been observed for reactions which proceed via an electron transfer. In its simple form the electron transfer model provides the basis for qualitative predictions about reactions and appears to apply to reactions of the alkaline earth metals with halogens. Although the alkaline earth metals have low ionization potentials, their divalent spin paired outer electron configuration and the presence of deep chemical wells in the potential surfaces to form stable triatomic molecules might preclude their participation in an electron transfer process. Their reactions with halogens do exhibit strong forward peaking and high internal excitation of the products.[12] These results are consistent with the predictions of the electron transfer model and indicate that the reaction intermediate dissociates into products before equipartitioning of reaction exothermicity can occur. A small fraction of collisions between barium and chlorine proceed via electronically excited long lived $BaCl_2^*$ which dissociates to $BaCl(C^2\pi) + Cl$.[13] It is interesting to note that the vibrational distribution of $BaCl(C^2\pi)$ corresponds to that expected for the break-up of a stabilized complex. Other reactions of barium also give visible chemiluminescence[14] and some offer evidence for other long-lived intermediates,[15] as will be discussed later.

Atomic mercury has an ionization potential[16] which is too high to allow its participation in an electron transfer process, but its first resonance excited state ($6\ ^3P_1$) has an ionization potential of 5.6 eV, close to those of lithium (5.4 eV) and strontium (5.7 eV).

Like the alkaline earths its ground state configuration is s^2, and it forms stable divalent gaseous compounds. The reactions of excited mercury atoms with halogens might proceed by an electron transfer mechanism, and this idea will be tested in this work, with specific emphasis on the bimolecular reactions which can form electronically excited species,

$$Hg(^3P_1) + XY(^1\Sigma^+) \rightarrow HgX(B^2\Sigma^+) + Y(^2P) . \qquad (2)$$

The $HgX(B^2\Sigma^+ \rightarrow X^2\Sigma^+)$ chemiluminescent emission will contain information about the distribution of reaction exothermicity among the products, which provides insight about the potential hypersurfaces and collision lifetime. An important difference between $Hg(^3P_1)$ and alkali or alkaline earths reactions with halogens is the fact that the electronic angular momentum of $Hg(^3P_1)$ removes the symmetry restrictions[17] which favor collinear trajectories for these latter reactions.

Energy transfer processes involving electronically excited mercury atoms have been known and exploited for a long time. Cario and Franck[18] observed mercury ($^3P_1$) sensitization of the decomposition of molecular hydrogen in 1922, and later were the first to observe mercury sensitized fluorescence from electronically excited thallium atoms.[19] Because $Hg(^3P_1)$ contains enough energy to break chemical bonds or to cause electronic excitation of the quenching gas, and its triplet spin character allows formation of spin states in the products which may not be accessible by direct absorption of light, mercury sensitization has

proved a useful technique in the study of radical species and of excited states of complex molecules, particularly for organic chemists. Several reviews are available.[5,20] Interest in the quenching processes of $Hg(^3P_1)$ by various gases led to the formulation of a simplified scheme by Stern and Volmer[21] which allowed quenching rates to be determined from the attenuation of resonance fluorescence by reactant gases. Early results were tabulated by Mitchell and Zemansky[22] who also discussed methods of dealing with the problem of imprisonment of resonance radiation. A more recent summary is included in reference 5. Of more interest to this work are studies which provide direct experimental evidence for the formation of mercury containing species as intermediates in quenching reactions. In a sophisticated flash photolytic set up Callear et al.[23] have observed absorption due to $HgH(X^2\Sigma^+)$ in the reaction of $Hg(^3P_1)$ with H_2, with a quantum yield of 0.70.[24] $HgCl(X^2\Sigma^+)$ has been observed in the quenching of $Hg(^3P_1)$ by HCl[25] and in the quenching of $Hg(^3P_0)$ by CH_3Cl.[26] Luminescence from eximers has also been observed in the reactions of $Hg(^3P_0)$ with NH_3, H_2O, alcohols and amines.[27] Some theoretical studies of $Hg(^3P)$ reactions have also been undertaken.[28]

There are relatively few molecules for which energetically accessible channels exist for the formation of electronically excited products in bimolecular atom transfer reactions with $Hg(^3P_1)$. In this work only molecular halogens have been studied, and, indeed, light emission corresponding to the transition $HgX(B^2\Sigma^+ \rightarrow X^2\Sigma^+)$ has been observed and shown to be consistent with its formation in reaction (2).

Although several early workers observed $HgX(B \rightarrow X)$ emission due to secondary processes in flame studies,[29] the only previously reported example of (2), involving $Hg(^3P_1) + I_2$, is hidden in fluorescence studies of I_2 by Duschensky and Pringsheim.[30] Currently molecular beam studies of the reactions of metastable $Hg(^3P_{2,0})$ with halogens and other compounds are underway at Oakridge.[31] These workers have observed $HgCl(B \rightarrow X)$ emission from $Hg(^3P_{2,0}) + Cl_2$ and $Hg(^3P_2)$ + chloromethanes.

In the present work a conventional glass flow system has been used to study the reactions accompanying the irradiation of flowing mixtures of mercury and halogens with mercury resonance radiation. Because of the short lifetime of the electronically excited species involved, estimated to be 10^{-6} - 10^{-7} sec, this experimental arrangement was not complicated by vibrational relaxation before light emission, in contrast to infrared chemiluminescence studies.[2] From the chemiluminescent spectrum accompanying the reaction of $Hg(^3P_1)$ with Cl_2, a crude vibrational distribution of $HgCl(B^2\Sigma^+)$ has been extracted. Kinetic studies of the light emission have established reaction (2) as the primary source for the formation of $HgCl(B^2\Sigma^+)$ and estimates of the rate constant for its production have been made. Chemiluminescent emission from excited mercurous halides has also been observed in the reactions of $Hg(^3P_1)$ with Br_2, I_2, and ICl. No chemiluminescence was observed in the reactions of the other resonance state of mercury, $Hg(^1P_1)$ with Cl_2 or $SnCl_4$.

These results will be discussed in a context which explores the possibility that these reactions proceed by an electron transfer mechanism. The possibility of chemical laser action in these reactions will also be discussed.

CHAPTER I REFERENCES

1. For a recent review, see J. L. Kinsey, MIP International Review of Science, Phys. Chem. Series 1, Vol 9, Butterworths, London, 1972, Chapter 6.

2. For a recent review, see J. C. Polanyi, MTP International Review of Science, Phys. Chem. Series 1, Vol. 9, Butterworths, London, Chapter 5.

3a. Quenching of $Na^*(3p^2P)$ by various gases B. L. Earl, R. R. Herm, S.-M. Lin and C. A. Mims, J. Chem. Phys. 56, 867 (1972).

3b. Quenching of $K^*(4p^2P)$ and $K^*(5p^2P)$ by various gases, B. L. Earl and R. R. Herm, J. Chem. Phys. 60, 4568 (1974).

4. Quenching of $Ar^*(4s\ ^3P_{0,2})$ by various gases, L. G. Piper, J. E. Velazco, and D. W. Setser, J. Chem. Phys. 59 3323 (1973).

5. Quenching of $Hg(6s\ ^3P_{0,1})$ by various gases, a now dated review, is included in J. C. Calvert and J. N. Pitts, Photochemistry, Wiley, New York, 1966.

6. Atomic absorption studies of the quenching of low lying electronic states of atoms, R. J. Donovan and D. Husain, Chem. Rev. 70, 489 (1970), and further work, for example, quenching of $Pb(6p^2\text{-}^1D_2)$ by various gases, D. Husain and J. G. F. Littler, Chem. Phys. Lett. 16, 145 (1972).

7a. E. H. Taylor and S. Datz, J. Chem. Phys. 23, 1711 (1955).

7b. S. Datz and E. H. Taylor, J. Chem. Phys. 25, 389, 395 (1956).

8. D. R. Herschbach, Adv. Chem. Phys. 10, 319 (1966).

9. J. L. McGee, J. Chem. Phys. 8, 687 (1940).

10. a. M. Polanyi, Atomic Reactions, Williams and Norgate, London, 1932,
b. M. G. Evans and M. Polanyi, Trans. Far. Soc. 35, 178 (1935).

11. See references 16, 34, and 79-82 of reference 1.

12. S.-M. Lin, C. A. Mims, and R. R. Herm, J. Chem. Phys. 58, 327 (1973).

13. a. C. D. Jonah and R. N. Zare, Chem. Phys. Lett. 9, 65 (1971).
b. M. Menzinger and D. J. Wren, Chem. Phys. Lett. 18, 431 (1973).

14. a. C. D. Jonah and R. N. Zare, J. Chem. Phys. 56, 263 (1972).
b. R. H. Obenauf, C. J. Hsu, and H. B. Palmer, J. Chem. Phys. 58 4693 (1973).
c. C. R. Jones, H. P. Broida, J. Chem. Phys. 60, 4369 (1974); R. W. Field, C. R. Jones, and H. P. Broida, J. Chem. Phys. 60, 4377 (1974).

15. R. H. Obenauf, C. J. Hsu, and H. B. Palmer, Chem. Phys. Lett. 17, 455 (1972).

16. C. E. Moore, Atomic Energy Levels, National Bureau of Standards, circular 467, Washington, 1952 and 1958.

17. P. B. Foreman, G. M. Kendall, and R. Grice, Mol. Phys. 23, 127 (1972).

18. G. Cario and J. Franck, Z. Physik 11, 161 (1922).

19. G. Cario and J. Franck, Z. Physik 17, 202 (1923).

20. a. H. E. Gunning and O. P. Strausz, Adv. in Photochemistry 1, 209 (1963).
b. R. J. Cvetanovic, Prog. Reaction Kinetics 2, 39 (1964).

21. O. Stern and M. Volmer, Physik 20, 183 (1919).

22. A. C. G. Mitchell and M. W. Zemansky, Resonance Radiation and Excited Atoms, Cambridge University Press, New York, 1961.

23. A. B. Callear and J. C. McGurk, Far. Trans. II, 68 289 (1972).

24. A. B. Callear and P. M. Wood, Far. Trans. II, 68, 302 (1972).

25. A. B. Callear and R. E. M. Hedges, Trans. Far. Soc. 66, 605 (1970).

26. A. C. Vikis and D. J. LeRoy, Chem. Phys. Lett. 21, 103 (1973).

27. L. F. Phillips, Accts of Chem. Res. 7, 135 (1974), and references there in.

28. a. K. J. Laidler, Chemical Kinetics of Excited States, Oxford University Press, New York, 1955.

b. P. G. Dickens, J. W. Linnett and O. Sovers, Disc. Far. Soc. 33, 52 (1962).

c. J. C. Light, J. Chem. Phys. 40, 3221 (1964), and P. Pechukas and J. C. Light, J. Chem. Phys. 42, 3281 (1965).

d. A. C. Vikis, and H. C. Moser, J. Chem. Phys. 53, 2333 (1970).

e. K. Yang, J. D. Paden, and C. L. Hassell, J. Chem. Phys. 47, 3824 (1967).

29. a. H. Fränz and H. P. Kallman, Z. Physik, 34, 924 (1925).

b. V. N. Kondratiev, Z. Physik 45, 67 (1927).

c. H. Tominaga and G. Okamoto, Bull. Chem. Soc. Japan 12, 401 (1937)

d. F. Haber and W. Zisch, Z. Physik 9, 302 (1922).

30. F. Duschinsky and P. Pringsheim, Physica 2, 923 (1935).

31. H. Krause and S. Patz, private communication.

II. EXPERIMENTAL DESIGN AND CONDITIONS

A. Introduction

The apparatus which was used to study reactions of excited mercury atoms with chlorine consisted of a glass and quartz vacuum system, a bank of low pressure mercury lamps, and a versatile light detection system. Several types of experiments were carried out with this apparatus. With the apparatus in the scanning configuration, the emission spectra of the mercury halides which accompany the reaction of $Hg(6^3P_1)$ with Cl_2, Br_2, I_2 and ICl were scanned using both photographic and photoelectric detection. Then various experiments were performed to establish the mechanism of formation of the chloride product and tb study its vibrational relaxation when varying pressures of helium or nitrogen also flowed through the system. The kinetics of the reaction of $Hg(^3P_1)$ with chlorine were studied with the apparatus in a configuration which allowed for monitoring the intensity of light emission along the reaction vessel axis as a function of incident light intensity and concentrations of mercury and chlorine. Finally attempts were made to find chemiluminescent emission accompanying reaction of $Hg(6^1P_1)$ with Cl_2 and $SnCl_4$.

A schematic diagram of the apparatus and light detection system in the scanning configuration is shown in Fig. II-1. Modifications of the apparatus for other parts of the experimental work will be discussed as they arise.

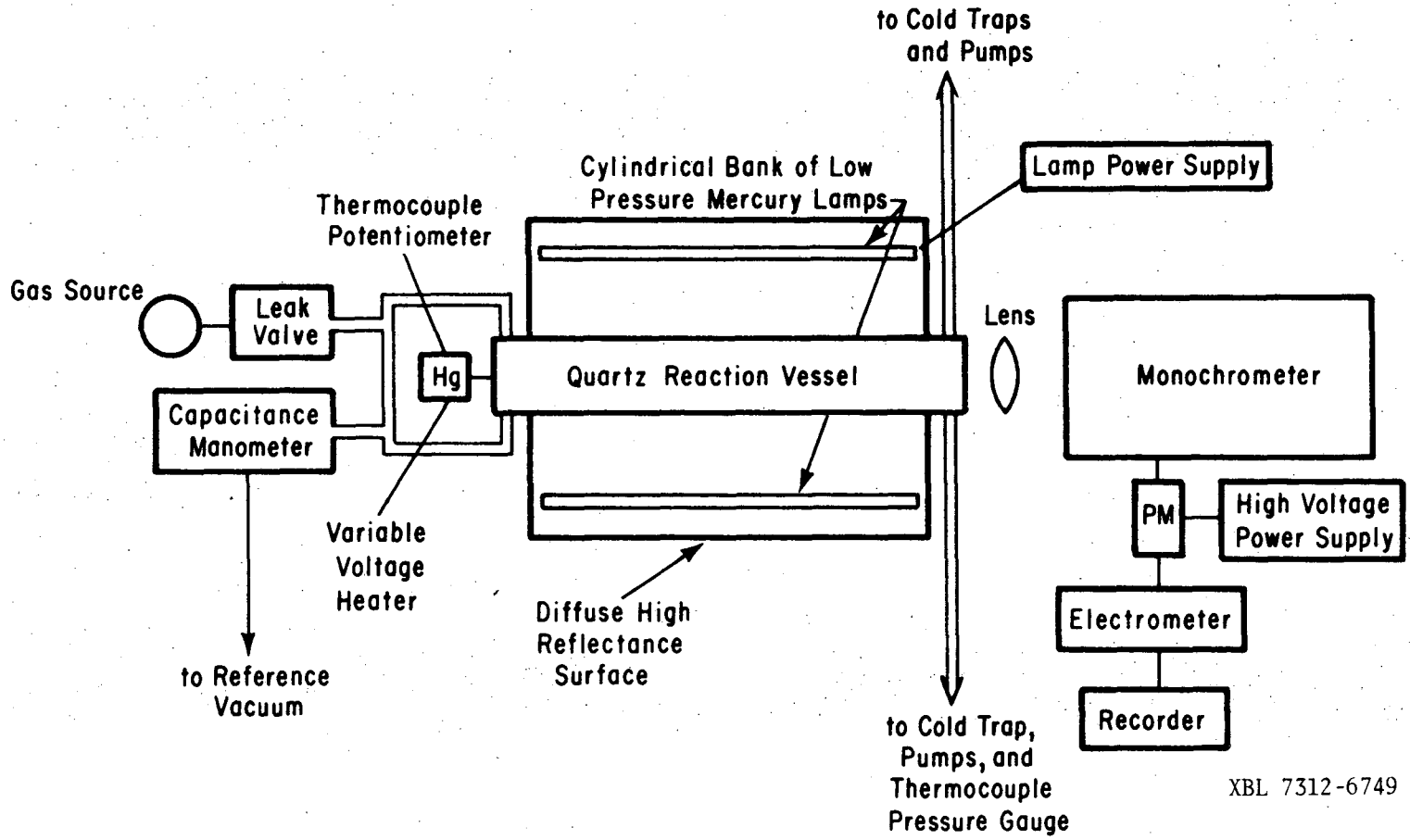

Fig. II-1. Schematic diagram of the apparatus and light detection system in the scanning configuration.

B. The Flow System

1. Reaction Vessels

The quartz reaction vessel formed the core of the flow system. The first vessel, constructed from General Electric type 204 clear fused quartz, incorporated two concentric tubes of inside diameters 51 mm and 75 mm and wall thickness 2 mm. The inner diameter was chosen several times larger than the diameter of the nearby glass tubing (id 9 mm) to minimize the pressure drop in the reaction vessel. These quartz tubes together transmitted about 70% of the incident radiation at 2537Å and less than 5% at 1849Å, allowing for about 10% loss due to surface reflection.[1] These were connected to the rest of the gas handling system via type 304 stainless steel flanges individually fitted at each end of the tubes. Leak tight sealing was accomplished with rubber O-rings. Figure II-2 shows the inlet end of the flange and quartz tube assembly with the mercury source attached. Gas inlet and outlet tubes were welded to the stainless steel bodies of the flanges. Swagelok fittings, kovar to glass seals, and glass ball joints connected the reaction vessel to the gas line at the inlet end. Cajon fittings at the outlet end allowed for easy glass to metal sealing and proved convenient when the reaction vessel had to be removed from the gas handling system for cleaning. The length from the center of the gas inlet arms to the center of the outlet arms was 43.8 cm, compared to the total irradiated length of 30.8 cm. The reaction vessel was mounted so that it could be aligned coaxially with the light detection system for experiments

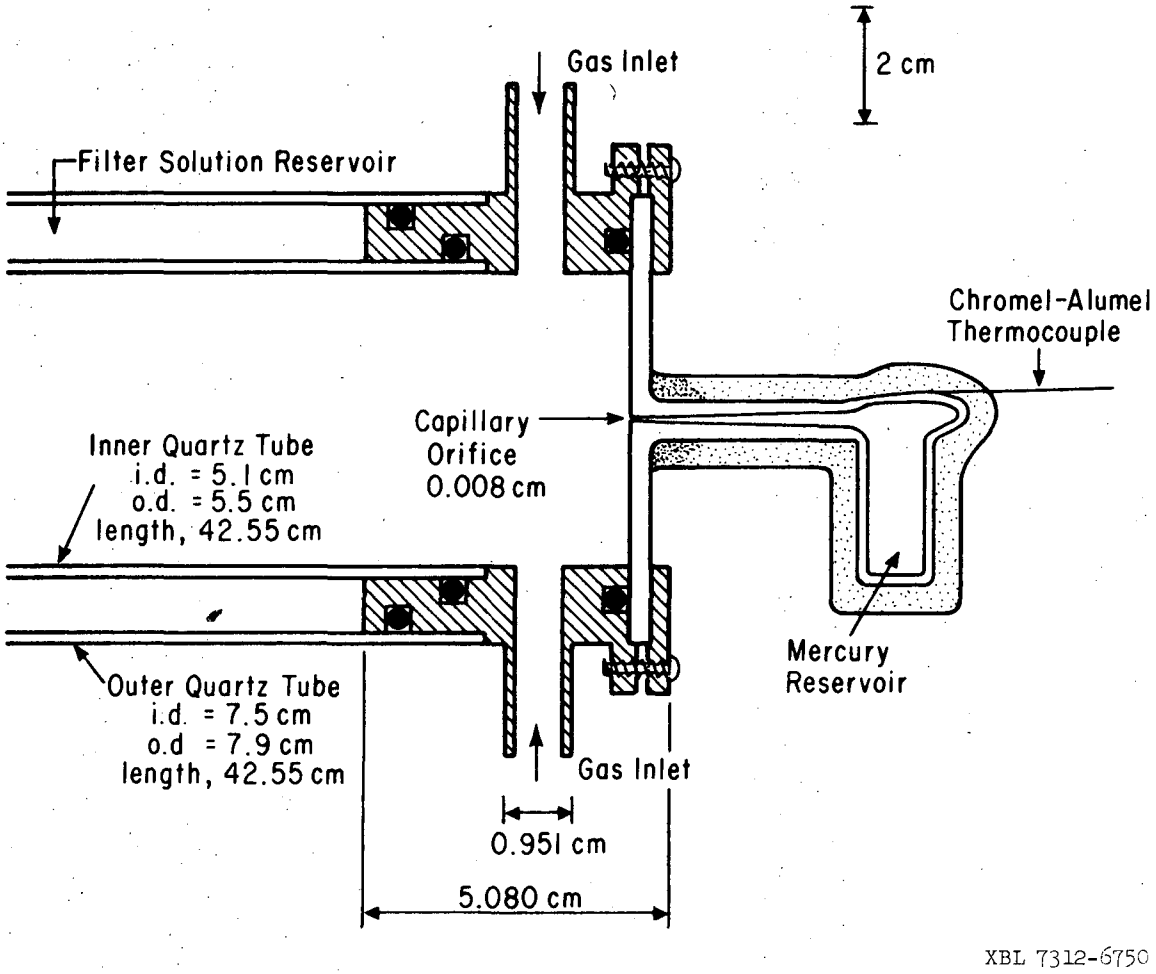

Fig. II-2. The inlet end of the reaction vessel: quartz tube and stainless steel flange assembly with the mercury reservoir in place.

in which emission spectra were scanned. It was supported at each end by a two piece aluminum disc of 1/8 in. thickness which was connected to the sturdy aluminum mount for the mercury lamps. In addition to the increased versatility of a reaction vessel which could be disassembled an important element in the choice of this design was the relative difficulty of fabricating a glass and quartz vessel incorporating two concentric tubes and removable windows. The stainless steel flanges and rubber O-rings proved resistant to the halogen compounds which were used in these studies.

Other design features are worth discussion. This assembly allowed for flexibility in choice and use of windows. A pyrex or quartz window of diameter 3 in. was used at the downstream end of the reaction vessel. The mercury source was incorporated into the pyrex window at the other end. This source window was replaced by other types of window for some experiments as will be discussed later. When necessary the windows could be removed easily for cleaning or replacement. It was also found that the reaction vessel could be cleaned internally without complete disassembly or loss of optical alignment by forcing paper swabs which had been soaked in ammonia through it, then then rinsing with distilled water and drying the inside. A black residue was formed and removed, indicating the presence of Hg_2Cl_2 according to[2]

$$Hg_2Cl_2(s) + 2NH_3 \rightarrow Hg(\ell) + HgNH_2Cl(s) + NH_4^+ + Cl^- .$$

This cleaning could be performed whenever the inside surface was thought to be contaminated by ultraviolet absorbing compounds. This design also permitted complete disassembly for cleaning when necessary. In that case the vessel was cleaned by rinsing the parts in methanol, and soaking the quartz tubes in hot chromic acid. To ensure the presence of a clean quartz surface, the tubes were rinsed in a 10% solution of HF for 30 seconds, followed by distilled water. Thorough cleaning of the reaction vessel was necessary after about 300 hours of exposure of the reaction vessel to ultraviolet irradiation. Cleaning without disassembly was performed whenever irregular conditions in the vessel demanded it, for example, after an air leak occurred while an experiment was in progress, or the ultraviolet transmission of the vessel was thought to be too low for any reason.

Another design feature of this reaction vessel was the optional outer quartz tube, which, when used, formed a 1 cm cavity surrounding the inner tube. This cavity was filled with a circulating solution consisting of 500 g/ℓ $NiSO_4$-$6H_2O$ and 75 g/ℓ $CoSO_4$-$7H_2O$. The solution was maintained at 45°C. This solution, which appeared black to the eye, transmitted 75% of the incident radiation at 2537Å[3] and had negligible transmittance from 3500Å to 5700Å. Its principal purpose was to prevent visible radiation at 4078Å and 4358Å from reaching the reaction vessel, since these lines could cause secondary absorption by $Hg(^3P_1)$. By eliminating most of the visible radiation from the lamps it was possible to perceive visually the green glow of HgCl(B→X) emission through the back window of the vessel, when the Hg pressure

was high enough. This was useful, especially in the initial experiments when the proper experimental conditions for producing the spectra were uncertain. Another advantage of using the filter solution was the reduction in fluorescence of the inner tube, presumably because of decreased transmission of short wavelength atomic lines which caused fluorescence of impurities in the fused quartz.[4] Since the filter solution had 50% transmission limits at 2250Å and 3300Å, radiation at 1849, 1942, 2224.7Å[5] could not reach the inner tube. It should also be mentioned that the transmission of the filter solution was constant to 2% after the first several hours of irradiation by the low pressure mercury lamps.

For some experiments a series of inert dull black baffles were inserted into the reaction vessel. They were constructed from anodized aluminum rings of outer diameter 2 in. and inner diameter 1 in. whose positions along the three threaded support rods were assigned so that no light originating from the walls of the reaction vessel or from the lamps could reach the cone of sight of the spectrometer. The baffles had two purposes, the first of which was to prevent detection of possible light emission from wall reactions. It was also necessary to use both the baffles and the filter solution to reduce the intensity of quartz fluorescence and background scattered visible light from the lamps so that the mercury halide emission spectrum could be photographed. Without these modifications the quartz fluorescence between 3000Å and 4500Å was about two orders of magnitude greater in intensity than that of the HgCl(B→X) emission

in this region and was found to be modulated at 120 hertz as were the exciting lamps. It did prove possible, however, to detect the HgX emission photoelectrically without use of filter solution or baffles as will be discussed later.

The second reaction vessel was constructed with an inner tube of "suprasil" purchased from the Amersil Quartz Division of Englehard Industries. This suprasil tube had an inner diameter of 50 mm and an outer diameter of 53 mm. According to the manufacturers this tube transmitted 90% of incident radiation at 2537Å and 80% at 1849Å, allowing for 10% loss in transmission due to surface reflection. This tube was purchased to permit investigation of reactions involving the singlet mercury resonance line at 1849Å. For these experiments the reaction vessel was assembled without the outer tube, but the flange design and mount for this vessel were entirely similar to those of the original tube. The fluorescence free characteristic of this vessel was exploited in the study of the $Hg(^3P_1)$ reaction with chlorine after it had been determined that there was no $HgCl^*$ emission due to reaction involving $Hg(^1P_1)$, and it became possible to study the short wavelength limit of the molecular emission with increased signal to noise ratios.

The suprasil tube and outer quartz tube were used together without filter solution or baffles for most photoelectric scans of the molecular emission spectra due to 2537Å irradiation which are presented in this work. The outer quartz tube and atmospheric oxygen absorbed the small output of 1849Å radiation from the germicidal lamps. For quantitative

kinetic studies the suprasil tube was used without the outer quartz tube.

Heat from the lamps maintained the reaction vessel at 45°C when at least 10 germicidal lamps were used. This temperature was sufficiently high to prevent condensation of solid products in the irradiated region of the vessel. Some condensation occurred on the downstream flange surfaces and the front window if the mercury pressure was too high. When this occurred the condensate could be removed by heating the window under vacuum without removing it.

2. The Mercury Source

The mercury capillary source is shown in Fig. II-2 as it was connected to the upstream flange of the reaction vessel. It was mounted in a 3 in. diameter pyrex window, with its 0.003 in. opening in the center. The reservoir was loaded with 2 cc of triply distilled reagent grade mercury, sealed, and then wound with 6 ft. of 10 ohm/ft. wire, insulated by layers of asbestos tape. It was necessary to concentrate the wire around the capillary orifice to keep it hotter than the major part of the reservoir and to ensure even flow of mercury into the reaction vessel. A chromel-alumel thermocouple for temperature measurement was attached to the glass body under the heating wire and electrically insulated from it. Control of the mercury flow rate was accomplished by connecting the heating wire to a variable voltage transformer. The flow rate of mercury from this source into the reaction vessel under vacuum was measured by weight loss of the whole source for known time periods, typically 36 hours.

The asbestos wrapping rapidly absorbed water vapor so the hot source was placed in a dessicator before it was weighed. The flow rate as a function of temperature is shown in Fig. II-3. For wavelength scans of the emission spectra of the mercurous halides the mercury source was operated typically at 508°K; the lowest source temperature for kinetic studies was 463°K. These temperatures gave flow rates of 2.83×10^{16} and 3.30×10^{15} atoms/sec respectively. The flow rate of mercury through the capillary is proportional to the square of the vapor pressure for viscous flow. The dependence of the vapor pressure on temperature is given by the Clausius-Clapeyron equation:

$$\frac{d(\ln P)}{d(1/T)} = \frac{-\Delta H_{vap}}{R} \quad . \tag{1}$$

Here ΔH_{vap} is the enthalpy of vaporization at the boiling point. For this mercury source the logarithm of the flow rate is indeed proportional to T^{-1}. Figure II-3 shows the flow rate as a function of T rather than T^{-1} for convenience in directly determining the flow rate from the capillary temperature.

The pressure of mercury in the vessel is related to its flow rate by

$$P_{Hg} = F_{Hg} P_{total} / (F_{Hg} + F_{Cl_2}) \tag{2}$$

where F is flow rate. Thus for a source temperature of 508°K, a chlorine pressure of 0.2 Torr and flow rate of 3.3×10^{18} mole/sec, the pressure of mercury was 1.7×10^{-3} Torr.

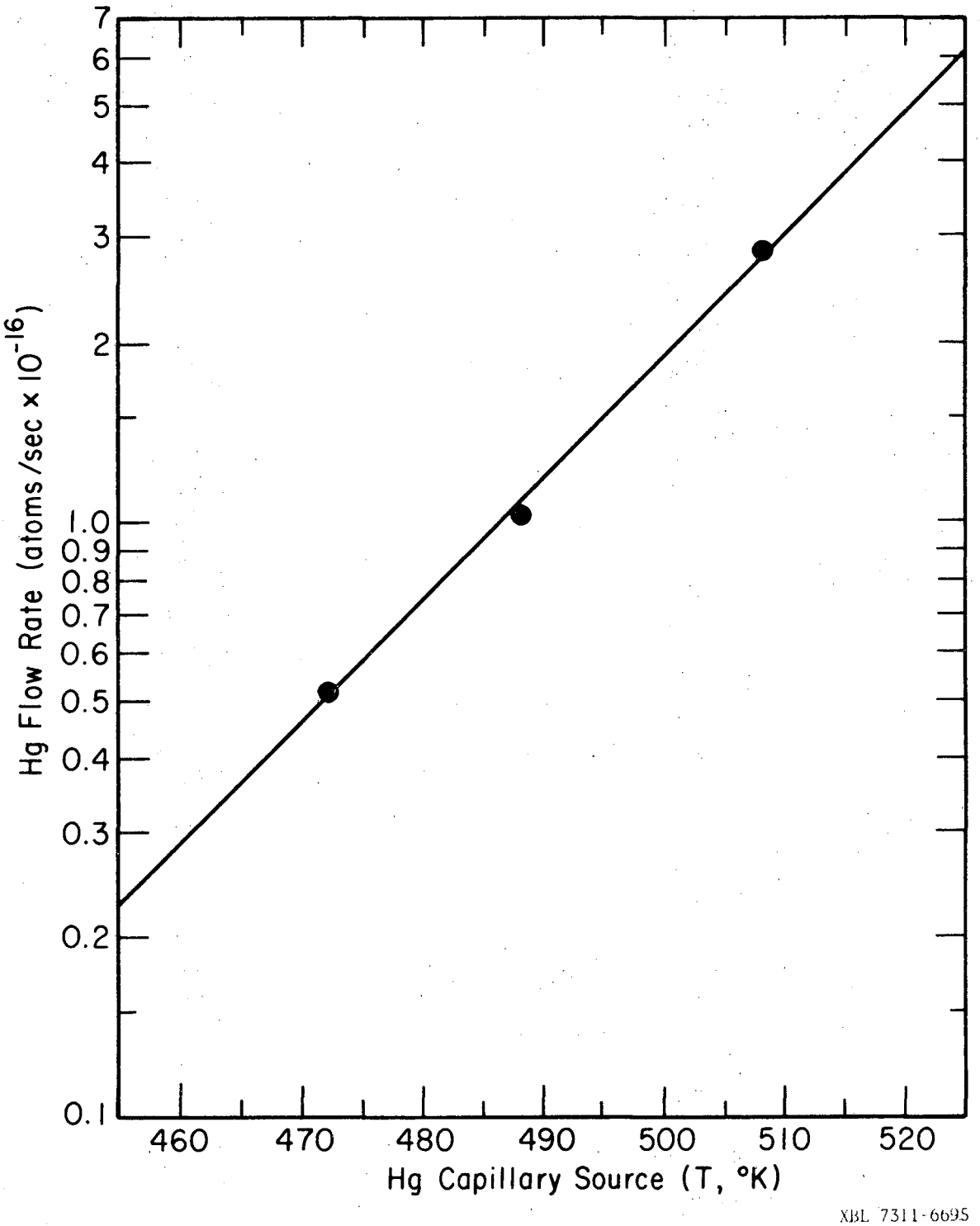

Fig. II-3. Mercury flow rate as a function of the temperature of the source.

This design provided a reproducible and steady flow rate of mercury which could be easily controlled. Other source designs were used before the capillary window source was constructed. In one such source helium or nitrogen bubbled through a heated reservior of mercury in an attempt to saturate the inert gas with mercury before it entered the reaction vessel where it was mixed with chlorine. Another source was a glass spiral about 20 cm in resultant length which contained a drop of mercury in each coil. This was heated in a water bath and again helium or nitrogen passed over the mercury. The flow rate and pressure of the carrier gas, as well as the mercury temperature, controlled the mercury pressure in the reaction vessel. These latter methods had several major disadvantages. Reproducible mercury pressure was difficult to obtain, and pressures of at least 50 Torr of carrier gas were necessary to produce high enough mercury concentration for detectable HgX light emission. Under these conditions the resultant HgX emission spectrum was vibrationally relaxed to an extent which depended on the carrier gas pressure. Another drawback to the early mercury sources was the fact that the gas mixture in the reaction vessel was certainly inhomogeneous and made kinetic studies extremely complicated. At one point chlorine gas was allowed to flow directly over a heated pool of mercury before the gas mixture entered the reaction vessel. Because of fairly rapid surface reaction this method was clearly a poor approach to mercury introduction. The window mounted capillary orifice source did not require the use of

a carrier gas so that vibrationally unrelaxed spectra could be obtained when low pressures of halogen gas were used, and contamination of the mercury presented no problem.

Under typical operating conditions the mercury source was heated to allow degassing, to permit temperature equilibration and to achieve a steady flow rate from the source before data collection.

3. Gas Sources and Pressure Measurement

High purity chlorine obtained from Matheson, of 99.5% purity, was used without purification. Bromine and iodine of analytical reagent grade were purchased from Mallinckrodt Chemical Works. Baker analyzed reagent $SnCl_4$ and practical grade ICl from Distillation Products Industries were used without further purification. In experiments with helium and nitrogen these gases passed through a cold trap at liquid nitrogen temperature before entering the flow system immediately down-stream of the chlorine entry port.

Reservoirs for liquid or solid reagents were constructed from glass tubes or bulbs with glass to kovar seals which allowed the reservoirs to be connected to the gas flow system by Swagelok fittings for easy interchange. For example, the ICl reservoir was essentially a tube 5 1/2 in. in total length and glass diameter of 5/8 in. Heating wire with asbestos tape insulation surrounded the reservoirs and was connected to a variable voltage transformer for temperature control.

Reproducible metering was achieved for chlorine, bromine, and iodine monochloride with a Granville Phillips Variable leak valve, type 203. To avoid condensation in the valve, for bromine the leak valve was maintained at 45°C with heating tape. The Br_2 reservoir was maintained at 28°C. For ICl the leak valve was also heated to 45°C but the reservoir was maintained at room temperature. For iodine the glass tubing leading to the reaction vessel was heated to 40°C to prevent condensation. The I_2 reservoir was operated at 30°C and the Nupro fine metering valve which replaced the Granville Phillips Variable Leak was maintained at about 70°C. In order to achieve a measurable steady pressure of $SnCl_4$, only crude metering could be accomplished using a glass stopcock between the room temperature reservoir and the vacuum line.

Pressure measurement of the flowing reactant gases was performed with a Datametrics Type 1023 Barocel Electronic Manometer which incorporated a Type 523-C pressure sensor. This differential manometer, sensitive in the range 1 millitorr to 10 Torr, operated as a high precision stable capacitave potentiometer in which a metal diaphragm separated two gas chambers, one of which connected to the gas line and the other to a reference vacuum or gas at known pressure. A difference in pressure between the two chambers caused deflection of the diaphragm, changing the relative capacitance of the diaphragm and the fixed capacitance plates in which it was mounted. A voltage proportional to the pressure difference between the ports and independent of the

nature of the gas was generated in the associated circuitry. The pressure sensor was factory calibrated, but calibration against an oil manometer was repeated periodically. Dow Corning 704 diffusion pump fluid of density 1.061 g/cm^3 was used in the manometer.

In order to measure the pressure of flowing gas in the reaction vessel, pressure measurements were made at two points in the apparatus simultaneously. Pressure probes of various lengths were incorporated into a pyrex window which replaced the mercury reservoir. The pressure probes were essentially glass tubes centered on the reaction vessel axis which extended into the reaction vessel distances 0.0, 7.6 and 22.8 cm past the upstream end of the illuminated region. The oil manometer monitored the pressure seen at the tube axis by one of these probes while the electronic manometer monitored the pressure of the flowing gas at a fixed point upstream of the reaction vessel. Calibration curves were then constructed which presented the reaction vessel pressure as a function of the upstream pressure at each measurement length. The reaction vessel pressure was typically 0.765 times the monitored pressure in the range 0.05 to 1.50 Torr. This is the result of the pressure gradient through the glass line and the difference in diameter between the glass tubing and the reaction vessel. During spectral scans and kinetic studies the reaction vessel pressure was related to the monitored pressure through the calibration curve for probe length 7.6 cm. The pressure drop measured between the shortest and longest probes was negligible at pressures less than 0.25 Torr. At 0.50 Torr average pressure,

$\Delta P/P = 0.020$. At 1.0 Torr average pressure, $\Delta P/P = 0.025$.

4. Flow Rate and Flow Velocity for Chlorine

For kinetic measurements in this system it was necessary to measure the flow rate of chlorine as a function of chlorine pressure in the reaction vessel. Such measurements were performed for both reaction vessels, although most of the significant kinetic results were produced in studies utilizing the suprasil vessel. A simple method was employed. Chlorine gas at a known pressure flowed through the system for a specified time, was condensed, and later allowed to reexpand into the evacuated glass line where its final static pressure was measured. The total volume of the flow system was extracted by allowing air at known pressure to expand from a known volume into the evacuated flow system where its final pressure was measured. Thus, the volumetric flow rate V' of chlorine is given by

$$V' = \frac{P_e V_e}{P_f t} \quad cm^3/sec \tag{3}$$

where P_e and V_e are expansion pressure and flow system volume in cm^3, respectively, P_f is the reaction vessel flow pressure, and t the time of flow in seconds. The transit time for gas between inlet and outlet arms of the reaction vessel is given by the ratio of the volume enclosed by these ports to the volumetric flow rate. For the suprasil vessel the transit time was found to be related to the reaction vessel pressure in Torr by an equation of the form

$$\frac{1}{\tau} = a\sqrt{P} + bP \quad \text{sec}^{-1} \tag{4}$$

where a and b have valves of 1.38 and 0.190, respectively, derived from a least squares deviation fit of the data. The average linear flow velocity v is given by

$$v = \frac{\ell}{\tau} = \frac{V'}{\pi r^2} \tag{5}$$

where distance between the centers of the inlet and outlet ports is ℓ = 43.8 cm for the suprasil vessel. Figure II-4 shows the linear flow velocity and transit time for the gas mixture as a function of chlorine pressure in the reaction vessel. The flow velocity calculated from Eq.(5) will be used frequently in subsequent data treatment. Note that typical flow velocity and transit-time are 27.8 cm/sec and 1.54 seconds, respectively, for P = 0.2 Torr.

Ferguson et al.[6] have shown that the flow velocity at radial distance r from the axis and distance along the cylindrical tube axis is given by

$$v(r,z) = \bar{v}(z)\left[\frac{2F_v}{F}\left(1 - \frac{r^2}{a^2}\right) + 2\frac{F_t}{F}\right] \tag{6}$$

where $\bar{v}(z)$ is the average flow velocity at z. $\bar{v}(z)$ depends on the pressure gradient along the axis. The term in brackets represents the affect of the viscous (F_v) and molecular (F_t) conductance on flow velocity, including the parabolic velocity profile of viscous flow. The flow velocity presented in Fig. II-4 is simply the average flow

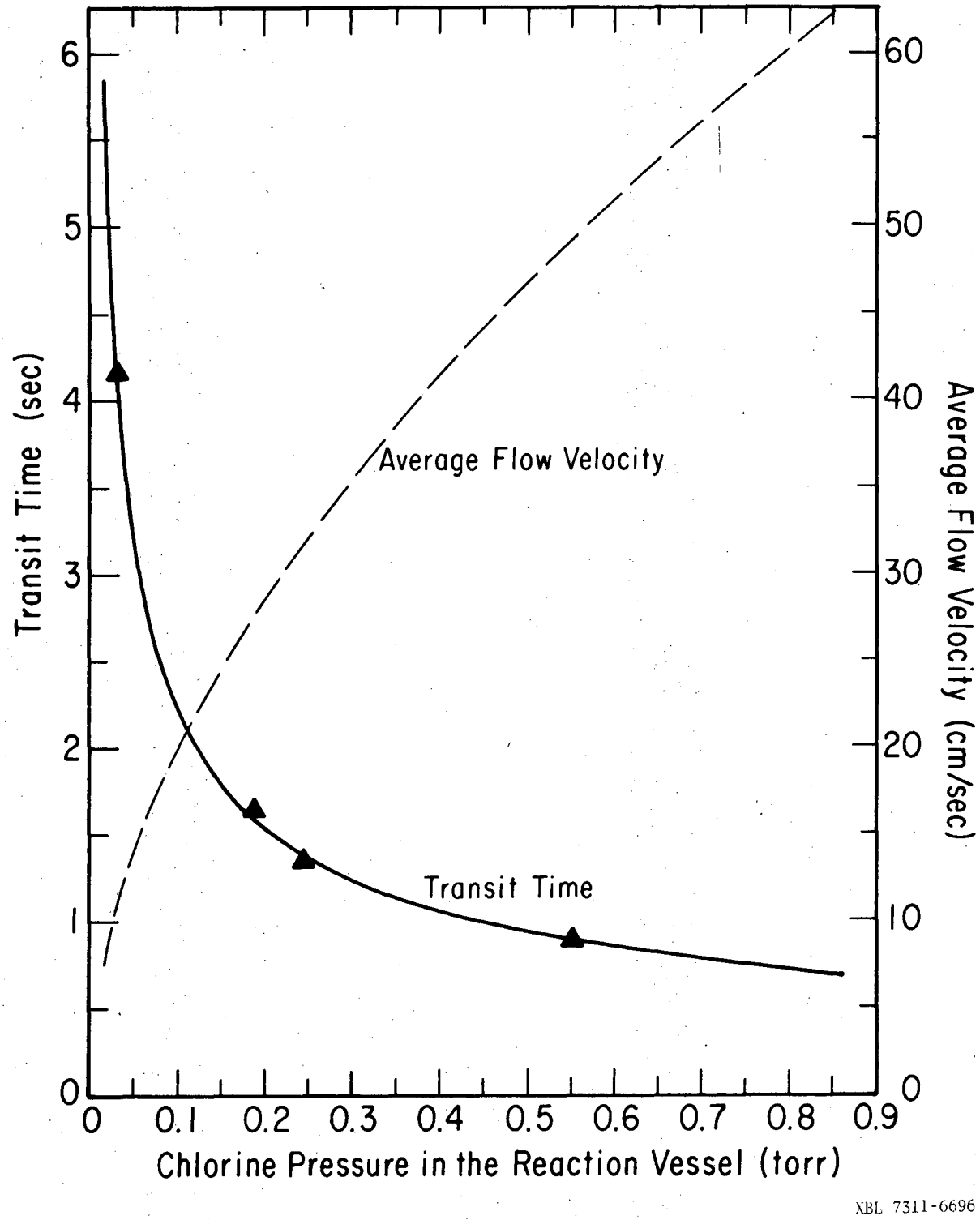

Fig. IV-4. Flow parameters. The average flow velocity is calculated from the transit time according to Eq. (5).

velocity for a planar velocity profile. Besides neglecting the actual parabolic velocity profile, the pressure drop along the reaction vessel axis has been neglected here. As mentioned earlier the pressure drop is no greater than 2% for pressure up to 1 Torr, so that $\bar{v}(z)$ is approximately independent of z, axial distance. This is important because in flow kinetic work the time scale is defined by $t = \frac{z}{v}$.

The axial distance required to establish a parabolic velocity profile is given by

$$\ell_e = 0.227\ aR \tag{7}$$

where a is the reaction vessel radius and R is the Reynold's number of the flow.[7] The Reynolds number, which is a measure of the turbulence of the flow, is given by

$$R = \frac{a\rho v}{\eta} \tag{8}$$

where ρ is the gas density, in g/cm^3 and η the viscosity in poise.[8] Using $\eta = 1.4\times10^{-4}$ poise at 45°C[9] and the flow velocities shown in Fig. II-4, ℓ_e varies from 0.10 cm at P = .05 Torr to 10.9 cm at P = 1.00 Torr. For P = 0.5 Torr, the maximum pressure for quantitative work, ℓ_e = 3.7 cm. Since the distance between the Cl_2 inlets and the beginning of the irradiated region of the vessel is 6.6 cm, the flow will be well developed before the gas mixture reaches the irradiated zone.

5. Flow Characteristics

In the quantitative studies of the flow system chlorine and mercury were admitted into the irradiated reaction vessel as described

earlier. Since no inert buffer gas was used the flow rate and pressure of chlorine determine the dominant hydrodynamic features of the flowing mixture. A convenient indicator of the nature of the flow is the Knudsen number, the ratio of the mean free path of the gas, L, to the cylindrical tube radius, a.[10] The mean free path is the average distance traveled by a gas molecule between collisions with other molecules and depends on the collision diameter δ and the concentration of the gas[11] as shown by kinetic theory:

$$L = \frac{1}{\sqrt{2}\pi n \delta} \tag{9}$$

Here n is the concentration of gas in particles/cm^3. Figure II-5 shows the variation of Knudsen number with pressure for chlorine, assuming a value of $\delta = 4.3$Å. δ is derived from Table I-A of Ref. 12. Dushman shows that for $L/a < .01$ the flow is almost entirely viscous; that is, the flow characteristics of the gas are essentially determined by the collisions of the molecules with each other rather than by collisions of the molecules with the walls, as is the case for free molecule flow. For $L/a > 100$ molecular flow dominates. According to this criterion for pressures higher than 0.16 Torr the flow is essentially viscous, but at lower pressures molecular flow characteristics appear. This is shown in the conductance of the cylindrical vessel. The conductance, defined as flow rate per unit pressure drop, along the axis, has been found by Knudsen to follow this empirical relationship for the transition range between viscous and molecular flow:

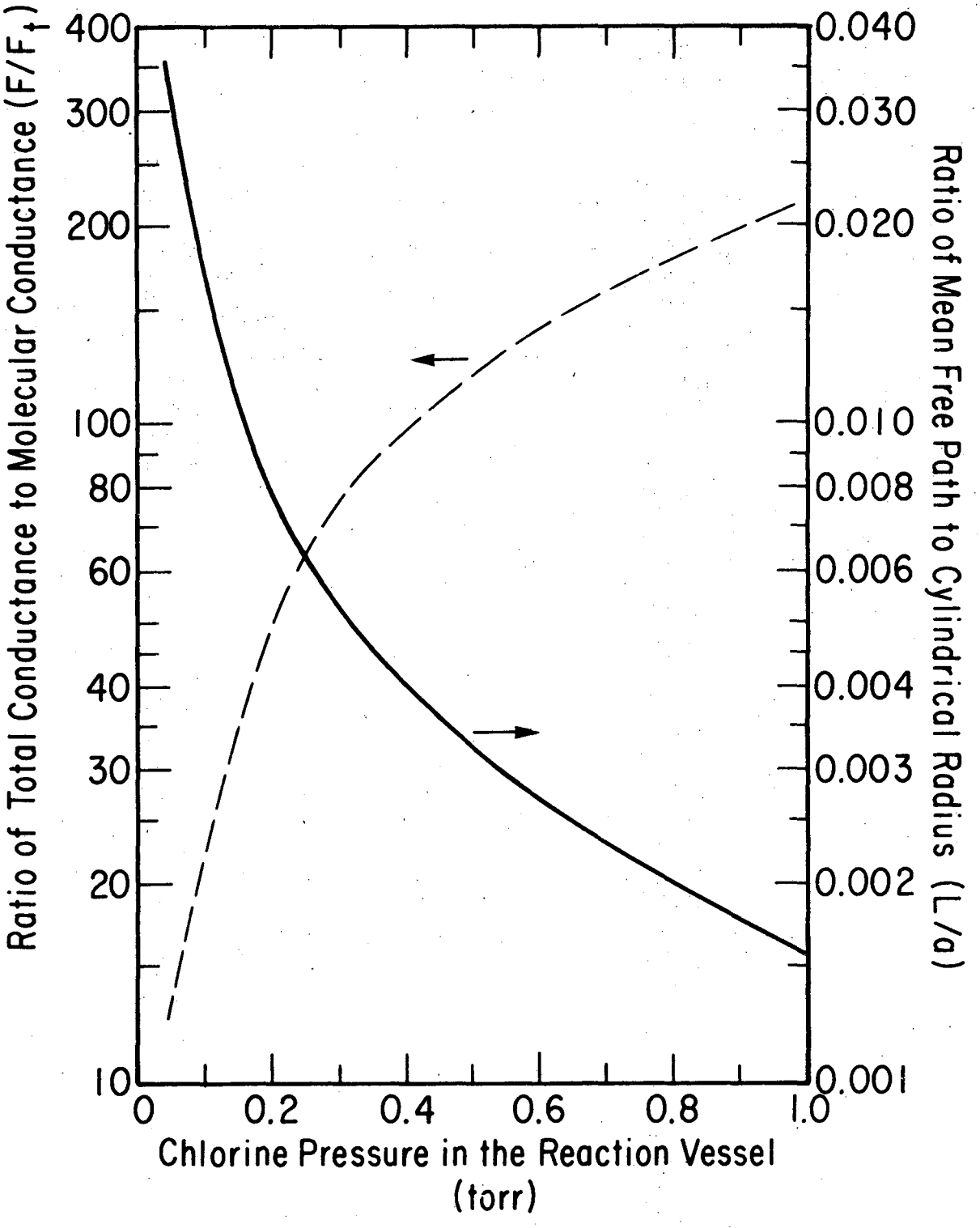

XBL 7311-6694

Fig. II-5. Flow characteristics. Knudsen number (L/a) and conductance ratio as a function of chlorine pressure in the reaction vessel.

$$F = F_v + zF_t \tag{10}$$

where F_v is the conductance for viscous or Poiseuille flow, F_t is the conductance for molecular flow and z is a factor dependent on the viscosity, pressure and average local velocity of the gas, which simplifies to

$$z = \frac{1 + 2.51(a/L)}{1 + 3.09(a/L)} \tag{11}$$

using kinetic theory.[13] For chlorine pressures above 0.05 Torr z has the constant value 0.810. Figure II-5 shows the ratio of total conductance to molecular conductance as a function of chlorine pressure for this reaction vessel. For P = .05 Torr (L/a = .0321) the flow is only about 8% molecular, so that deviation from viscous flow is significant but not dominating, for the lowest pressures used in these experiments. The coefficient of slip is also used as a measure of the deviation from viscous flow as the pressure is decreased. Molecules slip at the walls if instead of losing tangential velocity by collision with the walls they rebound with a fraction of their initial momentum. Using relationships given by Dushman for the coefficient of slip and for the correction of the conductance for slip[14] an estimate of 13% slip at the walls for P = .05 Torr is derived. Slip is about 1% at 1.0 Torr. These results show that the flow of gases in the reaction vessel is predominantly viscous but at very low pressures the deviation due to molecular flow cannot be ignored.

6. Diffusion Considerations

Mixing of chlorine and mercury in the reaction vessel occurs by radial diffusion. The homogeneity of the gas mixture depends on rapid diffusion. A measure of the effectiveness of diffusion mixing is given by the axial distance z through which the gas mixture passes when the average diffusion length is the cylindrical radius of the reaction vessel:[15]

$$\bar{x}^2 = r^2 = 2Dt = 2D\,\frac{z}{v} \tag{12}$$

the diffusion coefficient for the Hg + Cl_2 mixture has been estimated using the method of Hirschfelder et al.[16]

$$D_{12} = 0.002628\,\frac{\sqrt{T^3(M_1+M_2)/2M_1M_2}}{P\sigma_{12}^{\,2}\,\Omega_{12}^{(1,1)*}(T_{12}^*)}\ \text{cm}^2/\text{sec} \tag{13}$$

Here M_1 and M_2 are molecular weights, P is the total pressure in atm, $\sigma_{12} = \frac{1}{2}(\sigma_1+\sigma_2)$ is a molecular diameter measure, and $T_{12}^* = kT/\varepsilon_{12}$ where $\varepsilon_{12} = \sqrt{\varepsilon_1\varepsilon_2}$ is the estimated well depth of a Leonard Jones potential energy function describing the interaction of the two gases. $\Omega_{12}^{(1,1)*}(T_{12}^*)$ is a measure of the affect of the interaction potential on the diffusion coefficient. Table II-1 shows the values chosen for calculation of D_{12}. Figure II-6 shows the resultant diffusion coefficients and axial distance z for average diffusion length $\bar{x}^2 = r^2$ as a function of Cl_2 pressure. If a more attractive potential were assumed smaller values of D_{12} result. For pressures less than about

Table II-1. Values of Diffusion Coefficient Parameters for $Hg + Cl_2$ [a]

$$D_{12} = 0.002628 \frac{T^3 (M_1 + M_2)/M_1 M_2}{P\sigma_{12}^2 \Omega_{12}^{(1,1)*} (T_{12}^*)}$$

$\sigma(Hg)$	2.898Å
$\frac{\varepsilon}{k}$ (Hg)	851
$\sigma(Cl_2)$	4.29
$\frac{\varepsilon}{k}$ (Cl_2)	300
T_{12}^* (318°C)	0.627
$\Omega_{1,2}^{1,1}$ (T_{12}^*)	1.798

[a] J. O. Hirschfelder, C.F. Curtis and R.B. Bird, Molecular Theory of Gases and Liquids, Wiley, New York, 1964, Eq. 8.2-44, p. 539, and Table I-A.

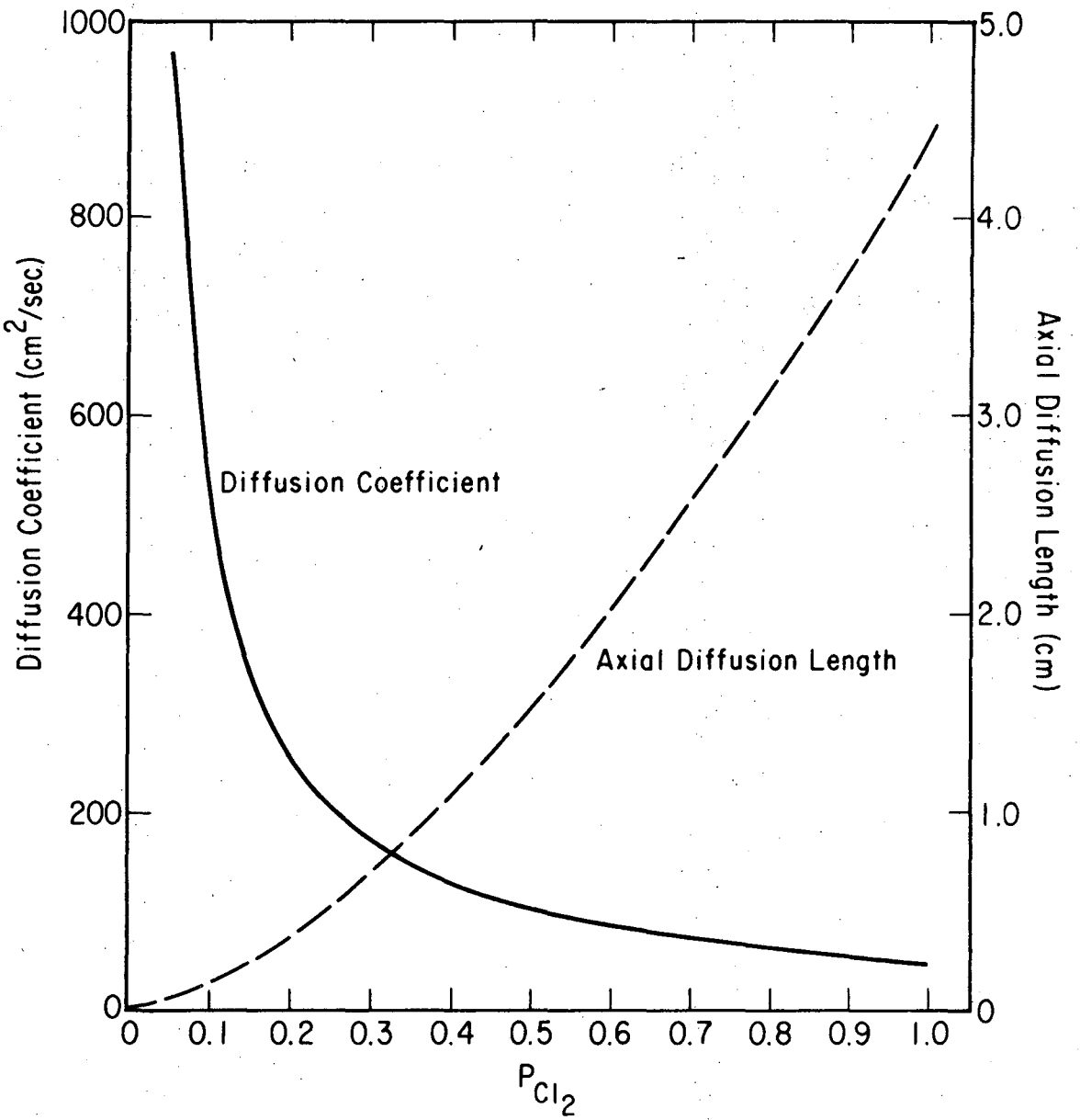

Fig. II-6. Diffusion coefficient and axial diffusion length as a function of chlorine pressure in the reaction vessel.

1.2 Torr radial diffusion will be established before the reacting mixture reaches the irradiated zone of the vessel. This places an upper limit on the total pressure for kinetic studies.

Although radial diffusion is rapid in this flow system and the reactants will be mixed before entering the irradiated zone, the assumption of a homogeneous gas mixture should be made cautiously because of the possibility of non-uniform irradiation. The simplest model of the flow system assumes a homogeneous distribution of reactants. The conditions required for homogeneity have been met as well as possible for quantitative work. The pressure of Cl_2 was kept below 0.5 Torr and the lowest possible mercury flow rates were used to minimize radiation imprisonment.

Because the reactions investigated here involve electronically excited species with lifetimes $\sim 10^{-7}$ sec, the time scale is very short compared to the transit time and diffusion time. Destruction of reacting species at the wall is unimportant here.

7. Experiments with Inert Gases

The influence of varying pressures of inert gases on the mercurous chloride emission spectrum was studied by adding the inert gas (helium or nitrogen) near the chlorine inlet into the system. The total pressure in the system was monitored upstream of the reaction vessel with the capacitance manometer used in the differential mode: air was added at the reference port of the manometer and its pressure measured with an oil or mercury manometer. In these experiments the flow was controlled by adjusting stopcocks down-stream of the reaction vessel.

C. Light Sources

1. General Electric Germicidal Lamps

Low pressure mercury lamps of two types were used in these experiments. Most of the work involving $Hg(6^3P_1)$ chemistry was performed using twenty four hot cathode germicidal lamps, type G8T5, purchased from General Electric Company. These lamps, of overall length 12 in. and outer diameter 0.625 in. were constructed from 9741 (Pyrex) 1 mm walled tubing, with transmission of about 60% at 2537Å and about 2% at 1849Å.[4] Each lamp contained a droplet of mercury in a few millimeters of argon. They were mounted coaxially with the reaction vessel at a radius of 4.0 in. from its axis. Six lamps were wired independently using ballasts and starters in the standard circuit for fluorescent lamps. The remaining lamps were wired in triplets with 120° between members so that considerable intensity variation was possible. Although these lamps operated in a frequency range of 10-160 hertz, no increase in emission signal to noise ratio was achieved when the line voltage at 60 hertz was replaced by a stable variable frequency power supply, even when lock-in detection techniques were employed. Therefore, in most experimental work, the lamps used line voltage without further voltage or current regulation. The output of the lamps was monitored frequently during quantitative work and data were time normalized when necessary, although lamp output usually did not vary by more than 1% during any experiment.

The entire lamp and reaction vessel assembly was surrounded by an aluminum cylinder of radius 6 in. which was coated internally with Eastman Kodak white reflectance paint. This paint had higher reflectance at 2537Å and better stability to continued ultraviolet irradiation than a similar coating of MgO. This surrounding cylinder also served as a heat reflector and helped maintain the reaction vessel at 45°C in thermal equilibrium with the lamps' walls. It has been determined that this type of lamp has maximum efficiency in production of the mercury resonance line at 2537Å at 45°C.[17] As mentioned earlier the heating of the reaction vessel by the lamps prevented condensation of solid products on the front window and flange ends of the reaction vessel.

Output radiation from these lamps is concentrated in the mercury resonance line at 2537Å. Output at 2537Å is 86% of the total power radiated in the ultraviolet and visible spectral region.[18] A slight ozone oder could be detected near the lamps, indicating that these lamps were radiating small amounts of the other mercury resonance line at 1849Å. Spokesmen from General Electric Company asserted that radiation at 1849Å comprises less than 0.5% of the total power output of these lamps. Absorption by atmospheric oxygen should render negligible the amount of this radiation reading the reaction vessel.

According to data of the producer,[18] the output power at 2537Å after use of the lamp for 100 hours is 1.3 watts. This gives a maximum illuminance at the reaction vessel axis of 0.95 milliwatt/cm^2 or 1.2×10^{15} photons/sec-cm^2 for one lamp. Thus for 24 lamps, the maximum

Another source of broadening is Lorentz broadening caused by collisions of mercury inthe lamp with the few Torr of argon present. The Lorentz half breadth is given by[21]

$$\Delta\nu_L = \frac{z_L}{\pi} \tag{14}$$

where z_L is the collision frequency in sec^{-1}. For 5 Torr of argon $\Delta\nu_L/\Delta\nu_D = 0.002$ for mercury resonance radiation.[22] Thus Lorentz broadening is unimportant for these lamps.

The simultaneous presence of seven stable isotopes of mercury also contributes to the width of the line. The two strongest hyperfine lines, due to mass 202 and 200, are separated by 0.0115Å and the other hyperfine lines are separated by approximately the same distances, so that the hyperfine structure is not resolved in Fig. II-7.

The absorbance of light from one mercury lamp caused by flowing mercury in the reaction vessel is presented as a function of mercury flow rate in Fig. II-8. The transmitted light of one lamp mounted parallel to the reaction vessel axis was monitored through the viewing tube (See Sec. II.F.) perpendicular to the axis at a distance of 1.8 cm from the upstream end of the irradiated region of the reaction vessel. The mercury vapor in the vessel does not follow the Beer Lambert law for light absorption for flow rate $> 10^{16}$ atoms/sec. The fractional absorption $(I_o-I)/I_o$ at a flow rate of 3.3×10^{15} atoms/sec is 0.08. This flow rate corresponds to the lowest flow rate of mercury which was used in kinetic studies. In order for the reaction mixture to be homogeneous with respect to incident light intensity it is wise to

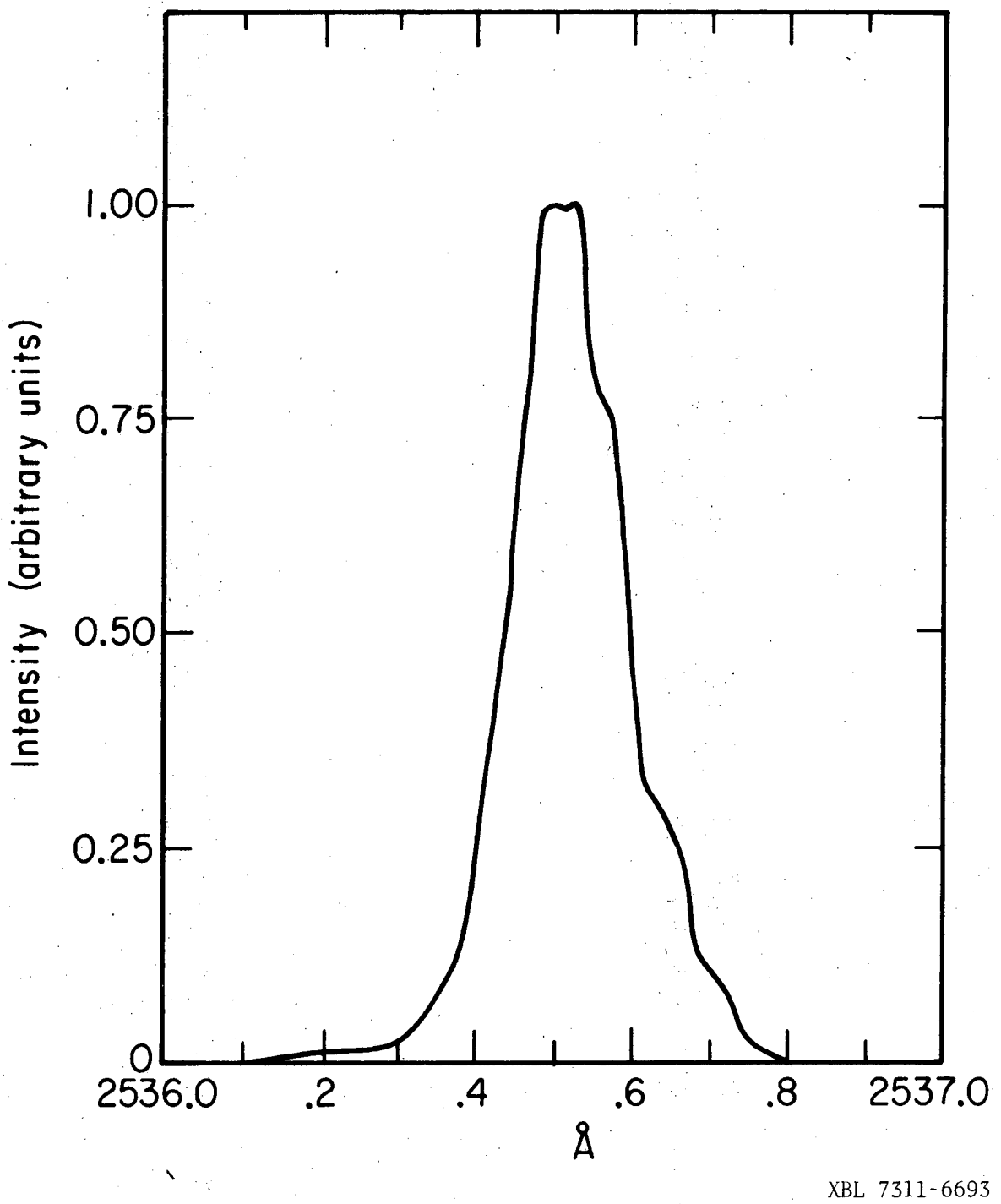

XBL 7311-6693

Fig. II-7. Profile of resonance radiation from the low pressure mercury lamps (General Electric G8T5), using 5μ slits and the fourth order of the spectrometer grating.

illuminance of 2.9×10^{16} photons/sec-cm^2 gives a photon density of 9.6×10^5 photons/cm^3 at the axis. This compares to a typical mercury concentration of 10^{13} atoms/cm^3.

The shape of the resonance line at 2537Å emitted by the germicidal lamps is shown in Fig. II-7. This photoelectric trace was taken in the fourth order of the grating with the spectrometer slits set at 5μ for a resolution of 0.012Å since the reciprocal linear dispersion is 2.5Å/mm in fourth order. The half width measured is 0.167Å compared to a Doppler width at 45°C of 0.0022Å.[19] (Both the lamp wall and reaction vessel had an equilibrium temperature under experimental conditions of 45°C.) The center of the lamp undoubtedly has hotter than the wall, so that the actual Doppler width of the lamp was larger than that of the absorbing mercury atoms near the walls of the lamp as well as mercury atoms in the reaction vessel. Other factors contribute to the breadth of the emission line. Probably the most important is self absorption inside the lamp. As shown in Fig. 1 of Ref. 20, the overall intensity of the emission line is reduced and its half width increases as the amount of self absorption increases, but an actual reversal or dip in the center of the emission line does not occur until the amount of self absorption is very large, as in a medium pressure mercury arc. The light source used here does not produce such a reversed line at 2537Å, but it is quite difficult to assess the actual amount of self absorption, and it is likely to be the chief source of line broadening in the lamps. To minimize reversal, low pressure mercury lamps must be cooled to wall temperatures of 20°C or less.

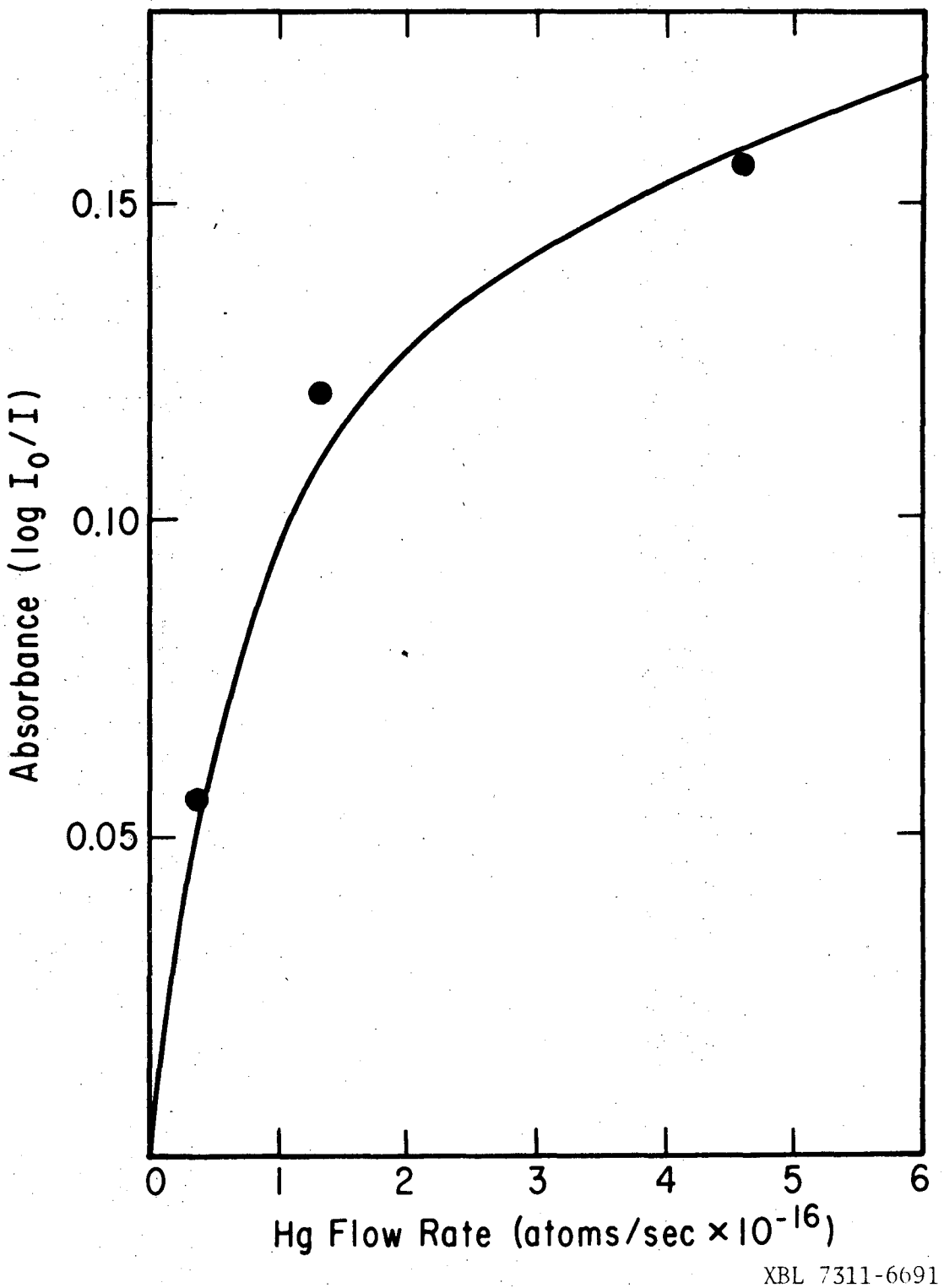

Fig. II-8. Absorbance of resonance radiation (2537Å) by flowing mercury in the reaction vessel.

keep light absorption lower than 10%. These absorption measurements were made without adding reactant gas. When Cl_2 was added the absorption decreased due to faster transit time of the reacting mixture through the vessel, so that the system did in fact remain fairly homogeneous with respect to incident radiation at 2537Å. However, because it was impossible to remove all Hg from the vessel, this absorption estimate is actually a lower limit and kinetic studies indicated that larger absorption of the incident light by mercury occurred.

2. Westinghouse Sterilamps

In attempts to study reactions of Hg 6^1P_1 atoms, low pressure mercury lamps rich in output of the singlet resonance line were used. Three Westinghouse "sterilamps," model 782H10, were mounted concentric with the reaction vessel at a radius of 3.25 in. and were surrounded by an aluminum reflector which was painted on the interior with Eastman white reflectance paint. These "cold cathode" lamps operated at around 300 volts with a much higher stability than the "hot cathode" germicidal lamps discussed previously. In cold cathode lamps, electron emission from the cathode to excite the discharge is produced by the affect of the high electric field rather than higher temperature at the cathode. Their output of 1849Å light was estimated by the manufacturer as 10% of the total ultraviolet output since the lamp material was quartz rather than pyrex. Lamp wall temperature was measured as 35°C.

During experiments with 1849Å radiation, the mount for the reaction vessel and lamps was sealed and flushed continuously with warm nitrogen to eliminate oxygen which absorbs 1849Å radiation to produce ozone. Ground state mercury has a much higher absorption coefficient for 1849Å radiation than for 2537Å radiation. The lifetime

for this spin allowed transition is 1.3×10^{-9} sec compared to 1.1×10^{-7} sec for the singlet triplet transition.[23] This facts mean that the self absorption in the lamp is higher for this transition, and that the 1849Å line is completely absorbed by the mercury in the tube at a lower mercury concentration. In a static system, Uphaus and Gunning reported complete absorption of 1849Å radiation at 0°C. At this temperature the 2537Å radiation had a fractional absorption of only 0.07, for a path length of 0.85 cm.[24] The short lifetime of $Hg(^1P_1)$ atoms also predicates that the time scale of collision and reaction phenomena is contracted and that the search for excited product molecules is made more difficult.

In experiments with 1849Å radiation secondary absorption measurements were performed at 4347.5Å to make sure that $Hg(^1P_1)$ atoms were indeed formed in the reaction vessel. The cylindrical enclosure surrounding the lamps and reaction vessel was alternately flushed with nitrogen and oxygen to determine whether the HgCl spectra which resulted were caused by irradiation by 1849Å or 2537Å. In both cases $Hg(^3P_1)$ was present. After it had been established that the emission spectra produced were identical in intensity and structure, these high ozone lamps were used to study the short wavelength limit of the HgCl* emission, since the signal to noise ratio of the spectra was improved by an order of magnitude compared to the spectra obtained using the germidical lamps. This increase in sensitivity proved important in interpreting the chemiluminescent spectra and in calculating the dissociation energy of the ground state of HgCl.

D. The Light Detection System

Light levels were high enough in these experiments to allow use of fairly simple and straightforward detection techniques. A versatile monochrometer formed the core of the light detection system. Photoelectric or photographic means could be used to record light signals.

1. The Monochrometer

The monochrometer used in these experiments was a Spex Industries model 1800 combined Spectrograph and Spectrometer, a f/7.5 three quarter meter focal length instrument with components arranged in a Czerny-Turner mount. The Bausch and Lomb certified precision plane diffraction grating with 1200 grooves/mm in a ruled area 102×102 mm was blazed at 7500Å in the first order. Weak satellites of strong lines from the mercury spectrum and perhaps a Hyman ghost were observed during scans of emission spectra. Ghosts and satellites are caused by ruling errors during the production of the grating and did not prove troublesome after they were understood.[25] No masking of this grating was necessary. A second grating, blazed at 2500Å with 600 grooves/mm was available for use, but better overall intensity and resolution were achieved for the ultraviolet region of the spectrum by using higher orders of the original grating. Kinematic mounting of the gratings provided for easy interchangeability with reseating accurate to 1Å, according to the manufacturer. The spectrometer had straight slits, Spex number 1411, with width variable between 5 microns and 3 millimeters and height variable from 1 to 20 mm at the entrance slit. The reciprocal linear dispersion or plate factor ranged from 10.4 to 9.6Å/mm in the

first order. Typical spectral scans conditions used a slit width of 250μ for a resolution of 2.5Å in first order and 1.25Å in second order, with a scan speed of 15 Å/minute.

2. Photographic Detection

For operation of the instrument as a spectrograph light diffracted at the grating was reflected onto the plate holder plane. The plate holder accommodated ten inch spectroscopic plates. Kodak 103A-O (2000Å to 5200Å) and 103A-F (4500-6900Å) plates were used for survey work, for recording spectra which were too unstable or noisy for photoelectric detection, and for higher resolution study of the emission spectra using a narrow slit and long exposure times. Plates were processed in Kodak D-19 Developer at room temperature with slight agitation for 4 minutes followed by one minute in water stopbath and 5 minutes in Kodak Rapid Fix with hardener. Later the plates were washed for 30 seconds in diluted Photoflo solution.

3. Photoelectric Detection.

For photoelectric detection, diffracted light from the grating was diverted from the plate holder area by an added mirror and reflected onto the exit slit and photomultiplier assembly. (Spex industries later discontinued this design and currently replace the plate holder with the slit and photomultiplier.) The phototube used in these experiments was an EMI 6256S tube with an end on 10 mm CsSbO cathode and fused silica window. The rated cathode sensitivity of the tube used was 68 μA/Lumen with overall sensitivity of 2000 A/L at -1760 volts at the cathode. At this voltage the gain was approximately 3×10^7.

The S type emitting surface of the tube had a maximum quantum efficiency of 16% at 3800Å. The tube could be used to a short wavelength limit of about 1650Å according to the manufacturers. The dark current in the tube with the cathode at -1760v measured 1×10^{-9} amp; cooling the tube reduced this by a factor of ten. Under normal scan conditions, cooling did not help the signal to noise ratio and was not used since most of the noise originated in the light source and differential signal levels were typically about 10^{-7} amp or higher. The voltage divider chain recommended by the manufacturer was used, with the cathode at high negative voltage and the anode close to ground potential. As expected AC detection with the anode at high positive voltage and the cathode at ground offered no advantage in noise reduction. The resultant anode current was fed into a Keithley 602 electrometer and measured either as current or across the an external load resistor as voltage. In most scans of the HgX(B→X) emission, the background signal from the fluorescing quartz and from the lamps had to be offset either by the zero adjustment of the electrometer or by an external variable DC voltage in series with the photomultiplier output across a 10^{7} ohm resistor. The electrometer in this case was floated and measured the sumeof the opposing voltages of the DC offset and the photomultiplier signal. One end of the photomultiplier output resistor was at ground potential. By using this external DC offset, differential amplification was achieved and resolution of fine spectral features in the emission signal was possible. The amplified 1 ma full scale output of the electrometer was fed into a Texas Instruments Servo Rectiriter II

recorder and was used with external RC filtering which allowed variation of the time constant up to 30 seconds. The recorder had variable chart speed (.5 cm/hour to 20 cm/minute) and variable full scale deflection (10-100 mv). These features provided convenient versatility in data acquisition.

When used as a spectrometer the grating of the Spex instrument was driven by a motor unit provided by a Servo Tek Products DC Velocity Servo Unit-model 584. Control of the scan speed was achieved with a ten turn potentiometer and scan speed could be varied in the range .25 - 500 Å/min reproducibly. A wavelength meter was attached to the grating drive unit, but it had an error of about - 6 Å/1000Å between 7000 and 12000Å and true wavelength readings were found by scanning the spectrum of a mercury lamp with no filtering of orders throughout the region of interest. The value of the correction term depended on the exact position of the mirror which deflected the reflected grating light onto the exit slit of the spectrometer. Since this mirror was removed each time the optical alignment of the reaction vessel was adjusted or checked, wavelength calibration scans had to be performed at least that frequently. The grating drive circuitry provided a low voltage pulse every 5.0 Å which activated an event marker solenoid at the second pen of the recorder, enabling wavelength calibration of the chart recorder output. Typical scan conditions and optical filters for recording $HgX(B^2\Sigma^+ \rightarrow X^2\Sigma^+)$ emission are shown in Table II-2.

Table II-2. Typical Scan Conditions for Recording HgX(B→X) Emission Spectra

a)	Variable	Typical Value
	Signal level	$.3\times10^{-7}$ amp
	Time constant	3 sec
	Slit width	250μ
	Wavelength drive	15 Å/minute
	Chart Speed	2.5 cm/minute
	Phototube cathode voltage	-1760 V
	Wavelength region	7000Å-11400Å I or 3500Å-5700Å II

b)	Wavelength Region-Å	Optical Filter-Corning numbers
	3000-4500	Pyrex 7740
	4500-5000	0-52 7380
	5000-5200	3-75 3389
	5200-5700	3-73 3060

E. Intensity Response of the Optical System

The response factor of the spectrometer and photomultiplier system was measured using the photo-feedback stabilized tungsten ribbon lamp and associated equipment which had been designed and assembled by Gabelnick.[26] Light from the General Electric 30A/T24/17 lamp which was emitted from a pinhole opening at the center of the lamp's quartz window illuminated the spectrometer slit while the lamp spectrum was scanned using the same optical filters and scan conditions as were used in the scans of the HgX emission spectra. The brightness temperature of the tungsten lamp was measured with a calibrated Leeds and Northrup model 8622-C optical pyrometer. The true temperature of the filament (2150°K) was obtained from the brightness temperature (1978°K) using Fig. 5 of Ref. 26. The emissivity of tungsten at 2150°K was interpolated from the published data of de Vos.[27] The true temperature and emissivity were used in this equation for the radiation for a non black body:[26]

$$Id\lambda = \frac{a\,\varepsilon(\lambda,T)\,d\lambda}{\lambda^4(e^{10^8\,hc/k\lambda T}-1)} \qquad (15)$$

Here I has units of quanta/sec/cm^2 of radiating surface/unit solid angle/unit wavelength (Å), λ is wavelength in Å; T, k, c and h have the usual meanings and values, a is a constant equal to 5.996×10^{34}, and $\varepsilon(\lambda,T)$ is the emissivity at λ and T, that is, the ratio of the intensity of radiation of the material used to the intensity of the

radiation of a true black body at the same temperature and wavelength. The relative response factor $R(\lambda)$ for this optical system was obtained by computing the ratio of the intensity calculated from Eq. (15) to the observed intensity at wavelength internals of 50Å. The resultant response factor curve is shown in Fig. II-9 for use of the spectrometer in the second order. The discontinuities in the curve reflect the use of the optical filters shown in Table II-1b. The intensity normalized spectra shown later were constructed using the data of Fig. II-9:

$$I = I_{measured} \times R(\lambda) \qquad (16)$$

F. Configuration and Alignment of the Optical System

Two configurations of the reaction vessel and light detection system were used. In the first, the optical axis of the spectrometer coincided with the axis of the cylindrical reaction vessel, so that the spectrometer viewed all emitted light in the reaction vessel as well as scattered light from the lamps. This is the arrangement simply illustrated in Fig. II-1. It was determined experimentally that the most efficient light collection resulted when light from the upstream end of the irradiated part of the reaction vessel was focused on the entrance slit of the spectrometer. Care was taken in alignment of the reaction vessel with respect to the spectrometer to ensure that the reaction vessel axis did in fact coincide with the spectrometer axis.

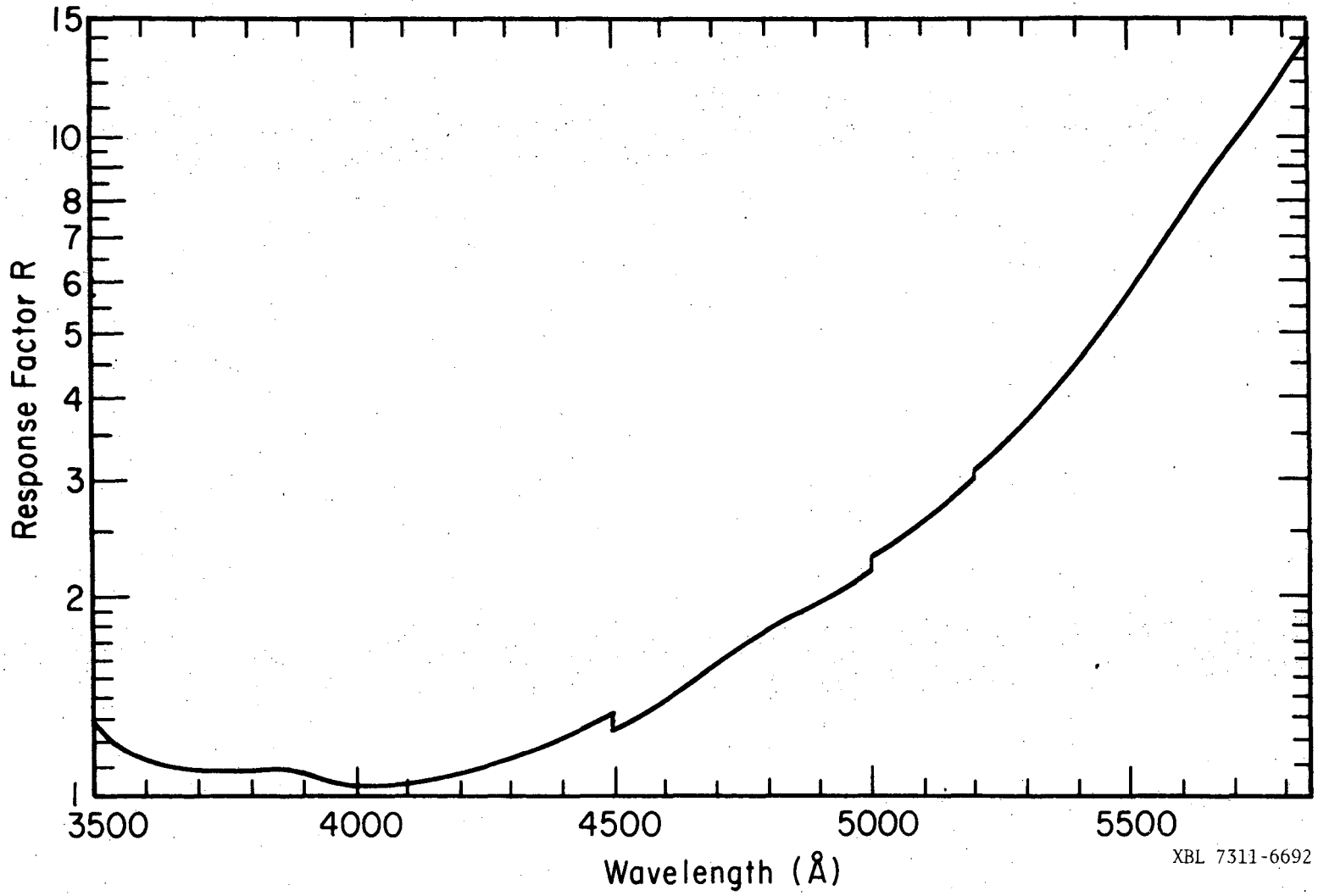

Fig. II-9. Second order response factor as a function of the first order wavelength.

With the spectrometer plate holder removed the image of the mercury capillary center and a string suspended through the center of the front window of the reaction vessel were viewed on the mirror which reflected the diffracted light from the grating. The green 5461Å line from the lamps surrounding the reaction vessel provided the light seen at this mirror. It was possible to visually align the reaction vessel so that its image was exactly centered and to ensure that light from the reaction vessel filled the grating with the lens in place.

In the second configuration of the reaction vessel and spectrometer the alignment was less precise, although the intensity of background mercury lines could be reproduced to within 2%. Here the entire reaction vessel assembly was turned 90° so that the spectrometer entrance axis was perpendicular to the reaction vessel axis. The four lamps which were closest to the plane of intersection were removed and a black cardboard viewing tube, 41.5 cm in length with an inside diameter of 2.0 cm, was mounted between the reaction vessel and the spectrometer slit. The end of the viewing tube which was tangent to the reaction vessel surface contained a slit 10 mm in height and 3 mm in width. The viewing tube height was adjusted so that its axis coincided with the spectrometer axis and the reaction vessel diameter. The aluminum cylinder which surrounded the lamps was held open slightly to allow for the viewing tube. Aluminum foil covered the part of the opening not blocked by the viewing tube. The apparatus was moved so that the spectrometer could monitor light variation along the cylindrical axis

of the reaction vessel. This configuration was used in quantitative kinetic studies of the reacting system. Wide slit settings, typically 0.5 mm, had to be used at the spectrometer as well as differential amplification because of the low light levels of HgCl* emission.

CHAPTER II REFERENCES

1. Fused Quartz Catalog, Lamp Glass Department, General Electric Company, Willoughby, Ohio, 1968, p 22.
2. F. A. Cotton and G. W. Wilkinson, Advanced Inorganic Chemistry, Interscience, New York, 1966, p. 618.
3. M. Kasha, J. Opt. Soc. Am. 38, 929 (1949).
4. a) H. W. Webb and H. A. Messenger, Phys. Rev. 34 1463 (1929).
   b) W. Coop and J. Hammond, J. Opt. Soc. Am. 52, 835 (1962).
5. L. R. Koller, Ultraviolet Radiation, Wiley, New York, 1952, p 33 and 148.
6. E. E. Ferguson, F. C. Fehsenfeld, and A. L. Schmeltekopf, Adv. At. Mol. Phys. 5, 1 (1969).
7. S. Dushman, Scientific Foundations of Vacuum Technique, 2nd edition, Wiley, New York, 1962, p. 84.
8. S. Dushman, ibid, p. 84.
9. Handbook of Chemistry and Physics, C. D. Hodgman, ed.; Chemical Rubber Company; Cleveland, 36th edition, 1954, p. 2010.
10. S. Dushman, loc.cit., p. 81.
11. S. Dushman, loc.cit., p. 28.
12. J. O. Hirschfelder, C. F. Curtis and R. B. Bird, Molecular Theory of Gases and Liquids, Wiley, New York, 1954, p. 1111.
13. S. Dushman, loc.cit., p. 106.
14. S. Dushman, loc.cit., p. 36 and 105.
15. A. G. Gaydon and H. G. Wolfhard, Flames, 2nd ed. MacMillan, New York, 1960, p. 137.

16. J. O. Hirschfelder, C. F. Curtis and R. B. Bird, Molecular Theory of Gases and Liquids, Wiley, New York, 1964, Eq. 8.2-44, p. 539.

17. W. E. Forsythe, Denison Univ. Bull, 26, 13 (1941), quoted by Koller, loc. cit, p. 60.

18. Germicidal Lamps, General Electric Company, publication TP-122.

19. J. G. Calvert and J. N. Pitts, Jr., Photochemistry, Wiley, New York, 1966, p. 58.

20. A. C. Mitchell and M. W. Zemansky, Resonance Radiation and Excited Atoms, Cambridge University Press, New York, 1961, p. 160.

21. A. C. Mitchell and M. W. Zemansky, ibid., p. 169.

22. G. H. Dicke, Rev. Mod. Phys. 20, 418 (1948).

23. Mitchell and Zemansky, loc.cit, p. 147.

24. R. A. Uphans and H. E. Gunning, JCP 21, 2229 (1953).

25. S. P. Davis, Diffraction Grating Spectrographs, Holt, Rinehait and Winston, New York, 1970, p. 15.

26. S. D. Gabelnick, Ph. D. Thesis, University of California, Berkeley, California, 1969.

27. J. C. de Vos, Physica 20, 690 (1954).

III. ORIGIN OF THE $HgX(B^2\Sigma^+ \rightarrow X^2\Sigma^+)$ EMISSION SPECTRA

A. The Proposed Mechanism for the Production of $HgX(B^2\Sigma^+)$

The simplest mechanism which is consistent with the observed behavior of the irradiated mixtures of mercury and halogens is

$$Hg(^1S_0) + h\nu(2537\text{Å}) \xrightarrow{k_1} Hg(^3P_1) \quad (1)$$

$$Hg(^3P_1) \xrightarrow{k_2} Hg(^1S_0) + h\nu(2537\text{Å}) \quad (2)$$

$$Hg(^3P_1) + XY(X^1\Sigma^+) \xrightarrow{k_3} HgX(B^2\Sigma^+) + Y(^2P) \quad (3)$$

$$HgX(B^2\Sigma^+) \xrightarrow{k_4} HgX(X^2\Sigma^+) + h\nu' \quad (4)$$

where

$$XY = Cl_2, Br_2, I_2 \text{ or ICl}.$$

Figure III-1 shows a Grotrian energy level diagram for atomic mercury. The most important transitions between energy levels for this work are the resonance lines at 1849Å and 2537Å. Reference will be made later to possible processes involving other energy levels. Two other quenching processes are possible for the destruction of $Hg(^3P_1)$:

$$Hg(^3P_1) + XY(X^1\Sigma^+) \xrightarrow{k_5} HgX(X^2\Sigma^+) + Y(^2P) \quad (5)$$

$$Hg(^3P_1) + XY(X^1\Sigma^+) \xrightarrow{k_6} Hg(^1S_0) + XY^* \quad (6)$$

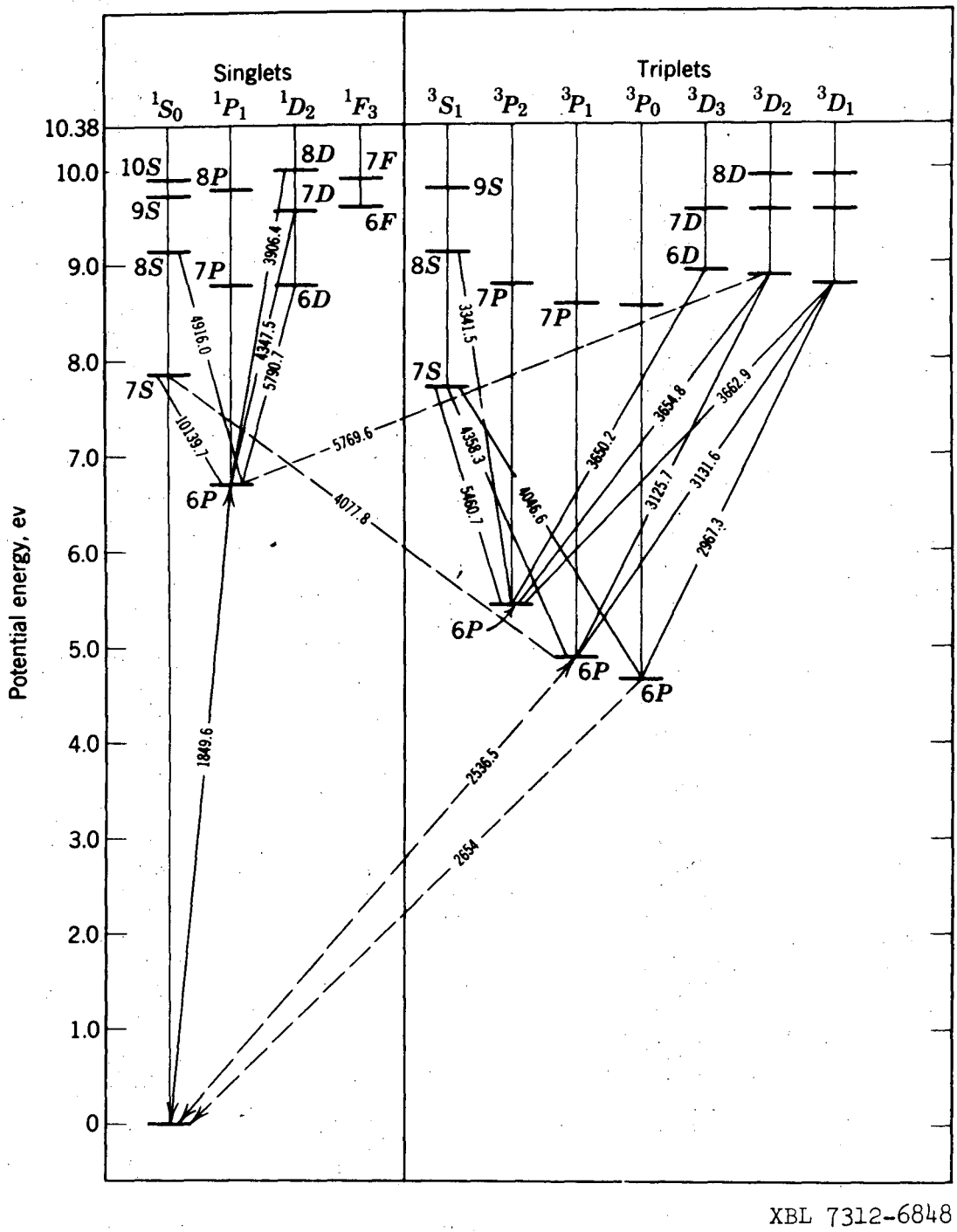

Fig. III-1. Energy level diagram for mercury. Spin forbidden transitions are indicated by dashed lines. From Fig. 2-10 of reference 9.

Here XY* represents a halogen molecule with vibrational or electronic excitation. Formation of $Hg(^3P_0)$ in a process analogous to (6) seems unlikely since halogenated molecules such as HCl, HBr and CH_3Br have been demonstrated to quench $Hg(^3P_1)$ with negligible formation of the metastable mercury species.[1] In the experiments described in this work no attempt has been made to determine the relative importance of processes (3), (5) and (6) in the quenching of electronically excited mercury atoms.

Table III-1 shows the exoergicity of Eq. (3), the bimolecular reaction between an excited mercury atom and a halogen molecule, for the halogen species studied in these experiments. The exoergicities of reaction are derived from spectroscopic data in the literature.[2,3,4] The maximum vibrational level of the $HgX(B^2\Sigma^+)$ molecule which can be populated if all the exoergicity of reaction is invested in vibration of the product molecule is also shown. Thermal energy will allow population of a few higher levels, depending on the size of $\omega_e x_e'$. For HgCl a value of D_o can be derived from the emission spectra observed here and will be presented later.

B. Qualitative Observations Which Support the Proposed Mechanism and Eliminate Other Possible Mechanisms For the Formation of $HgX(B^2\Sigma^+)$

Investigation of factors responsible for the production of HgX* and evaluation of experimental evidence for the proposed mechanism and its alternatives have been performed using only the $Hg^* + Cl_2$ system. With minor qualifications the same mechanism should be responsible

Table III-1. Exoergicity of Hg^* + XY → HgX + Y for XY = Cl_2, Br_2, I_2 and ICl.

a)

			ΔH
$Hg(6^3P_1)$	→	$Hg\ (6\ ^1S_o)$	- 4.86 eV
$XY(X^1\Sigma^+)$	→	$X(^2P) + Y(^2P)$	$D_o(XY)$
$Hg(6\ ^1S_o) + X(^2P)$	→	$HgX(X^2\Sigma^+)$	$-D_o(HgX)$
$HgX(X^2\Sigma^+)$	→	$HgX(B^2\Sigma^+)$	T_e

$$Hg(6^3P_1) + XY(X^1\Sigma^+) \rightarrow HgX(B^2\Sigma^+) + Y(^2P) \quad \Delta H_o = -4.88 + D_o(XY) - D_o(HgX) + Te$$

b)

Halogen	Product	$D_o^o(XY)^a$	$D_o^o(HgX)^b$	$T_e(HgX)^a$	ΔH_o	$v'_{max}{}^c$
Cl_2	HgCl	2.48	1.04[d]	2.90	-.52	23[d]
Br_2	HgBr	1.97	.71	2.91	-.69	45
I_2	HgI	1.54	.35	2.99	-.68	53
ICl	HgI	2.15	.35	2.99	-.09	6
ICl	HgCl	2.15	1.04	2.90	-.81	37

[a] G. Herzberg, Spectra of Diatomic Molecules 2nd edition, Van Nostrand Reinhold, New York, 1950.

[b] K. Wieland, Helv-Physica Acta 14, 420 (1941) and Z. für Electrochem., 64, 761 (1960).

[c]
$$v'_{max} = \frac{\omega_e + \left(\omega_e{}^2 + 4\omega_e x_e\ (\Delta H_o)\right)^{1/2}}{2\ \omega_e x_e} - \frac{1}{2} \quad cm^{-1}$$

[d] Experimentally observed values are D_o = 1.03 eV and v'_{max} = 29

for the production of HgX^* when the other molecular halogens react with excited mercury.

1. Participation of Ground State Species

The possibilities of reactions involving ground state species which could provide sources of $HgCl(X^2\Sigma^+)$ should be carefully considered. If there were an appreciable concentration of unexcited HgCl molecules, the (B→X) emission could be simple fluorescence from molecules which had absorbed visible radiation from the germicidal lamps.

The bimolecular reaction of ground state mercury atoms with molecular chlorine is endothermic,

$$Hg(6^1S_0) + Cl_2 \rightarrow HgCl(X^2\Sigma^+) + Cl \quad \Delta H_o = +1.44 \text{ eV} \qquad (7)$$

so that this source of $HgCl(X^2\Sigma^+)$ is eliminated at normal temperatures.

Stable $HgCl_2$ could be formed with Cl_2 as third body or it could be formed at the walls of the reaction vessel.

$$Hg(6^1S_0) + Cl_2 + M \xrightarrow{k} HgCl_2 + M \quad k = 10^{-15}(\text{mole/cm}^3)^{-2}\text{sec}^{-1} \qquad (8)$$

$$(M = Cl_2 \text{ or wall})$$

The three body collision rate constant can be estimated by analogy to the $Hg + Br_2 + M$ reaction investigated by Ogg et al.[5] For a total pressure of 1 Torr the time between gas phase three body collisions has a lower limit of about 10 sec, compared to a flow time for gas at this pressure in the reaction vessel of 0.5 sec. Therefore negligible

stable $HgCl_2$ will be formed in this way.

The importance of reaction at the walls of the quaftz vessel as a source of $HgCl_2$ or Hg_2Cl_2 can be neglected on several accounts. When the visible absorbing ultraviolet transmitting filter solution was used around the reaction vessel, the HgCl(B→X) emission could be perceived visually as a bright green glow which filled the cross section of the vessel homogeneously. This would not be the case for $HgCl^*$ formation in a process originating at the walls. When helium or nitrogen were used as inert carrier gases, mixed with Cl_2, the $HgCl^*$ emission spectrum was still observed under conditions in which diffusion of Hg to the walls was severely inhibited by the fast axial flow. Another argument against wall reactions comes from observation of the same emission spectrum with comparable intensity when inert dull black baffles were inserted into the irradiated reaction vessel and the mercury and chlorine admitted to it as usual. As described previously these anodized aluminium baffles were arranged along their supporting rods so that no light emitted from the walls of the reaction vessel could enter the cone of sight of the spectrograph. Only light emitted from products formed at the edge of the baffles would have been recorded under these conditions if wall reactions were important. Such an emission spectrum would be expected to exhibit greatly reduced intensity compared to the emission spectrum recorded under normal conditions. These experiments with the baffles show that the source of the $HgCl^*$ emission is not reaction at the vessel wall. The observed first order axial decay of the $HgCl^*$ emission as the incident light intensity is

varied also eliminates processes involving more than one light intensity dependent step such as:

$$Hg(6^3P_1) + Cl_2 + M \rightarrow HgCl_2^{\dagger} + M \quad (9)$$

$$HgCl_2^{\dagger} + h\nu\,(2537\text{Å}) \rightarrow HgCl(B^2\Sigma^+) + Cl \quad (10)$$

Here $HgCl_2^{\dagger}$ represents a molecule formed with some vibrational energy enabling it to be dissociated by light at 2537Å. Taken together these observations present a strong argument against the importance of wall reactions as a source of the HgCl(B→X) emission.

Even if there were a source of stable $HgCl_2$, light of 2537Å contains insufficient energy to dissociate $HgCl_2$ and to excite the HgCl product to the B state. For nonexcited $HgCl_2$ the maximum wavelength for which this would be possible is 2200Å, based on thermodynamic data of the Janaf tables[6] and Wieland's work.[7] To check these conclusions and the possibility of photolysis of $HgCl_2$ by short wavelength nonresonance light from the lamps or other processes involving only $HgCl_2$, $HgCl_2$ was allowed to flow into the irradiated reaction vessel through a window mounted source. This source was identical in design to the mercury source and was operated at 255°C, which was sufficient to cause condensation of salt on the cooler surfaces of the steel flanges. At this temperature the $HgCl_2$ vapor pressure in the reservoir was about 250 Torr.[8] No HgCl(B→X) emission was observed between 3000Å and 5700Å, confirming the non involvement of isolated $HgCl_2$ in processes which produce $HgCl(B^2\Sigma^+)$ in these experiments.

2. Isolation of the Necessary Exciting Radiation and the Role of $Hg(6^3P_1)$

With the flowing mercury and chlorine mixture in the usual experimental configuration, the quartz tube heated to 45°C by wire surrounding it, and the low pressure mercury lamps turned off, no $HgCl^*$ emission was observed between 3500Å and 5800Å. Similarly, when a pyrex cylinder of 2 mm wall thickness completely surrounded the area of the reaction vessel which was exposed to lamp inradiation no $HgCl^*$ emission was observed in that region. This thickness of pyrex glass has a low wavelength 50% transmission limit of 3170Å; 10% transmission occurs at 2970Å.[9] Here the mercury resonance line at 2537Å, which comprises 86% of the total germicidal lamp output, cannot reach the reaction vessel, and formation of $Hg(6^3P_1)$ by light absorption is impossible.

Isolation of the light reaching the reaction vessel to the wavelength region 2400Å to 3500Å was achieved by the use of the mickel sulfate-cobalt sulfate filter solution in the 1 cm thick cavity between the two quartz tubes. This filter solution transmitted about 60% of the incident radiation at 2537Å. $HgCl(B\rightarrow X)$ emission was observed with the same vibrational distribution but about half the intensity as that recorded when no filter solution was used.

These observations show that the presence of ultraviolet radiation between 2400Å and 3500Å is a necessary condition for the production of $HgCl^*$ emission but do not prove that $Hg(6^3P_1)$ is involved in a primary process to produce $HgCl^*$ emission. The fole of $Hg(6^3P_1)$ is clarified by the work of Duschinsky and Pringsheim who observed $HgI(B\rightarrow X)$ emission as a complication in their I_2 fluorescence experiments and decided to

investigate its origin.[10] The HgI(B→X) emission occurred upon irradiation of a Hg+I_2 mixture with unreversed mercury resonance radiation at 2537Å but was not present when the mixture was irradiated with reversed 2537Å radiation or with the cadmium resonance line at 2288Å. Irradiation of HgI_2 at λ = 2298Å or with 2537Å did not produce HgI emission. Consideration of these results leads to the conclusion that $Hg(^3P_1)$ is directly involved in the process producing the emission and excludes the photolysis of ground state HgI_2 as a source of HgI^*. These independent observations are supported by the first order dependence of the HgCl(B→X) emission intensity on initial ground state mercury concentration and on the intensity of incident radiation at 2537Å. The quantitative results referred to here will be presented and discussed in the next Chapter.

3. Possible Reaction Mechanisms Involving Excited Species

Several alternatives to the bimolecular reaction

$$Hg(6^3P_1) + Cl_2 \rightarrow HgCl(B^2\Sigma^+) + Cl \qquad (3)$$

can be postulated for the production of $HgCl(B^2\Sigma^+)$. Reaction channels which can produce higher excited states of HgCl should also be discussed.

Absorption by $Hg(6^3P_1)$ atoms inside the reaction vessel of light at 4358Å and 4078Å causes formation of $Hg(7^3S_1)$ and $Hg(7^1S_0)$ respectively, (See Fig. III-1). These higher excited states of mercury could react exothermically with chlorine to produce B, C, or D states of HgCl:

$$Hg(7^3S) + Cl_2 \rightarrow HgCl(D^2\pi_{3/2}) + Cl(^2P)\ \Delta H_0 = -1.74 \text{ eV} . \qquad (11)$$

Three experimental observations show that these reaction paths are unimportant. First, the C and D states of HgCl were never observed although a thorough search of the ultraviolet was made for them. The HgCl(B→X) spectrum would have been eliminated when the nickel sulfate-cobalt sulfate filter solution was used. This was not the case. Finally, the first order dependence of the $HgCl^*$ emission intensity on intensity of incident radiation at 2537Å eliminates these channels.

$Hg(6^3D_{1,2})$ states could, however, have been populated by absorption of light at 3132Å and 3126Å since the filter solution transitted these lines. Again, exothermic reaction paths exist for formation of HgCl in the B, C, or D states. The other arguments above also show that these processes do not occur.

The possibility of formation and excitation by absorption or collision of $HgCl(X^2\Sigma^+)$ is worth serious consideration. This non-adiabatic reaction path could produce ground state product with subsequent reexcitation:

$$Hg(6^3P_1) + Cl_2 \rightarrow HgCl(X^2\Sigma^+)^\dagger + Cl \qquad (12)$$

$$HgCl(X^2\Sigma^+) + h\nu \rightarrow HgCl(B^2\Sigma^+) \qquad (13)$$

(Here † represents some vibrational excitation). Table III-2 shows the energy available for excitation of $HgCl(X^2\Sigma^+)$ by absorption. Equation (13) is exoergic by about 1.1 eV for absorption of λ = 3126Å by HgCl. This would lead to maximum vibrational excitation at v' = 51.

Table III-2. Energy available for vibrational excitation of $HgCl(B^2\Sigma^+)$ after absorption by $HgCl(X^2\Sigma^+)$ of visible and near ultraviolet radiation from the mercury source.

Hg line[a] Å	E eV	$E-T_e$[b] eV
3125.67	3.96	1.06
3650.15	3.40	.50
4358.33	2.85	- .05
5460.74	2.27	- .63

[a] D. E. Gray, ed., American Institute of Physics Handbook, 2nd edition, McGraw Hill, New York, 1963.

[b] T_e = 23421 cm^{-1}, K. Wieland, Helv. Phys. Acta 14, 420 (1941).

The filter solution transmits light of this wavelength to the same extent as it transmits λ = 2537Å radiation. This mechanism is ruled out by the lack of observation of HgCl(B→X) vibronic bands originating in such high vibrational levels and by the first order dependence of the emission intensity on incident light intensity. The lack of significant change in the emission signal when the filter solution was used also confirms the absence of significant absorption of λ = 3650Å or 4358Å by $HgCl(X^2\Sigma^+)$ as a source of excited molecules. Alternatively $HgCl(X^2\Sigma^+)$ could be excited by collision with $Hg(^3P_1)$:

$$Hg(^3P_1) + HgCl(X^2\Sigma^+) \rightarrow Hg(^1S_0) + HgCl(B^2\Sigma^+) \quad \Delta H_o = -1.96 \text{ eV} \qquad (14)$$

$$\rightarrow Hg(^1S_0) + HgCl(C^2\pi_{1/2}) \quad \Delta H_o = -0.42 \text{ eV} \qquad (15)$$

$$\rightarrow Hg(^1S_0) + HgCl(D^2\pi_{3/2}) \quad \Delta H_o = -0.06 \text{ eV} \qquad (16)$$

This type of sensitized fluorescence process has been shown to be responsible for the HgCl(B→X) emission which is observed in a flow system in which $Hg(^3P_0)$ reacts with CH_3Cl.[12] In that case the bimolecular reaction to form $HgCl(B^2\Sigma^+)$ directly is endothermic by about 0.50 eV.[13] For reaction in this system, assuming a gas kinetic cross section of about 10Å^2 for reaction (14), a maximum population of $Hg(^3P_1)$ and $HgCl(B^2\Sigma^+)$ equal to the initial ground state mercury concentration, 10^{13} particles/cm^3, and a relative velocity of 3×10^4 cm/sec, the minimum time between collision of an HgCl molecule with an excited mercury

atom would be about 3×10^{-3} sec. A more reasonable guess of the $Hg(^3P_1)$ concentration is based on an estimate of 10^3 absorption events per mercury atom per second in this system. Since the lifetime of an $Hg(^3P_1)$ atom is 10^{-6} sec here, $[Hg(^3P_1)] \sim 10^{-3}[Hg(^1S_0)]$. Using this number the time between collision of $Hg(^3P_1)$ with HgCl is about 3 seconds. This should be compared with 3×10^{-6} sec which is estimated as the time between collisions for the postulated bimolecules reaction between $Hg(^3P_1)$ and chlorine at 0.3 Torr, relative velocity of 3×10^4 cm/sec, and a cross section of $\sim 10\text{Å}^2$. This means that collisional excitation of $HgCl(X^2\Sigma^+)$ would be, at the very least, three orders of magnitude less likely than bimolecular reaction between $Hg(^3P_1)$ and Cl_2 and therefore relatively unimportant as source of $HgCl(B^2\Sigma^+)$ or other excited states. This process would show second order dependence on incident light intensity and ground state mercury concentration, and the observation of first order dependence for each of these variables is a strong argument against the occurrence of this excitation process.

The participation of the mercury eximer Hg_2^* in the mechanism responsible for production of $HgCl(B^2\Sigma^+)$ can be eliminated on several grounds. Eximer formation requires stabilization by a third body:

$$Hg(^3P_{1,0}) + Hg(^1S_0) + M \rightarrow Hg_2(^3l_u) + M \quad M = Hg,\ Cl_2,\ N_2 \text{ or } He \qquad (17)$$

By analogy to the discussion above, such collisions would be several orders of magnitude less frequent than the postulated bimolecular

reactive collisions when low total pressures were employed. Hg_2($^3\Pi_u$ and ^3O_u) molecular emissions have been observed with maxima in the continuous spectra at 3350Å and 4850Å, respectively,[14] under conditions of high mercury concentration.[15] Eximer emission has also been observed easily in systems which produce high concentrations of the metastable species $Hg(^3P_0)$, for example when N_2 is used as a carrier gas.[16,17] In this work no Hg_2^* emission was observed when mercury, chlorine, and nitrogen flowed through the irradiated system. If eximer emission occurred when mercury and nitrogen alone were present it was too weak to be detected with these experimental arrangements. If the process responsible for the formation of $HgCl(B^2\Sigma^+)$ required eximer participation, the halide emission spectra would show second order dependence on ground state mercury concentration. First order dependence was observed.

The capillary mercury source could produce some Hg_x clusters which could absorb lamp radiation to produce Hg_2^*. Because the nozzle part of the source was maintained at a higher temperature than the main body of the reservoir, the likelihood of cluster formation has been considerably reduced. Initial experiments in a less sophisticated glass vacuum system used different mercury sources as discussed in Chapter II, and the same HgCl(B→X) emission was observed. In one such source helium gas passed through a temperature regulated glass coil containing mercury before the gas mixture flowed into the irradiated reaction vessel. Because the same molecular emission was observed in thatsystem where cluster formation was very unlikely it is safe to conclude that Hg_x clusters are not involved in any important reaction mechanism producing HgCl(B→X) emission.

Possible participation of excited electronic states of the molecular halogens should be mentioned. The homonuclear halogens absorb ultraviolet or visible light to excite a repulsive state ($^1\pi_u$) which dissociates into atoms.[18] For Cl_2 the maximum absorption occurs at about 3350Å with absorption coefficient ϵ = 64.3 liter/mole-cm.[19] Molecular chlorine is transparent to the mercury resonance line at 2537Å. Some absorption of lamp radiation at 3126Å and 3650Å can occur but the intensity of this radiation is two orders of magnitude less than that of the resonance line so that not much Cl atom will be produced in this way. Recombination processes involving Cl atoms would be too slow to be important.

The $Cl_2(A\ ^3\pi_{o+u})$ state has T_e = 18310.5 cm^{-1} so that[20] this state could be excited by absorption of λ = 5461Å radiation from the lamp or by quenching collision with $Hg(6^3P_1)$:

$$Hg(^3P_1) + Cl_2(X^1\Sigma^+g) \rightarrow Hg(^1S_0) + Cl_2(A\ ^3\pi_{o+u}) \quad \Delta H_o = -2.59\ eV \qquad (18)$$

In this work no extensive attempt was made to study this quenching process. The fact that the HgCl(B→X) emission spectrum recorded in the flow experiments was identical to that of a HgCl calibration lamp argues against the presence of much Cl_2 $A(^3\pi_{o+u})$ formed by either process since it would be expected to radiate and would be detected.

The involvement of Cl_2^* in an excitation process with HgCl such as

$$HgCl(X^2\Sigma^+) + Cl_2(A\ ^3\pi_{o+u}) \rightarrow HgCl(B^2\Sigma^+) + Cl_2(^1\Sigma^+_g) \qquad (19)$$

is negligible because the HgCl(B→X) emission would show second order dependence on light intensity and on Cl_2 pressure which contradicts experimental observations. Also the occurrence of the HgX emission when different halogens are used and its specificity to $\lambda = 2537\text{Å}$ radiation makes this excitation process unlikely.

CHAPTER III REFERENCES

1. A. B. Callear and R. E. M. Hedges, Trans. Far. Soc. 66, 605 (1970).
2. G. Herzberg, Spectra of Diatomic Molecules 2nd edition, Van Nostrand Reinhold, New York, 1950.
3. K. Wieland, Helv. Phys. Acta 14, 420 (1941).
4. K. Wieland, Z. für Electrochem. 64, 761 (1960).
5. R. A. Ogg, H. C. Martin, P. A. Leighton, J. Am. Chem. Soc. 58, (1936).
6. JANAF Thermochemical Tables, 2nd ed., Natl. Stand. Ref. Data System, National Bureau of Standards, [NSRDS-NBS37] D. R. Stull and M. Prophet, project directors.
7. K. Wieland, Helv. Chim. Acta 24, 1285 (1941).
8. R. Weast, editor, Handbook of Chemistry and Physics, 45th edition Chemical Rubber Company, Cleveland (1964).
9. J. G. Calvert and J. N. Pitts, Jr., Photochemistry, Wiley, New York, 1966, p. 748.
10. F. Duschinsky and P. Pringsheim, Physica 2, 923 (1935).
11. D. E. Gray, ed., American Institute of Physics Handbook, 2nd edition, McGraw Hill, New York, 1963.
12. A. C. Viskis and D. J. LeRoy, Chem. Phys. Lett. 21, 103 (1973).
13. V. I. Veyeneyev, et al, Bond Energies, Ionization Potentials, and Electron Affinities, tr. Scripta Technica, Ltd., Edward Arnold (Publishers), Ltd., 1966, p. 59.
14. Z. Mrozowski, Z. Phys. 106, 458 (1937).
15. R. V. Waddell and G. S. Hurst, J. Chem. Phys. 53 3892 (1970).
16. A. O. McCoubrey, Phys. Rev. 93, 1249 (1954).
17. J. M. Campbell, S. Penzes, H. S. Sandhu, O. P. Strausz, Int. J. Chem. Kinet. 3, 175 (1971).

18. Calvert and Pitts, loc.cit, p. 184.

19. G. E. Gibson and N. S. Bayliss, Phys. Rev. 44, 188 (1933).

20. Herzberg, loc.cit, p. 519.

IV. KINETIC STUDIES IN THE IRRADIATED Hg + Cl_2 FLOW SYSTEM

A. Introduction

The discussion of the previous section established the bimolecular reaction mechanism for production of $HgCl(B^2\Sigma^+)$ as the only plausible mechanism consistent with experimental results. The crucial step is

$$Hg(^3P_1) + Cl_2 \rightarrow HgCl(B^2\Sigma^+) + Cl$$

In this section quantitative kinetic data will be presented which have been obtained by monitoring the axial variation of HgCl(B→X) emission as a function of incident light intensity at 2537Å, chlorine pressure, and ground state mercury concentration. The object of these studies is the unequivocal determination of the order of the process producing $HgCl^*$ with respect to these factors. An estimate of the bimolecular rate constant has also been obtained. In order to extract this information the flow of gases through the reaction vessel must be understood, as well as the illumination geometry of the reaction vessel. The complicating effects of imprisonment of resonance radiation must also be discussed and treated in order to render the data meaningful.

The simplest description of the flow of gases in our reaction vessel can be made by assuming "plug flow". Here the mercury and chlorine are assumed to be homogeneously mixed before the mixture reaches the irradiated region of the reaction vessel. As discussed in Chapter II mixing by diffusion is complete before the gas mixture

reaches the illuminated region of the vessel for total pressure less than 1 Torr. A planar velocity profile is assumed for the gas mixture and the attenuation of reactants by diffusion is neglected. As discussed by Schmeltekopf, et.al.[1] this simple model should be corrected for radial and axial diffusion, for attenuation of reactive species by diffusion, and for the actual nonplanar velocity profile of the gas mixture, if reliable rate constants are to be extracted from kinetic measurements in flowing systems. For the flow system described in these experiments the data obtained do not warrant the use of such sophisticated treatment because of the addition of the complicating effects of radiation imprisonment and illumination geometry to the hydrodynamic problems of the flow system. Without simplification the model becomes mathematically untractable.

B. Schema of the Flow Experiments

This mechanism explains the origin of the HgCl(B→X) emission:

$$Hg + h\nu(2537\text{Å}) \xrightarrow{k_1} Hg^* \qquad (1)$$

$$Hg^* \xrightarrow{k_2} Hg + h\nu(2537\text{Å}) \qquad (2)$$

$$Hg^* + Cl_2 \xrightarrow{k_3} HgCl^* + Cl \qquad (3)$$

$$HgCl^* \xrightarrow{k_4} HgCl + h\nu(3550\text{-}5700\text{Å}) \qquad (4)$$

$$HgCl^* + Cl_2 \xrightarrow{k_5} HgCl + Cl_2^{\dagger} \qquad (5)$$

Process (5) will proceed slowly at low chlorine pressure and can be neglected to a first approximation. Its relative importance will be considered in section C-4 of this chapter. Here

$$Hg^* = Hg(6^3P_1) , \qquad HgCl^* = HgCl(B^2\Sigma^+) ,$$

and $Cl_2^{\dagger}$ is an electronically or vibrationally excited molecule.

Applying steady state formalism to this set of reactions involves assuming that the first step, light absorption by atomic mercury, is much slower than subsequent destruction of Hg^* by reemission of light or reaction with molecular chlorine. The rate constant for light absorption is $k_1 I$, where I is the light flux at the reaction vessel axis. I has maximum magnitude of 10^{16} photons/cm^2-sec and $k_1 = 1.23\times10^{-13}$ $cm^2/atom^2$ at 45°C. Therefore $k_1 I \sim 1000$ absorption events/sec per Hg atom. $k_2 = 10^6 - 10^7$ emissions/sec and $k_3(Cl_2) \sim 10^5 - 10^6$ collisions/sec for a cross section of $10Å^2$ and 0.3 Torr of chlorine. Light absorption is indeed the slow step. Steady state formalism yields the exact solutions to rate equations in this case after time

$$t > \frac{1}{k_2+k_3(Cl_2)} \quad \text{or} \quad t > 10^{-6} - 10^{-7} \text{ sec} .$$

These expressions for the steady state concentrations of intermediates Hg^* and $HgCl^*$ are obtained when process (5) is very slow:

$$(Hg^*) = \frac{k_1 I(Hg)}{k_2+k_3(Cl_2)} \tag{6}$$

$$(HgCl^*) = \frac{k_1 k_3 I(Hg)(Cl_2)}{k_4[k_2+k_3(Cl_2)]} \tag{7}$$

Besides depending on the rate of reaction, the axial variation of $(HgCl^*)$ is a function of the incident light intensity and the concentration of ground state mercury, both of which are dependent on the axial distance. When the flow velocity is known axial distance is the measure of time in this system. The chlorine gas concentration is very nearly uniform throughout the reaction vessel but the ground state mercury concentration will decay due to excitation and reaction, with the rate law:

$$\frac{d(Hg)}{dt} = - k_1 I(Hg) + k_2(Hg^*) = - \frac{k_1 k_3 I(Hg)(Cl_2)}{k_2+k_3(Cl_2)} = - k_4(HgCl^*) \tag{8}$$

The solution of this differential equation would be straightforward if radiation imprisonment could be assumed to be constant throughout the reaction vessel and to be independent of (Hg):

$$(Hg) = (Hg)_o \exp\left\{\frac{-k_1 k_3(Cl_2)}{k_2+k_3(Cl_2)} \int_o^t I dt'\right\} \tag{9}$$

This leads to

$$(HgCl^*) = \frac{k_1 k_3 I(Hg)_o (Cl_2)}{k_4[k_2+k_3(Cl_2)]} \exp\left\{-\frac{k_1 k_3 (Cl_2)}{k_2+k_3(Cl_2)} \int_o^t Idt'\right\} \qquad (10)$$

Since the Cl_2 pressure and initial mercury concentration (Hg_o) are experimental variables, if $\int_o^t I(t')dt'$ can be calculated, this mechanism can be tested by measurement of axial variation of $(HgCl^*)$. The integral $\int_o^t I(t')dt'$ is the total amount of radiation to which the reaction mixture has been exposed up to time t. Before discussing the affect of radiation imprisonment on the measured $(HgCl^*)$ a brief description of the experimental conditions will be given, and the derivation of $\int_o^t Idt'$ will be presented.

1. Comments on the Experimental Method

The reaction vessel and lamp assembly were turned 90° from the configuration shown in Fig. II-1 so that the cylindrical axis of the vessel was perpendicular to the spectrograph axis as discussed in section II-F. The viewing tube sampled the total light emission from a wedge shaped volume defined by the rectangular slit of the viewing tube and the diameter of the vessel. The volume element has been assumed to contain a homogeneous mixture of mercury and chlorine and to be irradiated uniformly by the lamps. The intensity of light emission from the volume element has been assumed to be proportional to the light emission at the point of intersection of the spectrograph axis with the cylindrical axis of the vessel.

The HgCl(B→X) emission was several orders of magnitude less intense when monitored this way compared to the configuration in which the cylindrical axis coincided with the spectrograph axis. This meant that wide spectrograph slits had to be used (~ .5 mm) with differential amplification of the $HgCl^*$ emission signal, and large time constants were necessary in the recorder circuitry. Time normalization of the data was essential. The $HgCl^*$ emission was monitored at $\lambda = 5558Å$. At this wavelength the maximum intensity occurs and $HgCl^*$ spectrum is almost continuous due to the overlap of many bands. Axial measurements at one wavelength were sufficient since previous work had shown in end on experiments that the dependence of the $HgCl^*$ emission on incident light intensity, on (Hg) and (Cl_2) was essentially the same at any wavelength.

Initial kinetic measurements of this kind were performed with the apparatus in the experimental configuration which was used to collect spectra. These measurements produced data which was difficult to interpret in a reliable way. The fall off of the $HgCl^*$ emission along the cylindrical axis for constant (Hg), (Cl_2) and $I_{2537Å}$ meant that the cone of sight of the spectrograph sampled a nonhomogeneous gas mixture even with no further inhomogeneity introduced by varying (Hg), (Cl_2) or $I_{2537Å}$. Monitoring the axial variation of $HgCl^*$ presented a much more straightforward method to make kinetic measurements. As low mercury flow rates were used as possible to minimize radiation imprisonment.

2. Axial Variation of the Incident Light Intensity

Calculation of the axial variation of the incident light intensity is a photometric problem. Figure IV-1 illustrates a simple geometric model which describes the illumination of the reaction vessel by the bank of lamps. The radiant flux I at point P on the reaction vessel axis due to illumination by one lamp is given by the inverse square law for oblique incidence:[3]

$$I = \int_{\phi_1}^{\phi_2} \frac{dL \cos\phi}{r^2} \tag{11}$$

Here dL is the luminous intensity of unit area of the lamp's emitting surface in the direction of ϕ. Luminous intensity is defined as the radiant flux per unit solid angle in the direction of P. The cylindrical electrical discharge mercury lamp is a light source whose brightness or luminous intensity per unit area obeys Lambert's law for diffuse radiating surfaces. This means that the lamp appears equally bright from all angles of observation. The lamp can be approximated as a linear light source extending in the x direction so that a unit of luminous intensity becomes

$$dL = Bdx \tag{12}$$

and the flux integral can be evaluated as

$$I_c(x) = \int_{-x_1}^{x_2} \frac{Bydx'}{(x'^2+y^2)^{3/2}} = \frac{B}{y}\left[\frac{x_1}{\sqrt{x_1^2+y^2}} + \frac{x_2}{\sqrt{x_2^2+y^2}}\right] = \frac{B}{y}(\sin\phi_1 + \sin\phi_2) \tag{13}$$

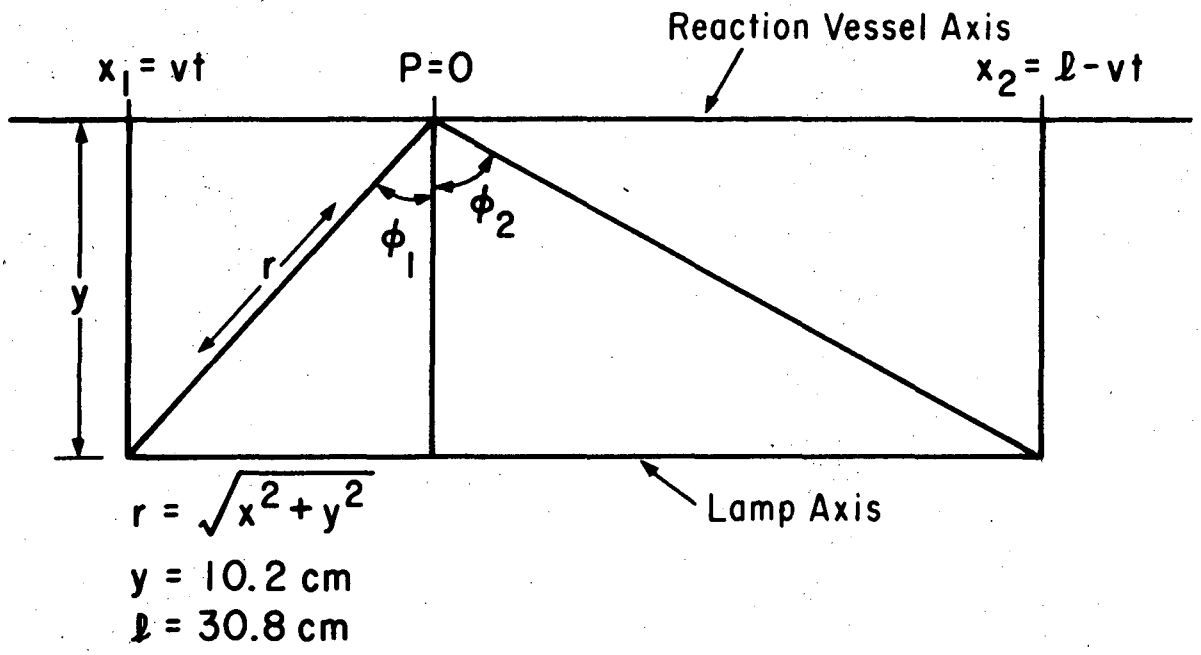

XBL 7311-6722

Fig. IV-1. Geometric model for the illumination of a point on the reaction vessel axis by one lamp. The radiant flux at P is given by $I = B \int_{\phi_1}^{\phi_2} \frac{\cos\phi dx}{R^2} = \frac{B}{y} (\sin \phi_1 + \sin \phi_2)$. B is the brightness of the lamp.

Here the origin of the coordinate system is taken as P, as illustrated in Fig. IV-1. The subscript c has been used here to specify the calculated flux $I_c(x)$. y is the perpendicular distance between the lamp axis and the cylindrical axis of the reaction vessel, constant for all experiments. B, the brightness, is proportional to the total number of lamps used since each lamp had equal light output to within 5%.

An experimental measure of the axial variation of the light flux is the variation of the background emission from the suprasil vessel as seen through the viewing tube with no chlorine present. This background emission, due to fluorescence of the vessel itself, was typically twenty times more intense than the $HgCl^*$ emission signal and therefore a DC offset voltage had to be used for differential amplification of the $HgCl^*$ signal as discussed previously. The background intensity at any point on the axis was found to be proportional to the intensity of any scattered mercury line from the lamp at that point, so that the background emission intensity could be used as a measure of the radiant flux along the axis. This function is designated as $I_e(x)$. Since the background light emission was due to fluorescence from the vessel, the viewing tube saw light from walls at perpendicular distance $y \pm 2.5$ cm. The resultant signal is not exactly a perpendicular to the incident lamp radiation at the vessel axis because of Eq. (11), but the effect of this small difference on subsequent data analysis is insignificant.

Figure IV-2 presents a comparison of the radiant flux calculated from the simplified lamp geometry, $I_c(x)$, with the background emission intensity at $\lambda = 5558\text{Å}$, $I_e(x)$, for a typical experiment. The flux functions are presented in arbitrary units and normalized to each other at the midpoint of the illuminated length of the axis. The calculated flux falls off less sharply near the upstream and downstream ends of the vessel than does the measured background emission. This reflects the fact that the discharge length in the lamps was 24.5 cm, compared to the vessel's irradiated length of 30.8 cm, and the simple model assumes a luminous source of the same length as the vessel axis. In spite of this the agreement between the calculated flux function and the measured values of the radiant flux is quite good. In the data analysis to be presented subsequently the measured background flux factor was used in preference to the calculated function.

In studying the kinetics of the flowing gas mixture it is important to know the total amount of light to which the mixture has been exposed up to point P along the axis, at time t. This depends on the flow velocity as well as the reaction length, which is the distance between the upstream end of the illuminated region of the vessel and P. For plug flow the flow velocity is assumed to be constant throughout the vessel and directed along the axis. Thus time and reaction length become equivalent parameters. The amount of light to which the reaction mixture has been exposed up to time t is given by the integral of the radiant flux. This can be calculated as

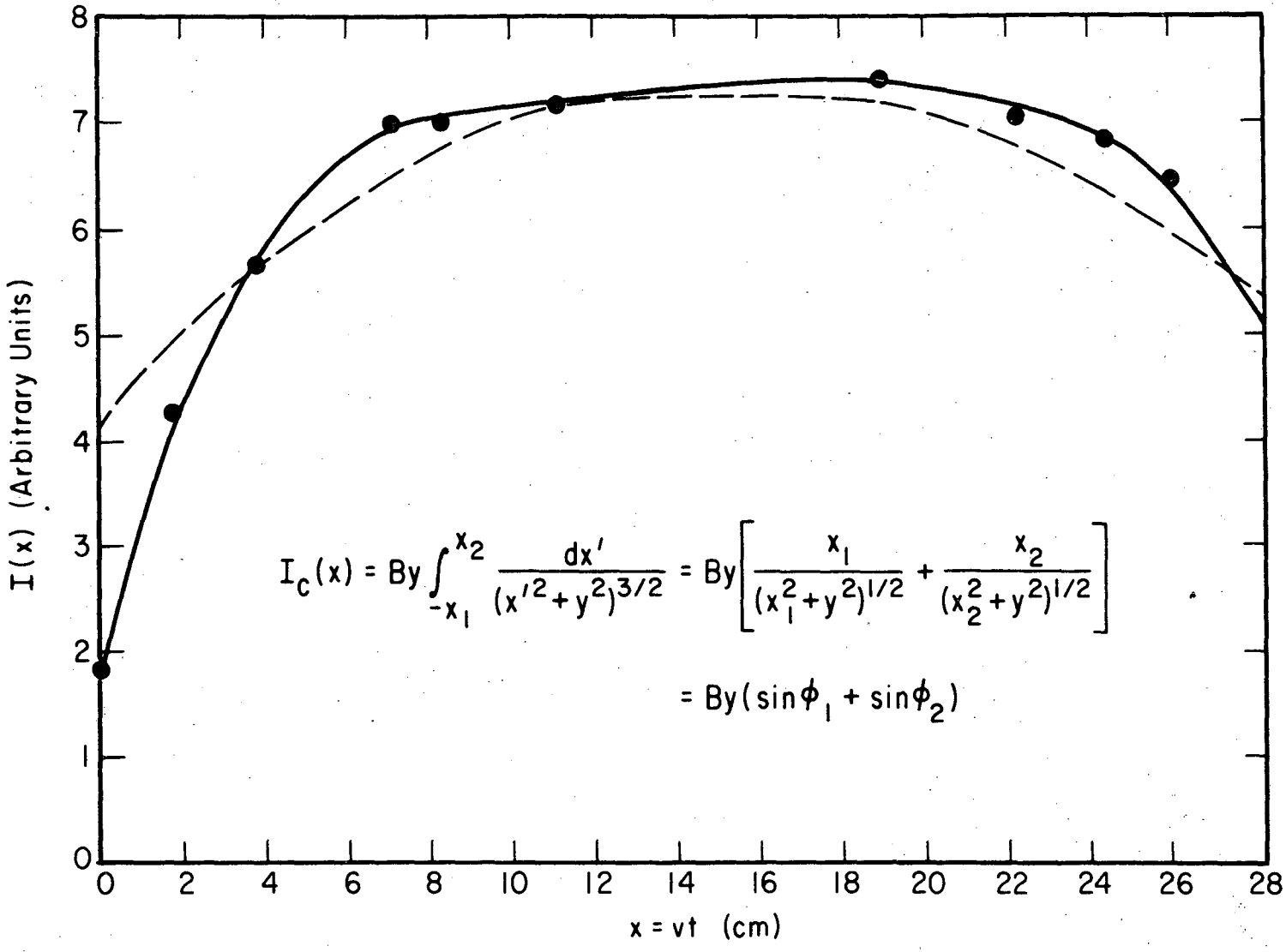

XBL 7311-6725

Fig. IV-2. Radiant flux as a function of the axial distance from the upstream end of the illuminated region of the reaction vessel. The solid line shows a smooth curve drawn through the points of measured background light emission at 5558Å. The dashed curve shows the radiant flux function calculated using the geometric model, Eq. (13).

$$\int_o^t I_c(t)dt = \frac{B}{y}\left[\int_o^t \frac{vt'dt'}{\sqrt{(vt')^2+y^2}} + \int_o^t \frac{(\ell-vt')dt'}{\sqrt{(\ell-vt)^2+y^2}}\right] \qquad (14)$$

From Fig. IV-1 it can be seen that $x_1 = vt'$ and $x_2 = \ell-vt'$ so that

$$\int_o^t I_c(t)dt = \frac{B}{vy}\left[\int_o^{vt} \frac{xdx}{\sqrt{x^2+y^2}} + \int_{\ell-vt}^{\ell} \frac{xdx}{\sqrt{x^2+y^2}}\right]$$

$$= \frac{B}{vy}\left[\sqrt{x_1^2+y^2} - \sqrt{x_2^2+y^2} + \sqrt{\ell^2+y^2} - y\right] \qquad (15)$$

Figure IV-3 compares the time independent portion of the calculated integrated flux function, $v\int_o^t I_c(t')dt'$, to the experimentally derived function $v\int_o^t I_e(t')dt'$ which was obtained by graphical integration of the background emission flux factor. The agreement between these functions is excellent and testifies to the validity of the simple geometric model. The difference between the calculated and experimental radiant flux functions which is apparent in Fig. IV-2 does not produce significant deviation between the integrated radiant flux functions. The experimental integrated flux factors were used at each monitoring position along the axis in subsequent data analysis.

3. Radiation Imprisonment

Because mercury atoms have a high absorption coeffieient for resonance radiation, there is significant probability that mercury in the reaction vessel will absorb radiation emitted by other mercury atoms in the vessel as well as lamp radiation. The probability of a photon escaping from the reaction vessel without being reabsorbed

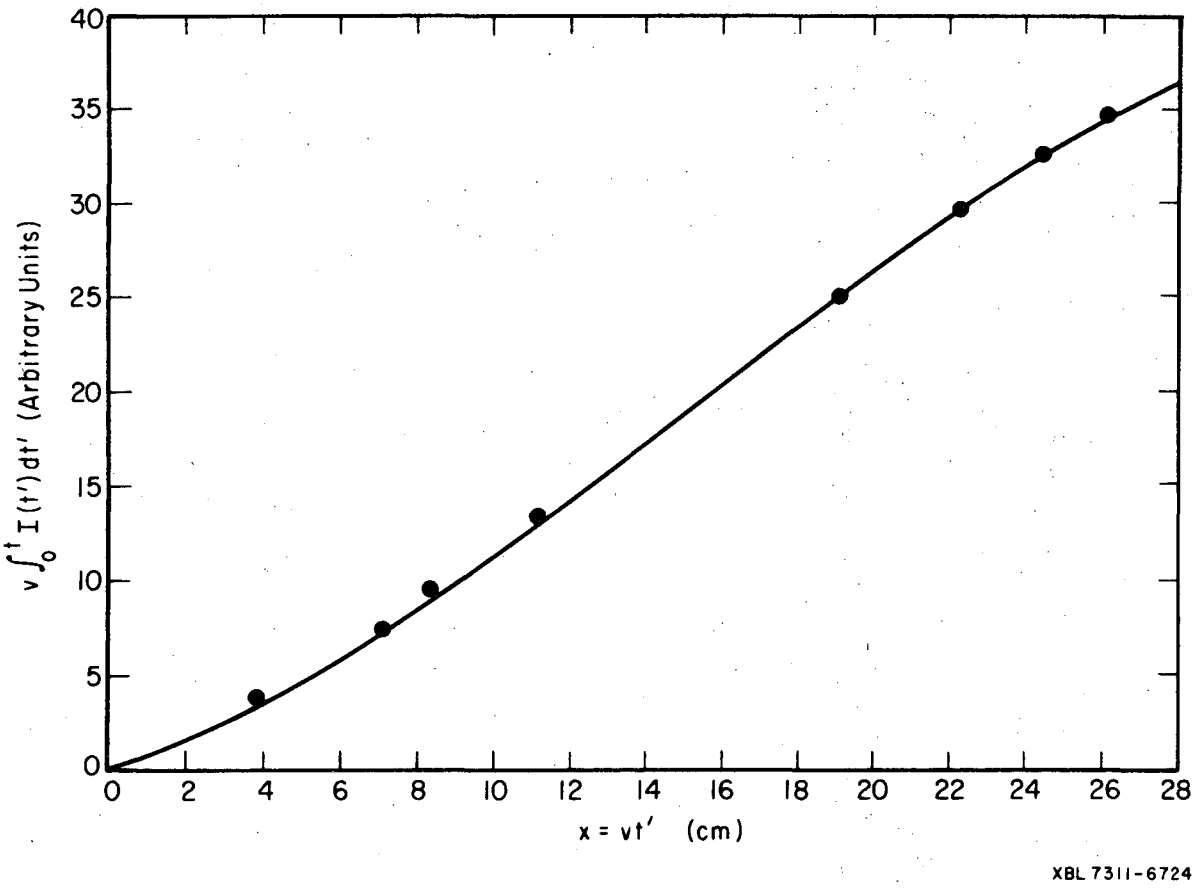

Fig. IV-3. Integrated radiant flux as a function of axial distance. The points have been obtained by graphical integration of the experimental flux function. The solid curve shows the integrated radiant flux obtained from the geometric model, Eq. (15).

depends on the concentration of mercury and on the path length through which it must travel. For mercury opacity greater than 10^{12} atoms/cm^2 this radiation imprisonment effect becomes important. Thus the time which a typical photon spends absorbed, τ, the lifetime of an excited mercury atom, is greater than the natural lifetime, τ_o, when imprisonment is present. A simple theoretical treatment of imprisonment was presented by Milne, as discussed by Mitchell and Zemansky.[4] Milne[5] set up differential equations for the radiation flux at any point in an infinite slab of thickness ℓ which contains atoms capable of absorbing the incident resonance radiation and reemitting it. The diffusion of radiation in his treatment is governed by

$$\frac{\partial}{\partial x^2}\left[(Hg) + \tau_o \frac{\partial (Hg)}{\partial t}\right] = 4k^2\tau_o \frac{\partial (Hg)}{\partial t} \qquad (16)$$

where k is the absorption coefficient at the center of the absorption line. Milne showed that the radiant flux I escaping from the slab at $x = \ell$ becomes

$$\pi I = A_1 e^{-\beta_1 t} + A_2 e^{-\beta_2 t} + \ldots \qquad (17)$$

Here the preexponential factors depend on the distribution of excited atoms at t=0, and the β_i are given by

$$\beta_i \tau_o = \frac{1}{1 + \left(\frac{k\ell}{\lambda_i}\right)^2} \qquad (18)$$

where λ_i is the ith root of the equation

$$\tan \lambda = \frac{k\ell}{\lambda} \qquad 0 < \lambda_1 < \pi/2 \tag{19}$$

Since $\beta_{i>1} \gg \beta_1$ for $t > 10^{-4}$ sec or so only the first term in the series is important. Thus β becomes the reciprocal of the actual imprisonment lifetime τ. Samson[6] showed that Eq. (18) predicts β in closer agreement to experimental data if, instead of k, an equivalent absorption coefficient $\bar{k}$ is used in Milne's treatment. $\bar{k}$ accounts for the assumed Doppler distribution in frequency of the absorption coefficient of the gas. The equivalent opacity at the center of the absorbing line, $\bar{k}_\ell$, is computed from

$$e^{-\bar{k}\ell} = \frac{\int_{-\infty}^{\infty} e^{-\omega^2} \, e^{-k\ell(e^{-\omega^2})} \, e\omega}{\int_{-\infty}^{\infty} e^{-\omega^2} \, d\omega} \tag{20}$$

where $\omega = \frac{2(\nu-\nu_o)}{\Delta\nu_D} \sqrt{\ln 2}$ for a Doppler line of breadth $\Delta\nu_D$ and center frequency ν_o. Using Milne's theory and Samson's tabulation of $\bar{k}$ one can calculate τ, the lifetime of imprisoned radiation in the reaction vessel. Although this approach is based on infinite slab geometry, reasonable agreement of calculated and observed values of τ is obtained if ℓ is assigned the value of the cylindrical radius, up to $(Hg)\ell = 3\times10^{13}$ atoms/cm^2. This is shown in Figs. 5 and 6 of Ref. 7. Rearranging Eq. (18) gives this expression for τ/τ_o, since $\beta = \tau^{-1}$

$$\tau = \tau_o \left[1 + \left(\frac{\bar{k}\ell}{\lambda}\right)^2\right] \tag{21}$$

For low opacity $\lambda \simeq \bar{k}\ell$ so that

$$\tau = \tau_o (1 + \bar{k}\ell) \tag{22}$$

A simple physical picture of imprisonment can be applied at low mercury opacity. The time required for a photon of resonance radiation to diffuse through the distance ℓ, after it has been initially absorbed by a ground state atom, is the sum of the lifetime of the excited atom τ_o and the time required for subsequent absorption and emission events, $\bar{k}\ell\tau_o$. Thus its imprisonment lifetime is given by Eq. (22). The probability that the photon will not be reabsorbed, $T(\ell)$, is then just a simple exponential decay function

$$T(\ell) = e^{-\bar{k}\,\ell} \tag{23}$$

For $(Hg)\ell \leq 1.2\times10^{13}$ atoms/cm^2 Yang[8] has shown that Eq. (22) predicts τ which is about 3% higher than his experimental values of τ.

As the mercury concentration increases λ in Eq. (21) approaches $\pi/2$ and τ increases as the second power of $\bar{k}$ and therefore as $(Hg)^2$. Milne's theory correctly predicts the qualitative behavior of τ for $(Hg)\ell > 3\times10^{13}$ atoms/cm^2 although its quantitative predictive limits have been exceeded. This happens because the equivalent absorption coefficient loses its meaning, and volume elements in the infinite slab in addition to that in the path of the exciting beam contribute to the detected light emission, making the choice of path length uncertain.

For mercury opacity $\geq 3\times10^{13}$ atoms/cm^2, the diffusion approach, even as modified by Samson to include the frequency dependence of the absorption coefficient, is no longer adequate, and most workers rely on the theoretical work of Holstein,[9] without assessing or even necessarily understanding his approach, especially since it correctly predicts τ for the region in which it has been tested[2] $2\times10^{14} \leq (Hg)\ell \leq 2\times10^{15}$ atoms/cm^2 and connects smoothly at $(Hg)\ell \simeq 3\times10^{14}$ atoms/cm^2 to the predictions of Samson's work and available experimental data. Holstein formulates the imprisonment problem as a general transport problem, sets up Boltzmann type integro differential equations involving $T(\ell)$ for which steady state solutions are obtained by variational methods. For cylindrical geometry Holstein derives this expression for τ

$$\tau = \frac{5}{8}\tau_o\, k\ell\, (\pi \ln k\ell)^{1/2} \quad . \tag{24}$$

with ℓ the cylindrical radius.

Experimentally measured values of τ/τ_o are presented in Fig. IV-4 for mercury opacity between 10^{12} and 5×10^{14} atoms/cm^2. The figure includes data from four independent sources. Yang[8] measured τ at 25°C by observing the variation of τkq with mercury concentration when the quenching molecule was ethylene. In these experiments the reciprocal of the quenching Q was plotted against the reciprocal of the quenching gas pressure, for which a straight line results when the Stern Volmer equation

$$\frac{1}{Q} = 1 + \tau kq(M) \tag{25}$$

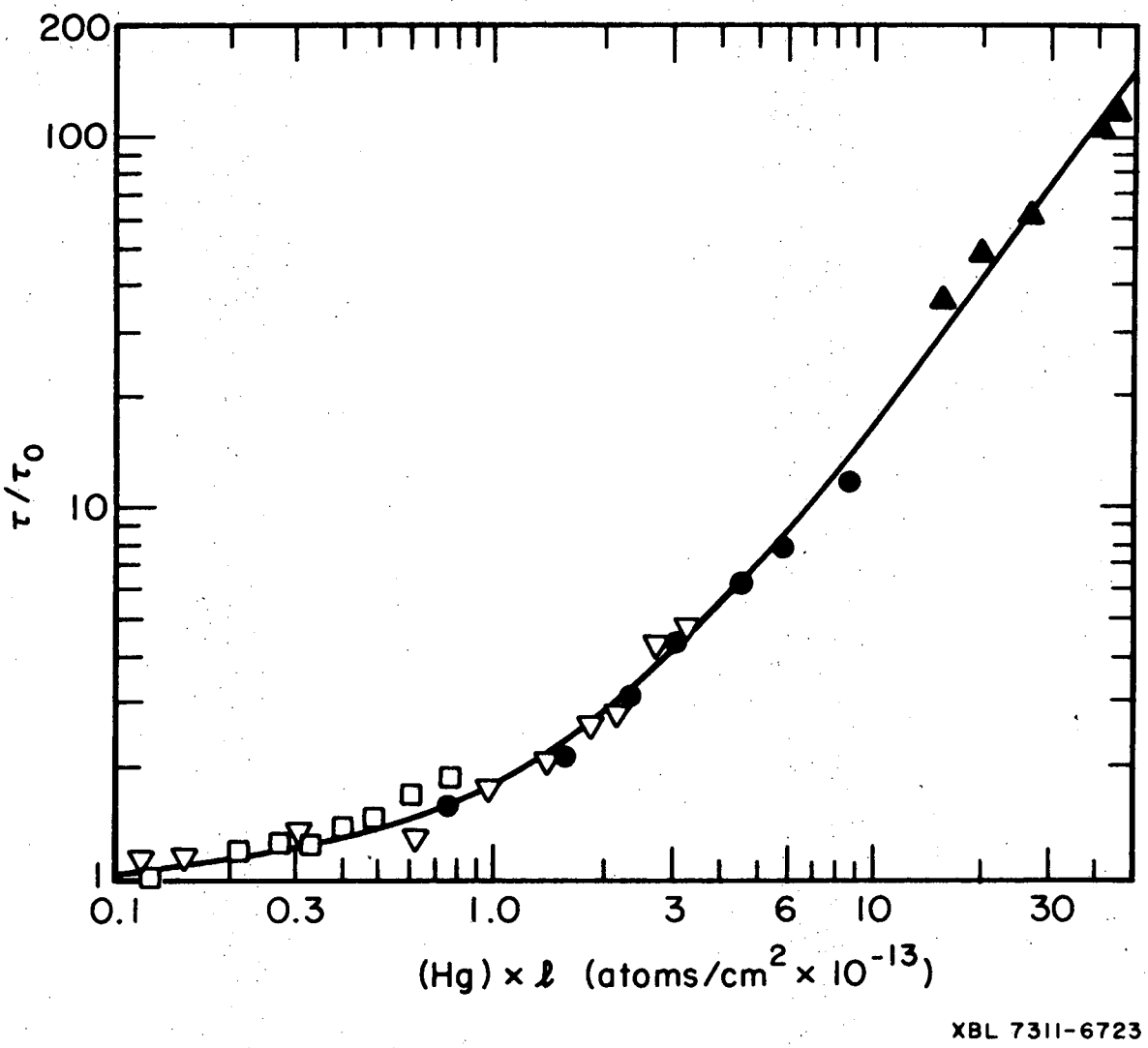

Fig. IV-4. Radiation imprisonment τ/τ_o as a function of mercury opacity. The data points give the results of various workers. ▽ - K. Yang, J. Am. Chem. Soc. 88, 4575 (1966); □ - J. V. Michael and C. Yeh, J. Chem. Phys. 53, 59 (1970); ● - L. B. Thomas and W. D. Gwinn, J. Am. Chem. Soc. 70, 2643 (1948); ▲- D. Alpert, A. O. McCoubrey, and T. Holstein, Phys. Rev. 76, 1257 (1949).

applies. The quenching is defined as the ratio of the intensity of fluorescent radiation with quenching gas M present to its intensity with no quenching gas present. The fluorescent radiation was measured perpendicular to the direction of the incident resonance radiation, and the value of k_q was derived from the value of τk_q extrapolated to zero mercury pressure. Since the quenching experiment was performed at many mercury pressures, values of $\tau = \tau(Hg)$ could be obtained in a straightforward way. The imprisonment path length through which fluorescent radiation had to travel to reach the photomultiplier was taken as the radius of the cylindrical cell, 1.27 cm.

Thomas and Gwinn[10] measured directly the quantum yield of $Hg(^3P_1)$ sensitized hydrogen decomposition at 30°C as a function of initial hydrogen and mercury pressures. Michael and Yeh[7] more recently measured a quantity proportional to the quantum yield of H atom formation at 27°C as a function of molecular hydrogen and mercury pressures. In both cases extrapolation to zero mercury concentration allowed estimation of the total cross section for quenching of $Hg(^3P_1)$ atoms and then evaluation of $\tau = \tau(Hg)\ell$ in a manner analogous to that of Yang. In both cases the cylindrical radius of the cell was used as the path length ℓ since the measurement of (H) or (H_2) was performed perpendicular to the direction of the incident resonance radiation which passed through the flat windows at the ends of the cylinders. Values of the radius were 1.125[10] and 1.956[7] cm.

The measured values of τ/τ_o of all of these workers fall on the same smooth curve, as shown in Fig. IV-4. Their derivation does not depend on any model for the imprisonment phenomenon but it does depend on the validity of the Stern-Volmer quenching formalism. As discussed by Mitchell and Zemansky[11] this approach to quenching is applicable as long as the concentration of quenching gas is low enough to avoid pressure broadening of the absorption coefficient of the metal atoms.

The data of the three works discussed above can be used to derive empirical expressions for the ratio τ/τ_o such that

$$\tau/\tau_o = a + b(Hg)\ell + c[(Hg)\ell]^2 \quad . \tag{26}$$

which are valid for specific ranges of mercury opacity. These least squares deviation expression and their ranges of applicability are

$$\tau/\tau_o = 0.952 + 0.925\times10^{-13}\ (Hg)\ell \tag{27}$$

when

$$1.0\times10^{12} \leqslant (Hg)\ell \leqslant 1.0\times10^{13}\ \text{atoms/cm}^2$$

for which the root mean square deviation, $(\Sigma\ d_i^{\,2}/n)^{1/2}$, in τ/τ_o is 0.114 for the thirteen data points of lowest opacity, and

$$\tau/\tau_o = 0.209 + 1.334\times10^{-13}\ (Hg)\ell \tag{28}$$

when

$$0.9\times10^{13} \leqslant (Hg)\ell \leqslant .90\times10^{14}\ \text{atoms/cm}^2$$

for which the rms deviation, for twelve data points, is 0.205. The data of these three groups of workers can be fit over the entire range of opacity by a quadratic function:

$$\tau/\tau_o = 0.836 + 1.008\times10^{-13}\ (\mathrm{Hg})\ell + 3.22\times10^{-28}\ [(\mathrm{Hg})\ell]^2 \qquad (29)$$

with rms deviation of 0.222.

Alpert, et al.[2] measured the imprisonment lifetime in pure mercury vapor, which was contained in a cylindrical vessel by observing the decay of 2537Å fluorescence perpendicular to the direction of the exciting radiation. They synchronized the chopped light source with the triggering of an oscilloscope. Mercury pressure varied from 2×10^{14} to 3×10^{16} atoms/cm^3 in a cylindrical vessel of radius 1.30 cm. Not all of their data is shown in Fig. IV-4. They note that below 1.5×10^{15} atoms/cm^3 of mercury, τ/τ_o agrees very well with the predictions of Holstein's theory for cylindrical geometry, although Fig. IV-4 shows that a straight line which fits smoothly through this data would not connect smoothly to the data collected by the other three groups of workers. The fact that Alpert et al. used pure mercury vapor at much higher concentrations than the other workers who used mercury along with a quenching gas may be related to this discrepancy. Mercury-mercury interactions may be affecting the imprisonment phenomenon at higher pressure.

A reasonable approach at constructing a function for τ/τ_o which is valid over the entire range of mercury opacity shown in Fig. IV-4 would seem to be the use of Eq. (29) for $(\mathrm{Hg})\ell \leq 0.6\times10^{+14}$ atoms/cm^2,

with the simplifications of Eqs. (27) and (28) for the opacity ranges shown. For $(Hg)\ell \geq .6\times10^{14}$ τ/τ_o can be estimated to within 25% of the experimental values by the smooth function which connects the highest points of Thomas and Gwinn's data with the data of Alpert, et al. This function is represented by

$$\tau/\tau_o = - 5.92 + 2.104\times10^{-13}\ (Hg)\ell + 1.989\times10^{-28}\ [(Hg)\ell]^2 \qquad (30)$$

in the range

$$0.6\times10^{14} \leq (Hg)\ell \leq 2.5\times10^{14}\ \text{atoms/cm}^2$$

with rms deviation in $\tau/\tau_o = 0.419$. The linear function

$$\tau/\tau_o = - 9.61 + 2.743\times10^{-13}\ (Hg)\ell \qquad (31)$$

fits more crudely, with rms deviation of 0.741 for the same range of mercury opacity represented by Eq. (30).

Table IV-1 presents the imprisonment functions which have been derived here as well as the opacity ranges for which each is valid. Most of the kinetic data which will be presented subsequently was obtained with initial mercury opacity $\leq 4\times10^{13}$ atoms/cm^2 so that Eq. (29) is the most useful imprisonment function for this work. Here the path length through which resonance radiation must diffuse has been taken as the radius of the reaction vessel. Since the exciting radiation cylindrically surrounds the reaction vessel, the diffusion length for the thin wedge which is subtended by the viewing tube varies between 0 and the value of the diameter of the vessel, 5.0 cm.

Table IV-1. Empirical Relations for the RAtio of Imprisonment Lifetime to Natural Lifetime for Mercury

Quadratic Functions	Opacity Range	RMS Deviation
$\tau/\tau_o = 0.84 + 1.01\times10^{-13}\ (Hg)\ell + 3.22\times10^{-28}\ [(Hg)\ell]^2$	$1.0\times10^{12} \leqslant (Hg)\ell \leqslant 9.0\times10^{13}$ atoms/cm^2	0.22
$\tau/\tau_o = -\ 5.92 + 2.10\times10^{-13}\ (Hg)\ell + 1.99\times10^{-28}[(Hg)\ell]^2$	$6.0\times10^{13} \leqslant (Hg)\ell \leqslant 2.5\times10^{14}$ atoms/cm^2	0.42
Linear Functions		
$\tau/\tau_o = 0.95 + 0.925\times10^{-13}\ (Hg)\ell$	$1.0\times10^{12} \leqslant (Hg)\ell \leqslant 1.0\times10^{13}$ atoms/cm^2	0.11
$\tau/\tau_o = 0.21 + 1.33\times10^{-13}\ (Hg)\ell$	$9.0\times10^{12} \leqslant (Hg)\ell \leqslant 9.0\times10^{13}$ atoms/cm^2	0.21
$\tau/\tau_o = -\ 9.61 + 2.74\times10^{-13}\ (Hg)\ell$	$6.0\times10^{13} \leqslant (Hg)\ell \leqslant 2.5\times10^{14}$ atoms/cm^2	0.74

The radius of the vessel is thus only a typical diffusion length which approximates the average length through which photons at 2537Å must undergo further absorption and emission processes after their initial capture by mercury atoms.

4. Axial Variation of the Ground State Mercury Concentration

Because of radiation imprisonment the lifetime of Hg^* in the reaction vessel depends on the ground state mercury concentration as discussed in the previous section. The steady state scheme which governs the reaction kinetics must be modified to include the affect of imprisonment. The rate equation for the destruction of ground state mercury, Eq. (8) becomes, using Eq. (26), since $k_2 = k_2^o \cdot \tau_o/\tau$

$$\frac{d(Hg)}{dt} = - \frac{k_1 k_3 \, I(Hg)(Cl_2)}{k_2^o\{a+b(Hg)\ell + c[(Hg)\ell]^2\}^{-1} + k_3(Cl_2)} = -k_4(HgCl^*) \qquad (32)$$

Rearranging Eq. (32) yields

$$- I \, dt = \frac{[k_2^o\{a+b(Hg)\ell + c[(Hg)\ell]^2\}^{-1} + k_3(Cl_2)] \, d(Hg)}{k_1 k_3 (Hg)(Cl_2)}$$

$$= \frac{k_2^o \, d(Hg)}{k_1 k_3 (Cl_2)(Hg)\{a+b(Hg)\ell + c[(Hg)\ell]^2\}} + \frac{d(Hg)}{k_1(Hg)} \qquad (33)$$

the solution of (33) when $c[(Hg)\ell]^2$ is very small compared to $b(Hg)\ell$ is

$$- \int_o^t I \, dt' = \frac{k_2^o}{a k_1 k_3 (Cl_2)} \ln \frac{(Hg)\,[a+b(Hg)_o\ell]}{(Hg)_o[a+b(Hg)\ell]} + \frac{1}{k_1} \ln \frac{(Hg)}{(Hg)_o} \qquad (34)$$

Here $(Hg)_o$ is the mercury concentration at t = 0, which occurs at the upstream end of the illuminated region of the reaction vessel. k_2^o is the decay constant for Hg^* when imprisonment is unimportant:[12]

$$k_2^o = \tau_o^{-1} = 0.876\times10^7 \text{ sec}^{-1} \tag{35}$$

Rearrangement of Eq. (34) yields

$$e^{-\frac{a\, k_1 k_3 (Cl_2)}{k_2^o} \int_o^t I\, dt} = \frac{a+b(Hg)_o}{a+b(Hg)} \left\{\frac{(Hg)}{(Hg)_o}\right\}^{\frac{k_2^o+k_3(Cl_2)}{k_2^o}} \tag{36}$$

In the most general situation Eqs. (32) and (33) show that the disappearance of unexcited mercury is controlled by a rate equation which contains terms which are up to third order in mercury concentration. This means that even explicit solution of Eq. (34) or (36) for (Hg[t]) is not straightforward.

It can be seen from Eq. (32) that at sufficiently small (Hg) the axial decay of mercury will be first order in (Hg) and that k_2 will be given by

$$k_2 = k_2^o/a \tag{37}$$

This occurs either for sufficiently low $(Hg)_o$ such that imprisonment is unimportant (a=1, $(Hg)\ell \leqslant 1.0\times10^{12}$ atoms/cm^2) or at sufficiently long times such that the initial unexcited mercury supply has been extensively depleted. Under these conditions the axial decay of (Hg) and of ($HgCl^*$) would follow Eqs. (9) and (10) respectively with $k_2 = k_2^o/a$.

Axial decay of mercury which is first order in (Hg) also occurs when the bimolecular reaction of Cl_2 with Hg^* completely dominates the reaction mechanism. Under these conditions an excited mercury atom is much more likely to react with Cl_2 than to radiate spontaneously its resonant photon and Eq. (32) becomes

$$\frac{d(Hg)}{dt} = - k_1 I(Hg) = -k_4 (HgCl^*) \quad . \tag{38}$$

In this work chlorine pressures such that process (3) and rate Eq. (38) dominate were not employed, because of the increased complication of diffusion and flow dynamic problems as the chlorine pressure was increased. At high chlorine pressures, chlorine itself would also begin to quench the $HgCl^*$ to an unknown extent.

For sufficiently high (Hg), $a \ll \{b(Hg)\ell + c[(Hg)\ell]^2\}$ and the solution of Eq. (33) contains a first order term, and a combined second and third order term in (Hg). Because of this complicated situation which results when radiation imprisonment is included in the search for axial mercury decay functions, kinetic inferences must be made from the data in a way which does not depend on the specific functional form of the axial mercury decay, as often as possible.

C. Results of the Kinetic Studies

1. Dependence of the HgCl(B→X) Emission on Incident Light Intensity

The order of the reaction producing $HgCl^*$ can be established without knowledge of the accurate axial decay function for mercury. The differential rate law

$$\frac{d(Hg)}{dt} = - \frac{k_1 k_3 \, I(Hg)(Cl_2)}{k_2 + k_3 \, (Cl_2)} = -k_4 (HgCl^*)$$

has a solution which is a function of the radiation flux integral $\int_o^t I dt'$

$$(Hg \, [\int_o^t I dt]) = f(\int_o^t I dt', \, (Hg)_o, \, (Cl_2)_o) \qquad (39)$$

$$\frac{(HgCl^*)}{I} = \frac{k_1 k_3 \, (Cl_2)(Hg \, [\int_o^t I dt'], \, (Hg)_o, \, (Cl_2)])}{k_4 \, (k_2 + k_3 \, (Cl_2))} \qquad (40)$$

Here $(HgCl^*)/I$ is the first order reduced emission intensity. $(Hg)_o$ is the initial mercury concentration. The chlorine pressure is assumed to be constant throughout the vessel so is not subscripted.

If the reaction producing $HgCl^*$ has first order dependence on incident light intensity all values of the first order reduced emission intensity will fall on the same curve when plotted against $\int_o^t I dt'$, even if there is appreciable absorption of the incident radiation.

Figure IV-5 presents a semilogarithmic plot of the results of a series of experiments in which the axial decay of $(HgCl^*)$ was monitored as the incident light intensity was varied. Both the $HgCl^*$ fluorescent signal and the radiant flux integral are given in arbitrary units.

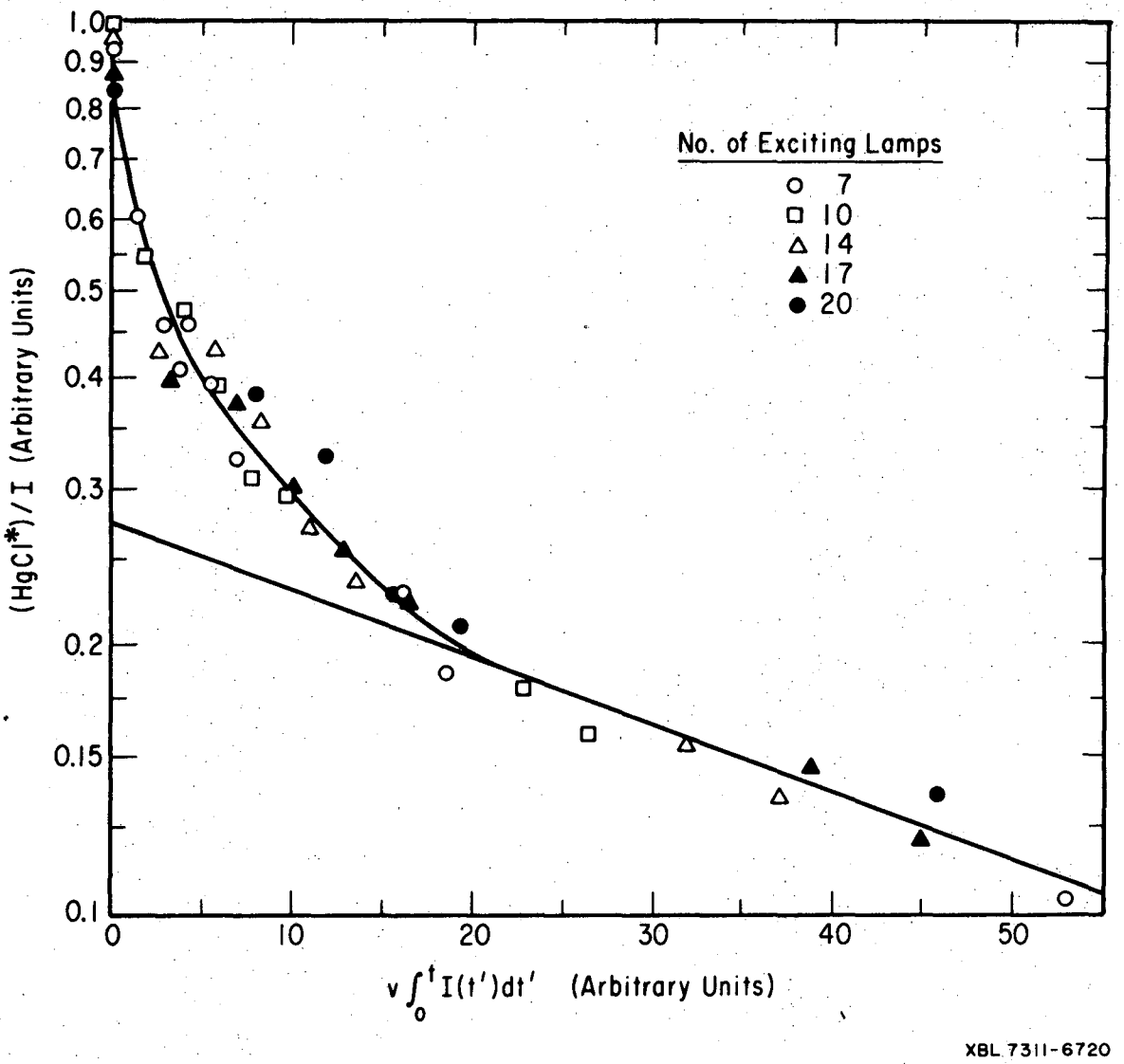

Fig. IV-5. Dependence of the fluorescence intensity on incident light intensity. Here the first-order reduced emission intensity, $(HgCl^*)/I$, is shown as a function of the radiant flux integral. The data were obtained at constant chlorine pressure by varying the incident intensity at each monitoring position.

The value of the radiant flux integral used for each point shown in Fig. IV-5 is proportional to the experimental value of the geometric portion of the integral of Fig. IV-3 and the number of lamps used. The first order reduced emission intensity at each monitoring point was obtained by dividing the $HgCl^*$ intensity by the product of the experimental radiant flux function $I_e(x)$ analogous to that shown in Fig. IV-2 and the number of lamps used. The background scattered light seen by the photomultiplier with twenty lamps in use was taken as the light independent part of $I_e(x)$. The initial mercury concentration, chlorine pressure, and flow velocity were held constant in these experiments. The light intensity was varied by switching on or off some of the lamps which surrounded the reaction vessel, taking care to illuminate the vessel evenly. To ensure constant temperature of the vessel, the full bank of lamps was turned on at each axial position for about 20 minutes before data were recorded. This also allowed the lamp intensity to return to a constant level. The data were time normalized by returning to the first position, full light intensity, before data at each position were recorded. Table IV-2 shows the important experimental parameters and the time normalized data.

The data illustrated in Fig. IV-5 do indeed conform to a single mercury decay function and are clearly consistent with a reaction mechanism which is first order in incident light intensity at 2537Å. It can be seen that the ground state mercury decay function falls by a factor of roughly ten for the range of $\int_0^t I dt'$ shown. This corresponds to a maximum illuminated length of 18.3 cm along the

Table IV-2. Axial $HgCl^*$ Emission Intensity Variation with Incident Radiant Flux.

a) Experimental Parameters

Mercury source temperature	488°K
Mercury flow rate	1.08×10^{16} atoms/sec
Initial mercury concentration	1.56×10^{13} atoms/cm^3
Chlorine pressure	0.361 Torr = 1.10×10^{16} molec/cm^3
Flow velocity	39.2 cm/sec
k_2	1.66×10^{6} sec^{-1}

b)

Monitoring Position cm	I Arbitrary Units	$v\int_0^t Idt'$ Arbitrary Units	$(HgCl^*)$ Arbitrary Units
0	0.354	0	1.08
	0.506	0	1.16
	0.708	0	2.24
	0.860	0	2.44
	1.120	0	2.77
1.8	0.572	1.26	1.73
	0.818	1.80	2.22
	1.143	2.52	2.20
	1.390	3.06	2.50
	1.638	3.62	3.36
3.6	0.631	2.80	1.32
	0.902	4.00	1.97
	1.261	5.60	2.47
	1.532	6.80	2.62
	1.804	8.00	3.18

Table IV-2 (Cont.)

Monitoring Position cm	I Arbitrary Units	$v\int_0^t Idt'$ Arbitrary Units	$(HgCl^*)$ Arbitrary Units
5.1	0.658	4.13	1.59
	0.941	5.90	1.75
	1.318	8.20	2.14
	1.600	10.00	2.13
	1.882	11.80	2.48
6.4	0.658	5.46	1.41
	0.940	7.80	1.60
	1.316	10.90	1.96
	1.598	13.25	2.24
	1.880	15.60	2.36
7.7	0.670	6.80	1.19
	0.957	9.70	1.39
	1.340	13.60	1.76
	1.629	16.50	2.03
	1.914	19.40	2.32
15.8	0.686	16.10	0.81
	0.980	22.90	0.91
	1.372	32.00	1.31
	1.668	38.90	1.35
	1.960	45.90	1.36
18.3	0.658	18.55	0.47
	0.940	26.50	0.79
	1.316	37.05	1.13
	1.598	45.00	1.22
	1.880	53.00	1.26

cylindrical axis of the reaction vessel. Detection efficiency limited further axial monitoring of the emission along the remaining 12.5 cm of irradiated axial reaction vessel length. When the first order reduced emission intensity has fallen to twenty percent of its value at t=0 the axial mercury decay function becomes first order, as expected from previous discussion.

By comparison Fig. IV-6 shows the second order reduced emission intensity $(HgCl^*)/I^2$ plotted against $\int_o^t Idt'$. Here the data do not fit a single decay function as smoothly. This means that reaction mechanisms which show second order dependence on incident light intensity are not influencing the production of $HgCl^*$ to an important extent. Two such processes, as discussed in Chapter III, would involve excitation of HgCl by light absorption or collision with excited mercury:

$$Hg(^1S_o) + h\nu(2537\text{Å}) \rightarrow Hg(^3P_1) \qquad \text{(III-1)}$$

$$Hg(^3P_1) + Cl_2 \rightarrow HgCl(X^2\Sigma^+)^\dagger + Cl \qquad \text{(III-12)}$$

$$HgCl(X^2\Sigma^+)^\dagger + h\nu' \rightarrow HgCl(B^2\Sigma^+) \qquad \text{(III-13)}$$

or

$$Hg(^3P_1) + HgCl(X^2\Sigma^+)^\dagger \rightarrow Hg(^1S_o) + HgCl(B^2\Sigma^+) \qquad \text{(III-14)}$$

In either case $(HgCl^*)/I^2$ would be a function of $\int_o^t Idt'$, although Eq. (III-14) would show second order dependence on $(Hg)_o$ at t=0 with Eq. (III-13) exhibiting first order behavior at t=0.

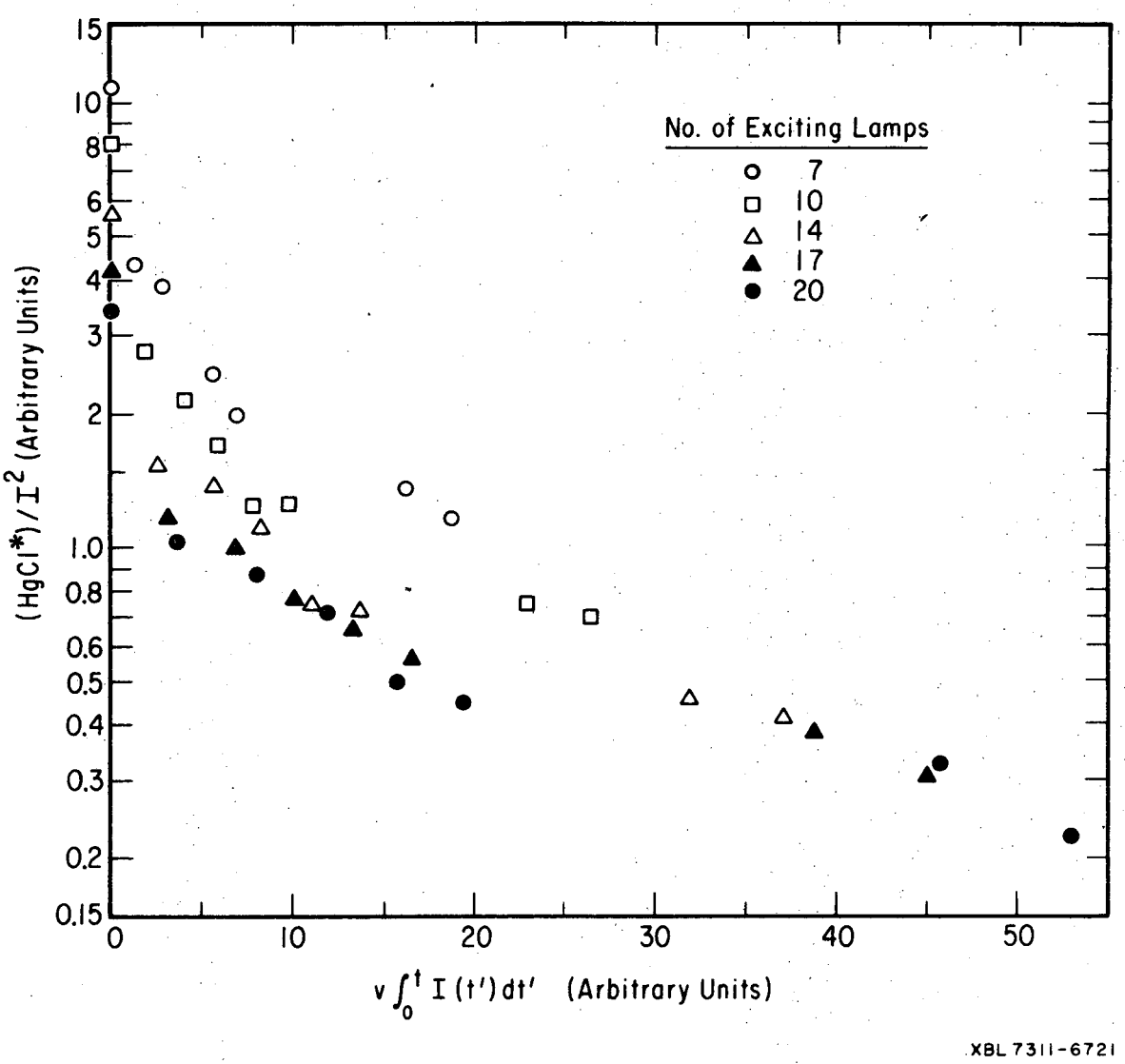

Fig. IV-6. Dependence of the fluorescence intensity on incident light intensity. Here the second order reduced emission intensity, $(HgCl^*)/I^2$, is shown as a function of the radiant flux integral. A reaction mechanism which has second order dependence on incident light intensity would produce data which fit a single smooth curve.

If the mechanism responsible for the formation of $HgCl^*$ is first order in exciting light intensity, the first order reduced emission intensity will be independent of the number of lamps used at time zero. This is indeed the case for the data presented here, and can be seen by referring to the data at $\int_o^t Idt'=0$ in Figs. IV-5 and IV-6. Thus it is clearly established that the most important process contributing to the formation of $HgCl^*$ shows first order dependence on the incident light intensity.

2. Dependence of the $HgCl^*$ Emission Intensity on Ground State Mercury Concentration and Chlorine Pressure

At the upstream end of the reaction vessel the dependence of the $HgCl^*$ emission intensity on ground state mercury concentration and chlorine pressure can be investigated without reliance on the axial mercury decay function. At the start of the illuminated region $t=0$ so that Eq. (10) becomes

$$(HgCl^*) = \frac{k_1 k_3 I(Hg)_o (Cl_2)}{k_4[k_2 + k_3(Cl_2)]} \qquad (41)$$

At low chlorine pressure $k_3(Cl_2) \ll k_2$ so that

$$(HgCl^*) = \frac{k_1 k_3 I(Hg)_o (Cl_2)}{k_2 k_4} \quad . \qquad (42)$$

The mercury concentration varies inversely with the chlorine flow rate and k_2 in turn depends on $(Hg)_o$, so that the order of the $HgCl^*$ forming step with respect to $(Hg)_o$ and (Cl_2) can be investigated by using appropriate reduced functions. First order dependence of $(HgCl^*)$ on

initial mercury concentration and on chlorine pressure predicts, respectively,

$$\frac{k_2 (HgCl^*)}{(Cl_2)} = \frac{k_1 k_3}{k_4} I(Hg)_o \quad (43)$$

and

$$\frac{k_2 (HgCl^*)}{(Hg)_o} = \frac{k_1 k_3}{k_4} I(Cl_2) \quad (44)$$

The initial mercury concentration can be calculated from the known flow rates of mercury and chlorine, as presented earlier, by

$$(Hg)_o = \frac{F_{Hg}(Cl_2)}{F_{Hg} + F_{Cl_2}} = \frac{F_{Hg} \tau_{Cl_2}}{V} \quad (II-2)$$

where F means flow rate in particles/sec, τ_{Cl_2} is the transit time for chlorine through the vessel, given by Eq. (II-4), and V is the volume of the reaction vessel between its inlet and outlet arms. k_2 is derived from Eqs. (29) and (35) with imprisonment path length ℓ chosen as the radius of the vessel, 2.5 cm.

Table IV-3 shows the values of important experimental parameters, the time normalized data points, and the imprisonment corrected values of the first order decay constant, k_2, which apply to an experimental determination of the variation of the $HgCl^*$ emission intensity with mercury and chlorine concentration at a monitoring position 3.86 cm from the upstream end of the illuminated zone of the vessel. The reaction mixture will have been perturbed slightly from its initial state but can still be described approximately by the initial conditions. Extrapolation of axial monitoring data to time = 0

Table IV-3. Variation of ($HgCl^*$) with $(Hg)_o$ and (Cl_2)

(Cl_2) Torr	(Cl_2) molec/cm^3 $\times 10^{15}$	$(Hg)_o$[a] atoms/$cm^3 \times 10^{-13}$	k_2[b] $sec^{-1} \times 10^{-6}$	$(HgCl^*)$[c] arbitrary units
0.043	0.131	1.31	1.95	0.46 ± .06
0.085	0.259	0.921	2.63	1.35 ± .25
0.129	0.394	0.702	3.23	1.89 ± .09
0.170	0.519	0.637	3.47	2.31 ± .06
0.252	0.768	0.518	4.00	2.55 ± .07
0.375	1.14	0.422	4.54	2.68 ± .05
0.580	1.77	0.330	5.18	2.27 ± .09

a Hg flow rate 3.30×10^{15} atoms/sec; source temperature 463°K

b $k_2 = k_2^o(\tau_o/\tau)$ $\quad k_2^o = 0.876 \times 10^7$ sec^{-1}

$\tau/\tau_o = 0.836 + 1.008 \times 10^{-13}(Hg)\ell + 3.22 \times 10^{-28}\ [(Hg)\ell]^2$; $\ell = 2.5$ cm

c Time normalized data at x = 3.86 cm from upstream end of the illuminated zone of the reaction vessel. 10 lamps were used through out.

for this series of experiments showed that the fluorescence at 3.86 cm had fallen typically to about 90% of its original value. Because the range in mercury and chlorine pressure at 3.86 cm was greater than for subsequent monitoring positions this data has been more useful for these tests. Table A-1 presents the complete axial $HgCl^*$ emission intensity data of which the work referenced here is part. The mercury flow rate of 3.30×10^{15} atoms/sec was chosen as low as consistent with detection efficiency in order to minimize the effects of radiation imprisonment and to keep the absorbance of resonance radiation small enough so that the incident light flux remains homogeneous thfoughout the reaction vessel.

Figure IV-7 shows the lefthand side of Eq. (43) plotted against initial mercury concentration, using the data presented in Table IV-3. At low $(Hg)_o$ the reduced emission intensity is first order in $(Hg)_o$. The negative deviation of the point at lowest (Hg) from linearity is what is to be expected if appreciable reaction is taking place and $k_3(Cl_2)$ becomes comparable to k_2. Since this point corresponds to the highest chlorine pressure of this experiment, 0.580 Torr, this is consistent with a reactive cross section of about $20Å^2$. As the mercury concentration increases above 0.637×10^{13} atoms/cm^3 the reduced emission intensity actually decreases. This behavior leads to the suspicion that at these mercury concentrations the incident light has been appreciably absorbed. Further increase in $(Hg)_o$ will produce no more increase in reduced emission intensity because the (Hg^*) has been limited by the flux of incident light at 2537Å rather

Fig. IV-7. Reduced fluorescence intensity, defined by Eq. (43), as a function of initial mercury concentration. The data were collected 3.86 cm downstream from the beginning of the irradiated region of the reaction vessel. The dashed and solid curves show attempts at estimating the saturation value of the reduced intensity, F_∞, as defined by Eqs. (47) and (48), which account for the attenuation of the incident intensity by absorption.

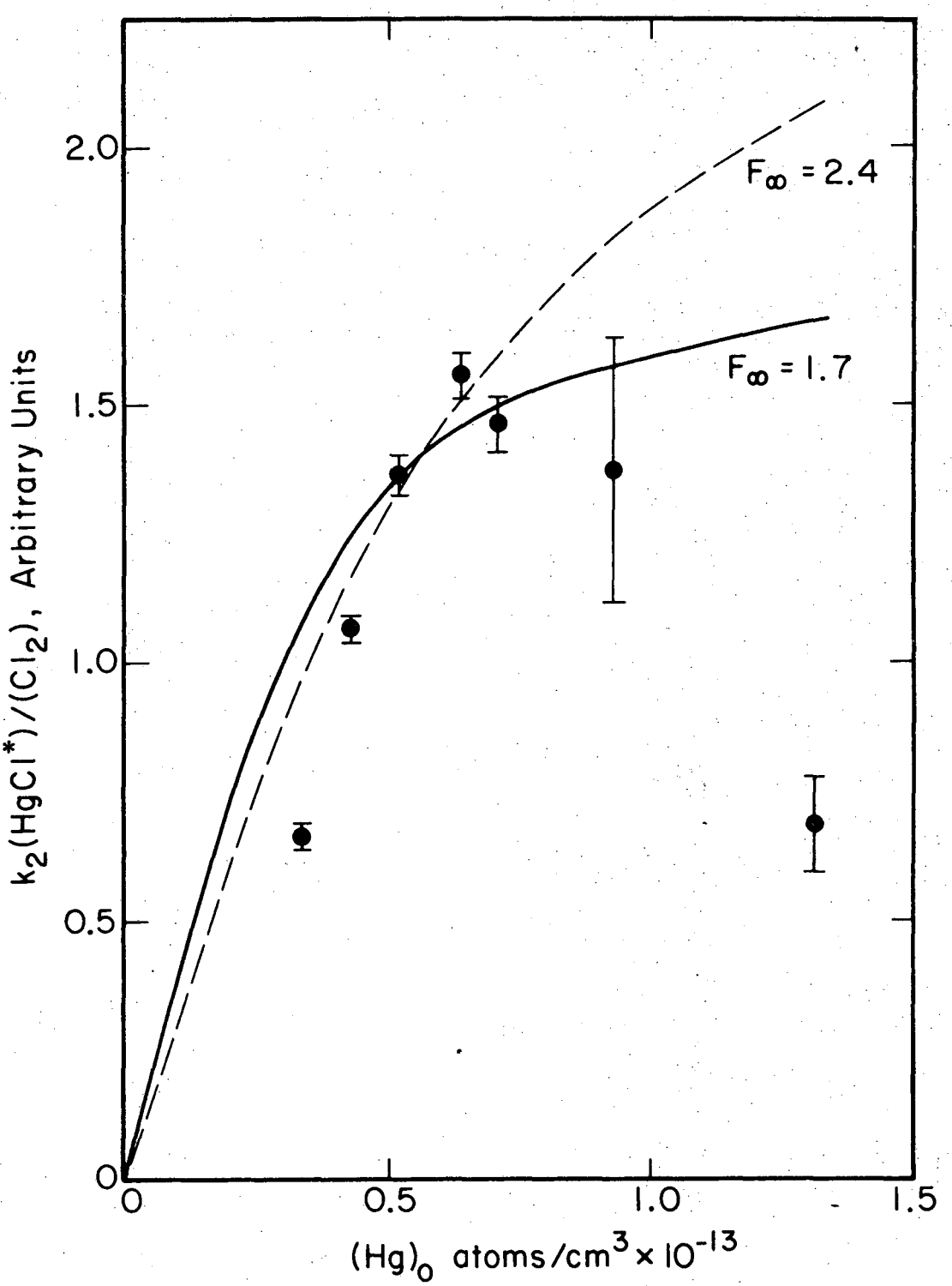
2.0
1.5
1.0
0.5
0
0
0.5
1.0
1.5
$F_\infty = 2.4$
$F_\infty = 1.7$
$k_2(HgCl^*)/(Cl_2)$, Arbitrary Units
$(Hg)_0$ atoms/cm^3 x 10^{-13}
XBL 7312-7110

Fig. IV-7.

than by $(Hg)_o$. The decrease at the points corresponding to the highest mercury concentrations may be due to nonhomogeneity in the reaction mixture present because of appreciable light absorption and the breakdown of viscous flow conditions at low chlorine concentration. Overcorrection of the data for radiation imprisonment at high (Hg) could also explain the decrease in reduced emission intensity at high (Hg), but there is no reason to suspect coupling between the extent of absorption and the amount of radiation imprisonment.

If the incident radiation I_o has been appreciably absorbed as it passes through the reaction vessel, the attenuation by absorption can be approximately described by Beer's law:

$$I = I_o e^{-k_1(Hg)\ell} \tag{45}$$

where I is the attenuated intensity, k_1 is the absorption coefficient and ℓ is the path length. The amount of excited mercury is then proportional to the fraction of incident light which has been absorbed, and

$$(Hg^*) = (Hg^*)_\infty (1 - e^{-k_1(Hg)\ell}) \ . \tag{46}$$

$(Hg^*)_\infty$ is the saturation value of the excited mercury concentration. A_∞^∞ is the number of absorption events per second. Thus the fluorescence intensity becomes

$$F = \frac{k_2(HgCl^*)}{(Cl_2)} = k_3 \frac{A_\infty (Hg^*)_\infty}{k_4} [1-e^{-k_1(Hg)\ell}] \tag{47}$$

in the limit of small $k_3(Cl_2)$. F is proportional to I_o-I. F_∞ is proportional to I_o when F_∞ is the saturation value of the reduced emission intensity. The extent of light absorption can be shown by plotting I/I_o as a function of mercury concentration. Since

$$\frac{I}{I_o} = 1 - \frac{I_o - I}{I_o} = 1 - \frac{F}{F_\infty} = e^{-k_1 \ell (Hg)_o} \qquad (48)$$

this information is readily available from the data shown in Table IV-2. Figure IV-8 shows $1-F/F_\infty$ plotted an exponential function of $(Hg)_o$ for $F_\infty = 1.70$ and 2.40. The slopes of the lines drawn through the experimental points can be chosen to agree with the values of $k_1\ell$ predicted when ℓ is chosen as the diameter (5.0 cm) and radius (2.5 cm) of the vessel. $k_1\ell = 6.16$ and 3.08×10^{-13} cm^3/atom for $F_\infty = 1.70$ and 2.40, respectively. These results show that appreciable absorption of incident resonance radiation occurs even at this low mercury flow fate. The absorbance is considerably greater for this experiment than is predicted from Fig. II-8 and points to error in the earlier absorbance measurements. The two curves shown in Fig. IV-7 show predictions of the reduced emission intensity from Eq. (47) for $F_\infty = 1.70$ and 2.40. The smaller value of F_∞ fits the experimental points better rather than the larger value which corresponds to less absorption. The deviation of measured values of the reduced emission intensity from the calculated curves at low $(Hg)_o$ is caused by the presence of appreciable reaction at high (Cl_2) so that Eqs. (42) to (44)

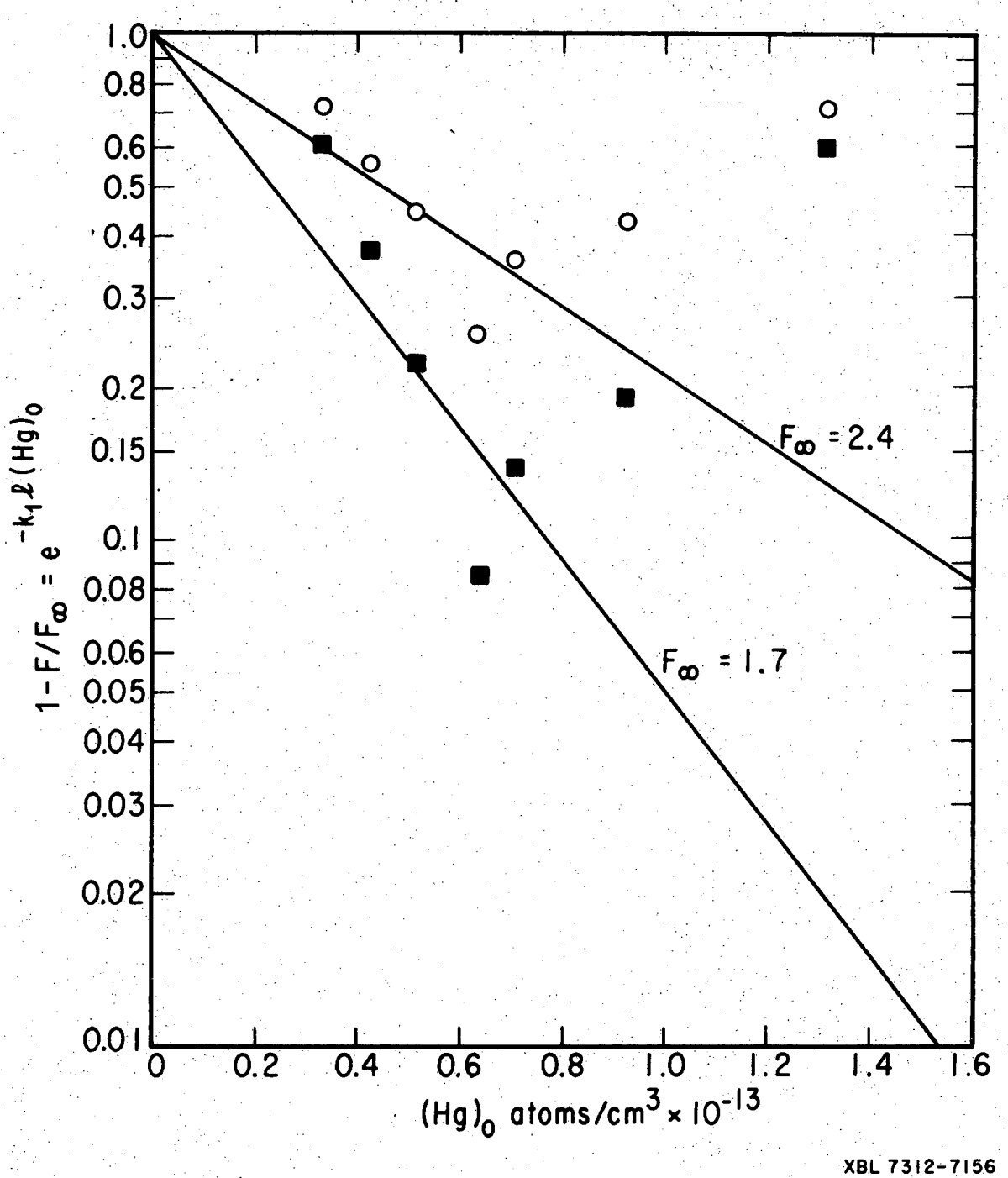

Fig. IV-8. A Beer's law plot of $I/I_o = 1-F/F_\infty$ versus initial mercury concentration. The open circles correspond to $F_\infty = 2.4$; the solid squares correspond to $F_\infty = 1.7$.

are no longer applicable since $k_3(Cl_2) \sim k_2$.

In summary, the dependence of the reduced emission intensity on mercury concentration is entirely consistent with a reaction mechanism which is first order in initial mercury concentration. Considerable absorption of the incident radiation flux occurs in the experimental work described here. Ninty percent of the incident light is absorbed at $(Hg)_o \sim 1\times10^{13}$ atoms/cm^3. It is important to note here that this estimate of the extent of absorption is consistent with the treatment of radiation imprisonment which was discussed earlier.

The dependence of the mechanism producing $HgCl^*$ on chlorine pressure can be studied by testing Eq. (44). Figure IV-9 shows the reduced emission intensity $k_2(HgCl^*)/(Hg)_o$ plotted as a function of (Cl_2), with no correction for the attenuation of the incident light by absorption. Rearrangement of Eq. (47) produces

$$\frac{k_2\ (HgCl^*)}{1 - \exp\{- k_1(Hg)_o \ell\}} = \frac{k_3}{k_4}\ A_\infty\ (Hg^*)_\infty (Cl_2) \qquad (49)$$

which allows for light absorption. Figure IV-10 illustrates the lefthand side of Eq. (49) plotted as a function of (Cl_2) for $F_\infty = 1.70$. The data are clearly consistent with a reaction mechanism which is first order in chlorine pressure. The deviation from linearity which each plot shows at the highest chlorine pressures points to the occurrence of appreciable reaction.

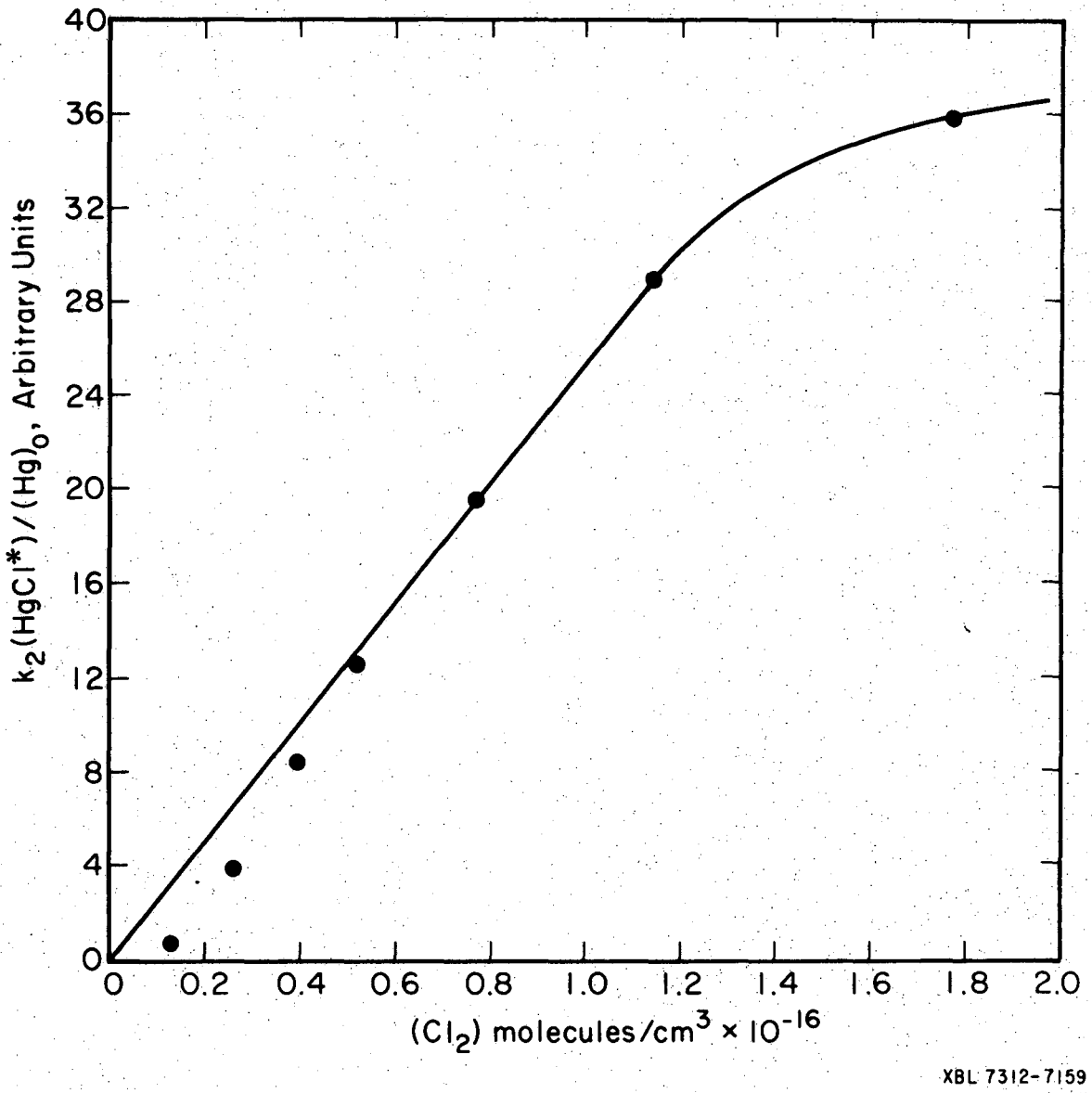

Fig. IV-9. The reduced fluorescence intensity, defined by Eq. (44), as a function of chlorine concentration. No absorption correction has been made.

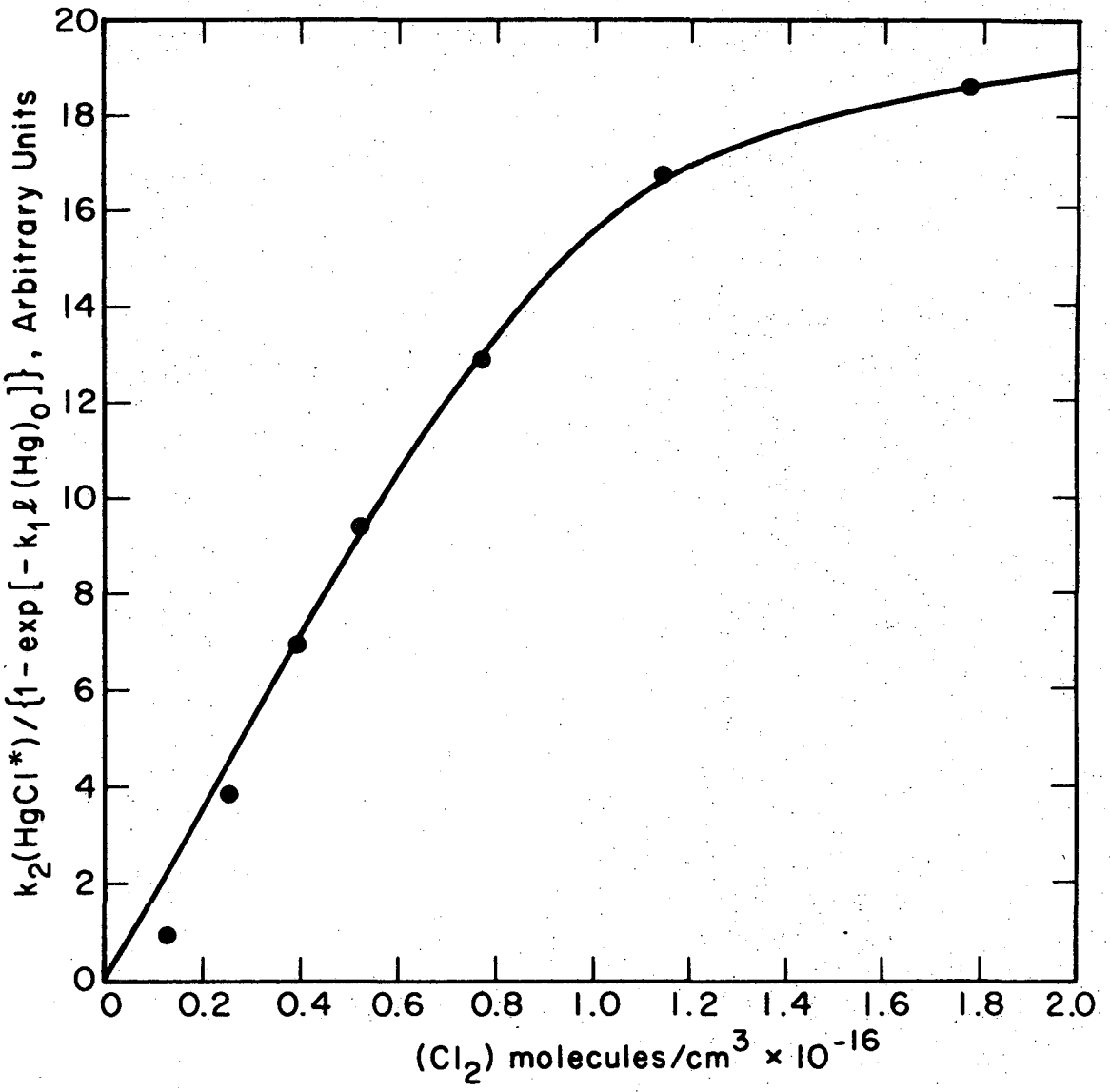

Fig. IV-10. The reduced fluorescence intensity for F_∞=1.70, defined by Eq. (49), as a function of chlorine concentration.

3. Estimates of the Rate Constant for $Hg^* + Cl_2 \rightarrow HgCl^* + Cl$

The deviation from linearity in the reduced emission intensity at high chlorine concentration which is present in Figs. IV-9 and 10 is an indication of the competition of reaction with spontaneous emission for the destruction of Hg^*, so that Eq. (41) describes the expected fluorescence intensity when no consideration is made for light absorption. Rearranging this equation produces the usable function

$$\frac{I\,(Hg)_o}{k_4(HgCl^*)} = \frac{k_2}{k_1\,k_3(Cl_2)} + \frac{1}{k_1} \quad . \tag{49a}$$

The incident light intensity I has been shown in the previous section to be dependent on the mercury concentration and to follow Beer's law for absorption, Eq. (45). Figure IV-11 shows $(Hg)_o/(HgCl^*)$ plotted against $k_2/(Cl_2)$ with no allowance made for this absorption. The data deviate from linearity most at low chlorine concentration. These points correspond to the highest mercury concentration and therefore are most affected by light absorption. If these points are neglected an estimate of k_3 is obtained from the ratio of the intercept of this plot to its slope:

$$k_3 = 0.48\times10^{-10}\ cm^3/molecule\text{-}sec \tag{50}$$

In the formalism of collision dynamics the bimolecular rate constant is related to the reactive cross section σ by[13]

$$k_3 = \sigma\bar{v}_{rel} \tag{51}$$

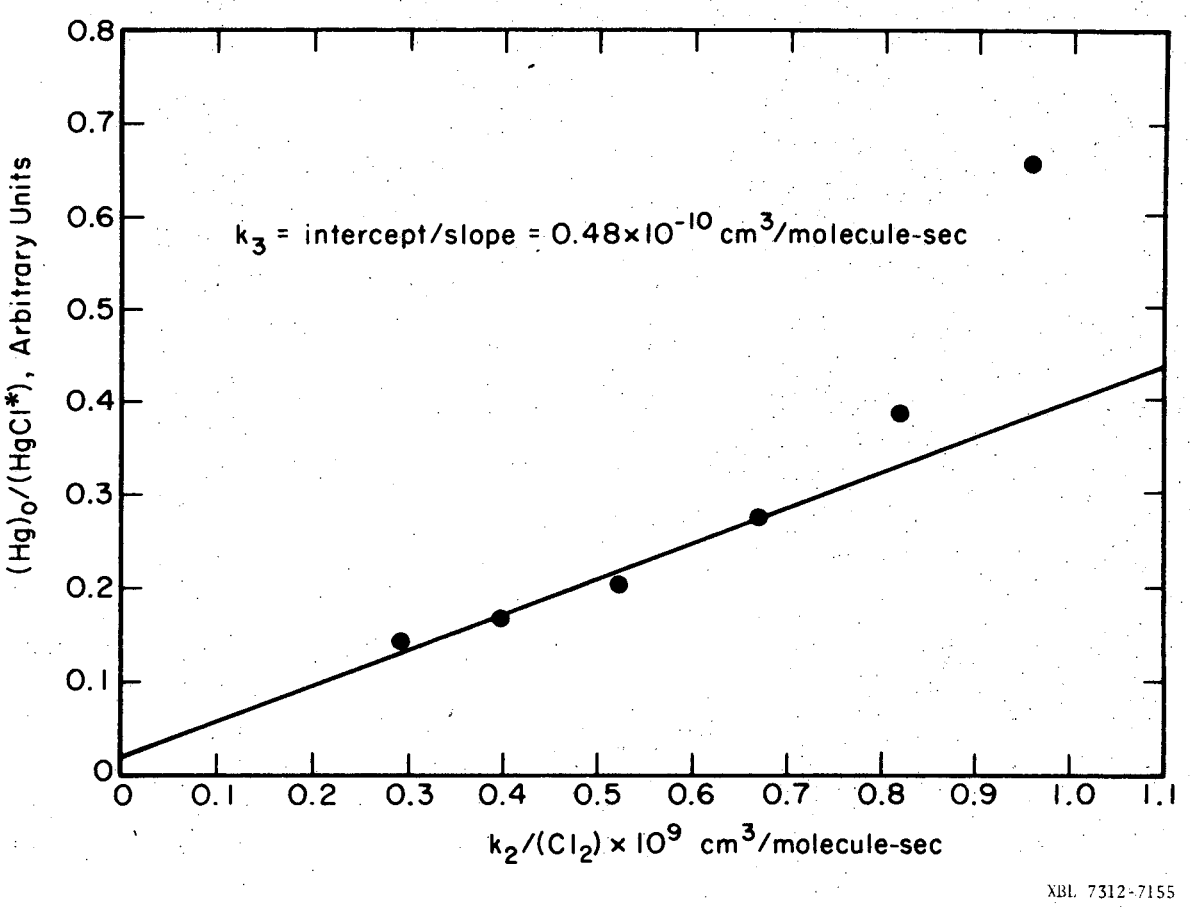

Fig. IV-11. The reciprocal reduced intensity as a function of the reciprocal of the chlorine concentration, Eq. (49a). No correction for absorption has been made.

where $\bar{v}_{rel}$ is the average relative velocity of the collision partners:

$$\bar{v}_{rel} = \left(\frac{8kT}{\pi m}\right)^{1/2} \qquad (52)$$

For $Hg^* + Cl_2$ at 318°K, $\bar{v}_{rel} = 3.586\times10^4$ cm/sec. Thus $\sigma = 13.4\text{Å}^2$ for $k_3 = 0.48\times10^{-10}$ cm^3/molecule-sec.

When light absorption is included and $k_3(Cl_2)$ is comparable to k_2, the $HgCl^*$ intensity follows

$$k_4(HgCl^*) = \frac{k_3 A_\infty (Hg^*)_\infty (Cl_2)(1 - e^{-k_1(Hg)_o \ell})}{k_2 + k_3(Cl_2)} \qquad (53)$$

which can easily produce

$$\frac{1-e^{-k_1(Hg)_o \ell}}{k_4(HgCl^*)} = \frac{k_2}{k_3 A_\infty (Hg^*)_\infty (Cl_2)} + \frac{1}{A_\infty (Hg^*)_\infty} \qquad (54)$$

Figure IV-12 shows $[1 - \exp(-k_1\ell(Hg)_o]/(HgCl^*)$ plotted as a function of $k_2/(Cl_2)$ for $F_\infty = 1.70$ and 2.40 using the data of Table IV-2. The ratios of intercepts to slopes give the estimates of k_3 which are presented in Table IV-4. The points corresponding to the highest and lowest values of $k_2/(Cl_2)$ were not considered in drawing the lines. As presented earlier $F_\infty = 1.7$ appears to fit the reduced emission intensity data of Fig. IV-7 better than $F_\infty = 2.4$. Thus, depending on the extent of absorption and the choice of the slope and intercept of Fig. IV-12, k_3 falls in this range

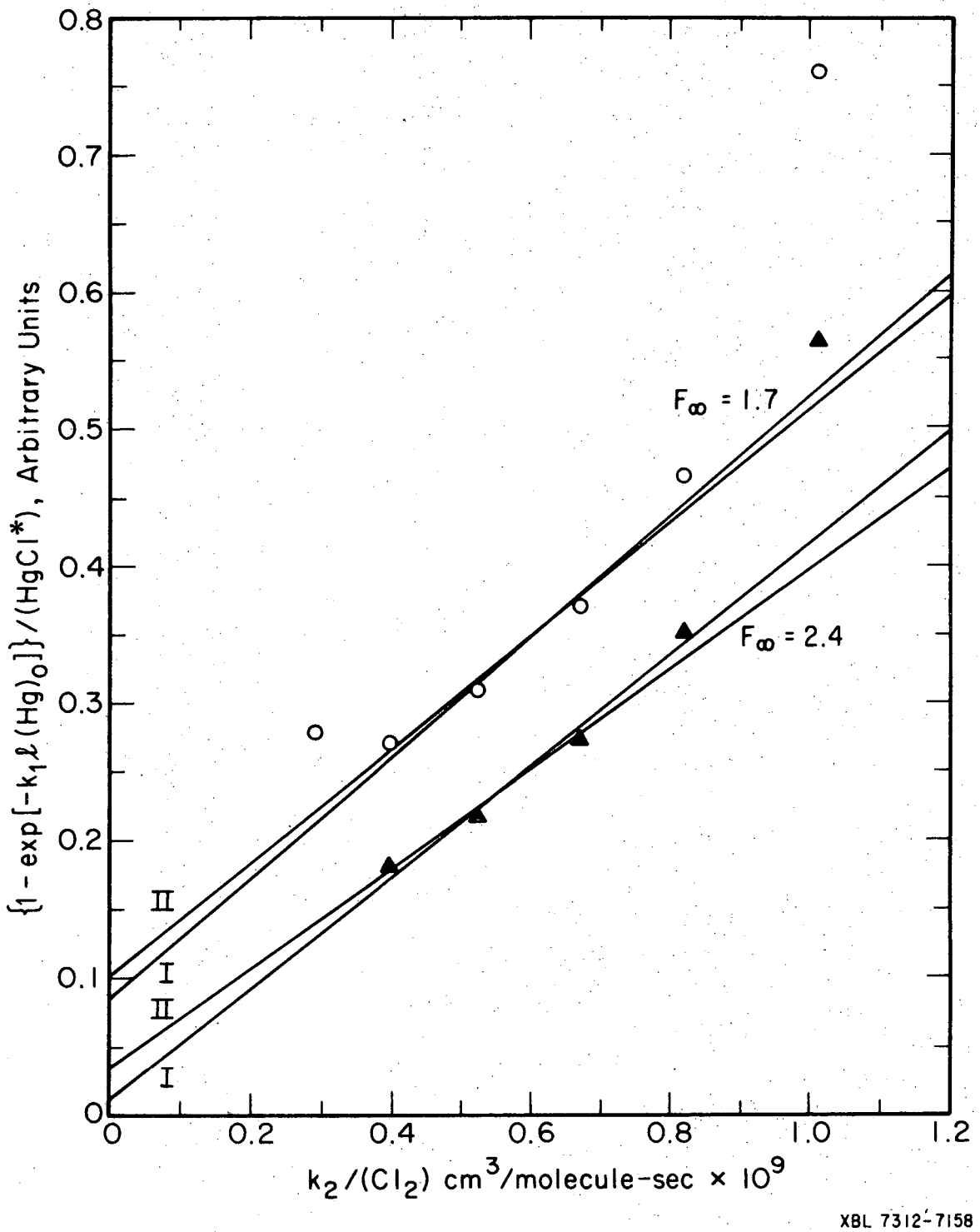

Fig. IV-12. The absorption corrected reduced emission intensity shown as a function of $k_2/(Cl_2)$. For each value of F_∞ the lines marked I and II indicate reasonable lines drawn through the data for $0.4\times10^{-9} \leq k_2/(Cl_2) \leq 0.9\times10^{-9}$. The resultant estimates of the bimolecular rate constant k_3 are shown in Table IV-4.

Table IV-4. Estimates of the Bimolecular Rate Constant for $Hg(^3P_1) + Cl_2 \rightarrow HgCl(B^2\Sigma^+) + Cl_2$

Conditions	Source	Intercept Arbitrary Units	Slope Arbitrary Units	$k_3 \times 10^{10}$ cm^3/molec-sec	σ Å^2
No treatment of light absorption	Fig. IV-11	0.018	0.383	0.480	15
$F_\infty = 1.70$	Fig. IV-12	0.0855	0.444	1.94	54
$F_\infty = 1.70$	Fig. IV-12	0.1021	0.414	2.47	69
$F_\infty = 2.40$	Fig. IV-12	0.0122	0.406	0.30	8.4
$F_\infty = 2.40$	Fig. IV-12	.0338	0.368	0.93	26
Axial variation of HgCl* with $\int_0^t Idt'$ and $F_\infty = 1.70$	Fig. IV-5	-[a]	-[a]	0.19	5.2

a See Equations (58-65)

$$0.30\times10^{-10} \leq k_3 \leq 2.5\times10^{-10} \text{ cm}^3/\text{molecule-sec} \qquad (55)$$

with reactive cross section

$$8.4 \leq \sigma \leq 69 \text{ Å}^2 \qquad (56)$$

The greater the extent of light absorption, the larger an estimate of k_3 results.

This estimate of the range of the bimolecular rate constant k_3 must not be taken as a definitive determination for several reasons. First, the treatment of radiation imprisonment depends on knowledge of the ground state mercury concentration and on choice of the imprisonment path length. Any nonhomogeneity in the reaction mixture at the monitoring point will produce uncertainty in knowledge of (Hg) and affect the amount of imprisonment. The radius of the reaction vessel seems the best choice for a typical imprisonment path length since that distance can vary between zero and the diameter of the vessel. Another caution applies to the treatment of the extent of absorption. Beer's law has been assumed to describe the absorption of resonance radiation by mercury atoms throughout the range of mercury concentration shown in Table IV-3, but the absorption deviates negatively from Beer's law predictions as the mercury concentration is increased. Even if Beer's law adequately describes the variation of absorbance with mercury concentration there is uncertainty in the appropriate choice of absorption path length, especially since choice of either

the radius or diameter yields a reasonable fit to the data of Fig. IV-7. With no correction of the data for absorption a value of k_3 results which is at the low end of the range shown in expression (55). More confidence could be placed in a value of k_3 which had been obtained from several measurements of the variation of $HgCl^*$ intensity with mercury and chlorine concentrations if lower mercury concentrations were used so that radiation imprisonment and attenuation of the incident light flux by absorption could be ignored. The positive aspect of presenting such a measurement of the range of k_3 is the fact that this knowledge adds further confidence to the reaction mechanism which has been postulated to explain the origin of the $HgCl(B^2\Sigma^+) \rightarrow HgCl(X^2\Sigma^+)$ emission.

The cross section range given by (56) can be compared to an estimaterof the hard sphere collision cross section

$$\sigma_{HS} = \pi \left(\frac{d_{Hg} + d_{Cl_2}}{2} \right)^2 \qquad (57)$$

For the molecular diameters d listed in Table II-1, $\sigma_{HS} = 40\text{Å}^2$. Thus this work predicts a reactive cross section comparable to the gas kinetic collision cross section.

An estimate of the lower limit of the bimolecular rate constant can be derived using the data presented in Fig. IV-5 which shows the variation of $(HgCl^*)/I$ with the incident radiant flux integral $\int_o^t I dt'$. As discussed in section B.4, for sufficiently long reaction time the mercury concentration will have fallen to such an extent that radiation

imprisonment becomes unimportant and the axial variation of mercury is a simple exponential decay. Here the straightforward decay function of Eq. (9) holds for (Hg), and ($HgCl^*$) varies according to Eq. (10). Thus, the slope of the first order line at high $\int_o^t Idt'$ on Fig. IV-5 can be used to estimate k_3 if absolute values of $\int_o^t Idt'$ and k_1 are known, since

$$\ln\left\{\frac{k_4(HgCl^*)}{I}\right\} = \ln\left\{\frac{k_1k_3(Hg)_o(Cl_2)}{k_2 + k_3(Cl_2)}\right\} - \frac{k_1k_3(Cl_2)}{k_2+k_3(Cl_2)} \int_o^t Idt' \quad . \qquad (58)$$

$\int_o^t Idt'$ can be estimated from the rated maximum illuminance perpendicular to the lamp axis at 10.16 cm from that axis.

$$I(15.8\ cm) = 9.5\ milliwatts/cm^2 = 1.20\times10^{15}\ photons/cm^2\text{-}sec \qquad (59)$$

for 1 lamp, or

$$\int_o^t I(t)dt = (L\times1.2\times10^{15}\ photons/cm^2\text{-}sec)\ t \qquad (60)$$

where L is the number of lamps and t is the reaction time. At the midpoint of the illuminated region of the reaction vessel t = 15.8 cm/ 39.2 cm/sec = 0.413 sec and, for 10 lamps,

$$\int_o^{0.413} Idt' = 4.8\times10^{15}\ photons/cm^2 \quad . \qquad (61)$$

For x=15.8 cm $v\int_o^t Idt = 22.9$ in the arbitrary units of Fig. IV-5 so that

$$\int_o^t Idt' = 2.1\times10^{14}\ photons/cm^2 \text{ per arbitrary unit of } v\int_o^t Idt'. \qquad (62)$$

This estimate of $\int_o^t Idt'$ applies only to the data of Table IV-2 and Figs. IV-5 and 6. The incident light flux will be attenuated by light absorption. Figure IV-5 shows that (Hg) ~ $0.38(Hg)_o = 5.9\times10^{12}$ atoms/cm^3. when $v\int_o^t Idt' = 20.0$ arbitrary units, for which $I/I_o = 9.4\times10^{-3}$, using $(Hg)_o$ from Table IV-2, $k_1 = 1.23\times10^{-13}$ cm^3/Hg atom and assuming Beer's law absorption with $F_\infty = 1.70$.

$$\int_o^t I_o dt' \sim 2.0\times10^{12} \text{ photons/cm}^2\text{/A.U.} \qquad (63)$$

Using Eq. (58) yields the slope S of Fig. IV-5 as

$$S = \frac{k_1 k_3(Cl_2)}{k_2+k_3(Cl_2)} = 0.89\times10^{-14} \text{ cm}^2 \qquad (64)$$

Rearranging Eq. (64) produces, for $k_2 = 3.81\times10^6$ sec^{-1} and $(Cl_2) = 1.10\times10^{16}$ mole/cm^3

$$k_3 = 0.19\times10^{-11} \text{ cm}^3\text{/molec-sec} \qquad (65)$$

and

$$\sigma = 5.2 \text{ Å}^2 .$$

This method of estimating the bimolecular rate constant predicts a value which is up to an order of magnitude lower than that obtained from the ($HgCl^*$) dependence on $(Hg)_o$ and (Cl_2) at t=0 as discussed earlier in this section. Because the mercury concentration was known more accurately in that work, the effects of radiation imprisonment and incident light absorption could be at least approximately treated, giving more credence to k_3 implied by that work. The second method

of estimating k_3 relies on the applicability of a first order axial decay function for mercury which may not be correct, especially due to the complications of uncertainty in knowledge of the extent of radiation imprisonment and light absorption. The latter method also relies on an estimate of the light output of the lamps from the manufacturer's data which is almost certainly higher than the light flux transmitted through the suprasil vessel, which may have been contaminated by ultraviolet absorbing compounds present, for example. Thus this estimate of k_3 is a lower limit only.

4. Quenching of $HgCl^*$ Emission by Chlorine

The possibility of appreciable quenching of $HgCl^*$ by Cl_2 has been ignored in these kinetic studies. It is possible to assess the relative importance of

$$HgCl^* + Cl_2 \rightarrow HgCl + Cl_2^{\dagger} \qquad (5)$$

by reference to experimental data. If process (5) is important, the initial state of the reaction mixture will follow

$$(HgCl^*) = \frac{k_3(Hg^*)(Cl_2)}{k_4+k_5(Cl_2)} = \frac{k_1k_3I(Hg)_o(Cl_2)}{[k_2+k_3(Cl_2)][k_4+k_5(Cl_2)]} \qquad (66)$$

rearranging Eq. (66) yields

$$k_1k_3\frac{I(Hg)_o(Cl_2)}{(HgCl^*)} = k_2k_4 + (k_3k_4+k_2k_5)(Cl_2) + k_3k_5(Cl_2)^2 \qquad (67)$$

If appreciable absorption of incident radiation is occurring, the emission intensity is more accurately described by

$$(HgCl^*) = \frac{k_3 A_\infty (Hg^*)_\infty (Cl_2) [1 - e^{- k_1 \ell (Hg)_o}]}{[k_2 + k_3(Cl_2)][k_4 + k_5(Cl_2)]} \qquad (68)$$

Inversion and rearrangement of Eq. (68) produces

$$\frac{k_3 A_\infty (Hg^*)_\infty (Cl_2)(1-e^{- k_1 \ell (Hg)_o})}{(HgCl^*)} = k_2 k_4 + (k_3 k_4 + k_2 k_5)(Cl_2) + k_3 k_5 (Cl_2)^2 \qquad (69)$$

Figure IV-13 shows $(Cl_2)(1-e^{- k_1 \ell (Hg)_o})/(HgCl^*)$ plotted as a function of (Cl_2) for the data shown in Table IV-3, with $F_\infty = 1.70$. Neglecting the two points of lowest chlorine concentration, the deviation from linearity becomes important only for $(Cl_2) > 1.2 \times 10^{16}$ molecules/cm^3, and part of this deviation is due to the variation of k_2 with (Cl_2). These results show that quenching of $(HgCl^*)$ by (Cl_2) is unimportant for the intermediate range of (Cl_2) which has been utilized for most of this work.

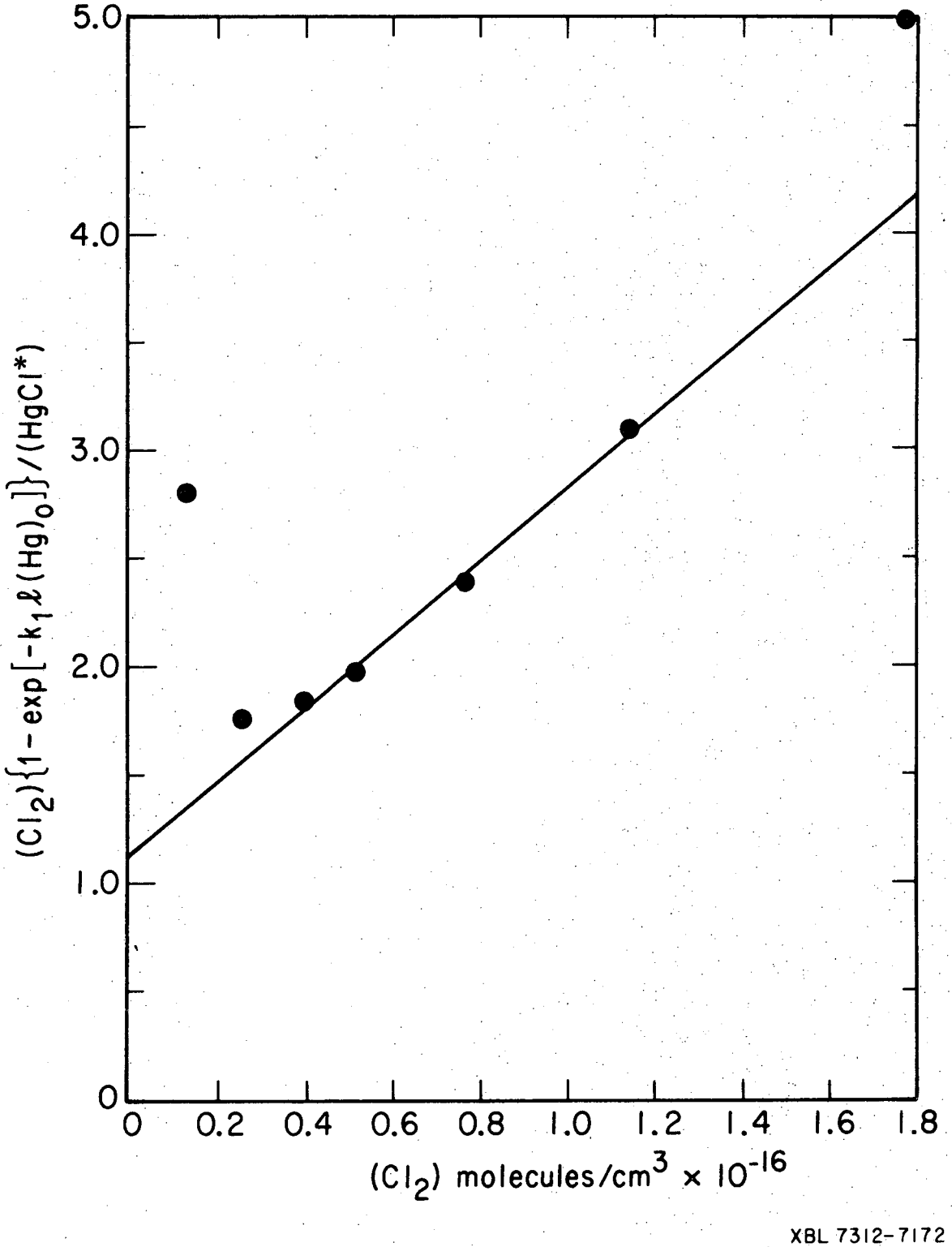

Fig. IV-13. A test for quenching of ($HgCl^*$) by Cl_2. The ordinate variable is defined by Eq. (69).

CHAPTER IV REFERENCES

1. E. E. Ferguson, F. C. Fehsenfeld, and A. L. Schmeltekopf, Adv. At. Mol. Phys. 5, 1 (1969).
2. D. Alpert, A. O. McCoubrey, T. Holstein, Phys. Rev. 76, 1257 (1949).
3. Morgan, Geometric and Physical Optics, McGraw Hill, New York, 1953, Chapter 9.
4. A. C. Mitchell and M. W. Zemansky, Resonance Radiation and Excited Atoms, Cambridge University Press, New York, 1961, p. 230.
5. E. A. Milne, Journ. Lond. Math. Soc. 1, 1 (1926).
6. E. W. Samson, Phys. Rev. 40, 940 (1932).
7. J. V. Michael and C. Yeh, J. Chem. Phys. 53, 59 (1970).
8. K. Yang, J. Am. Chem. Soc. 88, 4575 (1966).
9. T. Holstein, Phys. Rev. 72, 1212 (1947).
10. L. B. Thomas and W. D. Gwinn, J. Am. Chem. Soc. 70, 2643 (1948).
11. A. C. Mitchell and M. W. Zemansky, loc. cit., p. 192.
12. A. Lurio, Phys. Rev. 140, A1505 (1965).
13. H. S. Johnston, Gas Phase Reaction Rate Theory, Ronald, New York, 1966, p. 102.

V. SPECTROSCOPIC STUDIES OF THE HgX (B-X) EMISSION

A. Introduction

The chemiluminescence which accompanies the reaction of $Hg(6^3P_1)$ with the halogens has been established to originate from the bimolecular process

$$Hg(^3P_1) + XY \rightarrow HgX(B^2\Sigma^+) + Y$$

which is followed by light emission

$$HgX(B^2\Sigma^+) \rightarrow HgX(X^2\Sigma^+) + h\nu \quad .$$

In this chapter the resultant spectra will be presented and discussed. The intensity variation among the vibronic bands contains information about the distribution of energy between the products of the reaction. The principal goal of these studies has been to extract this information because of the insight it provides about the dynamics of the reaction. It is also possible to obtain an estimate of the dissociation energy of the ground state of HgX from its chemiluminescent spectrum, and this has been done for HgCl. Similarly, the energy distribution results apply to the $Hg^* + Cl_2$ system only. For the other halogen species studied here only the emission spectra themselves will be presented and discussed.

B. Characterization of the Emission for $Hg^* + Cl_2$

1. Comparison of the Chemiluminescence Spectrum to the Spectrum of HgCl(B→X)

Vibrational analysis of the HgX(B→X) spectra has been performed by Wieland for HgCl,[1] HgBr and HgI.[2] Very complicated emission spectra were obtained by electric discharge of HgX_2 and only when large amounts of nitrogen were added to the Geissler tube to relax vibrational energy could he begin to order the observed bands. Figure V-1a shows a photograph of the HgCl(B→X) emission which was obtained by Tesla discharge of a small amount of slightly warmed $HgCl_2$ in 5 Torr of Argon. With slit width of 50 microns exposure time for the 103aF plate was 30 seconds. The pronounced intensity maximum at about 5550Å for HgCl and the sharp fall off to the red of that maximum are characteristic features of the HgX spectra. Both red and blue shaded bands appear, and except for the v'=0 progression which is indicated on the figure, it is difficult to see much of the ordering of vibronic bands in the region shown. The presence of two stable isotopes of chlorine in an abundance ratio of mass 35 to mass 37 of 3 to 1 introduces further complication. Wieland deconvoluted this spectrum by using pure $HgCl_2{}^{37}$ in the discharge tube and by observing the simplification of the band structure as the pressure of nitrogen was increased. The blue shaded bands disappeared entirely, the extent of the emission towards the violet decreased, and he could pick out the low v' progressions.

The well ordered red shaded bands at low wavelength with no nitrogen could then be assigned to high v' transitions. After constructing estimates of the potential curves for the B and X states of HgCl the reversal in shading could be understood, and the blue shaded could be tied to the same electronic transition. A large displacement of the upper state potential to larger r compared to the ground state is indicated by the intensity maximum in the v'=0 progression at v"=21 or 22 and by their red shaded character. Further discussion of the potential curves for HgCl will be presented later.

The emission spectrum obtained upon irradiation of Hg and Cl_2 in the flow system is shown in Fig. V-1b and c. Chlorine pressure was 0.35 Torr in the reaction vessel with Hg flow rate of 3.5×10^{16} atoms/sec; the same grating setting and Plate type were used as for part d of this figure. Part d shows the background light emission with no mercury or chlorine in the irradiated system. The plate records the scattered light from the exciting lamps. With slit width of 150 microns the exposure time was 150 minutes for parts d and b. Part c is another print made from the same plate as part b. The suprasil vessel was used with no filter solution or baffles. The comparison of the chemiluminescence spectrum to that of the known discharge source of HgCl had to be made photographically because the instability of the discharge and the electronic noise caused by the Tesla spark made photoelectric detection impossible.

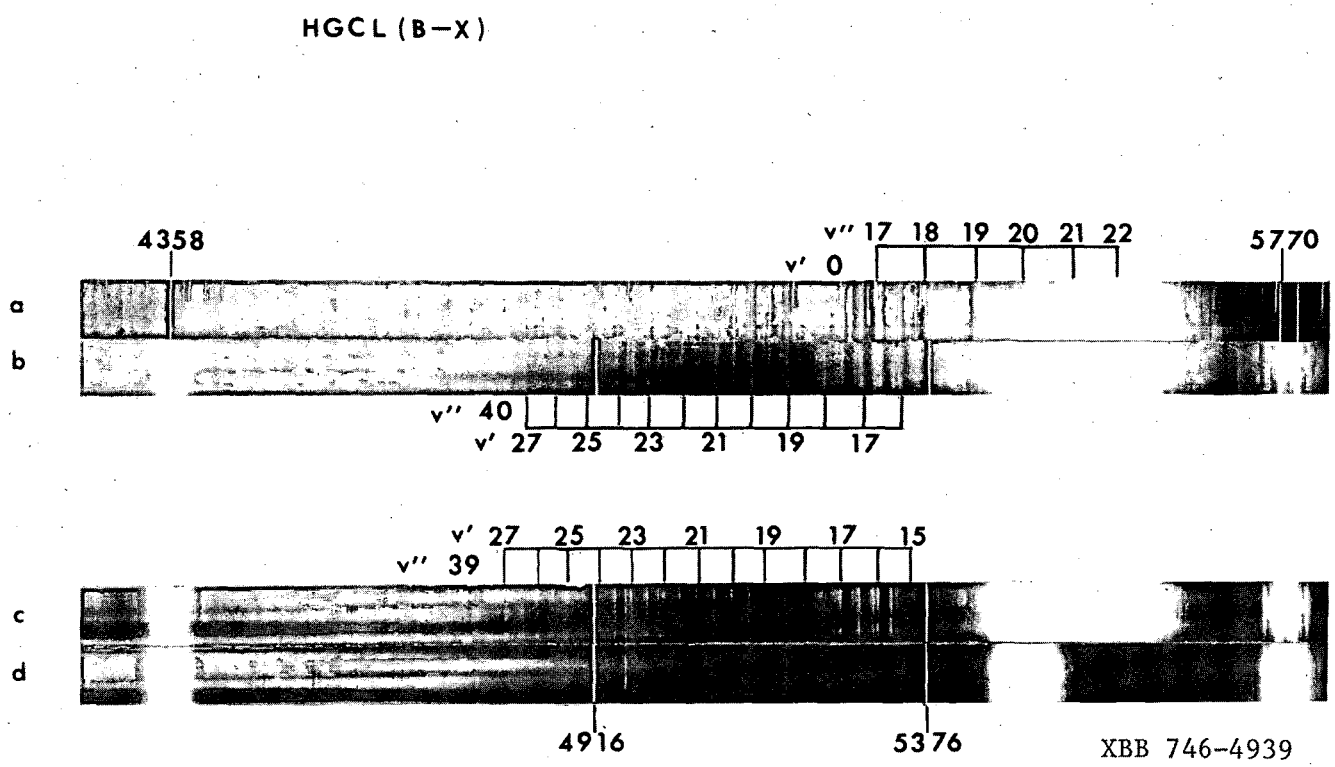

Fig. V-1. $HgCl(B^2\Sigma^+ \rightarrow X^2\Sigma^+)$ emission spectra. a) Tesla discharge of warmed $HgCl_2$ + 5 Torr of Argon b) and c) Emission from $Hg(^3P_1)$ + Cl_2 (0.35 Torr) d) Background emission from the reaction vessel. Wavelengths of atomic Hg lines are indicated.

Direct comparison of parts a and b shows that nearly all the band structure of the chemiluminescence spectrum appears on the discharge spectrum but the converse is not true. The blue shaded bands, some of which are indicated on parts b and c with v'=27 to 15 and v"=39 and 40, are common to both the emission spectrum of HgCl excited by Tesla discharge of $HgCl_2$ and to the chemiluminescence spectrum, but the intense sequences whose first members originate in v'=0 are completely missing from parts b and c. The discharge spectrum is more complicated than the chemiluminescence spectrum and also has appreciable intensity beyond both the short and long wavelength limits of the latter. This occurs because the discharge spectrum reflects a different vibrational population of the parent HgCl* molecule. In both cases the upper state population is non-thermal, and apparently very little population of the low v' levels of the product HgCl* results from the bimolecular reaction of Hg* with Cl_2. It is important to note that the discharge does indeed produce the same molecular spectrum as Wieland observed in his Geissler tube, and he has unambiguously assigned it to the transition $HgCl(B^2\Sigma^+ \rightarrow X^2\Sigma^+)$. His spectra are reproduced in reference 3 for natural HgCl and in reference 1 for $HgCl^{37}$. These observations establish that the molecular emission which has been observed to accompany the reaction of $Hg(^3P_1)$ with Cl_2 is due to radiation from $HgCl(B^2\Sigma^+)$.

2. Spectroscopic Information for $HgCl(B^2\Sigma^+)$ and $HgCl(X^2\Sigma^+)$

Table V-1 shows the spectroscopic constants derived for HgCl from vibrational analysis of the (3000-5700Å) emission. Except for the dissociation energy of the ground state, these are Wieland's values. The energy $\bar{\nu}$ in cm^{-1} emitted or absorbed by HgCl during a vibronic transition in this region is given by the difference in energy between the two levels[4]

$$\bar{\nu} = T_e + G' - G''$$

$$= T_e + \omega_e'(v'+\tfrac{1}{2}) - \omega_e x_e'(v'+\tfrac{1}{2})^2 - [\omega_e''(v''+\tfrac{1}{2}) - \omega_e x_e''(v''+\tfrac{1}{2})^2 + \omega_e y_e(v''+\tfrac{1}{2})^3 - \omega_e z_e''(v''+\tfrac{1}{2})^4].$$

As is conventional the superscript prime refers to the upper state and the double prime to the lower state involved in the transition, with v' and v" labeling the vibrational levels. T_e measures the difference in energy between the potential minima of the states. G' and G" give the vibrational energy measured from the respective minima. Note that whereas the upper state can be described by a potential energy function which predicts energy levels which are quadratic in (v'+1/2), the lower state needs a potential function which produces terms up to $(v'+1/2)^4$ in its energy expression.

The dissociation energies reflect the relative instability of the ground state compared to the upper state. For both states values of D_e^o were obtained from Birge-Sponer plots of the observed vibrational quanta as a function of v according to

$$\Delta G(v+\tfrac{1}{2}) = G(v+1) - G(v) \qquad (2)$$

Table V-1. Spectroscopic Constants for $HgCl^{35}$

	$HgCl(X^2\Sigma^+)$	$HgCl(B^{2+})$
ω_e	292.61[a]	192.0 $v' \leq 30$
		186.3 $v' \geq 30$
$\omega_e x_e$	1.6025	0.50 $v' \leq 30$
		0.40 $v' \geq 30$
$\omega_e y_e$	1.493E-02	
$\omega_e z_e$	3.3E-05	
r_e	2.5Å	3.15
D_e^o	8463[b]	21753
	1.05 eV	2.70 eV
T_e		23421
μ	29.79 amu	

[a] All values in cm^{-1} unless otherwise noted. These constants are derived from the vibrational analysis of HgCl; see K. Wieland, Helv. Phys. Acta 41, 420 (1941).

[b] This estimate of D_e^o is based on the Birge Sponer extrapolation illustrated in Fig. V-2. An experimental estimate from the low wavelength limit of the chemiluminescence spectrum predicts $D_e^o \geq 1.05$ eV. See section V.D.3.

where G(v) represents the vibrational term value. For an energy function which is quadratic in v, $\Delta G(v+1/2)$ is linear in v, since

$$\Delta G(v+\tfrac{1}{2}) = \omega_e - 2\omega_e x_e (v+1). \tag{3}$$

The dissociation energy, calculated from the minimum of the quadratic function becomes

$$D_e^o = \frac{\omega_e^2}{4\omega_e x_e} \tag{4}$$

For most molecular states this value is higher than the true dissociation energy since (v+1/2) terms of higher power than 2 are required to predict the position of vibrational levels. If curvature can be seen in a Birge-Sponer diagram, a more accurate estimate of the dissociation energy results when the curve is extrapolated to $\Delta G(v+1/2) = 0$, and

$$D_o^o = \sum_{v=0}^{v_{max}} \Delta G(v+1/2) \tag{5}$$

where v_{max} is the vibrational level nearest to which the extrapolated value of $\Delta G(v+1/2)$ is zero. Figure V-2 shows a Birge-Sponer plot for the ground state of HgCl, using its average vibrational spacings as derived from the positions of bands of constant v' as listed in Table 1 of reference 1. The lines marked I and II indicate that in some restricted ranges of v, $\Delta G(v+1/2)$ is linear in v. Reference will be made later to these lines in the derivation of quasi-Morse

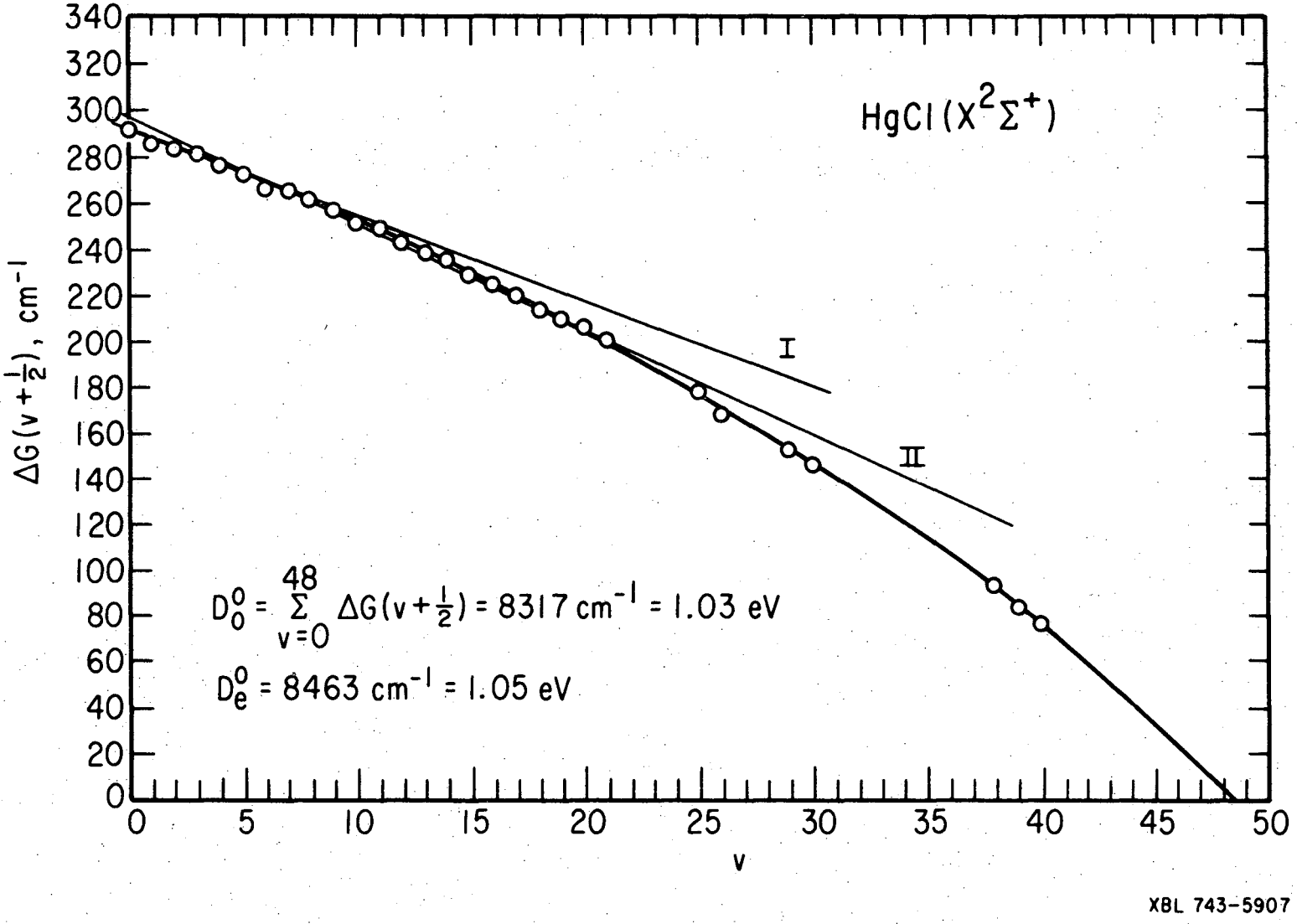

Fig. V-2. Birge Sponer extrapolation for HgCl($X^2\Sigma^+$). Two regions of approximate linearity are marked I and II.

parameters for HgCl. The curve drawn shows the expected non-linearity in v, but a reasonable extrapolation can be made to $\Delta G(v+1/2) = 0$, which predicts from Eq. (5).

$$D_o^o = 8317 \text{ cm}^{-1} = 1.03 \text{ ev} \qquad (6)$$

and

$$D_e^o = D_o^o + \omega_e/2 - \omega_e x_e/4 = 8463 \text{ cm}^{-1} = 1.05 \text{ ev} .$$

This value of D_e^o is shown in Table V-1 for $HgCl(X^2\Sigma^+)$. For the B state a Birge - Sponer plot should be linear in v. Wieland estimates its dissociation energy D_o^o as 21753 cm^{-1} or 2.70 ev.

Rotational analysis of the vibronic bands would be required to derive accurate values of the equilibrium internuclear separation in each of these states. For such a heavy molecule the rotational levels are very close together so high resolving power is required of the spectrometer and a high intensity source of the emission is necessary. Alternatively, infrared studies of allowed rotational and vibrational transitions within each electronic state could be used to derive values of r_e. As expected such studies have not been made, so other methods of estimating r_e for the ground state must be used. Once an estimate of r_e'' is made, r_e' can be deduced from the intensity variation of the observed bands, and potential energy curves can be drawn for the two states.

Wieland argues that since average energy per bond in $HgCl_2$ is higher than that of HgCl(2.02 ev[5] compared to 1.05 ev), and the symmetric vibrational frequency in $HgCl_2$ is 362 cm^{-1} compared to 293 cm^{-1} for the fundamental frequency in the diatomic molecule, it can be expected intuitively that the bond length is shorter in the triatomic than in the diatomic molecule because of the stronger bonding between the atoms. Wieland quotes three measurements of the bond length in $HgCl_2$, obtained from x-ray and electron diffraction studies, which give an average value of 2.29±0.04Å.[6,7] For HgCl Wieland eventually chose to use r_e''=2.5Å, apparently somewhat arbitrarily. Since the most intense emission band from v'=0 has v"=21, he assigned r_e'=3.15Å because a quasi-Morse potential predicts this as the classical turning point r^+ for v"=21. These values come close to satisfying the empirical rule discovered by Birge and Mecke[8] that for different electronic states of the same molecule,

$$\omega_e r_e^2 = \text{constant}$$

For r_e'' = 2.50Å this rule is best satisfied for r_e' = 3.09Å, but our Franck-Condon factor calculations for these values of equilibrium internuclear distances would predict the most intense emission band from v'=0 to occur to v"=18.

Other methods can be used to estimate the equilibrium internuclear separation in HgCl. A useful empirical relation is Badger's rule.[9a] This relates the internuclear separation to the force constant for infinites simally small displacement of the nuclei from their equilibrium positions:[10]

$$F = 5.883 \times 10^{-2} \mu_A \omega_e \text{ dynes/cm}$$

for μ_A, the reduced mass in amu and the vibrational frequency in cm^{-1}. As revised by Herschbach and Johnston,[9b,c] Badger's rule can be used for estimating internuclear distances from knowledge of ω_e and the row in the periodic table in which each atom occurs, according to

$$r_e = a_{ij} - b_{ij} \log_{10} F$$

for i and j labeling the rows of the atoms. Johnston has presented a table containing a_{ij} and b_{ij} values for i and $j \leq 4$ and has shown the validity of the predicted r_e values by comparison to experimental data. Mercury, however, belongs to row 5, and only hydride r_e values are known for fifth row compounds. Figure V-3 shows Johnston's values of a_{2j} and b_{2j} for $j \leq 4$ from which it is possible to extrapolate a_{25} and b_{25} values of 2.64Å and 0.82, respectively, which apply to HgCl. For ω_e=292.6 cm^{-1} r_e"=2.50Å using these empirical extrapolated constants. Surprisingly close agreement to Wieland's estimate of r_e" is found. Admittedly this estimate is obtained crudely and should not be taken as a definitive value for r_e". For the B state of HgCl with ω_e=192 cm^{-1} Badger's rule predicts r_e'=2.70Å which is certainly too small if r_e" is close to 2.5Å and the vibrational analysis of the emission spectrum is correct. Badger's rule holds less well for ionically bound gaseous molecules than for covalently bound molecules, so the estimate of r_e for the ground state of HgCl is expected to be more reliable than that for the B state which has appreciable ionic character.

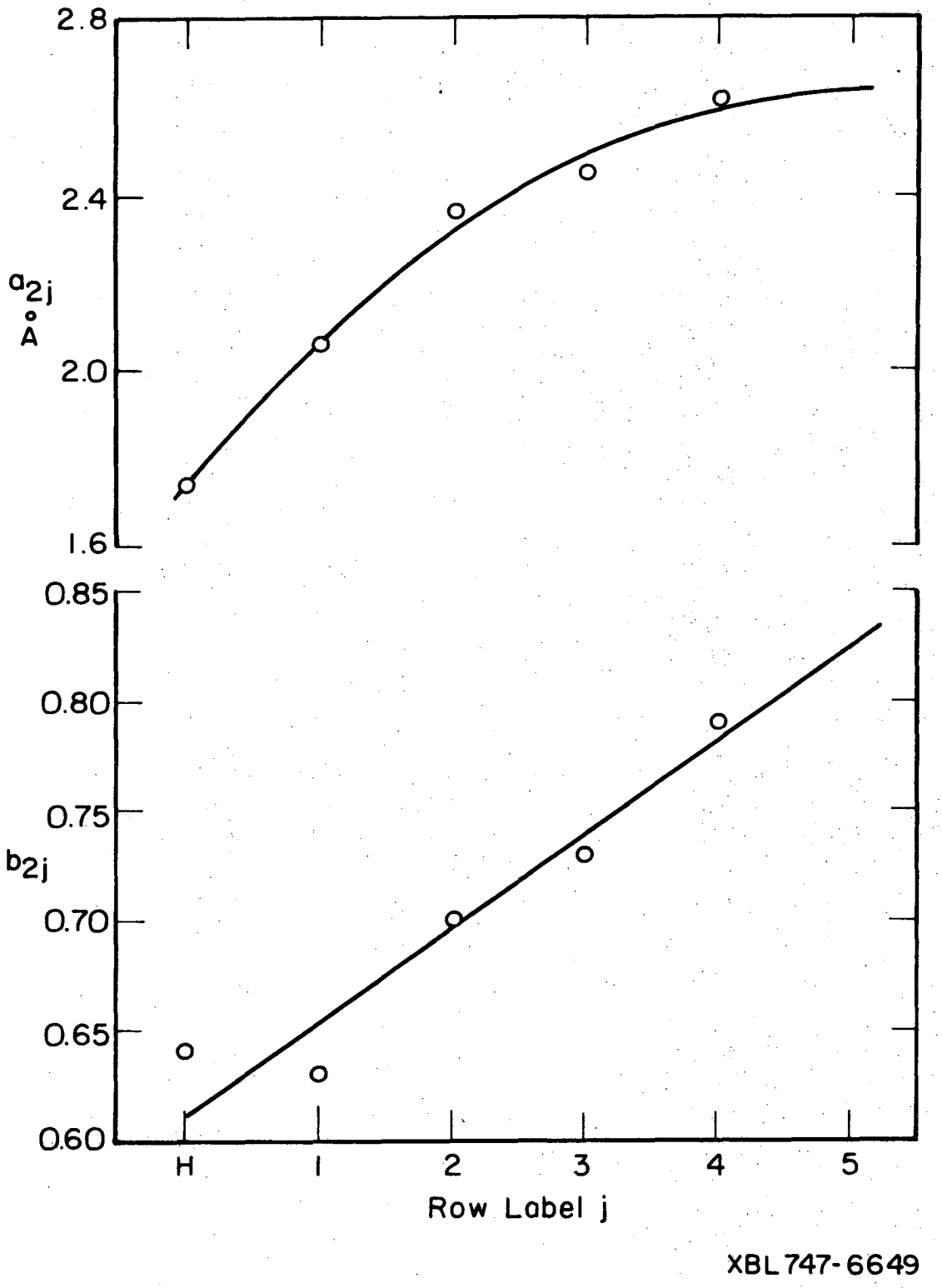

Fig. V-3. Badger's rule parameters for compounds of the second row of the periodic chart.

The dissociation energy of alkali halide molecules into ions, $D_o(M^+X^-)$, correlates well with the bond length of the ionic molecule.[11] The bond length of the B state of HgCl can be estimated from that correlation and it gives an idea of r_e to be expected if the B state dissociates to ions. The ionic dissociation energy is

$$D_o(M^+X^-) = D_o(MX) + I(M) - E(X) \qquad (10)$$

where $D_o(MX)$ is the dissociation energy of the neutral molecule, I(M) is the ionization potential of M and E(X) is the halogen atom electron affinity. For $D_o^o(HgCl^*) = 2.69$ eV,[12] $I(Hg\,^3P_1) = 5.57$ eV,[13] and $E(Cl) = 3.61$ eV,[14] $D_o(Hg^+Cl^-) = 4.65$ eV. Thus Fig. 5 of reference 11 predicts $r_e' = 2.9$Å. Since the B state is not really an ionic state, its actual equilibrium internuclear separation is expected to be greater than this since the attractive force is less coulombic and the nuclei are further separated than for alkali metals.

The Badger's rule estimate of $r_e'' = 2.50$Å and the ionic model's prediction of $r_e' > 2.9$Å do not contradict Wieland's crude estimates of $r_e'' = 2.50$Å and $r_e' = 3.15$Å. In the calculation of the relative population of vibrational levels of $HgCl^*$ formed in the $Hg^* + Cl_2$ reaction, it will be shown subsequently that accurate knowledge of the internuclear separation in either state is not essential and that only their relative separation must be well estimated in order to construct a meaningful set of overlap integrals which can be combined with spectral intensities to extract vibrational populations.

C. Background Information for the Interpretation of Spectral Intensities

The intensity of an emission band in quanta/sec is related to the population $N_{v'}$, of the level v' by[15]

$$I = N_{v'}A_{v'v''} = \frac{64\pi^4}{3h} N_{v'}\nu^3_{v'v''} |R^{v'v''}|^2 . \quad (11)$$

Here $A_{v'v''}$ is the transition probability, the Einstein coefficient for spontaneous emission, $\nu_{v'v''}$ is the frequency of the transition, and $R_{v'v''}$ is the transition moment or matrix element.

$$R_{v'v''} = \langle \psi_e'\psi_v^{v'} |\vec{M}|\psi_e''\psi_v^{v''}\rangle \quad (12)$$

Here ψ_e and ψ_v refer to electronic and vibrational wavefunctions respectively and $\vec{M}$ is the dipole moment operator. In order to extract relative vibrational populations from the observed intensities of the vibronic bands of HgCl it becomes necessary to calculate their transition moments, or to use sum rules, or both. Because the motion of the electron involved in the transition is fast compared to the nuclear motion in vibration, the electronic motion is only slightly dependent on the nuclear positions, and the transition moment can be expressed as the product of an average value of the electronic moment for all transitions involving the same electronic states, $\bar{R}_e$, and the overlap integral formed from the vibrational wavefunctions of the two states when the Born-Oppenheimer approximation holds, so that

$$\vec{R}_{v'v''} = \vec{R}_e \langle \psi_v^{v'} | \psi_v^{v''} \rangle \quad . \tag{13}$$

The emission intensity then becomes

$$I_{v'v''} = CN_{v'} \nu^3_{v'v''} \vec{R}_e^{\,2} |\langle \psi_v^{v'} | \psi_v^{v''} \rangle|^2 \quad . \tag{14}$$

The square of the overlap integral, shown in Eq. (14), is the Franck-Condon factor for the transition. Franck-Condon factors have been calculated for HgCl by finding vibrational wavefunctions for each state which are solutions to the radial Schrodinger equation, using Morse or quasi-Morse potential energy expressions for each state. The subsequent parts of this section describe the potential energy functions which can be derived from the previous spectral analysis and also discuss the calculation of Franck-Condon factors for HgCl.

1. Potential Curves and Dissociation Products for HgCl

The Morse function can be used to describe the variation of the potential energy with internuclear distance for electronic states of molecules as long as the vibrational term values are quadratic in (v+1/2). The Morse potential predicts energy levels close to those experimentally observed when it is used in the Schrodinger equation. It yields analytical wavefunctions which can be used relatively easily to calculate overlap integrals which are needed to derive the relative populations of the vibrational levels of an electronic state. The Morse potential is given by

$$V(r-r_e) = D_e(1-\exp[-\beta(r-r_e)])^2 \quad . \tag{15}$$

D_e and r_e have the usual meanings and β is related to spectroscopic constants by[16]

$$\beta = \sqrt{\frac{2\pi^2 c\mu}{D_e h}}\ \omega_e = 0.12177\ \omega_e \sqrt{\frac{\mu}{D_e}} \qquad (16)$$

for D_e and ω_e in cm^{-1} and μ in atomic mass units. The Morse dissociation energy is given by

$$D_e = \frac{\omega_e^2}{4\omega_e x_e} \qquad (17)$$

The Morse potential fills two requirements for a useful potential. It predicts a minimum in energy at $r=r_e$ and makes $V(r-r_e)\rightarrow D_e$ as $r\rightarrow\infty$ but it does not predict $V(r-r_e) = \infty$ as $r \rightarrow 0$ as a true potential would. The fact that most electronic states require a vibrational potential whose term values are more than quadratic in $(v+1/2)$ means that the Morse function can usually be use accurately only for low vibrational levels of an electronic state. However, for the B state of HgCl a Morse function is expected to accurately describe the energy levels and wavefunctions for $v \leqslant 30$. For the ground state a simple Morse function is hopeless since the vibrational energy expression requires terms up to $(v+1/2)^4$. It is possible to construct a quasi-Morse potential energy function for the ground state from several pieces, each of which is valid for a limited range of v, and each of which is quadratic in $(v+1/2)$. For such regions the change in vibrational spacings is linear in v. Two regions of approximate linearity are

indicated in Fig. V-2 for HgCl($X^2\Sigma^+$). Quasi-Morse constants have been derived from the slopes and intercepts of lines I and II according to Eq. (3). These are presented in Table V-2 along with the applicable ranges in vibrational quantum number. Figure V-4 shows potential energy diagrams for the B and X states of HgCl. For the ground state the potential is a composite smooth curve obtained from the two quasi-Morse potential functions whose constants are presented in Table V-2. For the B state the potential curve is composed of two smoothly connected Morse pieces which have been constructed from Wieland's original constants as presented in Table V-1. The vibrational levels shown in the figure indicate the vibrational term values predicted by Wieland's original constants as given in Table V-1. The shape of the Morse function does not depend on the choice of r_e, so that the uncertainty in the choice of r_e'' does not yet introduce difficulty. The figure shows r_e'' = 2.50Å and r_e' = 3.12Å, the values of the internuclear separations which were ultimately used in the calculation of overlap integrals for vibronic transitions involving these states.

The energy difference between the electronic states at large internuclear distance indicates that the dissociation products are ground state atoms for the X state and Hg(^3P_o) or Hg($^3P_1$) and a ground state Cl atom fro the B state, since

$$T_e + D_e' - D_e'' = 4.55 \text{ eV} \qquad (18)$$

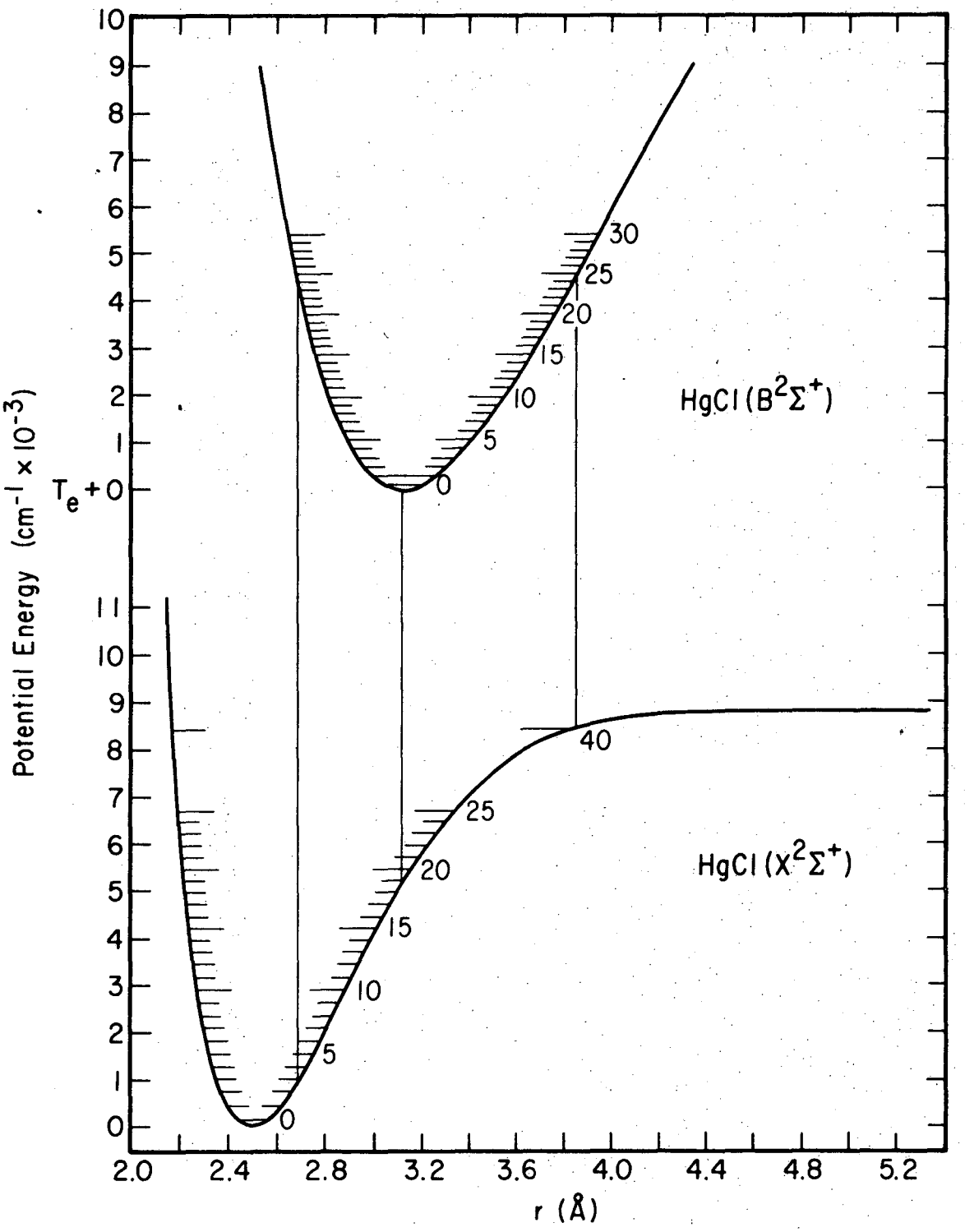

Fig. V-4. Potential curves for $HgCl(B^2\Sigma^+)$ and $(X^2\Sigma^+)$. The vertical lines show a red shaded and a blue shaded band from v'=25 and a red shaded band from v'=0.

Table V-2. Quasi-Morse Parameters for $HgCl^{35}$ ($X^2\Sigma^+$)

	$0 \leq v \leq 9$	$9 \leq v \leq 22$
ω_e	294.5[a]	303.1
$\omega_e x_e$	1.89	2.33
D_e^o	11472[b]	9857
r_e	2.5Å[c]	2.5Å

[a] All values in cm^{-1} except as noted.

[b] The Morse potential predicts $D_e^o = \frac{\omega_e^2}{4\omega_e x_e}$.

[c] The best fit of predicted Franck-Condon factors to the observed intensity envelopes for constant v' or v", for r_e"=2.5Å, occurs for r_e'=3.12Å. These values of the internuclear distance were used in the overlap integral calculation whose results are presented in Table V-3.

and Hg(^3P_o) lies 4.65 eV above the ground state. Hg($^3P_1$) is not ruled out, however. The Birge-Sponer extrapolation estimate of D_e' may provide a value lower than the true dissociation energy of the B state, since the vibrational analysis indicates that for $v'>30$ the potential energy function is converging less rapidly than for $v'\leqslant 30$. Gaydon[17] illustrates Birge-Sponer extrapolations for several molecular states which have appreciable ionic character, and the long range attractive force makes for weaker convergence of the potential energy function than is expected from a function whose vibrational term value is quadratic in (v+1/2). The appreciable ionic character of the B state of HgCl is indicated by the presence of an avoided crossing of this state by the ionic state of the same symmetry ($^2\Sigma^+$). The separated ions lie at an energy above the dissociation limit of the ground state defined by the difference between the ionization potential of mercury in its excited state and the electron affinity of atomic chlorine, or between 1.96 and 2.17 eV above the dissociation limit of the B state. The zero order crossing distance r_c can be found from the coulombic energy expression

$$\frac{e^2}{r_c} = I(Hg\,^3P) - E(Cl) \qquad (19)$$

which gives r_c between 6.6 and 7.3Å. The effect of the interaction between this ionic state and the B state of HgCl is a net mixing of the two states so that the B state is stabilized appreciably by the strong attractive potential of the ionic interaction.

2. Franck-Condon Factor Calculations for HgCl

Franck-Condon factors have been calculated for B→X transitions in HgCl using Morse potential energy functions. The calculations used a computer program developed by S. Gabelnick[18] and were performed on a CDC 7600 computer at Lawrence Berkeley Laboratory. The program proceeds by constructing radial solutions to the Schrodinger equation using Morse potential parameters,[19] testing the orthogonality of the resultant set of vibrational wavefunctions for each state, and finally by numerical integration to produce the overlap integrals. The program also calculates r-centroids for each transition but they are not used here since the variation of the electronic transition moment with internuclear separation is neglected.

For the B state of HgCl Wieland's values of ω_e, $\omega_e x_e$, and r_e were used initially, for $v \leq 30$, as listed in Table V-1. For the ground state the quasi-Morse parameters of Table V-2 were used in calculating FC factors for the appropriate span of vibrational levels. This means that the useful set of FC factors for $v' \leq 30$ is composed of two subsets, with one valid for low v" and the other valid for high v". When transitions from one level in the upper state occur to a wide range of lower levels, the FC factors from both subsets are needed. Because they are separately normalized they must be used in tandem in this case.

By varying the Morse parameters for each state and repeating the calculation of FC factors it is possible to find the set of potential parameters which most closely reproduces the observed variation in intensity of emission from a particular upper level to all lower levels.

The best set of potential parameters reproduces the Franck-Condon envelope for the whole emission spectrum. For HgCl it has been found that the calculated Franck-Condon envelope is most sensitive to the difference between r_e'' and r_e' and is relatively insensitive to variations of ω_e and $\omega_e x_e$ which are within the experimental error of the vibrational analysis ($\leq$10%). For $r_e'' = 2.50$Å, the best fit to the observed Franck-Condon envelope for the whole spectrum occurs for $r_e' = 3.12$Å. This is a compromise value, since levels of high v' are fit best by a slightly smaller value of r_e' (3.10Å) and levels of low v' are fit best by $r_e' = 3.14$Å. This compromise reflects the limitations of the Morse and quasi-Morse potential functions in describing the real potential energy functions. Table V-3 presents the Franck-Condon factors which provide the best fit to the Franck-Condon envelope to the Fortrat parabola and which have been used in calculation of relative popultions of the vibrational levels of the B state of HgCl. Parts a and b of the table present FC factors which are valid for $0 \leq v'' \leq 9$ and $9 \leq v'' \leq 22$ respectively but the range of v" for which the overlap integrals have been calculated has been extended somewhat for each case.

Table V-3 shows that the overlap integrals for high v' do not decrease much below 10^{-3} for transitions to v" between the classical turning points of the upper state potential curve. This means that the resultant emission spectrum will be composed of so many weak bands that it appears continuuous, with a banded structure superimposed by only the strongest transitions. Transitions to the r^+ side of the ground state potential have greater intensity because of the larger

Table V-3. Franck-Condon Factors for HgCl(B→X)

a) FC factors based on quasi-Morse parameters valid for $0 \leq v' \leq 9$[a] and Morse parameters for $0 \leq v' \leq 30$.[b]

v'\v"	0	1	2	3	4	5	6	7
0	1.898E-17	1.676E-15	7.104E-14	1.924E-12	3.739E-11	5.550E-10	6.542E-09	6.282E-08
1	4.627E-16	3.831E-14	1.516E-12	3.817E-11	6.861E-10	9.365E-09	1.008E-07	8.777E-07
2	5.777E-15	4.486E-13	1.659E-11	3.883E-10	6.454E-09	8.099E-08	7.960E-07	6.276E-06
3	4.922E-14	3.586E-12	1.239E-10	2.697E-09	4.146E-08	4.782E-07	4.288E-06	3.058E-05
4	3.218E-13	2.200E-11	7.104E-10	1.438E-08	2.045E-07	2.166E-06	1.771E-05	1.140E-04
5	1.721E-12	1.105E-10	3.334E-09	6.277E-08	8.250E-07	8.024E-06	5.972E-05	3.467E-04
6	7.841E-12	4.727E-10	1.333E-08	2.334E-07	2.835E-06	2.530E-05	1.712E-04	8.932E-04
7	3.129E-11	1.771E-09	4.671E-08	7.601E-07	8.527E-06	6.973E-05	4.282E-04	2.003E-03
8	1.116E-10	5.933E-09	1.462E-07	2.212E-06	2.290E-05	1.714E-04	9.535E-04	3.983E-03
9	3.610E-10	1.803E-08	4.154E-07	5.838E-06	5.576E-05	3.815E-04	1.917E-03	7.121E-03
10	1.073E-09	5.035E-08	1.084E-06	1.415E-05	1.245E-04	7.774E-04	3.519E-03	1.156E-02
11	2.958E-09	1.304E-07	2.623E-06	3.177E-05	2.574E-04	1.464E-03	5.947E-03	1.718E-02
12	7.622E-09	3.156E-07	5.930E-06	6.664E-05	4.964E-04	2.565E-03	9.317E-03	2.346E-02
13	1.848E-08	7.190E-07	1.261E-05	1.314E-04	8.987E-04	4.209E-03	1.360E-02	2.957E-02
14	4.242E-08	1.550E-06	2.538E-05	2.448E-04	1.535E-03	6.497E-03	1.857E-02	3.443E-02
15	9.259E-08	3.177E-06	4.854E-05	4.332E-04	2.485E-03	9.472E-03	2.377E-02	3.699E-02
16	1.930E-07	6.216E-06	8.857E-05	7.306E-04	3.828E-03	1.308E-02	2.859E-02	3.654E-02
17	3.855E-07	1.166E-05	1.548E-04	1.179E-03	5.625E-03	1.716E-02	3.231E-02	3.290E-02
18	7.403E-07	2.101E-05	2.598E-04	1.824E-03	7.909E-03	2.142E-02	3.427E-02	2.662E-02
19	1.371E-06	3.650E-05	4.201E-04	2.715E-03	1.066E-02	2.545E-02	3.402E-02	1.883E-02
20	2.454E-06	6.127E-05	6.558E-04	3.895E-03	1.381E-02	2.883E-02	3.145E-02	1.102E-02
21	4.256E-06	9.961E-05	9.907E-04	5.398E-03	1.720E-02	3.110E-02	2.682E-02	4.652E-03
22	7.165E-06	1.572E-04	1.451E-03	7.236E-03	2.062E-02	3.191E-02	2.078E-02	8.533E-04
23	1.173E-05	2.410E-04	2.063E-03	9.397E-03	2.384E-02	3.108E-02	1.422E-02	9.328E-05
24	1.872E-05	3.600E-04	2.854E-03	1.184E-02	2.655E-02	2.860E-02	8.125E-03	2.121E-03
25	2.913E-05	5.243E-04	3.845E-03	1.448E-02	2.851E-02	2.471E-02	3.388E-03	6.060E-03
26	4.431E-05	7.457E-04	5.051E-03	1.722E-02	2.948E-02	1.983E-02	6.235E-04	1.066E-02
27	6.593E-05	1.037E-03	6.477E-03	1.991E-02	2.932E-02	1.451E-02	6.385E-05	1.464E-02
28	9.609E-05	1.411E-03	8.116E-03	2.240E-02	2.800E-02	9.377E-03	1.531E-03	1.699E-02
29	1.373E-04	1.882E-03	9.946E-03	2.453E-02	2.558E-02	5.013E-03	4.492E-03	1.720E-02
30	1.926E-04	2.462E-03	1.193E-02	2.614E-02	2.225E-02	1.875E-03	8.185E-03	1.531E-02
31	2.655E-04	3.161E-03	1.402E-02	2.711E-02	1.829E-02	2.356E-04	1.178E-02	1.188E-02
32	3.598E-04	3.988E-03	1.614E-02	2.734E-02	1.405E-02	1.452E-04	1.453E-02	7.785E-03
33	4.799E-04	4.946E-03	1.822E-02	2.679E-02	9.884E-03	1.438E-03	1.594E-02	3.967E-03
34	6.304E-04	6.034E-03	2.017E-02	2.546E-02	6.157E-03	3.769E-03	1.579E-02	1.225E-03

Table V-3. (Continued)

a) FC factors based on quasi-Morse parameters valid for $0 \leq v'' \leq 9$[a] and Morse parameters for $0 \leq v' \leq 30$.[b]

v'\v"	8	9	10	11	12	13	14	15
0	5.007E-07	3.354E-06	1.907E-05	9.271E-05	3.870E-04	1.392E-03	4.320E-03	1.158E-02
1	6.285E-06	3.744E-05	1.870E-04	7.862E-04	2.787E-03	8.316E-03	2.078E-02	4.306E-02
2	4.031E-05	2.130E-04	9.302E-04	3.362E-03	1.001E-02	2.438E-02	4.767E-02	7.262E-02
3	1.758E-04	8.210E-04	3.119E-03	9.601E-03	2.369E-02	4.586E-02	6.695E-02	6.798E-02
4	5.854E-04	2.405E-03	7.891E-03	2.045E-02	4.091E-02	6.054E-02	6.050E-02	3.211E-02
5	1.583E-03	5.693E-03	1.598E-02	3.428E-02	5.392E-02	5.692E-02	3.202E-02	2.806E-03
6	3.615E-03	1.130E-02	2.679E-02	4.650E-02	5.465E-02	3.584E-02	5.642E-03	5.462E-03
7	7.147E-03	1.923E-02	3.792E-02	5.140E-02	4.127E-02	1.157E-02	1.339E-03	2.573E-02
8	1.245E-02	2.853E-02	4.567E-02	4.573E-02	2.068E-02	1.294E-04	1.591E-02	3.359E-02
9	1.935E-02	3.718E-02	4.669E-02	3.124E-02	4.319E-03	6.073E-03	2.954E-02	2.042E-02
10	2.704E-02	4.266E-02	3.984E-02	1.432E-02	2.908E-04	2.002E-02	2.758E-02	3.579E-03
11	3.413E-02	4.292E-02	2.716E-02	2.552E-03	8.053E-03	2.807E-02	1.339E-02	1.218E-03
12	3.896E-02	3.736E-02	1.322E-02	4.226E-04	1.961E-02	2.365E-02	1.494E-03	1.231E-02
13	4.009E-02	2.727E-02	3.104E-03	6.937E-03	2.578E-02	1.141E-02	1.807E-03	2.183E-02
14	3.690E-02	1.557E-02	3.568E-05	1.664E-02	2.248E-02	1.586E-03	1.142E-02	1.928E-02
15	2.984E-02	5.738E-03	3.947E-03	2.312E-02	1.268E-02	9.649E-04	1.964E-02	8.376E-03
16	2.048E-02	5.145E-04	1.174E-02	2.267E-02	3.287E-03	8.223E-03	1.888E-02	5.057E-04
17	1.106E-02	8.613E-04	1.895E-02	1.601E-02	2.147E-05	1.633E-02	1.052E-02	2.297E-03
18	3.794E-03	5.690E-03	2.198E-02	7.245E-03	3.846E-03	1.875E-02	2.167E-03	1.033E-02
19	2.495E-04	1.241E-02	1.960E-02	1.128E-03	1.111E-02	1.408E-02	2.684E-04	1.611E-02
20	8.265E-04	1.803E-02	1.325E-02	3.959E-04	1.655E-02	6.205E-03	5.201E-03	1.450E-02
21	4.716E-03	2.031E-02	6.031E-03	4.575E-03	1.677E-02	7.006E-04	1.203E-02	7.470E-03
22	1.022E-02	1.854E-02	1.082E-03	1.069E-02	1.201E-02	7.721E-04	1.512E-02	1.225E-03
23	1.532E-02	1.362E-02	1.812E-04	1.517E-02	5.411E-03	5.518E-03	1.242E-02	4.507E-04
24	1.836E-02	7.537E-03	3.131E-03	1.574E-02	7.931E-04	1.117E-02	6.289E-03	4.906E-03
25	1.846E-02	2.496E-03	8.105E-03	1.236E-02	3.677E-04	1.390E-02	1.167E-03	1.043E-02
26	1.574E-02	1.015E-04	1.264E-02	6.948E-03	3.776E-03	1.220E-02	2.208E-04	1.267E-02
27	1.117E-02	8.370E-04	1.477E-02	2.151E-03	8.658E-03	7.390E-03	3.473E-03	1.021E-02
28	6.180E-03	4.035E-03	1.373E-02	2.952E-05	1.219E-02	2.450E-03	8.281E-03	5.112E-03
29	2.180E-03	8.251E-03	1.015E-02	1.179E-03	1.259E-02	5.387E-05	1.139E-02	9.332E-04
30	1.587E-04	1.186E-02	5.573E-03	4.673E-03	9.859E-03	1.155E-03	1.098E-02	1.907E-04
31	4.413E-04	1.361E-02	1.781E-03	8.679E-03	5.529E-03	4.725E-03	7.540E-03	2.901E-03
32	2.672E-03	1.303E-02	4.859E-05	1.137E-02	1.707E-03	8.578E-03	3.215E-03	6.956E-03
33	5.995E-03	1.044E-02	7.552E-04	1.166E-02	2.196E-05	1.066E-02	3.855E-04	9.711E-03
34	9.344E-03	6.774E-03	3.361E-03	9.599E-03	9.596E-04	1.002E-02	3.472E-04	9.604E-03

[a] listed in Table V-2.

[b] listed in Table V-1.

Table V-3. (Continued)

b) FC factors based on quasi-Morse parameters for $9 \leq v' \leq 22$[a] and Morse parameters for $0 \leq v' \leq 30$.[b]

v'\v"	0	1	2	3	4	5	6	7
0	1.684E-17	1.634E-15	7.584E-14	2.240E-12	4.728E-11	7.584E-10	9.606E-09	9.853E-08
1	4.099E-16	3.717E-14	1.606E-12	4.392E-11	8.536E-10	1.253E-08	1.441E-07	1.331E-06
2	5.112E-15	4.335E-13	1.744E-11	4.419E-10	7.910E-09	1.062E-07	1.109E-06	9.217E-06
3	4.352E-14	3.454E-12	1.294E-10	3.039E-09	5.012E-08	6.158E-07	5.836E-06	4.358E-05
4	2.845E-13	2.114E-11	7.379E-10	1.607E-08	2.441E-07	2.742E-06	2.357E-05	1.579E-04
5	1.522E-12	1.059E-10	3.446E-09	6.955E-08	9.733E-07	9.998E-06	7.783E-05	4.670E-04
6	6.938E-12	4.523E-10	1.372E-08	2.567E-07	3.308E-06	3.105E-05	2.186E-04	1.172E-03
7	2.771E-11	1.693E-09	4.788E-08	8.305E-07	9.851E-06	8.438E-05	5.365E-04	2.561E-03
8	9.893E-11	5.664E-09	1.494E-07	2.402E-06	2.621E-05	2.047E-04	1.173E-03	4.967E-03
9	3.206E-10	1.721E-08	4.233E-07	6.305E-06	6.326E-05	4.498E-04	2.316E-03	8.665E-03
10	9.547E-10	4.804E-08	1.102E-06	1.520E-05	1.401E-04	9.054E-04	4.179E-03	1.373E-02
11	2.637E-09	1.244E-07	2.660E-06	3.398E-05	2.874E-04	1.685E-03	6.946E-03	1.990E-02
12	6.811E-09	3.013E-07	6.005E-06	7.097E-05	5.503E-04	2.920E-03	1.070E-02	2.652E-02
13	1.656E-08	6.868E-07	1.276E-05	1.394E-04	9.894E-04	4.740E-03	1.537E-02	3.257E-02
14	3.810E-08	1.482E-06	2.564E-05	2.589E-04	1.679E-03	7.241E-03	2.064E-02	3.689E-02
15	8.339E-08	3.040E-06	4.898E-05	4.566E-04	2.702E-03	1.045E-02	2.598E-02	3.848E-02
16	1.743E-07	5.957E-06	8.933F-05	7.678E-04	4.137E-03	1.429E-02	3.071E-02	3.675E-02
17	3.492E-07	1.118E-05	1.560E-04	1.235E-03	6.045E-03	1.855E-02	3.407E-02	3.181E-02
18	6.727E-07	2.019E-05	2.618E-04	1.907E-03	8.452E-03	2.291E-02	3.544E-02	2.449E-02
19	1.250E-06	3.513E-05	4.233E-04	2.832E-03	1.133E-02	2.695E-02	3.443E-02	1.618E-02
20	2.244E-06	5.908E-05	6.609E-04	4.054E-03	1.460E-02	3.019E-02	3.104E-02	8.475E-03
21	3.904E-06	9.624E-05	9.986E-04	5.606E-03	1.809E-02	3.220E-02	2.570E-02	2.834E-03
22	6.594E-06	1.521E-04	1.463E-03	7.500E-03	2.158E-02	3.264E-02	1.916E-02	1.721E-04
23	1.083E-05	2.338E-04	2.081E-03	9.723E-03	2.480E-02	3.136E-02	1.242E-02	6.665E-04
24	1.734E-05	3.499E-04	2.879E-03	1.223E-02	2.747E-02	2.842E-02	6.503E-03	3.747E-03
25	2.708E-05	5.106E-04	3.881E-03	1.493E-02	2.932E-02	2.411E-02	2.253E-03	8.281E-03
26	4.132E-05	7.277E-04	5.100E-03	1.772E-02	3.013E-02	1.891E-02	1.826E-04	1.289E-02
27	6.169E-05	1.014E-03	6.544E-03	2.045E-02	2.977E-02	1.343E-02	3.831E-04	1.633E-02
28	9.021E-05	1.383E-03	8.204E-03	2.297E-02	2.821E-02	8.305E-03	2.524E-03	1.775E-02
29	1.293E-04	1.848E-03	1.006E-02	2.510E-02	2.556E-02	4.118E-03	5.942E-03	1.688E-02
30	1.820E-04	2.423E-03	1.207E-02	2.670E-02	2.201E-02	1.296E-03	9.794E-03	1.406E-02
31	2.517E-04	3.117E-03	1.419E-02	2.762E-02	1.787E-02	5.839E-05	1.323E-02	1.006E-02
32	3.422E-04	3.940E-03	1.635E-02	2.778E-02	1.351E-02	3.942E-04	1.556E-02	5.868E-03
33	4.578E-04	4.896E-03	1.846E-02	2.715E-02	9.304E-03	2.072E-03	1.637E-02	2.418E-03
34	6.032E-04	5.985E-03	2.045E-02	2.573E-02	5.610E-03	4.688E-03	1.556E-02	3.951E-04

Table V-3. (Continued)

b) FC factors based on quasi-Morse parameters for $9 \leq v' \leq 22$[a] and Morse parameters for $0 \leq v' \leq 30$.[b]

v'\v"	8	9	10	11	12	13	14	15
0	8.328E-07	5.871E-06	3.482E-05	1.747E-04	7.443E-04	2.697E-03	8.310E-03	2.173E-02
1	1.002E-05	6.221E-05	3.201E-04	1.368E-03	4.853E-03	1.421E-02	3.400E-02	6.527E-02
2	6.178E-05	3.367E-04	1.496E-03	5.409E-03	1.578E-02	3.657E-02	6.539E-02	8.549E-02
3	2.594E-04	1.237E-03	4.720E-03	1.429E-02	3.367E-02	5.972E-02	7.452E-02	5.600E-02
4	8.325E-04	3.458E-03	1.124E-02	2.808E-02	5.206E-02	6.682E-02	5.041E-02	1.218E-02
5	2.173E-03	7.816E-03	2.141E-02	4.326E-02	6.050E-02	5.053E-02	1.523E-02	1.280E-03
6	4.792E-03	1.481E-02	3.369E-02	5.347E-02	5.249E-02	2.217E-02	5.922E-07	2.193E-02
7	9.154E-03	2.406E-02	4.456E-02	5.303E-02	3.168E-02	2.360E-03	1.144E-02	3.681E-02
8	1.541E-02	3.399E-02	4.979E-02	4.106E-02	1.026E-02	2.713E-03	2.919E-02	2.605E-02
9	2.313E-02	4.206E-02	4.662E-02	2.276E-02	1.828E-04	1.693E-02	3.163E-02	5.994E-03
10	3.119E-02	4.558E-02	3.553E-02	6.761E-03	4.722E-03	2.877E-02	1.759E-02	6.136E-04
11	3.792E-02	4.294E-02	2.050E-02	5.083E-05	1.704E-02	2.730E-02	2.895E-03	1.197E-02
12	4.155E-02	3.443E-02	7.224E-03	3.972E-03	2.623E-02	1.498E-02	1.104E-03	2.301E-02
13	4.085E-02	2.243E-02	4.392E-04	1.392E-02	2.547E-02	2.981E-03	1.088E-02	2.062E-02
14	3.561E-02	1.059E-02	1.689E-03	2.261E-02	1.609E-02	4.186E-04	2.034E-02	8.700E-03
15	2.687E-02	2.441E-03	8.788E-03	2.462E-02	5.249E-03	7.331E-03	2.012E-02	3.908E-04
16	1.671E-02	3.004E-05	1.717E-02	1.918E-02	6.775E-05	1.633E-02	1.125E-02	2.919E-03
17	7.599E-03	3.183E-03	2.230E-02	9.969E-03	2.844E-03	1.968E-02	2.235E-03	1.172E-02
18	1.672E-03	9.717E-03	2.177E-02	2.336E-03	1.031E-02	1.517E-02	3.499E-04	1.713E-02
19	3.570E-05	1.644E-02	1.620E-02	5.441E-05	1.666E-02	6.810E-03	5.834E-03	1.422E-02
20	2.477E-03	2.047E-02	8.513E-03	3.458E-03	1.768E-02	7.975E-04	1.298E-02	6.309E-03
21	7.602E-03	2.032E-02	2.285E-03	9.771E-03	1.311E-02	7.991E-04	1.569E-02	5.470E-04
22	1.335E-02	1.628E-02	1.131E-08	1.506E-02	6.146E-03	5.845E-03	1.217E-02	1.207E-03
23	1.770E-02	1.011E-02	2.072E-03	1.645E-02	1.012E-03	1.175E-02	5.518E-03	6.732E-03
24	1.928E-02	4.211E-03	6.936E-03	1.348E-02	2.987E-04	1.438E-02	6.711E-04	1.198E-02
25	1.772E-02	6.046E-04	1.201E-02	7.944E-03	3.757E-03	1.225E-02	6.146E-04	1.278E-02
26	1.368E-02	2.617E-04	1.494E-02	2.695E-03	8.868E-03	7.019E-03	4.686E-03	8.859E-03
27	8.505E-03	2.864E-03	1.458E-02	9.767E-05	1.255E-02	2.017E-03	9.602E-03	3.377E-03
28	3.763E-03	7.082E-03	1.128E-02	1.128E-02	9.869E-04	9.469E-07	1.199E-02	1.714E-04
29	7.320E-04	1.117E-02	6.575E-03	4.496E-03	9.920E-03	1.687E-03	1.049E-02	1.033E-03
30	6.124E-05	1.364E-02	2.366E-03	8.691E-03	5.361E-03	5.660E-03	6.300E-03	4.854E-03
31	1.652E-03	1.371E-02	1.603E-04	1.157E-02	1.493E-03	9.458E-03	2.032E-03	8.794E-03
32	4.774E-03	1.150E-02	5.313E-04	1.195E-02	5.710E-07	1.102E-02	3.057E-05	1.031E-02
33	8.345E-03	7.873E-03	3.030E-03	9.813E-03	1.269E-03	9.676E-03	1.096E-03	8.628E-03
34	1.128E-02	4.045E-03	6.486E-03	6.200E-03	4.393E-03	6.291E-03	4.280E-03	4.958E-03

Table V-3. (Continued)

b) FC factors based on quasi-Morse parameters for $9 \leq v' \leq 22$[a] and Morse parameters for $0 \leq v' \leq 10$.[b]

v'\v"	16	17	18	19	20	21	22	23
0	4.807E-02	8.942E-02	1.389E-01	1.781E-01	1.861E-01	1.553E-01	1.008E-01	4.896E-02
1	9.741E-02	1.064E-01	7.389E-02	1.979E-02	2.139E-03	5.709E-02	1.420E-01	1.745E-01
2	7.268E-02	2.815E-02	7.850E-08	3.120E-02	7.837E-02	5.908E-02	4.048E-03	3.288E-02
3	1.446E-02	2.512E-03	4.057E-02	5.958E-02	1.788E-02	5.905E-03	6.165E-02	5.944E-02
4	3.087E-03	3.799E-02	4.682E-02	7.582E-03	1.320E-02	5.381E-02	2.257E-02	6.353E-03
5	3.118E-02	4.174E-02	6.712E-03	1.225E-02	4.475E-02	1.304E-02	1.096E-02	5.047E-02
6	3.988E-02	1.021E-02	7.099E-03	3.835E-02	1.325E-02	8.338E-03	4.101E-02	5.867E-03
7	1.731E-02	1.686E-03	3.139E-02	1.820E-02	3.151E-03	3.480E-02	8.104E-03	1.632E-02
8	2.343E-04	2.123E-02	2.507E-02	2.010E-05	2.706E-02	1.443E-02	7.306E-03	3.153E-02
9	8.966E-03	2.892E-02	3.247E-03	1.559E-02	2.248E-02	7.055E-04	2.845E-02	3.967E-03
10	2.442E-02	1.333E-02	3.906E-03	2.615E-02	1.879E-03	1.904E-02	1.323E-02	7.886E-03
11	2.336E-02	2.768E-04	1.967E-02	1.183E-02	6.012E-03	2.213E-02	1.738E-04	2.417E-02
12	8.851E-03	6.413E-03	2.157E-02	3.727E-05	2.067E-02	4.730E-03	1.426E-02	1.097E-02
13	5.355E-05	1.883E-02	7.972E-03	8.150E-03	1.662E-02	1.822E-03	2.013E-02	1.067E-04
14	5.628E-03	1.916E-02	1.759E-07	1.893E-02	2.675E-03	1.472E-02	6.425E-03	1.167E-02
15	1.611E-02	8.094E-03	6.870E-03	1.484E-02	1.879E-03	1.737E-02	3.979E-04	1.785E-02
16	1.840E-02	2.019E-04	1.637E-02	3.282E-03	1.246E-02	6.102E-03	1.029E-02	6.895E-03
17	1.067E-02	3.705E-03	1.531E-02	6.217E-04	1.626E-02	5.023E-05	1.609E-02	4.820E-05
18	1.882E-03	1.246E-02	5.951E-03	8.470E-03	8.233E-03	6.877E-03	8.337E-03	7.484E-03
19	6.097E-04	1.568E-02	6.708E-05	1.480E-02	4.644E-04	1.418E-02	3.219E-04	1.425E-02
20	6.718E-03	1.029E-02	3.473E-03	1.160E-02	2.597E-03	1.119E-02	3.351E-03	9.276E-03
21	1.316E-02	2.569E-03	1.081E-02	3.515E-03	1.017E-02	2.856E-03	1.110E-02	1.133E-03
22	1.373E-02	1.159E-04	1.344E-02	2.330E-05	1.290E-02	2.207E-04	1.194E-02	1.491E-03
23	8.363E-03	4.343E-03	8.958E-03	4.057E-03	7.885E-03	5.452E-03	5.299E-03	8.321E-03
24	2.120E-03	1.030E-02	2.399E-03	1.014E-02	1.435E-03	1.100E-02	1.668E-04	1.136E-02
25	5.203E-05	1.224E-02	4.792E-05	1.156E-02	4.603E-04	1.016E-02	2.286E-03	6.889E-03
26	3.153E-03	8.753E-03	3.376E-03	7.246E-03	5.094E-03	4.388E-03	8.031E-03	1.050E-03
27	8.270E-03	3.174E-03	8.573E-03	1.755E-03	9.788E-03	2.002E-04	1.026E-02	6.752E-04
28	1.118E-02	7.672E-05	1.077E-02	9.119E-05	9.764E-03	1.534E-03	6.746E-03	5.327E-03
29	9.853E-03	1.469E-03	8.294E-03	3.149E-03	5.395E-03	6.260E-03	1.635E-03	9.103E-03
30	5.542E-03	5.687E-03	3.510E-03	7.640E-03	9.780E-04	9.294E-03	1.058E-04	7.908E-03
31	1.386E-03	9.217E-03	2.726E-04	9.540E-03	2.650E-04	7.850E-03	3.106E-03	3.352E-03
32	2.359E-05	9.507E-03	7.606E-04	7.466E-03	3.346E-03	3.565E-03	7.176E-03	1.643E-04
33	1.958E-03	6.577E-03	4.131E-03	3.326E-03	7.173E-03	3.324E-04	8.358E-03	1.116E-03
34	5.568E-03	2.608E-03	7.601E-03	3.472E-04	8.512E-03	6.473E-04	5.790E-03	4.772E-03

Table V-3. (Continued)

b) FC factors based on quasi-Morse parameters for $9 \leq v'' \leq 22$[a] and Morse parameters for $0 \leq v' \leq 10$.[b]

v'\v"	24	25	26	27	28	29	30
0	1.670E-02	3.567E-03	3.640E-04	4.505E-06	2.336E-06	6.048E-07	4.035E-10
1	1.299E-01	5.967E-02	1.548E-02	1.678E-03	8.473E-06	2.278E-05	3.753E-06
2	1.399E-01	1.836E-01	1.180E-01	3.723E-02	4.159E-03	5.672E-07	1.105E-04
3	1.508E-03	6.019E-02	1.844E-01	1.734E-01	6.629E-02	7.279E-03	4.214E-05
4	6.489E-02	3.631E-02	9.115E-03	1.486E-01	2.150E-01	9.821E-02	9.871E-03
5	9.953E-03	2.406E-02	6.259E-02	1.081E-03	1.036E-01	2.421E-01	1.287E-01
6	2.351E-02	3.965E-02	5.074E-04	5.562E-02	1.477E-02	6.689E-02	2.598E-01
7	3.280E-02	4.489E-04	4.258E-02	8.114E-03	3.193E-02	2.870E-02	4.340E-02
8	1.589E-04	3.205E-02	9.240E-03	2.283E-02	2.599E-02	1.123E-02	3.371E-02
9	2.065E-02	1.552E-02	1.106E-02	2.648E-02	4.993E-03	3.668E-02	1.227E-03
10	2.300E-02	1.778E-03	2.808E-02	8.269E-05	3.115E-02	5.268E-05	3.682E-02
11	1.150E-03	2.260E-02	3.814E-03	2.166E-02	5.360E-03	2.322E-02	4.659E-03
12	9.317E-03	1.495E-02	7.302E-03	1.651E-02	8.037E-03	1.583E-02	1.183E-02
13	2.086E-02	1.392E-05	2.131E-02	1.600E-08	2.207E-02	4.785E-04	2.193E-02
14	8.306E-03	1.110E-02	7.872E-03	1.308E-02	5.241E-03	1.725E-02	1.450E-03
15	2.086E-04	1.779E-02	6.840E-04	1.692E-02	2.890E-03	1.360E-02	8.619E-03
16	1.045E-02	5.595E-03	1.271E-02	2.684E-03	1.606E-02	1.153E-04	1.730E-02
17	1.577E-02	5.383E-04	1.454E-02	2.901E-03	1.068E-02	8.585E-03	3.980E-03
18	6.505E-03	1.003E-02	3.136E-03	1.357E-02	1.812E-04	1.480E-02	2.034E-03
19	1.668E-06	1.389E-02	1.218E-03	1.097E-02	5.956E-03	4.623E-03	1.260E-02
20	5.876E-03	5.588E-03	1.004E-02	1.227E-03	1.318E-02	5.491E-04	1.008E-02
21	1.254E-02	1.225E-06	1.211E-02	2.311E-03	7.259E-03	8.797E-03	7.679E-04
22	9.322E-03	5.074E-03	4.382E-03	1.017E-02	1.563E-04	1.135E-02	3.075E-03
23	1.790E-03	1.117E-02	2.491E-05	1.028E-02	3.762E-03	3.843E-03	1.035E-02
24	6.347E-04	8.849E-03	4.807E-03	3.066E-03	1.013E-02	1.125E-04	8.320E-03
25	6.256E-03	2.100E-03	1.014E-02	1.413E-04	8.321E-03	5.362E-03	1.284E-03
26	1.026E-02	2.864E-04	8.095E-03	4.897E-03	1.808E-03	9.667E-03	1.084E-03
27	7.603E-03	4.881E-03	2.077E-03	9.331E-03	4.380E-04	6.236E-03	6.775E-03
28	2.023E-03	9.113E-03	1.669E-04	7.177E-03	5.217E-03	7.776E-04	8.630E-03
29	8.597E-05	7.699E-03	4.046E-03	1.804E-03	8.635E-03	9.795E-04	4.135E-03
30	3.343E-03	2.734E-03	3.129E-03	1.524E-04	6.146E-03	5.645E-03	1.402E-04
31	7.547E-03	6.561E-06	7.433E-03	3.606E-03	1.377E-03	7.926E-03	1.777E-03
32	8.081E-03	2.060E-03	3.107E-03	7.362E-03	2.102E-04	5.028E-03	6.0515-03
33	4.665E-03	6.084E-03	1.038E-04	6.979E-03	3.447E-03	8.910E-04	7.103E-03
34	8.899E-04	7.676E-03	1.298E-03	3.181E-03	6.788E-03	3.520E-04	3.856E-03

Table V-3. (Continued)

b) FC factors based on quasi-Morse parameters for $9 \leq v' \leq 22$[a] and Morse parameters for $0 \leq v' \leq 10$.[b]

v'\v"	31	32	33	34	35	36	37
0	1.417E-08	6.271E-11	3.887E-10	4.598E-09	9.973E-08	2.104E-06	6.270E-05
1	1.002E-07	1.401E-07	7.924E-10	1.752E-09	5.080E-09	3.339E-09	9.215E-08
2	1.045E-05	1.534E-06	5.716E-07	5.020E-08	1.219E-08	8.335E-09	1.659E-06
3	3.570E-04	1.456E-05	1.016E-05	1.115E-06	4.947E-07	1.832E-08	1.850E-08
4	4.298E-04	8.540E-04	5.325E-06	4.044E-05	5.835E-07	2.530E-06	1.616E-07
5	1.056E-02	1.869E-03	1.569E-03	9.152E-06	1.067E-04	8.470E-07	7.848E-06
6	1.539E-01	8.453E-03	5.485E-03	2.178E-03	1.895E-04	1.858E-04	2.264E-05
7	2.747E-01	1.704E-01	4.016E-03	1.238E-02	2.076E-03	9.193E-04	1.800E-04
8	3.141E-02	2.911E-01	1.740E-01	2.057E-04	2.249E-02	9.359E-04	2.561E-03
9	2.998E-02	2.803E-02	3.103E-01	1.604E-01	3.127E-03	3.290E-02	9.322E-06
10	6.856E-04	2.121E-02	3.173E-02	3.296E-01	1.270E-01	2.079E-02	3.725E-02
11	3.075E-02	5.844E-03	1.126E-02	4.265E-02	3.411E-01	7.770E-02	5.802E-02
12	1.172E-02	2.345E-02	1.402E-02	3.323E-03	6.125E-02	3.324E-01	2.692E-02
13	3.625E-03	1.667E-02	1.780E-02	2.444E-02	5.004E-06	8.575E-02	2.905E-01
14	2.161E-02	2.412E-04	1.812E-02	1.487E-02	3.794E-02	3.275E-03	1.093E-01
15	6.716E-03	1.737E-02	4.632E-04	1.649E-02	1.505E-02	5.613E-02	1.326E-02
16	2.251E-03	1.180E-02	1.220E-02	2.580E-03	1.270E-02	1.912E-02	8.020E-02
17	1.537E-02	2.371E-05	1.460E-02	7.933E-03	5.532E-03	7.746E-03	2.895E-02
18	9.408E-03	1.059E-02	9.004E-04	1.500E-02	5.141E-03	9.150E-03	2.860E-03
19	5.204E-06	1.277E-02	5.824E-03	3.126E-03	1.372E-02	3.760E-03	1.410E-02
20	7.315E-03	1.725E-03	1.324E-02	2.479E-03	5.444E-03	1.149E-02	3.658E-03
21	1.227E-02	2.667E-03	4.855E-03	1.168E-02	7.136E-04	7.350E-03	8.721E-03
22	4.423E-03	1.086E-02	3.258E-04	7.587E-03	9.288E-03	7.751E-05	8.921E-03
23	1.631E-04	8.083E-03	7.618E-03	1.197E-04	9.192E-03	6.895E-03	9.406E-06
24	6.272E-03	6.427E-04	9.862E-03	4.329E-03	1.126E-03	9.722E-03	4.885E-03
25	9.933E-03	2.329E-03	2.968E-03	9.644E-03	1.935E-03	2.469E-03	9.567E-03
26	4.803E-03	8.437E-03	2.667E-04	5.427E-03	8.188E-03	5.970E-04	3.608E-03
27	6.666E-05	7.636E-03	5.469E-03	1.423E-04	7.070E-03	6.327E-03	6.913E-05
28	2.786E-03	1.785E-03	8.430E-03	2.667E-03	1.180E-03	7.711E-03	4.610E-03
29	7.608E-03	3.597E-04	4.349E-03	7.442E-03	8.486E-04	2.556E-03	7.578E-03
30	6.995E-03	4.673E-03	1.550E-04	6.266E-03	5.584E-03	8.096E-05	3.748E-03
31	2.230E-03	7.544E-03	1.859E-03	1.428E-03	7.000E-03	3.669E-03	5.650E-05
32	2.516E-05	4.934E-03	6.079E-03	2.885E-04	3.119E-03	6.716E-03	2.139E-03
33	2.765E-03	7.917E-04	6.485E-03	3.818E-03	4.236E-05	4.497E-03	5.844E-03
34	6.289E-03	4.769E-04	2.801E-03	6.450E-03	1.816E-03	6.551E-04	5.284E-03

Table V-3. (Continued)

b) FC factors based on quasi-Morse parameters for $9 \leq v'' \leq 22$[a] and Morse parameters for $0 \leq v' \leq 10$.[b]

v'\v"	38	39	40	41	42	43	44
0	3.643E-03	1.025E-01	8.315E+00	3.424E+02	2.061E+04	2.211E+05	3.992E+06
1	1.328E-05	2.869E-03	9.739E-01	7.788E+01	5.401E+03	1.408E+05	4.335E+06
2	1.043E-04	1.533E-03	2.881E-01	2.840E+01	2.127E+03	7.116E+04	2.806E+06
3	1.511E-06	2.199E-04	6.519E-02	8.605E+00	7.221E+02	3.286E+04	1.550E+06
4	5.959E-06	4.037E-05	1.451E-02	2.543E+00	2.338E+02	1.393E+04	7.602E+05
5	2.255E-07	1.512E-05	3.628E-03	7.761E-01	7.667E+01	5.587E+03	3.455E+05
6	7.844E-06	1.261E-05	7.555E-04	2.127E-01	2.356E+01	2.150E+03	1.480E+05
7	1.268E-04	1.063E-06	3.397E-04	6.232E-02	7.295E+00	7.979E+02	6.069E+04
8	3.694E-05	3.325E-04	8.645E-05	1.840E-02	2.175E+00	2.869E+02	2.391E+04
9	4.694E-03	1.362E-04	3.635E-04	6.565E-03	6.521E-01	1.007E+02	9.149E+03
10	3.171E-03	5.435E-03	1.488E-03	3.901E-04	2.097E-01	3.440E+01	3.399E+03
11	2.898E-02	1.496E-02	2.954E-03	2.745E-03	5.715E-02	1.178E+01	1.234E+03
12	1.076E-01	1.028E-02	3.353E-02	8.538E-05	1.373E-03	3.983E+00	4.397E+02
13	2.683E-04	1.443E-01	2.260E-04	4.579E-02	3.245E-04	1.088E+00	1.550E+02
14	2.113E-01	2.201E-02	1.351E-01	2.650E-02	4.235E-02	2.090E-01	5.250E+01
15	1.196E-01	1.112E-01	8.972E-02	7.297E-02	9.635E-02	1.638E-01	1.594E+01
16	2.607E-02	1.039E-01	2.841E-02	1.560E-01	7.386E-03	2.993E-01	5.313E+00
17	1.086E-01	3.298E-02	6.267E-02	5.043E-05	1.537E-01	5.075E-02	2.805E+00
18	4.707E-02	1.335E-01	2.532E-02	1.797E-02	2.141E-02	5.259E-02	1.161E+00
19	6.468E-05	7.447E-02	1.397E-01	6.883E-03	1.262E-06	3.042E-02	1.170E-01
20	2.182E-02	2.264E-03	1.058E-01	1.120E-01	1.683E-03	7.282E-03	8.754E-03
21	5.167E-03	3.449E-02	1.167E-02	1.252E-01	5.481E-02	2.991E-02	3.807E-04
22	5.598E-03	9.654E-03	5.407E-02	2.572E-02	1.125E-01	6.655E-03	4.133E-02
23	1.063E-02	2.407E-03	1.995E-02	7.930E-02	3.378E-02	6.549E-02	3.200E-03
24	6.596E-05	1.332E-02	1.667E-04	3.952E-02	1.006E-01	2.428E-02	1.935E-02
25	3.302E-03	2.509E-05	1.837E-02	1.276E-03	6.837E-02	9.942E-02	5.310E-03
26	9.174E-03	2.023E-03	7.479E-05	2.801E-02	8.912E-03	9.583E-02	6.521E-02
27	4.302E-03	8.962E-03	9.156E-04	1.308E-03	4.501E-02	2.308E-02	1.004E-01
28	1.722E-05	4.465E-03	9.391E-03	9.427E-05	6.485E-03	7.006E-02	3.484E-02
29	3.279E-03	1.806E-04	4.041E-03	1.116E-02	4.465E-04	1.996E-02	9.553E-02
30	7.005E-03	2.377E-03	4.271E-04	2.958E-03	1.562E-02	4.301E-03	4.393E-02
31	4.551E-03	6.256E-03	1.870E-03	7.692E-04	1.316E-03	2.529E-02	1.481E-02
32	4.040E-04	4.972E-03	5.473E-03	1.747E-03	1.421E-03	2.376E-05	4.371E-02
33	1.110E-03	8.386E-04	5.121E-03	4.665E-03	2.138E-03	3.023E-03	1.919E-03
34	4.787E-03	5.087E-04	1.189E-03	5.152E-03	3.718E-03	3.568E-03	7.184E-03

[a] listed in Table V-2.

[b] listed in Table V-1.

overlap integrals for the less steep side. For transitions with high v' these bands are actually blue shaded, and are the most intense banded features of the chemiluminescence spectrum. The reversal in shading is due to the change of sign of the difference of the rotational constants $B_{v'}$ and $B_{v''}$ for the two states. For the red shaded bands $B_{v'}<B_{v''}$. Since the rotational constant is proportional to the average value of $\frac{1}{r^2}$ for that vibrational level, this is expected since $r_e'>r_e''$. For high v" that soft potential means that the HgCl molecule spends most of its time with the atoms widely separated and $\frac{1}{r^2}$ is smaller than for low v". Thus $B_{v'}>B_{v''}$ and blue shaded bands result. These blue shaded bands have not been used in determination of the vibrational distribution because of the uncertainty in knowledge of the shape of the potential curve for the ground state at high v". The number of blue shaded bands which appear is limited by the fact that many transitions from high v' will radiate to the adjoining dissociation continuum of the ground state. We have made no attempt to calculate the overlap integrals for these discrete to continuous transitions.

Because the HgCl potential curves are only approximately known and the internuclear separations are a sophisticated guess at best, it is important to estimate the uncertainty introduced in using them for calculation of vibrational populations. The overlap integrals are most sensitive to small changes in the relative internuclear separation of the two electronic states. As the relative internuclear separation is varied the Franck-Condon envelope and the Fortrat parabola

change such that emission from one v' takes place to a different range of v" states. The summed overlap integrals for comparable widths (v',Δv"), for different relative internuclear separations, ought to be fairly constant for each v'. Figure V-5 shows that this is true for HgCl. The overlap integrals for v'=0 and v'=15 are shown as a function of v" for r_e'=3.12Å and several choices of r_e". The increment in r_e" from the somewhat arbitrarily chosen value of 2.50Å is 0.25Å, which is larger than the uncertainty of our estimate. For v'=0, the summed overlap integrals agree with each other, although the predicted transitions occur to smaller v" as r_e" is increased. For v'=15 some of the FC factors have appreciable value at v" higher than the initial envelope, but it is important to note that the envelope has constant width Δv" and the summed FC factors for the envelope agree to within ten percent. This means that even though the potential curves are only approximately correct, the summed overlap integrals can be used with some confidence to calculate vibrational populations, as long as reasonable matching occurs between the observed and calculated Franck-Condon envelopes.

D. Results of the Spectroscopic Studies for $Hg^* + Cl_2$

1. HgCl ($B^2\Sigma^+ \rightarrow X^2\Sigma^+$) Spectra from the Irradiated Flow System

The most intense emission which accompanies the reaction of Hg^* with Cl_2 comes from the blue shaded bands of HgCl (B→X) which originate in high v'. The short wavelength onset of the chemiluminescence at 3550Å corresponds to red shaded bands which originate in the same v'

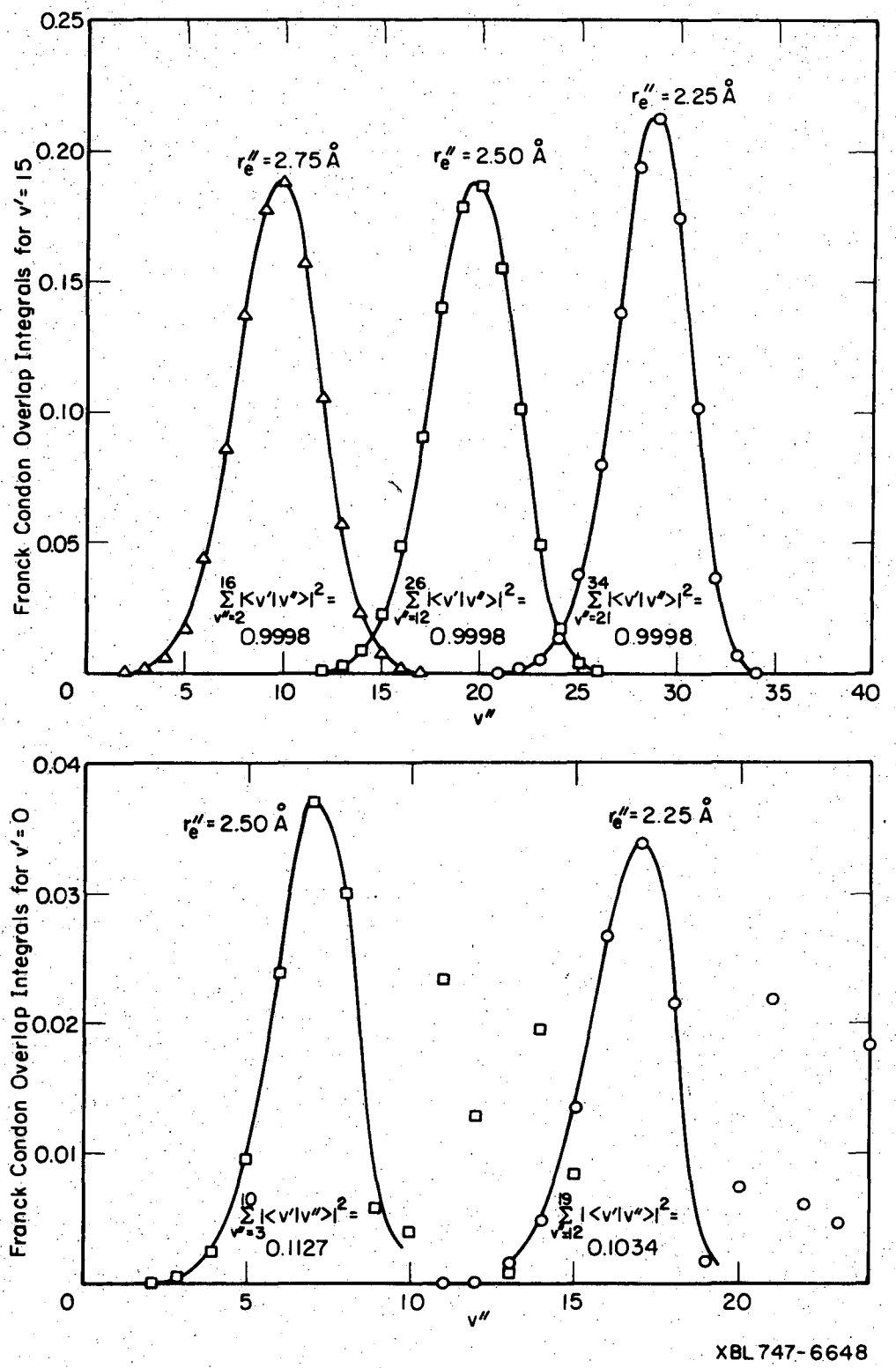

Fig. V-5. Franck-Condon overlap integrals for r_e'=3.12Å and several values of r_e'', for v'=15 and v'=0.

levels ($v' \leqslant 29$). The difference in observed intensity parallels the order of magnitude difference in overlap integrals which can be seen in Table V-3. Since such high vibrational levels are populated in HgCl, a good check on the proposed mechanism to explain their origin is observation of the change in the emission spectrum as a large amount of inert carrier gas is added to the flow system. If these vibrational levels have been populated in the bimolecular collision between Hg* and Cl_2 the addition of a buffer gas will cause relaxation to the thermal vibrational distribution, without quenching of the electronic excitation. The HgCl* emission spectrum will reflect the change in vibrational distribution.

Figure V-6 presents HgCl ($B \rightarrow X$) spectra which have been obtained by photoelectric scans of the light emission from the flow tube between 4800Å and 5670Å. The emission below 4800Å was scanned and analyzed but it is not shown in this figure. The upper part of each section of the figure shows the spectrum recorded with the Hg flow rate at 6.0×10^{15} atoms/sec and with chlorine pressure at 0.29 Torr in the reaction vessel. The lower part of each section shows the light emission present when helium at 200 Torr flowed through the irradiated system, with Hg flow rate at 3.0×10^{16} atoms/sec and chlorine partial pressure at the monitoring point at 1.0 Torr. For these scans the reaction vessel axis was aligned to be coincident with the spectrometer axis as described in section II-F. Scan conditions are listed in Table II-2. The time normalized spectra have been corrected for the response of the detection system according to Eq. (II-15). The relative intensity scales are

Fig. V-6(a,b,c). Photoelectric scans of the chemiluminescent emission, corrected for the response of the detection system. The upper part of each section of the figure shows the HgCl(B→X) emission from $Hg(^3P_1)$ + Cl_2 with no buffer gas. The lower part shows the emission with 200 Torr of helium added to the irradiated system. Wieland's assignments of v',v" from reference 1 are included in parentheses. Bracketed values, [v',v"] refer to possible new assignments. Asterisks refer to (v',v") for HgCl.[37]

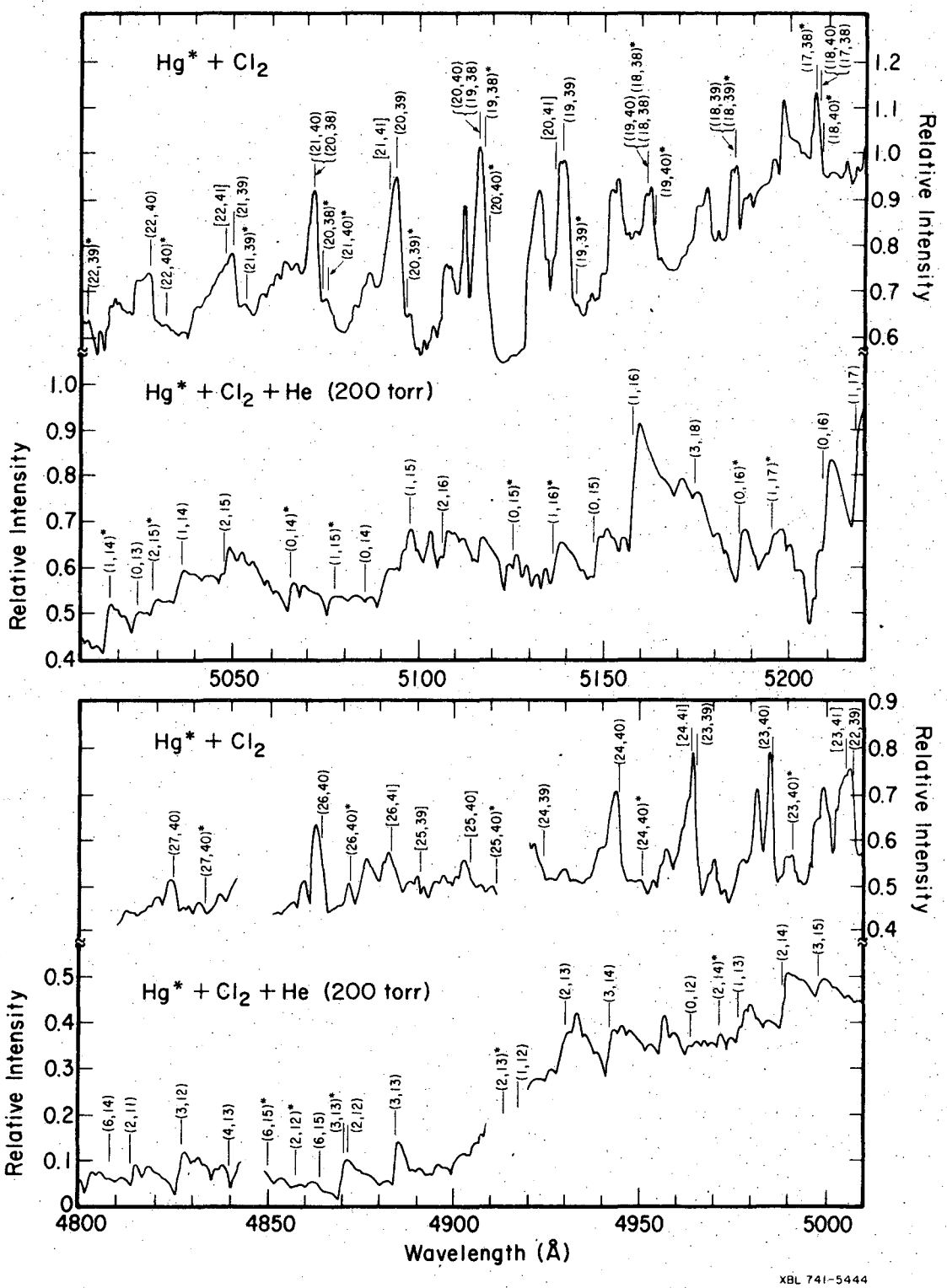
Hg* + Cl2
Hg* + Cl2 + He (200 torr)
Relative Intensity
Wavelength (Å)
XBL 741-5444

Fig. V-6(a).

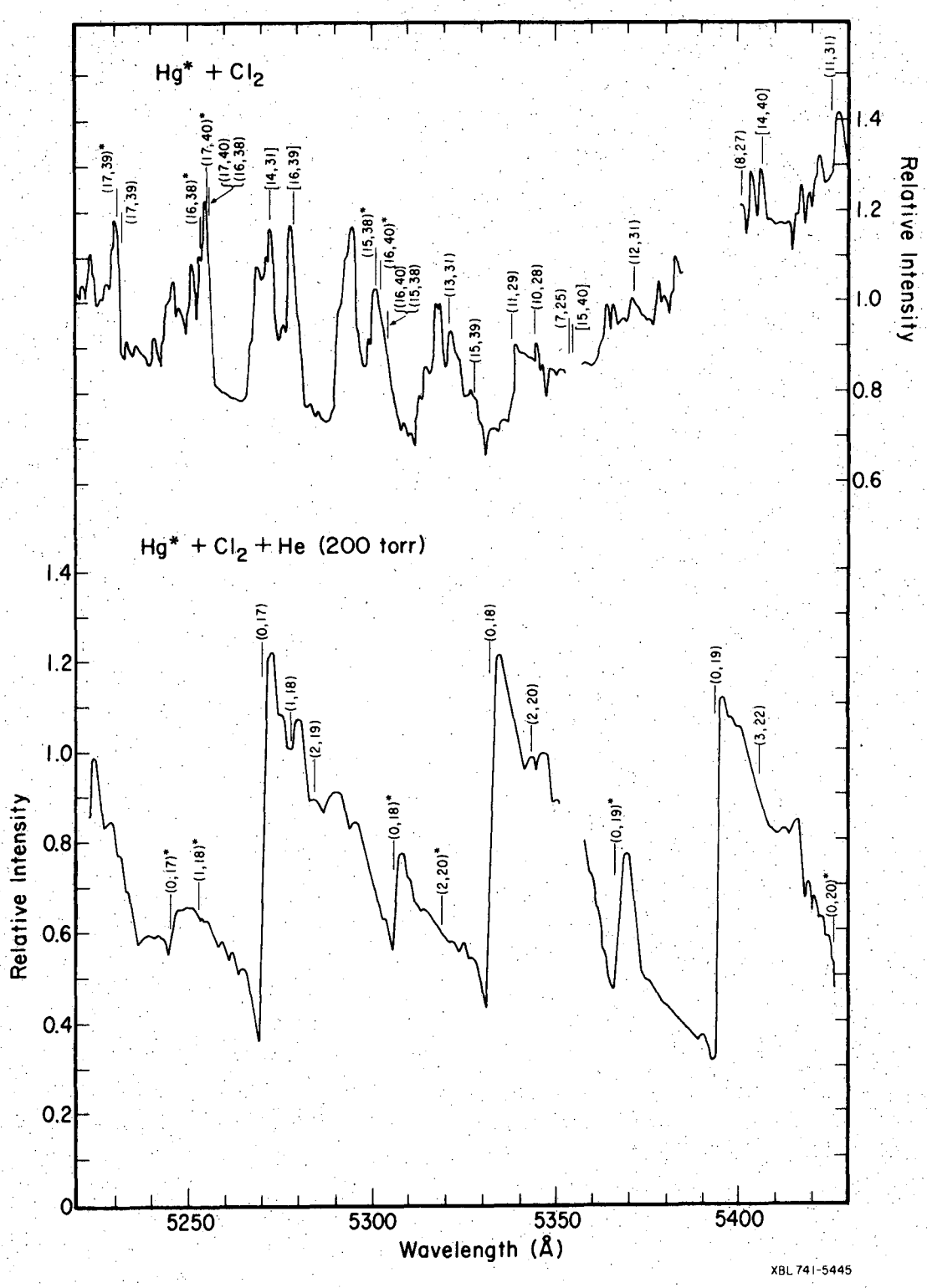
Hg* + Cl2
Hg* + Cl2 + He (200 torr)
Relative Intensity
Wavelength (Å)
5250
5300
5350
5400
0
0.2
0.4
0.6
0.8
1.0
1.2
1.4
(17,39)*
(17,39)
(16,38)*
(17,40)*
(17,40)
(16,38)
(14,31)
(16,39)
(15,38)*
(16,40)*
(16,40)
(15,38)
(13,31)
(15,39)
(11,29)
(10,28)
(7,25)
(15,40)
(12,31)
(8,27)
(14,40)
(11,31)
(0,17)*
(1,18)*
(0,17)
(1,18)
(2,19)
(0,18)*
(2,20)*
(0,18)
(2,20)
(0,19)*
(0,19)
(3,22)
(0,20)*
XBL 741-5445

Fig. V-6(b).

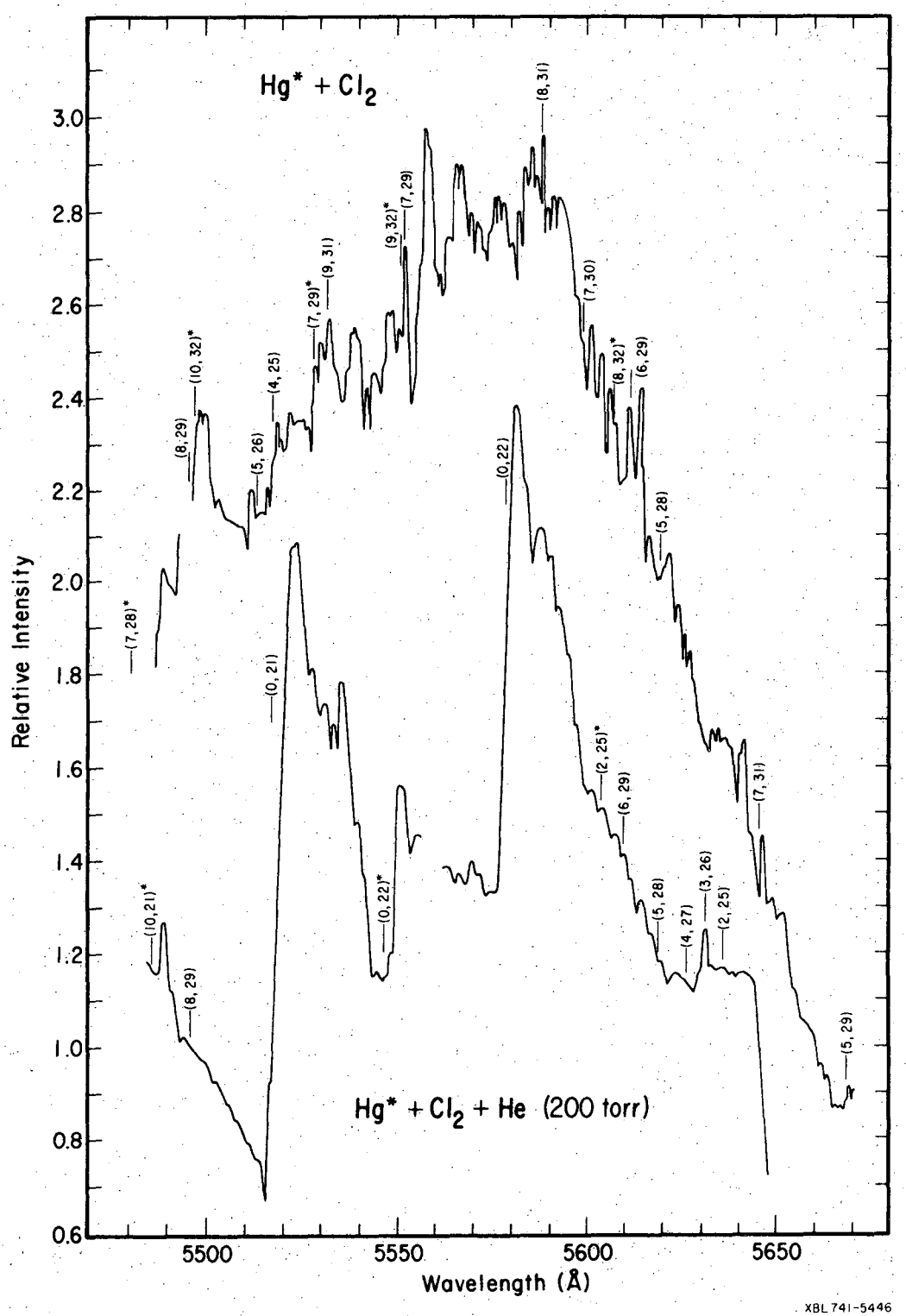
Hg* + Cl2
Hg* + Cl2 + He (200 torr)
Relative Intensity
Wavelength (Å)
3.0
2.8
2.6
2.4
2.2
2.0
1.8
1.6
1.4
1.2
1.0
0.8
0.6
5500
5550
5600
5650
(7, 28)*
(10, 21)*
(8, 29)
(0, 21)
(10, 32)*
(5, 26)
(4, 25)
(7, 29)*
(9, 31)
(9, 32)*
(7, 29)
(8, 31)
(7, 30)
(8, 32)*
(6, 29)
(5, 28)
(0, 22)
(0, 22)*
(2, 25)*
(6, 29)
(5, 28)
(4, 27)
(3, 26)
(2, 25)
(7, 31)
(5, 29)
XBL 741-5446

Fig. V-6(c).

continuous from one section of the figure to the next, but the reader is cautioned to observe the generally different ordinate origins for the spectra with and without helium present. The spectra have been presented in this way to emphasize their different appearance. Most of the main features of the upper curves can be assigned to the blue shaded bands of HgCl as indicated on the figure. Wieland's band edge assignments are indicated in parentheses for both spectra, with the v' value given first. Asterisks refer to band assignments for HgCl.[37] The heavy isotope of chlorine accounts for about one fourth of the HgCl* emission.[20] Several new blue shaded bands are indicated in brackets, for example, [25,40]. Extensive vibrational relaxation occurs with 200 Torr of helium; exclusively red-shaded bands originating in low v' are seen. The v'=0 progression is especially predominant. There are no common features to these two spectra, except for the intensity maxima at 5580-5590Å. The short wavelength cut off with helium present occurs at about 4750Å, but with no quenching gas present the HgCl (B→X) system extends to 3550Å with approximately constant intensity from 3800Å to 4800Å. A tabulation of the observed intensities of the red shaded bands for both scan conditions is included in Table V-4 and Table V-5 with work on the vibrational distributions.

Emission spectra were also obtained for Hg* + Cl_2 with helium pressure at 50 and 100 Torr, and with nitrogen at 10 Torr. With 50 Torr of helium the spectrum contains both the blue shaded bands which are characteristic of high v' population, and the simpler appearing red

shaded sequences originating in low v'. With 100 Torr of helium the blue shaded bands are entirely absent in the emission, and the photoelectric traces look qualitatively similar to those obtained with 200 Torr of helium.

Because molecular nitrogen causes efficient spin-orbit relaxation of $Hg(^3P_1)$,[29] a high concentration of the metastable $Hg(^3P_0)$ was present in the $Hg^* + Cl_2 + N_2$ studies. The presence of $Hg(^3P_0)$ was confirmed by monitoring the absorption of the 4078Å light of a low pressure mercury lamp along the axis of the vessel as the nitrogen concentration was varied. This radiation causes the excitation $Hg(6^3P_0 - 7^3S_1)$. Because the bimolecular reaction of $Hg(^3P_0)$ with Cl_2 is exoergic by 0.32 eV, compared to 0.53 eV for $Hg(^3P_1) + Cl_2$, only about 14 vibrational levels of the B state could be populated. At this pressure of nitrogen some collisional relaxation of the vibrational energy of HgCl* is expected, but the emission spectrum should still contain some evidence about the original vibrational manifold. The HgCl(B→X) emission shows primarily the red shaded structure typical of population of low v' states; however, the intensity of emission features originating in $v' \leq 12$ is strong, in addition to the characteristic emission from v'=0 and 1. The blue shaded bands originating in $v' \geq 15$ are present but are very weak compared to the dominant red shaded bands, which also have the largest Franck-Condon factors in this region. No attempt was made to extract the original vibrational distribution for the reaction of $Hg(^3P_0)$ with Cl_2. What is relevant here is the qualitative observation that the metastable specie reacts with chlorine in a manner which is analogous to the $Hg(^3P_1)+Cl_2$ process.

The appearance of the spectra is worthy of further comment. In both cases but especially when no helium is present, the band structure appears to be superimposed on a continuum (or unresolved discrete spectrum). For the region below 4800Å the spectra with no helium is at most one third discrete emission, except at the short wavelength limit where only bands can be seen. In the region of the maximum intensity the vibrationally relaxed spectrum, although simplified substantially, still shows sequences of bands ($\Delta v = v' - v''$ constant) which are poorly resolved. In the non-relaxed spectrum much overlapping of discrete features is apparent and can be seen by the non-uniform widths of the bands. The narrowest bands with a half width of ≤ 2Å, (23,40) for example, correspond to band shapes predicted using Wieland's potential curves and values of $\frac{\bar{I}}{r^2}$ for a rotational temperature of about 320°K. The red shaded bands are somewhat more spread out due to larger differences between B'_v and $B_{v''}$ and a reasonable half width is 5Å at 320°K. The resolution of the detection was 1.25Å for the conditions used to record these spectra. Because so few states have appreciable population with helium present, the spectrum is greatly simplified and the problems caused by extensive overlap of many bands are reduced. The continuous emission in the spectrum with no helium present, to the extent that it appears, must come from two sources. First, true continuous emission, either from HgCl* in high v' radiating to the dissociation continuum of HgCl, or from an excited $HgCl_2$ species formed in the collision of Hg* with Cl_2. The other source of continuous

emission is just the inability of the detection system to resolve very closely spaced bands. This latter possibility was studied carefully by photographing the emission from the HgCl* lamp with narrowed slits in the second order of the spectrograph. Here with resolution of 0.25Å very many closely spaced bands are apparent, and Wieland's assignments refer to only the strongest features. These are the most intense members of sequences. No attempt was made at assignment of these newly observed bands. Their presence is certainly consistent with the calculations discussed earlier, which predict many transitions with small but non-negligible overlap integrals, which had not been resolved by Wieland's photographs either. The low intensity of the chemiluminescence from $Hg^* + Cl_2$ and the complicating effects of fluorescence from the reaction vessels made high resolution studies difficult. However, some photographs were obtained at intermediate resolution in the second order. These indicate the same type of structure as obtained from the high resolution photographs of the HgCl* lamp emission. With this information it can be concluded that the apparent continuum is at least half due to unresolved banded structure. Most of the true continuous emission is likely to occur close to the intensity maximum at 5580Å. The emission below 4800Å is predominantly discrete.

2. Vibrational Distributions of HgCl ($B^2\Sigma^+$) from $Hg^* + Cl_2$

With the previous discussion in mind one can proceed to extract an estimate of the relative population of the vibrational levels of HgCl* which is formed in the bimolecular collision of Hg* with Cl_2. The total intensity of a vibronic transition in emission was previously given by Eq. (11):

$$I_{v'v''} = N_{v'}A_{v''} = \frac{64}{h} N_{v'}\nu^3_{v'v''}|R^{v'v''}|^2 \quad .$$

The principal quantity of interest is, of course, $N_{v'}$, the population of level v'. The electronic transition mement has been assumed to vary only slightly with internuclear separation, so that

$$I_{v'v''} = C\, N_{v'}\nu^3_{v'v''} \langle \psi^{v'}_{v} | \psi^{v''}_{v} \rangle \quad . \tag{20}$$

Because the spectrum present when no quenching gas is used contains unresolved discrete and continuous emission, the total intensity recorded at a particular wavelength λ_o and slit width will have contributions from several bands and from the possible continuum. The slit function of the detection system will allow light of a certain wavelength spread around λ_o into the photomultiplier. This situation implies that area measurements of the banded features can not be easily defined. The only meaningful approach is measurement of peak heights of banded features relative to the unresolved emission. At the maximum in intensity of an emission band this relative peak height will be a measure of the true intensity of the band. As long as the rotational envelope does not change much in width for the set of red shaded bands, relative populations of the v' levels can be calculated from peak heights. The approach used here has been measurement of peak height above the unresolved emission for all red shaded bands in the HgCl* spectra obtained with and without the use of helium as carrier gas.

The peak height at the maximum is actually a differential intensity, dI, related to I by differentiation of Eq. (20). Since the spectral intensities have been recorded as a function of wavelength,

$$dI_{v',v''} = C'N_{v'}\nu^2|\langle\psi_v^{v'}|\psi_v^{v''}\rangle|\ d\nu = \frac{CN_{v'}}{\lambda 4}\ |\langle\psi_v^{v'}|\psi_v^{v''}\rangle|^2\ d\lambda \qquad (21)$$

and the peak height will be proportional to dI for an infinitessimal wavelength interval $d\lambda$ between λ and $\lambda+d\lambda$.

If all the emission from one level v' could be resolved and measured, vibrational sum rules could be applied, since

$$\sum_{v' \text{ or } v''}^{\text{all possible}} |\langle\psi_v^{v'}|\psi_v^{v''}\rangle|^2 = 1 \qquad (22)$$

if the vibrational wavefunctions are normalized properly. This is out of the question here because the emission is only partly resolved. A sum rule approach is helpful with this analysis, however, since the accuracy of the sums of Franck-Condon factors from one v' is better than the FC factor of any individual transition from that level. The population of level v' in arbitrary units is related to the intensities of observed transitions from v' by

$$N_{v'} = (\Sigma_{v''}\ dI_{v',v''}/\nu^4_{v',v''})/\Sigma_{v''}|\langle\psi_v^{v'}|\psi_v^{v''}\rangle|^2 \qquad (23)$$

where both summations extend over the same values of v".

Table V-4 presents the peak height intensity measurements and overlap integrals which have been used to calculate the vibrational distribution for HgCl* with no helium present. The resultant values of N_v, are presented in Table V-5 and plotted as a function of vibrational level in Fig. V-7. Only red shaded bands have been considered, and most of these lie below 4800Å and so do not appear in Fig. V-6. When the bands of a single progression radiate to a wide range of v" levels the population N_v, has been calculated using overlap integrals based on both the low v" and high v" quasi-Morse potential functions. Data points and overlap integrals marked by asterisks show poor correspondence between intensity and overlap integral. The vibrational populations shown in Table V-5 have been calculated first excluding these points. Below these values for each v' are shown the relevant sums and N_v, values calculated when the * points are included. In this way crude error limits can be set on the values of N_v, obtained in this analysis. Uncertainty in initial measurements adds an error of ± 10% to weak bands and less to strong bands. It is important to note that the relative intensities of bands in the emission spectra are reproducible to within ten percent for both conditions.

In Fig. V-7 the populations N_v, have been normalized so that the smoothed values N^*_v,(s) sum to 1.00. The N^*_v,(av) values are the normalized populations averaging the low v" and high v" fit results when both have been computed.

Table V-4. Vibrational Distribution Data: Frequency Normalized Intensities and Overlap Integrals for $HgCl(B^2\Sigma^+)$ formed by $Hg^* + Cl_2$ with no helium.

v'	v"	λ Å	$\bar{\nu}$ cm^{-1}	$\frac{dI}{\nu^4}$	$\lvert\langle v'\rvert v''\rangle\rvert^2$ low v" fit	$\lvert\langle v'\rvert v''\rangle\rvert^2$ high v" fit
4	10	4672.3	21397	1.99*[a]		1.12E-02*[a]
4	11	4727.5	21147	2.12		2.81E-02
4	12	4783.8	20898	2.57		5.21E-02
5	9	4577.5	21840	2.28*		7.82E-03*
5	10	4632.0	21583	1.85		2.14E-02
5	11	4686.5	21332	3.08		4.33E-02
5	12	4741.2	21086	2.30		6.05E-02
5	13	4796.3	20842	2.36		5.05E-02
6	8	4585.7	22287	1.35*	3.62E-03*	4.79t-03*
6	9	4538.4	22028	1.50	1.13E-02	1.48E-02
6	10	4592.2	21770	1.36	2.68E-02	3.37E-02
6	11	4645.8	21519	2.71	4.65E-02	5.35E-02
6	12	4699.9	21271	2.34	5.46E-02	5.25E-02
6	13	4754.2	21028	.825	3.58E-02	2.22E-02
6	14	4808.4	20791	1.56	5.64E-02	2.53E-02
7	7	4397.3	22735	1.28*	2.00E-03*	2.56E-03*
7	8	4448.5	22473	1.14	7.15E-03	9.15E-03
7	9	4501.0	22211	1.26	1.92E-02	2.41E-02
7	10	4553.3	21956	1.09	3.79E-02	4.46E-02
7	11	4606.6	21702	1.55	5.14E-02	5.30E-02
7	12	4659.4	21456	1.55	4.13E-02	3.17E-02
7	13	4712.8	21213	1.51	1.16E-02	2.36E.03
7	14	4766.3	20975	1.48	1.34E-03	1.14E-02

Table V-4. (Continued)

v'	v"	λ Å	$\bar{\nu}$ cm^{-1}	$\frac{dI}{\nu^4}$	$\lvert\langle v'\rvert v''\rangle\rvert^2$ low v" fit	$\lvert\langle v'\rvert v''\rangle\rvert^2$ high v" fit
8	6	4261.6	23459	1.07*	9.53E-04*	1.17E-03*
8	8	4412.7	22655	1.91	1.24E-02	1.54E-02
8	9	4463.6	22397	2.10	2.85E-02	3.40E-02
8	10	4515.4	22140	1.59	4.57E-02	4.98E-02
8	11	4567.6	21887	.80	4.57E-02	4.11E-02
8	12	4619.8	21640	.71	2.07E-02	1.03E-02
9	6	4277.8	23370	2.09*	1.92E-03*	2.32E-03*
9	7	4327.0	23104	1.19	7.12E-03	8.66E-03
9	9	4377.4	22838	1.57	3.72E-02	4.21E-02
9	10	4478.6	22322	1.45	4.67E-02	4.66E-02
9	11	4529.8	22070	1.79	3.12E-02	2.28E-02
9	12	4581.3	21822	.95	4.32E-03	1.83E-04
9	13	4633.6	21580	1.23	6.07E-03	1.69E-02
9	14	4685.5	21341	2.25	2.95E-02	3.16E-02
10	6	4244.9	23551	1.49	3.52E-03	4.18E-03
10	7	4293.4	23285	2.44	1.16E-02	1.37E-02
10	8	4344.0	23020	1.63	2.70E-02	3.12E-02
10	9	4392.4	22760	1.35	4.27E-02	4.56E-02
10	10	4443.4	22504	1.48	3.98E-02	3.55E-02
10	11	4494.3	22251	.83	1.43E-02	6.76E-03
10	13	4593.9	21762	1.85	2.00E-02	2.88E-02
10	14	4644.9	21523	1.38	2.76E-02	1.76E-02
10	15	4695.7	21290	2.47*	3.58E-03*	6.14E-04*
10	16	4747.0	21060	1.81	1.30E-02	2.44E-02

Table V-4. (Continued)

v'	v"	λ Å	$\bar{\nu}$ cm^{-1}	$\frac{dI}{\nu^4}$	$\lvert\langle v'\rvert v''\rangle\rvert^2$ low v" fit	$\lvert\langle v'\rvert v''\rangle\rvert^2$ high v" fit
11	6	4212.5	23722	1.33*	5.95E-03*	6.95E-03*
11	7	4260.7	23464	1.97	1.72E-02	1.99E-02
11	8	4308.2	23202	1.40	3.41E-02	3.79E-02
11	10	4407.0	22685	1.06	2.72E-02	2.05E-02
11	11	4456.3	22434	1.16*	2.55E-05*	5.08E-05*
11	12	4505.7	22188	1.79	8.05E-03	1.70E-02
11	13	4556.0	21943	1.42	2.81E-02	2.73E-02
11	14	4606.2	21704	2.04	1.34E-02	2.89E-03
12	5	4133.6	24185	1.61*	2.56E-03*	2.92E-02*
12	6	4181.0	23911	2.19	9.32E-03	1.07E-02
12	7	4227.9	23646	2.40	2.35E-02	2.65E-02
12	8	4275.8	23381	3.76	3.90E-02	4.16E-02
12	9	4323.9	23121	1.90	3.74E-02	3.44E-02
12	11	4420.9	22613	.65	4.23E-03	3.97E-03
12	12	4469.8	22366	.98	1.96E-02	2.62E-02
12	13	4518.3	22126	2.04	2.36E-02	1.50E-02
12	14	4566.4	21893	1.29	1.49E-02	1.10E-03
12	15	4617.6	21650	.93	1.23E-02	2.30E-02
13	5	4103.6	24362	2.32*	4.21E-03*	4.74E-03*
13	6	4149.4	24093	1.82	1.36E-02	1.54E-02
13	7	4196.4	23823	1.92	2.96E-02	3.26E-02
13	8	4243.3	23560	1.49	4.01E-02	4.08E-2
13	9	4290.6	23300	.96	2.73E-02	2.24E-2
13	10	4338.3	23044	1.13	3.10E-03	4.39E-04
13	11	4386.3	22792	1.14	6.94E-03	1.39E-02
13	12	4433.9	22547	1.72	2.58E-02	2.55E-02
13	13	4482.6	22302	1.17	1.14E-02	2.98E-03
13	14	4531.3	22063	1.31	1.81E-03	1.09E-02

Table V-4. (Continued)

v'	v"	λ Å	$\bar{\nu}$ cm^{-1}	$\frac{dI}{\nu^4}$	$\lvert\langle v'\rvert v''\rangle\rvert^2$ low v" fit	$\lvert\langle v'\rvert v''\rangle\rvert^2$ high v" fit
14	6	4119.5	24268	2.30	1.86E-02	2.06E-02
14	7	4164.6	24005	3.07	3.44E-02	3.69E-02
14	8	4211.6	23738	1.93	3.69E-02	3.56E-02
14	9	4258.1	23478	1.06	1.56E-02	1.06E-02
14	10	4305.2	23221	.99*	3.57E-05*	1.69E-03*
14	12	4398.9	22726	1.69	2.25E-02	1.61E-02
14	13	4447.2	22480	.64	1.59E-03	4.19E-04
15	4	3999.8	24994	1.51*	2.49E-03*	2.70E-03*
15	6	4090.0	24443	2.41	2.38E-02	2.60E-02
15	7	4134.1	24182	1.93	3.70E-02	3.85E-02
15	8	4180.1	23916	.92	2.98E-02	2.69E-02
15	9	4226.9	23652	.87	5.74E-03	2.44E-03
15	11	4319.0	23147	2.00	2.31E-02	2.46E-02
15	13	4412.6	22656	1.14	9.65E-04	7.33E-03
15	14	4459.5	22418	1.81	1.96E-02	2.01E-02
16	5	4015.9	24894	.71	1.31E-02	1.43E-02
16	7	4104.8	24355	2.13	3.65E-02	3.68E-02
16	8	4149.9	24090	1.66	2.05E-02	1.67E-02
16	9	4195.4	23829	1.19*	5.14E-04*	3.00E-05*
16	10	4240.6	23575	1.62	1.17E-02	1.25E-02
16	11	4286.4	23323	1.97	2.27E-02	6.10E-03
16	12	4332.3	23076	.85	3.29E-03	1.03E-02
17	4	3944.8	25343	1.21*	5.62E-03*	
17	5	3987.9	25069	1.00	1.72E-02	
17	11	4254.7	23497	1.34	1.60E-02	

Table V-4. (Continued)

v'	v"	λ Å	$\bar{\nu}$ cm^{-1}	$\frac{dI}{\nu^4}$	$\lvert\langle v'\rvert v''\rangle\rvert^2$ low v" fit	$\lvert\langle v'\rvert v''\rangle\rvert^2$ high v" fit
18	3	3875.3	25797	1.13*	1.82E-03*	
18	4	3917.9	25517	.98	7.91E-03	
18	5	3960.5	25242	.93	2.14E-02	
18	6	4003.1	24972	1.21	3.43E-02	
18	11	4223.6	23699	1.29	7.24E-03	
19	3	3849.7	25969	1.18*	2.72E-03*	
19	4	3891.3	25691	.80	1.07E-02	
19	5	2591.6	25416	1.18	2.54E-02	
19	6	3975.8	25145	.98	3.40E-02	
20	3	3824.2	26141	1.07*	3.89E-03*	
20	4	3865.4	25863	.90	1.38E-02	
20	5	3907.0	25588	.33	2.88E-02	
20	6	3948.8	25317	1.56	3.14E-02	
21	2	3758.6	27172	.98*	9.91E-04*	
21	3	3799.2	26314	.69	5.40E-03	
21	4	3840.3	26032	.44	1.72E-02	
21	5	3880.9	25760	.73	3.11E-02	
21	6	3922.3	25488	.84	2.68E-02	
22	2	3734.9	26766	.68*	1.45E-03*	
22	3	3775.1	26482	.85	7.23E-03	
22	4	3815.0	26205	.76	2.06E-02	
22	5	3856.0	25926	.53	3.19E-02	
23	2	3711.0	26939	1.07*	2.06E-03*	
23	3	3751.1	26651	1.38	9.40E-03	
23	4	3790.5	26374	1.03	2.38E-02	
23	5	3830.9	26096	.52	3.11E-02	
23	6	3870.8	25827	.41	1.42E-02	

Table V-4. (Continued)

v'	v"	λ Å	$\bar{\nu}$ cm^{-1}	$\frac{dI}{\nu^4}$	$\lvert\langle v'\rvert v''\rangle\rvert^2$ low v" fit	$\lvert\langle v'\rvert v''\rangle\rvert^2$ high v" fit
24	2	3688.9	27101	.75*	2.85E-03*	
24	4	3764.9	26542	1.03	2.66E-02	
24	5	3806.5	26265	.39	2.86E-02	
24	6	3845.5	25995	.43	8.12E-03	
24	7	3885.9	25723	.37	2.12E-03	
25	2	3665.6	27273	.49*	3.84E-03*	
25	4	3743.6	26709	.50	2.85E-02	
25	5	3782.1	26433	.62	2.47E-02	
25	6	3821.3	26162	.15	3.39E-03	
26	2	3643.7	27437	.96*	5.05E-03	
26	3	3681.2	27157	.44	1.72E-02	
26	4	3718.7	26875	.63	2.95E-02	
26	5	3758.5	26599	.27	1.98E-02	
27	1	3585.1	27885	.21*	1.04E-03*	
27	2	3621.6	27604	.34	6.48E-03	
27	3	3657.4	27319	.21	1.99E-02	
28	1	3564.4	28055	.10*	1.41E-03*	
28	2	3600.2	27768	.14	8.12E-03	

[a]Asterisks(*) refer to the transition from one v' for which agreement between observed intensity and overlap integral is the worst for that vibrational level. See Table V-5, footnote d.

Table V-5. Vibrational Distribution Results: Summed Intensities, Summed Overlap Integrals and Vibrational Populations for $HgCl(B^2\Sigma^+)$ formed from $Hg^* + Cl_2$ with no helium

v'	$\Sigma \frac{dI}{\nu^4}$ [a]	$\Sigma\lvert\langle v'\rvert v''\rangle\rvert^2$ low v''	$\Sigma\lvert\langle v'\rvert v''\rangle\rvert^2$ high v''	N_v,(low v'')	N_v,(high v'')	N_v^*,(s) [b]	N_v^*,(av) [c]
4	4.69 [d]		0.0802		58.5	.0251	.0417
	6.68		0.0914		73.1		.0522
5	9.59		0.1757		54.58	.0310	.0389
	11.87		0.1835		64.69		.0462
6	10.29	0.2314	0.2020	44.47	50.94	.0365	.0340
	11.64	0.2350	0.2048	49.53	56.84		.0379
7	9.58	0.1699	0.1764	56.39	54.31	.0411	.0395
	10.86	0.1719	0.1790	63.18	60.67		.0442
8	7.11	0.1530	0.1506	46.47	47.21	.0459	.0334
	8.18	0.1540	0.1518	53.12	53.89		.0382
9	10.43	0.1621	0.1689	64.34	61.75	.0500	.0450
	12.52	0.1640	0.1702	76.34	73.56		.0535
10	14.26	0.1973	0.2076	72.28	68.69	.0542	.0503
	16.73	0.2031	0.2084	82.37	80.28		.0580
11	9.68	0.1281	0.1255	75.57	77.13	.0579	.0545
	12.17	0.1367	0.1325	89.03	91.85		.0645
12	16.14	0.1838	0.1825	87.81	88.44	.0608	.0629
	17.75	0.1864	0.1854	95.23	95.48		.0681

Table V-5. Vibrational Distribution Results: Summed Intensities, Summed Overlap Integrals and Vibrational Populations for HgCl($B^2\Sigma^+$) formed from Hg* + Cl_2 with no helium (Continued).

v'	$\Sigma \frac{dI}{\nu^4}$ [a]	$\Sigma\|\langle v'\|v''\rangle\|^2$ low v''	$\Sigma\|\langle v'\|v''\rangle\|^2$ high v''	N_v,(low v'')	N_v,(high v'')	N_v^*,(s) [b]	N_v^*,(av) [c]
13	12.66	0.1594	0.1649	79.42	76.77	.0622	.0557
	14.98	0.1638	0.1696	91.45	88.33		.0641
14	10.69	0.1296	0.1202	82.48	88.94	.0628	.0612
	11.68	0.1296	0.1219	90.12	95.82		.0663
15	11.08	0.1401	0.1458	79.09	75.99	.0621	.0553
	12.59	0.1426	0.1485	88.29	84.78		.0617
16	8.94	0.1073	0.0967	83.32	92.45	.0603	.0627
	10.13	0.1078	0.0967	93.97	104.76		.0709
17	2.34	0.0332		70.48		.0547	.0503
	3.55	0.0388		91.49			.0653
18	4.41	0.0708		62.25		.0478	.0444
	5.54	0.0726		76.31			.0544
19	2.96	0.0701		42.23		.0410	.0302
	4.14	0.0728		56.87			.0406
20	2.79	0.0740		37.70		.0363	.0269
	3.86	0.0779		49.55			.0353
21	2.70	0.0805		33.54		.0319	.0239
	3.68	0.0814		45.21			.0322
22	2.14	0.0597		35.85		.0280	.0256
	2.82	0.0612		46.08			.0329

Table V-5. Vibrational Distribution Results: Summed Intensities, Summed Overlap Integrals and Vibrational Populations for $HgCl(B^2\Sigma^+)$ formed from $Hg^* + Cl_2$ with no helium (Continued).

v'	$\Sigma \frac{dI}{\nu^4}$ [a]	$\Sigma\|\langle v'\|v''\rangle\|^2$ low v''	$\Sigma\|\langle v'\|v''\rangle\|^2$ high v''	N_v,(low v'')	N_v,(high v'')	N^*_v,(s) [b]	N^*_v,(av) [c]
23	3.34	0.0785		42.55		.0280	.0304
	4.41	0.0806		54.71			.0390
24	2.22	0.0655		33.89		.0225	.0242
	2.97	0.0682		43.55		.0225	.0311
25	1.27	0.0566		22.44		.0201	.0160
	1.76	0.0604		29.14			.0208
26	1.34	0.0665		20.15		.0178	.0144
	2.28	0.0715		31.89			.0228
27	0.55	0.0264		20.83		.0155	.0149
	0.76	0.0274		27.74			.0198
28	0.14	0.0081		17.28		.0133	.0123
	0.24	0.0095		25.26			.0180

[a] From Table V-4

[b] N^*_v,(s) values obtained by from a smooth curve through the average N_v, values and normalized such that $\sum_{v'=4}^{28} N^*_v,(s) = 1.00$

[c] N^*_v,(av) values are normalized to the curve as indicated above. N_v,(low v'') and N_v,(high v'') values are averaged where both have been computed.

[d] The first line of results for each v' excludes the transition which shows worst agreement between intensity and overlap integral (points marked * in Table V-4). The second line of results includes that transition.

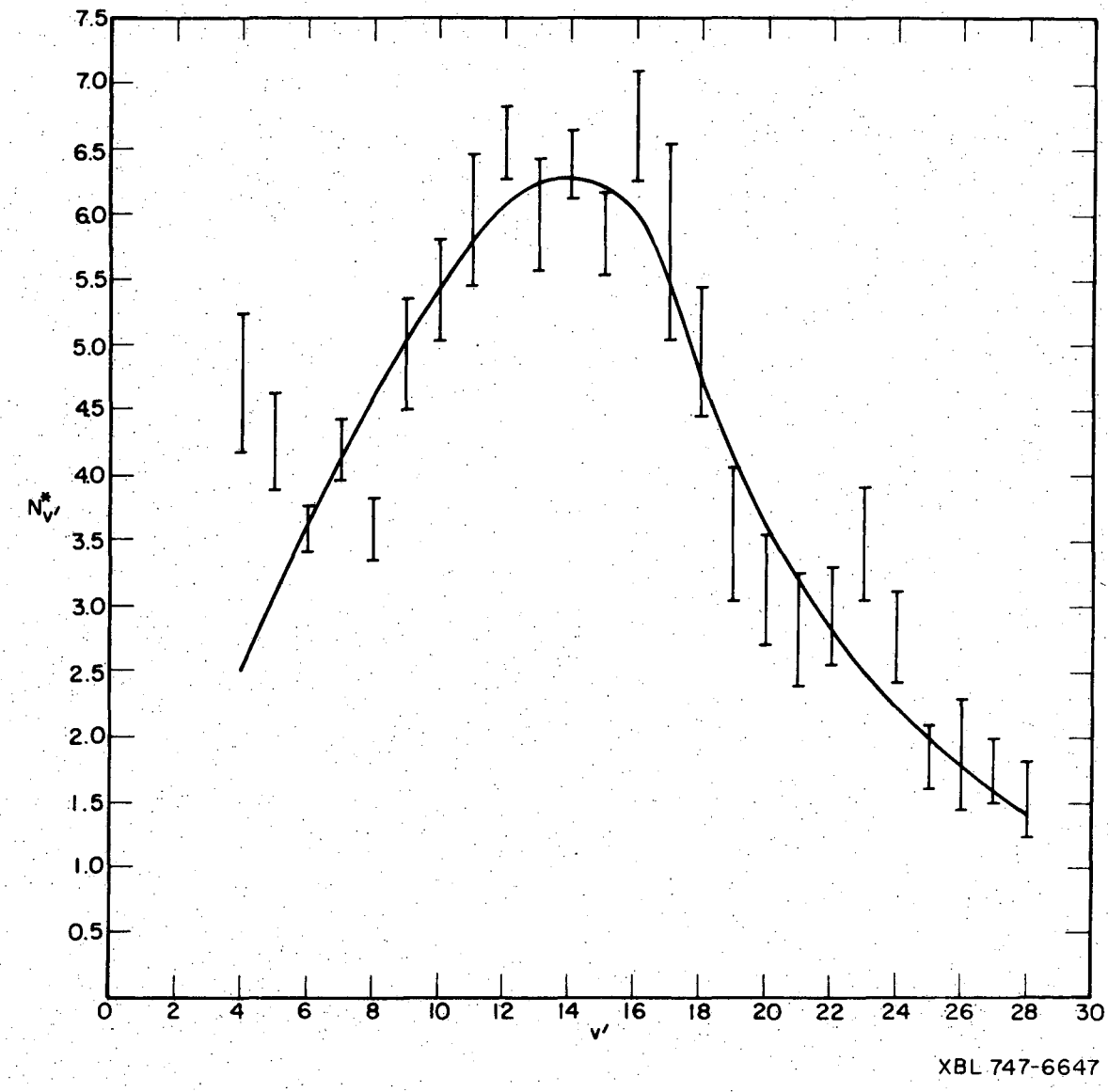

Fig. V-7. Vibrational distribution for $HgCl(B^2\Sigma^+)$. Data bars correspond to $N^*_{v'}(av)$ computed as described in the text. The smooth curve connects the points $N^*_{v'}(s)$, shown in Table V-5. No buffer gas was used.

The vibrational distribution is definitely non thermal, with maximum population occurring in v' = 14. Half the $HgCl^*$ molecules are formed in levels 10 to 17, with appreciable population of levels up to the limit defined by the exoergicity of the reaction, v' = 29. There may be quenching of vibrational energy indicated by an increase in population at very low v', although this is dubious. Emission from levels below v'=4 could not be detected at all, as shown in Fig. V-6 for these conditions.

When large amounts of helium flow through the irradiated vessel in addition to mercury and chlorine, only very low vibrational levels of $HgCl^*$ are represented in emission. Table V-6 gives spectral intensities and overlap integrals for the $HgCl^*$ emission under these conditions, as shown in Fig. V-6. Table V-7 presents the vibrational populations derived from this data. The population of each level is reported relative to $N_{v'=0} = 1.00$, for comparison to the thermal population expected for 295°K. (Helium flowed through the vessel too fast to reach thermal equilibrium with the irradiated vessel at 318°K.) The thermal population of v' relative to v'=0 is given by

$$N_{v'} = \frac{N}{Q_v} \exp[-E_{vib}(v')/kt] \qquad (24)$$

where N is the total population of the electronic state, Q_v is the vibrational partition function, and $E_{vib}(v')$ is the amount of energy in excess of that of v'=0 of level v'. The exponential part of Eq. (24) is also shown as a function of v' in Table V-7 for 295°K. Figure V-8

Table V-6. Vibrational Distribution Data: Frequency Normalized Intensities and Overlap Integrals for HgCl($B^2\Sigma^+$) formed from Hg* + Cl_2 + Helium (200 Torr).

v' v"	λ Å	$\bar{\nu}$ cm^{-1}	dI/ν^4	$\lvert\langle v'\lvert v''\rangle\rvert^2$ high v" fit
0 13	5025.0	19895	3.22	2.70E-03
0 14	5085.6	19658	1.02	8.31E-03
0 15	5146.8	19428	6.38	2.17E-03
0 16	5208.5	19194	14.90	4.81E-02
0 17	5270.5	18969	65.48	8.94E-02
0 18	5332.1	18749	62.72	1.389E-01
0 19	5393.7	18535	67.12	1.781E-01
0 21	5517.2	18120	129.42	1.553E-01
0 22	5583.5	17920	101.84	1.008E-01
0 23	5638.9	17729	5.58*[a]	4.90E-02*[a]
1 13	4976.7	20088	2.59*	1.42E-02*
1 14	5036.4	19850	4.53	3.40E-02
1 15	5097.5	19612	6.07	6.53E-02
1 16	5157.5	19384	19.81	9.74E-02
1 17	5217.8	19160	19.88	1.064E-01
1 18	5278.1	18941	13.99	7.39E-02
2 12	4871.7	20521	3.10	1.58E-02
2 13	4930.1	20278	5.91	3.66E-02
2 14	4988.6	20040	4.65	6.54E-02
2 15	5047.8	19805	3.96	8.55E-02
2 16	5106.1	19579	4.29	7.63E-02
2 17	5166.3	19351	3.00	2.12E-02
2 18	5227.0	19131	9.85	3.51E-02
2 19	5284.8	18917	1.72	3.12E-02
2 20	5343.7	18708	2.61*	7.84E-02*

Table V-6. Vibrational Distribution Data: Frequency Normalized Intensities and Overlap Integrals for HgCl($B^2\Sigma^+$) formed from Hg* + Cl_2 + Helium (200 Torr).

v' v"	λ Å	$\bar{\nu}$ cm^{-1}	dI/ν^4	$\lvert\langle v' \rvert v'' \rangle\rvert^2$
3 12	4827.2	20710	4.94	3.37E-02
3 13	4884.3	20468	5.30	5.97E-02
3 14	4924.0	20229	5.97	7.45E-02
3 15	5000.1	19993	2.69	5.60E-02
3 16	5058.2	19764	1.24	1.45E-02
3 17	5116.3	19540	3.79	2.51E-03*
3 18	5174.3	19321	1.43	4.06E-02
3 19	5232.5	19106	0.22	5.96E-02
3 21	5348.5	18692	0.42	5.91E-03
4 13	4839.9	20656	2.80	6.68E-02
4 14	4896.8	20416	1.61	5.04E-02
4 17	5067.5	19728	2.11	1.22E-02
4 18	5124.6	19508	2.07*	3.09E-03*
4 20	5238.5	19084	2.11	1.32E-02
4 21	5295.1	18880	1.57	5.38E-02

[a]The same convention as used in Table V-4.

Table V-7. Vibrational Distribution Results: Summed Intensities, Summed Overlap Integrals and Vibrational Populations for $HgCl(B^2\Sigma^+)$ formed from Hg* + Cl_2 + Helium (200 Torr).

v'	G_o cm^{-1}	$\Sigma \frac{dI}{\nu^4}$	$\Sigma\|\langle v'\|v''\rangle\|^2$ high v''	$N_{v'}$	$N_{v'}$(av)	$N_{v'}$(rel)	$e^{-G_o hc/kt}$ (T=295°C)
0	0.0	452.10[a]	0.7238	624.62	613.53	1.000	1.000
		457.68	0.7728	592.24			
1	191	64.28	0.3770	170.50	170.72	0.278	0.394
		66.87	0.3912	170.93			
2	381	36.48	0.3671	99.37	93.56	0.152	0.156
		29.09	0.4455	87.74			
3	570	22.21	0.3445	64.50	69.71	0.114	0.062
		26.00	0.3470	74.93			
4	758	10.20	0.1964	51.93	56.72	0.092	0.025
		12.27	0.1995	61.50			

[a]The same convention as used in Table V-5.

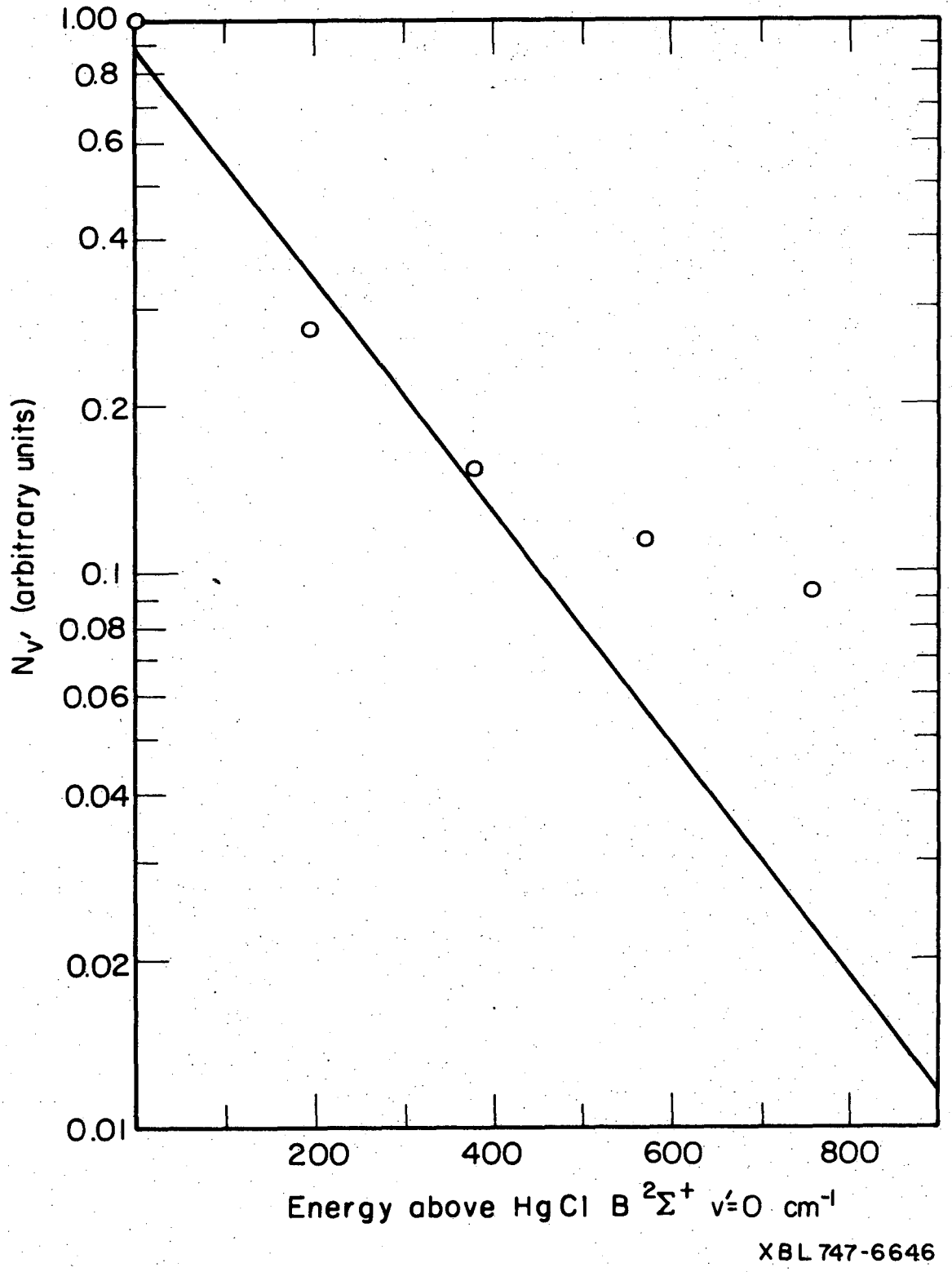

Fig. V-8. Vibrational distribution for HgCl($B^2\Sigma^+$) when 200 Torr of helium is added to the flow system.

shows the relative population as a function of $E_{vib}(v')$ and v'. The straight line shows the best fit of the thermal population at 295°K to the data points. These results show that a pressure of 200 Torr of helium is fairly efficient at relaxing the vibrational energy of $HgCl^*$ but it does not produce the thermal vibrational population at $v' \geq 3$. The fact that most of the vibrational energy of $HgCl^*$ is quenched, however, does make a strong case for the formation of vibrationally hot molecules via the bimolecular reaction rather by an alternative process such as light absorption.

3. The Dissociation Energy of HgCl ($X^2\Sigma^+$)

The short wavelength limit of the chemiluminescent emission can be used to estimate the dissociation energy D_o^o of HgCl formed in the reaction

$$Hg(^3P_1) + Cl_2 \rightarrow HgCl(B^2\Sigma^+) + Cl \ .$$

By energy balance

$$E_{int}(Hg^*) + E_{int}(Cl_2) + E_{tr}(Hg^* + Cl_2) + D_o^o(HgCl)$$

$$= E_{int}(HgCl^*) + E_{int}(Cl) + E_{tr}(HgCl^* + Cl) + D_o^o(Cl_2) \ . \qquad (25)$$

Here D_o^o is the dissociation energy of ground state HgCl, E_{int} is the internal energy of chlorine (0.084 eV at 318 K), E_{tr} is the relative translational energy of reactants or products

$$E_{tr}(Hg^* + Cl_2) = \frac{3}{2} kT = 0.041 \text{ eV at } 318°K) \ ,$$

and $E_{int}(Cl) = 0.0$ or 0.11 eV for a $^2P_{3/2}$ or $^2P_{1/2}$ Cl product respectively. The short wavelength limit of the $HgCl^*$ emission corresponds to emission from the 29th vibrational of excited HgCl, at 3.534 eV above v''=0. With $E_{int}(Hg^*) = 4.86$ eV and $D_o^o(Cl_2) = 2.475$ eV, the dissociation energy of unexcited HgCl is then

$$D_o^o[HgCl(X^2\Sigma^+)] = 1.03 \text{ eV} + E_{int}(Cl) + E_{tr}(HgCl^* + Cl) \qquad (26)$$

or

$$D_o^o[HgCl(X^2\Sigma^+)] \geq 1.03 \text{ eV} = 8309 \text{ cm}^{-1} .$$

Of course, any limit of this sort on a bond energy which is arrived at by measurements of reaction energy partitioning is always uncertain to the extent of any possible activation energy for reaction. However, the large reactive cross section estimates presented in Chapter IV as well as the similarities in behavior of the present reaction to reactions of alkali atoms with halogens, which are known to proceed with no activation energy, indicate that this could not introduce an uncertainty much in excess of kT in the present case. Adding the zero point energy to this limit gives $D_e^o[HgCl(X^2\Sigma^+)] \geq 1.05$ eV. This limit is also in excellent agreement with the value of $D_o^o = 1.03$ eV derived by a Birge-Sponer extrapolation in this chapter and with the value of $D_o^o = 1.0 \pm 0.1$ eV recommended by Gaydon.[17]

E. Spectroscopic Studies of $Hg(^3P_1)$ + Br_2, I_2, and ICl

1. HgBr (B→X) and HgI (B→X) Spectra Obtained from the Irradiated Flow System

$Hg(^3P_1)$ reacts with molecular bromine and iodine in a manner which is completely analogous to its reaction with chlorine. Figure V-9 shows a photoelectric scan of the emission which accompanies the reaction of $Hg(^3P_1)$ with Br_2 in the irradiated flow system. The trace includes the response factor of the detection system as plotted in Fig. II-9. Scan conditions as noted in Table II-2 were used except that the spectrometer slits were 200 microns. At a mercury flow rate of 3.2×10^{16} atoms/sec the most intense chemiluminescent emission occurred with bromine pressure at 0.30 Torr in the reaction vessel. The vessel axis was coincident with the spectrometer axis.

Figure V-10 shows the light emission which accompanies the reaction of $Hg(^3P_1)$ with molecular iodine at 0.34 Torr in the reaction vessel. All other conditions were the same as for studies of $Hg(^3P_1)$ + Br_2. No photographs of the chemiluminescent emissions were taken, unfortunately.

Inspection of the figures of reference 2 and consideration of the information supplied recently by Wieland to Rosen's tabulation,[21] show that Hg^* + Br_2 and I_2 give the same emission as that assigned by Wieland to the (B→X) systems of HgBr and HgI, with no inert gas. For these heavy molecules the spectra are even more complicated than the analogous system of HgCl. Wieland made progress in the vibrational analysis only by adding large amounts of either argon or nitrogen to his Geissler tubes of $HgBr_2$ and HgI_2. As observed for $HgCl^*$ gross

Fig. V-9. Photoelectric scan of the chemiluminescent emission which accompanies the reaction of $Hg(^3P_1)$ with bromine, corrected for the response of the detection system. (v',v") assignments of known $HgBr(B^2\Sigma^+)$ bands are indicated in parentheses, followed by estimates of the intensity of these bands in the presence of 100 Torr of Argon, taken from reference 2.

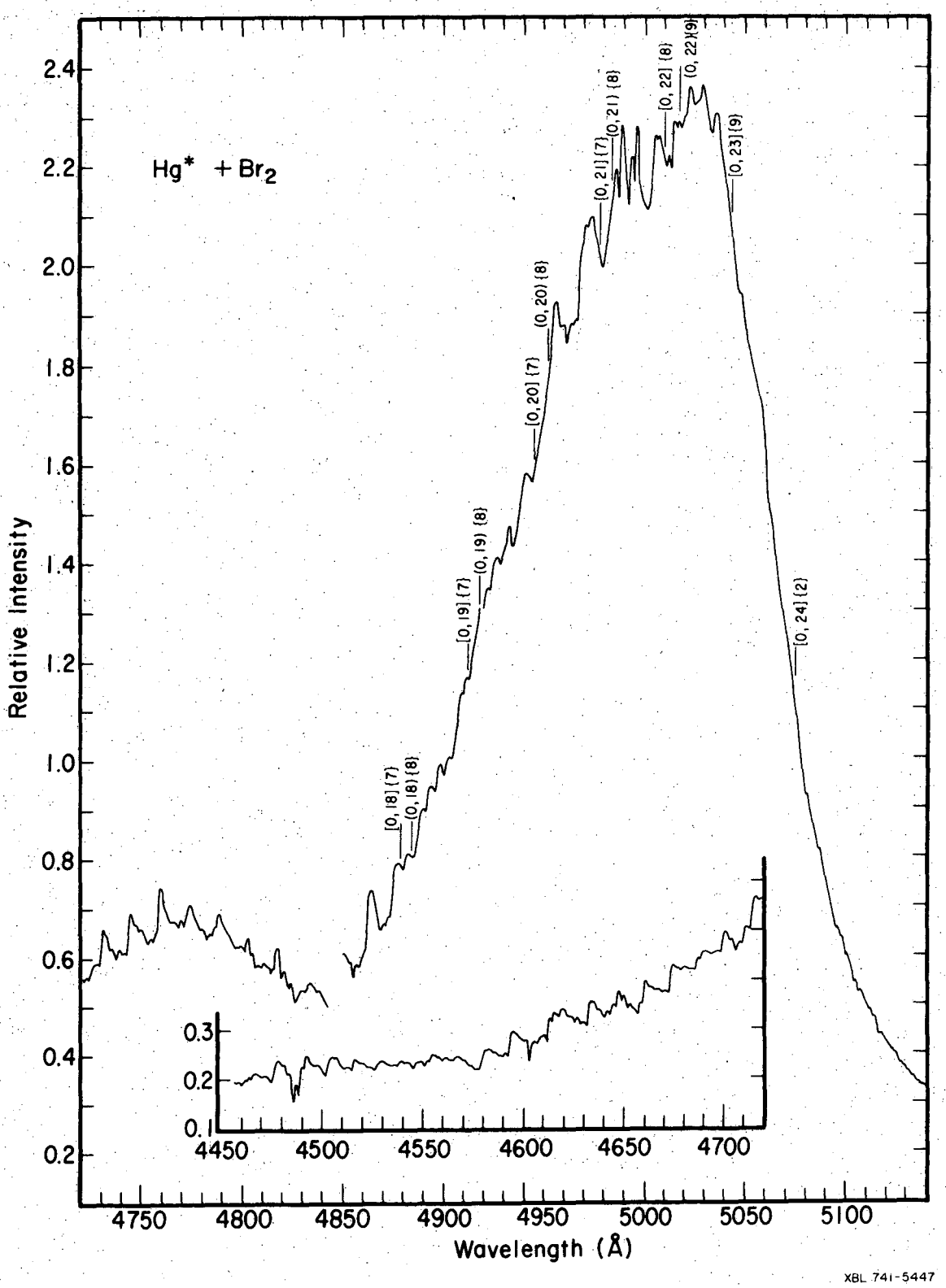

Fig. V-9.

Fig. V-10. Photoelectric scan of the chemiluminescent emission which accompanies the reaction of $Hg(^3P_1)$ with iodine, corrected for the response of the detection system. (v',v") assignments of known $HgI(B^2\Sigma^+)$ bands are indicated in parentheses, followed by estimates of the intensities of these bands in the presence of 460 Torr of Argon, taken from reference 2.

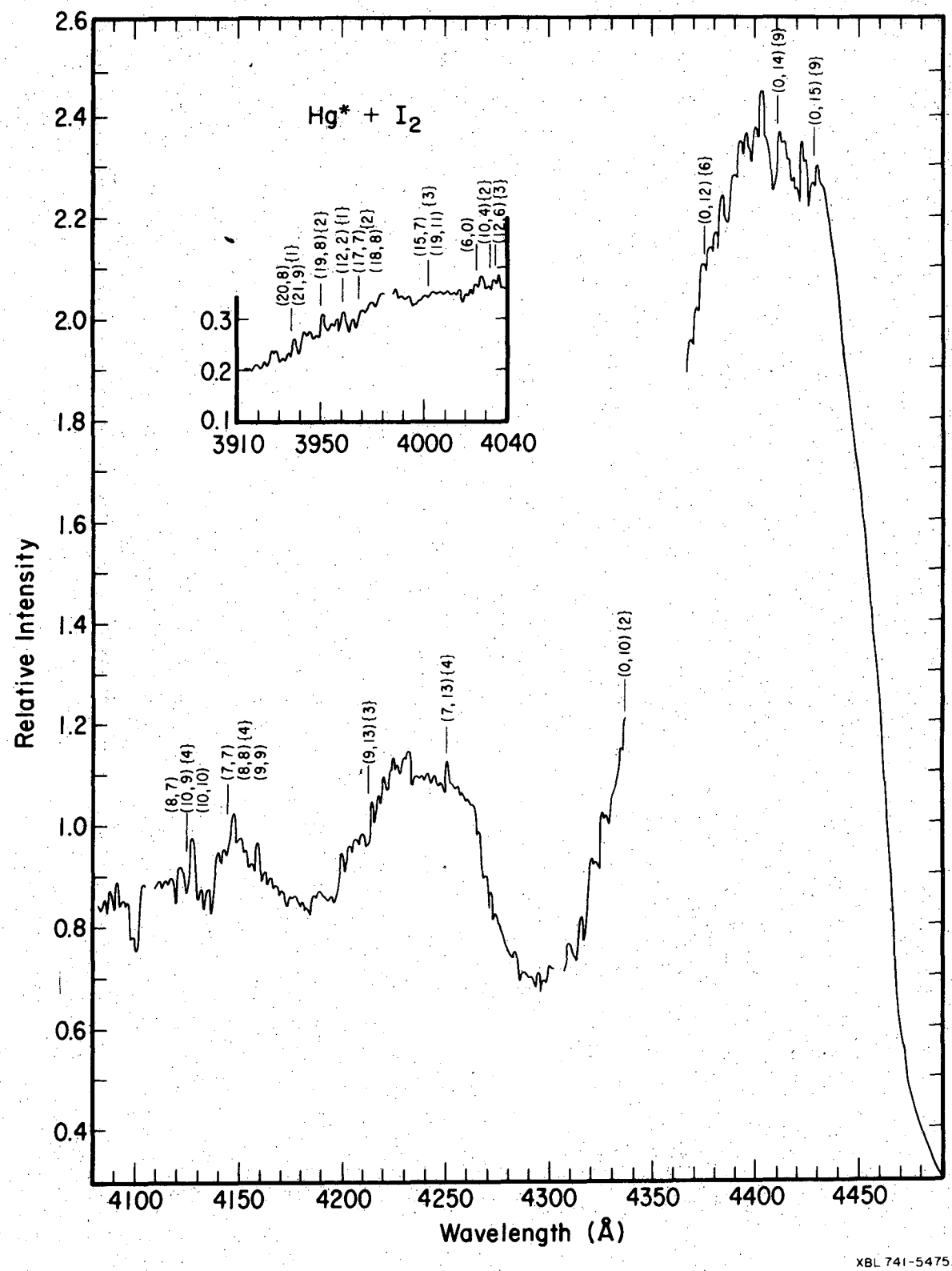
Hg* + I2
Relative Intensity
Wavelength (Å)
(8,7)
(10,9) {4}
(10,10)
(7,7)
(8,8) {4}
(9,9)
(9,13) {3}
(7,13) {4}
(0,10) {2}
(0,12) {6}
(0,14) {9}
(0,15) {9}
(20,8)
(21,9) {1}
(19,8) {2}
(12,2) {1}
(17,7) {2}
(18,8)
(15,7)
(19,11) {3}
(6,0)
(10,4) {2}
(12,6) {3}
XBL 741-5475

Fig. V-10.

changes in the appearance of the spectra are seen when the inert gas is present. The resultant vibrational relaxation and simplification of the spectra allow assignment of most of the emission features, but the non-relaxed spectra are disappointingly complex. Table V-8 shows the molecular constants he extracted from vibrational analysis of the simplified spectra. It should be noted that the B and X states of HgBr and HgI are more weakly bound than those of HgCl and that the vibrational frequencies are smaller as well. The band heads which are indicated in Figs. V-9 and 10 are based on Wieland's analysis.

For Hg^* + Br_2 and I_2 it is clear from the figures that HgX^* is not formed in v'=0 for either case. For Hg^* + Br_2 the unassigned peaks between 4600 and 4850Å are those seen by Wieland with no inert gas in his discharge tube, as listed in Rosen's tabulation. For Hg^* + I_2 many HgI^* bands due to population of $v' \geq 6$ can be recognized. The problems caused by overlap of many weak bands make it impossible to determine the extent to which continuous emission is contributing to the Hg^* + Br_2 and Hg^* + I_2 chemiluminescence.

Table III-1 shows that the bimolecular reaction to produce $HgX(B^2\Sigma^+)$ is exoergic by 0.69 and 0.68 eV for Br_2 and I_2, respectively. Levels up to v'=45 and 53 could be populated if all the exoergicity were invested in vibration of the product molecule. Emission from up to v'=21 can be seen in the spectrum of HgI^*, and emission from higher levels occurs beyond the lower limit of these studies. Although the spectra are less resolved than that of $HgCl^*$ it seems safe to assert that the reaction dynamics are similar for the series Hg^* + Cl_2, Br_2, and I_2.

Table V-8. Spectroscopic Constants for HgBr and HgI

	$HgBr^{79}(X^2\Sigma^+)$ [a]	$HgBr^{79}(B^2\Sigma^+)$	$HgI(X^2\Sigma^+)$	$HgI(B^2\Sigma^+)$
ω_e	188.13[b]	136.275	125.0	110.45
$\omega_e x_e$	0.9665	0.280	1.0($v' \leq 7$) 1.5($v' > 7$)	0.15
$\omega_e y_e$	0.0094	-	-	-
T_e	0	23485	0	24187.1
D_o^o	5740	19930	2850	16300

[a] Values taken from K.Wieland, Z.für Electrochem. 64 769 (1960).

[b] cm^{-1} throughout the table.

2. Results from the Study of $Hg(^3P_1)$ + ICl

Intuitively one expects the reaction of Hg^* with ICl to proceed in a completely analogous way to its reaction with the homonuclear halogens. Since two electronically excited products of different mass can be formed, their spectral intensities and vibrational distributions should provide some insight into their relative rates of formation.

The chemiluminescence which accompanies the reaction of Hg^* with ICl was monitored under the same experimental conditions as were used for $Hg^* + Br_2$ and I_2. ICl at a pressure of 0.05 Torr flowed through the irradiated system as described in Section II. In hindsight one can observe that more effort should have been made to purify the sample and to prevent contamination due to I_2.

Between 3600 and 5800Å weak emission was seen due to HgCl(B→X), and strong emission was seen from HgI(B→X). In addition to these systems strong fluorescence was seen from $I_2(B^3\pi_{o^+_u}, v'=25 \rightarrow X^1\Sigma^+_g)$. This fluorescence was two orders of magnitude more intense than the $HgCl^*$ emission which occurred in the same spectral region (5300-5700Å). Because ICl disproportionates to I_2 and Cl_2 at room temperature with $K_{dissoc}=1.3\times10^{-3}$,[22] the presence of I_2 in the vessel could not be eliminated. The HgI^* emission observed was completely similar in appearance to that occurring with $Hg^* + I_2$. Because the bimolecular reaction of Hg^* with ICl is exoergic by only 0.09 eV for formation of the iodide product, compared to 0.81 eV for the chloride (Table III-1),

emission from only the first six vibrational levels would be seen if only ICl were present in the flow system. Therefore much of the observed HgI^* emission is certainly due to $Hg^* + I_2$. The fact that the $HgCl^*$ emission was so weak indicates either that there was less ICl and Cl_2 than I_2 in the reaction vessel, or that the reaction of Hg^* with ICl or Cl_2 is much slower than with I_2. It is interesting to note here that in reactions of alkali and alkaline earth metals with ICl, the major product appears to be the metal chloride.[23]

The I_2 fluorescence is worthy of further comment. Molecular iodine absorbs the Hg 5461Å line to excite v=25, J=34 of the B state.[24] The resultant fluorescence has been well studied.[25] Steinfeld et al. have investigated energy transfer processes involving this specific excitation by observing the change in the fluorescence spectrum as various quenching gases are added to the iodine system.[26] When low pressures of quenching gases are present the fluorescence spectrum reflects the subsequent vibrational and rotational energy transfer from v'=25, J=34. The I_2 fluorescence observed in the present studies was extremely sensitive to the presence of mercury. With mercury at less than 0.05 Torr, fluorescence was observed from the nearby vibrational levels of I_2^* (v' between 24 and 27). With no mercury only the v'=25 progression was observed. This suggests that Hg is efficient in energy transfer processes with I_2. No detailed studies of this phenomenon were made here. Fluorescence from ICl would occur in the same spectral region,[27] but the spin selection rule holds more

strongly for ICl than for I_2 so that its absorption of radiation at 5461Å is diminished. Predissociation due to interaction of the $^3\pi(0_u^+)$ state with the nearby 0^+ state[28] also decreases the likelihood of observing this fluorescence. No emission from ICl^* was observed here.

F. Experiments with $Hg(6\ ^1P_1)$

Comparativily few studies involving the singlet mercury resonance state, $Hg(6\ ^1P_1)$, have been performed. Although mercury photosensitization processes involving 1849Å radiation have been exploited,[30] studies of quenching rates are scanty.[31] As mentioned in section II.C.2, we investigated the possibility of chemiluminescence accompanying the reaction of $Hg(^1P_1)$ with Cl_2 and $SnCl_4$. These compounds were chosen because the biomolecular reaction to form $HgCl(B^2\Sigma^+)$,

$$Hg(^3P_1) + SnCl_4 \rightarrow HgCl(B^2\Sigma^+) + SnCl_3$$

is endoergic by 0.34 eV and therefore any observed chemiluminescence would unambiguously involve $Hg(^1P_1)$. Another reason for study of $Hg(^1P_1) + SnCl_4$ is that insight could be gained about the relative reactivity of the singlet and triplet species and the extent to which the singlet species might react in a manner analogous to the reactions of alkali metals with halogens. $SnCl_4$ has been shown to react with alkali metals with somewhat larger cross sections than have been found with diatomic halogens,[32] so its use is appropriate in this context. $Hg(^1P_1) + Cl_2$ was studied because by this time the emission which is characteristic of $Hg(^3P_1) + Cl_2$ was well understood, and new spectral

features due to reaction of chlorine with $Hg(^1P_1)$ could be easily noticed and analyzed. The C and D states of HgCl could be populated,

$$Hg(^1P_1) + Cl_2 \rightarrow HgCl(C^2\pi_{1/2}, v'=0) + CL(^2P_{3/2}) \quad \Delta E_o = -0.78 \text{ eV}$$
$$HgCl(D^2\pi_{3/2}, v=0) + Cl(^2P_{3/2}) \quad \Delta E_o = -0.30 \text{ eV}$$

and the chemiluminescence from these states would occur between roughly 2400 and 3000Å.

As discussed earlier, the suprasil reaction vessel and cold cathode lamps were used. The lamps were high in output of the resonance radiation at 1849Å necessary to excite mercury to the singlet state. The enclosure surrounding the lamps and the irradiated area of the reaction vessel was sealed and continuously flushed with nitrogen or oxygen to minimize or maximize the absorption of incident radiation at 1849Å as desired. Absorption of the 4347.5Å radiation from a low pressure Hg lamp was used as a monitor for the presence of $Hg(^1P_1)$ and experiments were performed at Hg flow rates of 3.0×10^{16} atoms/sec where maximum secondary absorption occurred. Under these conditions appreciable concentrations of $Hg(^3P_1)$ were found as expected.

1. Results for $Hg(^1P_1) + Cl_2$

Neither photographs nor photoelectric detection, using the second order of the spectrometer showed any sign of HgCl(C→X) or (D→X) emission between 2000 and 3000Å, indicating that $Hg(^1P_1)$ does not react fast enough, or at all, with Cl_2 to form these states of HgCl. The (B→X) emission was observed strongly and its intensity was not changed when oxygen rather than nitrogen flowed through the lamp and reaction vessel enclosure. $Hg(^1P_1)$ is not, therefore, involved in a

chemiluminescent bimolecular reaction with Cl_2.

2. Results for $Hg(^1P_1) + SnCl_4$

The B state of HgCl is energetically accessible in the reaction of $Hg(^1P_1)$ with $SnCl_4$,

$$Hg(^1P_1) + SnCl_4 \rightarrow HgCl(B^2\Sigma^+, v=0) + SnCl_3 \quad \Delta E_o = -1.48 \text{ eV}$$

and the formation of the C state is only slightly endoergic,

$$Hg(^1P_1) + SnCl_4 \rightarrow HgCl(C^2\pi_{1/2}, v=0) + SnCl_3 \quad \Delta E_o = +0.06 \text{ eV} .$$

With Hg flow rate of 3.0×10^{16} atoms/sec and $SnCl_4$ pressure of 1.65 Torr at the monitoring point, no emission was seen from either state of HgCl, or, continuous emission, was seen between 2400Å and 5700Å. These results indicate that $Hg(^1P_1)$ does not react in a manner analogous to $Hg(^3P_1)$ and further implications of these studies will be discussed subsequently.

CHAPTER V REFERENCES

1. K. Wieland, Helv. Phys. Acta 14, 420 (1941).
2. K. Wieland, Z. für Electrochem. 64, 761 (1960).
3. K. Wieland, Z. für Phys. Chem. B. 42, 422 (1939).
4. G. Herzkerg, Spectra of Diatomic Molecules, 2nd Edition, Van Nostrand, Princeton, 1950, Eqs. (IV.12) and (IV.14).
5. JANAF Thermochemical Tables, 2nd ed., Natl. Stand. Ref. Data System, National Bureau of Standards, D. R. Stull and M. Prophet, project divetors.
6. A. Gregg et al, Trans. Far Soc. 33 852 (1937).
7. a) M. Brauve and S. Knoke, Z. Phys. Chem. 1323, 163 (1933).
   b) L. R. Maxwell and C. M. Mosley, Phys. Rev. 57, 21(1939).
8. a) R. T. Birge, Phys. Rev. 25 240 (1925)
   b) R. Mecke, Z. Physik 32, 823 (1925).
9. a) R. M. Badger, J. Chem. Phys. 2, 128 (1934) and 3, 710 (1935).
   b) D. R. Herschbach and V. W. Laurie, J. Chem. Phys. 35, 458 (1961).
   c) H. S. Johnston, Gas Phase Reaction Rate Theory, Ronald Press, New York, 1966, Table A-2, p. 75.
10. G. Herzberg, loc. cit., Eq. (III.91), p. 89.
11. R. R. Herm and D. R. Herschbach, J. Chem. Phys. 52, 5783 (1970), Fig. 5.
12. See Section V.C.1.

13. V. I. Vedeneyev, et al., Bond Energies, Ionization Potentials and Electron Affinities, Edward Arnold, London, 1966, p. 152.

14. R. S. Berry, Chem. Rev. 69, 533 (1969).

15. G. Herzberg, loc.cit., p.20 ff., 199 ff.

16. G. Herzberg, loc.cit., Eq. (III,100) p. 101.

17. A. G. Gaydon, Dissociation Energies and Spectra of Diatomic Molecules, Third edition, Chapman and Hall, London, 1968.

18. S. D. Gabelnick, Ph.D. Thesis, University of California, Berkeley (1968); Lawrence Radiation Laboratory Report 18623, January (1969).

19. P. M. Morse, Phys. Rev. 34, 57 (1929); corrections as noted for example, in G. D. Brabson, J. Chem. Ed. 50, 397 (1973); numerical procedures, R. N. Zare, J. Chem. Phys. 40, 1934 (1964).

20. Natural abundances of the chlorine isotopes are Cl^{35}, 75.53%; Cl^{37}, 24.47%. R. Weast, editor, Handbook of Chemistry and Physics, 45th edition, Chemical Rubber Company, Cleveland (1964).

21. International Tables of Selected Constants, Number 17. Spectroscopic Data Relative to Diatomic Molecules, B. Rosen, editor, Pergamon, New York, 1970.

22. F. A. Cotton and G. Wilkinson, Advanced Inorganic Chemistry, Interscience, New York, 1966, p. 460.

23. a) Alkali metals + ICl: G. M. Kwei, I. A. Norris, and D. R. Herschbach, J. Chem. Phys. 52, 1317 (1970).

b) Alkaline earth metals + ICl: C. A. Mims, S.-M. Lin, and R. R. Herm, J. Chem. Phys. 58, 1983 (1973).

24. A summary of I_2 fluorescence studies appears in J. A. Coxon, "Low Lying States of Diatomic Halogen Molecules," Molecular Spectroscopy Vol. 1, The Chemical Society, London, 1973, Chapter 4.

25. a) F. Rossler, Z. für Physik 96, 251 (1931).
b) J. C. Polanyi, Can. J. Chem. 36, 121 (1958).
c) C. Arnot and C. A. MacDowell, Can J. Chem. 36, 114, 1322 (1958).

26. a) J. I. Steinfeld and W. Klemperer, J. Chem. Phys. 42, 3475 (1965).
b) J. I. Steinfeld, R. N. Zare, L. Jones, M. Lesk, and W. Klemperer, J. Chem. Phys. 42, 25 (1955).

27. G. W. Holleman and J. I. Steinfeld, Chem. Phys. Lett. 12, 431 (1971).

28. W. G. Brown and G. E. Gibson, Phys. Rev. 40, 529 (1932).

29. G. G. Matland, Phys. Rev. 92, 637 (1953).

30. J. R. McNesby and M. Okabe, Adv. in Photochem. 3, 157 (1964).

31. A. Granzow, M. Z. Hoffman, and N. N. Lichtin, J. Phys. Chem. 73, 4289 (1969).

32. a) K. R. Wilson and D. R. Herschbach, J. Chem. Phys. 49, 2676 (1968),
b) D. D. Parrish and R. R. Herm, J. Chem. Phys. 51, 5467 (1969),
c) S. J. Riley and D. R. Herschbach, J. Chem. Phys. 58, 27 (1973).

VI. DISCUSSION OF THESE EXPERIMENTAL RESULTS AND COMPARISON TO RELATED WORK

The results presented in this work have shown that $Hg(^3P_1)$ reacts with molecular halogens to produce electronically excited products in the bimolecular process

$$Hg(^3P_1) + XY(^1\Sigma^+) \rightarrow HgX(B^2\Sigma^+) + Y(^2P) \qquad (1)$$

where XY is Cl_2, Br_2, I_2 or ICl. The resultant HgX(B→X) emission shows that a large fraction of the reaction exothermicity appears as vibration in the mercurous halide product. From kinetic studies, the cross section for formation of $HgCl(B^2\Sigma^+)$ from the reaction of excited mercury with chlorine is estimated to be roughly the same as the gas kinetic collision cross section, ~ $40Å^2$. These results give some insight into the reaction dynamics, and of course this is the ultimate aim of these experimental studies. In this section we will compare information gained from this work to results of molecular beam studies of alkali[1,2] and alkaline earth[3] metal reactions with halogens, and discuss the relevance of the electron transfer model to reactions involving excited mercury atoms.

A. The Electron Transfer Mechanism for $Hg(^3P_1) + Cl_2(^1\Sigma_g^+)$

The group IA and IIA metal reactions with halogens exhibit several features which are consistent with qualitative predictions based on an electron transfer model for reaction. These features which have been probed by molecular beam studies, are forward peaking in the

angular distribution of metal halide product with respect to the direction defined by the incoming metal atom's velocity, large reaction cross section, and high internal excitation of the metal halide product, as shown by its small recoil velocity. The essential idea of the electron transfer model, first proposed by McGee,[4] is that the metal atom tosses its loosely held outer electron to the incoming halogen molecule while the reactants are far enough apart so that internuclear repulsion is weak. The coulombic attraction of the resultant ion pair accelerates the collision, and essentially every ion pair formed leads to formation of a metal halide product. The distance between the metal atom and halogen molecule at the time of the electron transfer can be estimated from the difference between the ionization potential of the atom and the vertical electron affinity of the halogen molecule.

$$r_x = e^2/[IP(Me) - EA_v(XY)] \qquad (2)$$

Near r_x the potential hypersurface which describes the reaction undergoes an abrupt change from the covalent character of the reactants to the ionic character of the intermediate. Thus the potential hypersurface could be called diabatic in zero order, where the surfaces would actually cross each other. The reaction cross section becomes

$$\sigma_R = \pi r_x^2 \qquad (3)$$

in this lowest-order electron transfer model. It can be seen from (2) that the electron transfer will occur at sufficiently large internuclear separations as to be out of range of chemical forces only for reactants for which IP-EA is relatively small. Thus, the alkali metal reactions with halogens are ideal candidates for this mechanism, since their ionization potentials are low, and have ns^1 as an outer electron configuration. The divalent alkaline earth metals have low ionization potentials, but because of their paired spin ns^2 configuration and because potential hypersurfaces to form stable dihalides have deep wells, their reactions with halogens might not proceed via a similar one electron transfer mechanism. However, experimental evidence[3] supports such a model for their reactions with halogens to form monohalide products analogous to (1). It is interesting to note, however, that a small fraction of reactions of barium with chlorine[5] produce a visible chemiluminescence from the electronically excited dihalide and monohalide

$$Ba + Cl_2 \rightarrow BaCl_2^* \rightarrow BaCl\ C(^2\pi) + Cl(^2P) \qquad (4)$$

the forward peaked product angular distributions and the high internal excitation of the product halide, observed for both alkali and alkaline earth reactions with halogens, suggest that the ion pair intermediate is extremely short lived and that the products separate before the exothermicity can be equipartitioned among the available modes of the complex. In contrast, the reactions of alkali metals with $SnCl_4$ and SF_6[6] show angular distributions which are symmetric about 90° in the

center of mass system. This is evidence for the formation of long lived collision complexes. Measurement of the vibrational energy of CsF formed from Cs + SF_6[7] shows a Boltzmann distribution which is also consistent with the formation of a long lived intermediate. The reactions of $Hg(^3P_1)$ with molecular halogens present an interesting case for testing the applicability of the electron transfer model for several reasons. $Hg(^3P_1)$ has an ionization potential between that of strontium and barium (5.6 eV compared to 5.7 and 5.2 eV, respectively). Like the alkaline earth metals it is a divalent species, but the outer electron is in a p orbital, which affects the symmetry requirements of the relevant potential hypersurfaces. Again, the existence of stable dihalides of mercury brings to mind the possibility of deep chemical wells in the potential surfaces which might lead to formation of long lived complexes, whose presence would be refected in the nature of the energy distribution between the products. Here direct measurement of the vibrational distribution is possible because the mercurous halide is formed in a short lived electronically excited state, whose vibronic emission spectra can be observed before secondary collisions distort the initial product vibrational manifold.

The reactive collisions of alkali and alkaline earth metals with halogens are restricted from the broadside C_{2v} approach trajectories by symmetry restraints.[8] This is not so for $Hg(^3P_1)$ + halogens. For Me representing an alkali or alkaline earth atom, for the family of reactions

$$Me(^{1,2}S_g) + X_2(^1\Sigma_g^+) \rightarrow Me^+(^{1,2}S_g) + X_2^-(^2\Sigma_u^+) \rightarrow MeX(^{1,2}\Sigma^+) + X(^2P_u) \qquad (5)$$

the totally symmetric reactants transform as the A_1 irreducible representation for C_{2v} symmetry,[9] but the ionic intermediates transform as B_2. The products give A_1, B_1 and B_2. Thus, since there is no ionic potential surface of C_{2v} symmetry which correlates with the reactants, broadside attack of the metal atom on the halogen molecule is symmetry forbidden. A collinear approach is not forbidden because Σ representations of $C_{\infty v}$ exist for reactants, products and the ionic intermediate in (5). For $Hg(^3P_1) + X_2$ the reactants transform as $A_1 + B_1 + B_2$ under C_{2v} symmetry, with the ionic intermediate and products having the same symmetry constraints as imposed in (5). Thus, broadside attack as well as a collinear approach of $Hg(^3P_1)$ to the molecular halogen is possible. In an electron transfer process the excited mercury loses its p electron to the empty antibonding σ_n orbital of X_2, and a configuration with C_{2v} symmetry can be imagined in which the empty p orbital is partly delocalized into the π system of X_2. The stability and lifetime of such an ionic intermediate would be reflected in the vibrational distribution of the $HgX(B^2\Sigma^+)$ product.

In Table VI-1 electron transfer model predictions of the reactive cross section are compared to the imcomplete molecular beam experimental data, for the reactions of alkali and alkali metals and $Hg(^3P_1)$ with molecular chlorine. r_x has been calculated from Eq. (2) using the measured adiabatic electron affinity of Cl_2.[10] Since the vertical electron affinity is probably smaller than the adiabatic, r_x values may be too large. As the ionization potential increases the electron

Table VI-1. Alkali and Alkaline Earth Reactions with Cl_2 Compared to $Hg(^3P_1) + Cl_2$.

M	IP[a] eV	r_x[b] Å	σ_{et} $Å^2$	σ_{obs} $Å^2$	ΔD_o kcal/mole	f_{int}^{mp}[h]	ref
Li	5.4	5.0	78	87	54	0.86	c
K	4.3	7.9	200	300	44	0.91	d
Rb	4.2	8.6	230	310	44	0.96	d
Cs	3.9	10.4	340	310	49	0.96	d
Mg	7.6	2.8	25		17	0.89	e
Ca	6.1	4.0	50		37	0.90	e
Sr	5.7	4.5	63		39	0.90	e
Ba	5.2	5.3	88	60[f]	48	0.94	e
$Hg(^3P_1)$	5.6	4.7	69	8.70	12	0.51[g]	

[a] Ionization Potentials from C.E. Moore, Atomic Energy Levels, National Bureau of Standards, NBS Circular 467, Washington, 1952 and 1958.

[b] Adiabatic Electron Affinity of Cl_2=2.52 eV from W.A. Chupka and J. Berkowitz, J. Chem. Phys. 54, 1885 (1951).

[c] D.D.Parrish and R.R. Herm, J. Chem. Phys. 51, 5467 (1969).

[d] R. Grice and P.B. Empedocles, J. Chem. Phys. 48, 5352 (1968).

[e] S.M. Lin, C.A. Mims, and R.R. Herm, J. Chem. Phys. 58, 327 (1973).

[f] C.D. Jonah and R.N. Zare, Chem. Phys. Lett. 9, 65 (1971).

[g] $f_{vib}^{m.p.}$ has been used here.

[h] $f_{vib}^{mp} \sim 1 - \frac{E'}{\Delta D_o + E}$ where E and E' are most probable values of the relative translational energy for reactants and products.

transfer occurs when the reactants are closer together. The long range coulombic attraction can be offset by internuclear repulsion, and thus the model breaks down. With a crossing distance of 2.8Å the Mg+Cl_2 reaction should not be well described by the electron transfer model. The ionic and covalent potential surfaces for $Hg(^3P_1)$ + Cl_2 cross at 4.7Å, which is close to the crossing distances for Ba and Sr. For Ba+Cl_2 the reactive cross section estimate of 60$Å^2$ compares favorably to the electron transfer prediction. The $Hg(^3P_1)$ + Cl_2 reaction cross section range, 8-70$Å^2$, is consistent with the model's order of magnitude. Forward peaking of the product halide with respect to the direction of the incoming metal has been observed in the molecular beam studies mentioned here. Of course no comparison can be made on this point for the reaction of excited mercury with halogens. Trajectory calculations which include electron transfer do not agree on the type of exit channel interaction needed on the potential hypersurface to produce forward peaking or the high internal excitation of the molecular product and the two-body electron transfer model needs more sophistication. However, if the reaction of $Hg(^3P_1)$ with halogens is analogous to the alkali and alkaline earth reactions, the $HgX(B^2\Sigma^+)$ product should be vibrationally hot.

The primitive molecular beam studies referred to in Table VI-1 show very high internal excitation of the chloride product. The fraction of reaction exothermicity invested in internal excitation, f_{int} can be inferred from the translational recoil velocity. In experiments without

velocity analysis the product kinetic energy is estimated from the Lab ↔ center of Mass transformation and cannot be uniquely determined. Nevertheless, reactions of both alkali and alkali metals with chlorine show most probable values of $f_{int} \geq 0.90$.

B. Energy Partioning

The vibrational distribution derived from analysis of the HgCl(B→X) emission and presented in Fig. V-7 can be used to determine the most probable value of the fraction of reaction exothermicity invested in product vibration, if it is assumed that the probability of formation of HgCl(B,v') is proportional to $N_{v'}$, the population of level v'. This also requires that our vibrational distribution reflect the initial distribution and has not been affected by relaxational processes. Another inherent assumption is that the partial sum rule approach for FC factors which has been applied to obtain N_v according to Eq. (V-23) is correct. Thus, the values of $N^*_{v'}(s)$ from Table V-5 and Fig. V-7 have been used in Fig. VI-1, which shows the probability of formation of $HgCl^*$ as a function of the fraction of reaction exothermicity invested in vibration. The total product energy corresponds to $f_{vib}=1.0$ at v'=29. In addition to $P(f_{vib})$ is shown $P^o(f_{vib})$ which gives the probability of forming $HgCl^*$ as a function of f_{vib}, assuming equipartitioning of the reaction exothermicity among the available vibrational, rotational and translational degrees of freedom. Treating the diatomic product as a vibrating rotor gives this normalized expression for $P^o(f_{vib})$:[11]

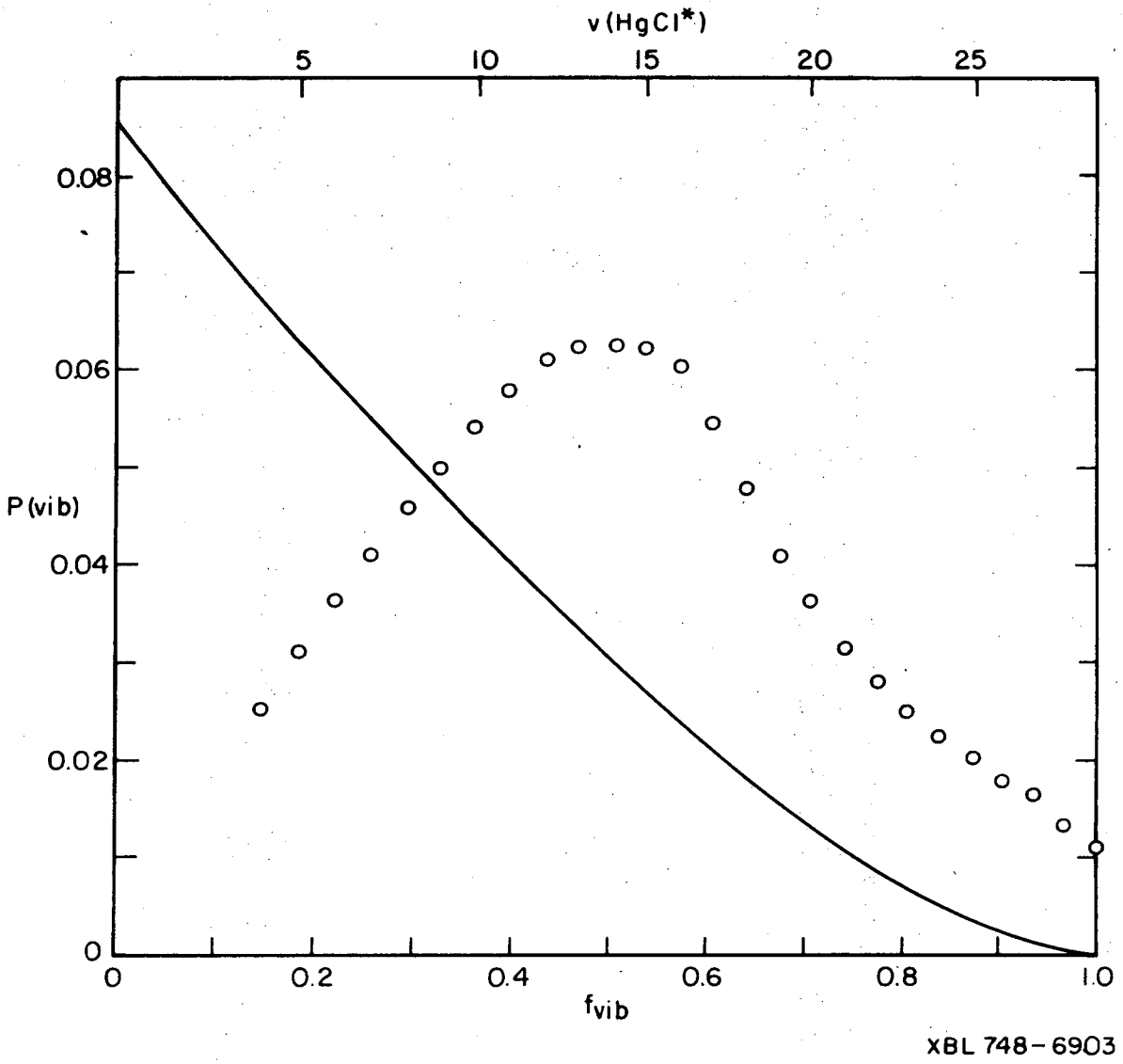

Fig. VI-1. The probability of formation of $HgCl(B^2\Sigma^+)$ as a function of the fraction of available energy invested in vibration, f_{vib}. The smooth curve shows $P^o(f_{vib})$ based on equipartitioning of the available energy, calculated from Eq. (6). Data points present the experimentally observed values of $P(f_{vib})$.

$$P^{o}(f_{vib}) = \frac{(1 - f_{vib})^{3/2}}{\sum_{v=0}^{29} (1 - f_{vib})} \qquad (6)$$

Equipartitioning of the exothermicity of reaction is characteristic of the breakup of a long lived complex. Figure VI-1 shows that $HgCl(B^2\Sigma^+)$ is certainly not formed via a long lived complex. The most probable experimental value of f_{vib} is 0.51, compared to f_{vib}=0.0 for a statistical complex. For HgCl $\langle f_{vib} \rangle$, the average value, is given by

$$\langle f_{vib} \rangle = \sum_{v=0}^{29} f_{vib} P(f_{vib}) = 0.53 \qquad (7)$$

Ben-Shaul et al.[11] outline a concise formalism for expressing the divergence of a measured energy distribution from statistical predictions. They define the surprisal of a distribution, when only the total energy and vibrational distribution are known, as

$$I(v|E) = -\log \omega(v|E) \qquad (8)$$

where $\omega(v|E) = P(f_{vib})/P^{o}(f_{vib})$. E is the total available product energy. The entropy deficiency of the energy distribution can be computed from

$$\Delta S(v) = k \sum_{v=0}^{v^*} P(f_{vib})\, I(v|E) \qquad (9)$$

where k is the Boltzmann constant. The derivative of the surprisal with respect to f_{vib} gives the parameter λ_{vib} from which a vibrational temperature can be computed.

$$\lambda_{vib} = - d \log \omega(f_{vib})/df_{vib} \tag{10}$$

and

$$kT_{vib}\lambda_{vib} = E \ , \tag{11}$$

Figure VI-2 shows ω_{vib} plotted semilogarithmically as a function of f_{vib} for $HgCl(B^2\Sigma^+)$. The curvature which is apparent and enhanced at the extremes of the plot reflects the arbitrary character of the smooth curve drawn through the data of Fig. V-7, rather than an inherent dependence of λ_{vib} on f_{vib}. The line drawn through the center region shows $\lambda_{vib} = -2.7$, for which $T_{vib} = -2600°K$. This reflects the substantial vibrational inversion which we have already noted. In the surprisal formalism an equilibrium distribution has $\lambda_{vib} = 0$, and positive values of λ_{vib} correspond to over population of the lowest vibrational levels accessible. The entropy deficiency of this vibrational distribution, computed from Eq. (9), is 1.23 cal/mole-°K.

C. Comparison to Related Work

Table VI-2 summarizes the results of the previous section and compares them to energy distributions derived from molecular beam and infrared chemiluminescence experiments for the reaction

$$K + I_2 \rightarrow KI + I \tag{12}$$

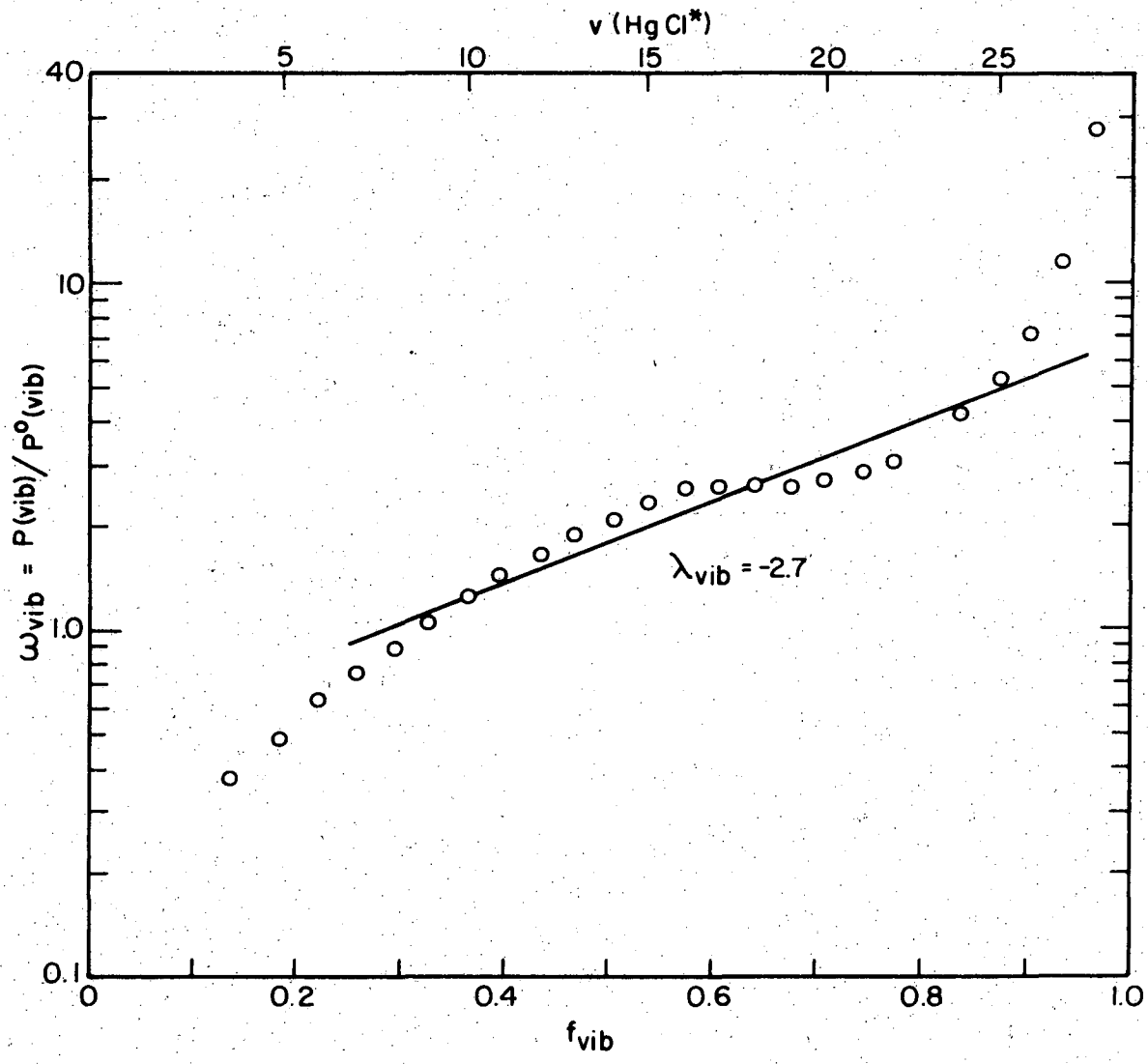

XBL 748-6902

Fig. VI-2. The ratio of the observed probability of formation of $HgCl(B^2\Sigma^+)$ with f_{vib} to the probability calculated by assuming equipartitioning of the available energy, ω_{vib}, as a function of f_{vib}. $\lambda_{vib} = -d \log \omega_{vib}/df_{vib}$.

Table VI-2. Product Energy Distributions

a) Spectroscopic results for $Hg^* + Cl_2 \rightarrow HgCl^* + Cl$	
Total Exothermicity E	14 kcal/mole
λ_{vib}	-2.7
T_{vib}	-2600°K
$\Delta S(vib)$	1.23 cal/mole-°K
$\langle f_{vib} \rangle$	0.53
b) Velocity analysis results for $K + I_2 \rightarrow KI + I$[a]	
Total Exothermicity	44.5 kcal/mole
λ_{trans}^{I}	15
T_{trans}^{I}	1500°K
λ_{trans}^{II}	4.4
T_{trans}^{II}	5000°K
$f_{trans}^{m.p.}$	0.03
$\Delta S(trans)^{I}$	1.4 cal/mole-°K
c) Velocity analysis and electric deflection results for $Rb+Br_2 \rightarrow RbBr+Br$[b]	
Total Exothermicity	45 kcal/mole
$\langle f_{trans} \rangle$	0.07
$\langle f_{vib} \rangle$	0.82
$\langle f_{rot} \rangle$	0.11

Table VI-2. Product Energy Distributions
(Continued)

d) Infrared chemiluminescence results for $H + Cl_2 \rightarrow HCl + Cl$[c]

Total Exothermicity	49 kcal/mole
$\langle f_{trans} \rangle$	0.54
$\langle f_{vib} \rangle$	0.39
$\langle f_{rot} \rangle$	0.07

[a] K.T. Gillen, A.M. Rulis, and R.B. Bernstein, J. Chem. Phys. 54, 2831 (1971).

[b] R.Grice, J.E. Mosch, S.A. Saffron, and J.P. Toennies, J. Chem. Phys. 53, 3376 (1970).

[c] From Table 5.1 of Polanyi, MTP International Review of Science, Physical Chemistry Series 1, Volume 9, Butterworths, London, 1972.

has been investigated using combined velocity selection and velocity analysis by Gillen et al.[12] Surprisal analysis has been applied to the translational recoil data from these experiments in reference 11, and the results are included in Table VI-2. An interesting finding is that a plot of $-\log \omega(f_{trans})$ vs f_{trans} shows two linear regions. The component with low translational temperature probably corresponds to the forward peaked product, whereas the high T_{trans} component may correspond to a backward peaked product formed with higher translational energy. The net fraction of exothermicity invested in product recoil energy is still very small, since $f_{trans} = 0.03$. Grice et al.[13] have studied the reaction

$$Rb + Br_2 \rightarrow RbBr + Br \qquad (13)$$

using velocity analysis and electric deflection so that both the recoil velocity and product rotational energy could be measured simultaneously. By difference the average vibrational energy is $\langle f_{vib} \rangle = 0.82$. The average fraction of available energy observed in vibration of $HgCl^*$, 0.53, is thus substantially smaller than in the analogous reactions of $K + I_2$ and $Rb + Br_2$. This may be due to a somewhat longer lived collision complex in the $Hg^* + Cl_2$ case, or may be an artifact of a somewhat relaxed vibrational distribution. The basic idea that the reaction of Hg^* with Cl_2 proceeds via an electron transfer mechanism and yields high internal excitation is still supported, and this reaction does appear to be analogous to the reactions of alkali and alkaline earth metals with halogens. The product energy distribution for another

reaction which is highly exothermic but does not proceed via formation of an ionic intermediate,

$$H + Cl_2 \rightarrow HCl + Cl \qquad (14)$$

is also shown in Table VI-2.[14] The infrared chemiluminescence of excited HCl was monitored using arrested relaxation to obtain relative populations of $HCl(X'\Sigma^+, v, J)$ levels. Here little rotational excitation occurs and the fraction of available energy released as translation is higher than in the analogous alkali studies quoted above. $\langle f_{vib} \rangle$ = 0.39 and $\langle f_{trans} \rangle$ 0.54. This behavior is rationalized by suggesting that the product energy distribution depends on the exit channel repulsion, and that for light attacking atoms this results is anomalously low internal excitation in the product. This could not explain the low $\langle f_{vib} \rangle$ for $Hg(^3P_1) + Cl_2$ and suggests that, if this value reflects the initial vibrational distribution, the potential hypersurface governing the reaction differs somewhat in character for $Hg(^3P_1) + Cl_2$ from those for alkali and alkaline earth reactions with halogens.

As mentioned in the introduction to this work, some reactions of $Hg(^3P_1)$ have been shown to proceed by bimolecular atom transfer. The reactions of $Hg(^3P_{1,0})$ with molecular hydrogen[15] and alkanes[16] produce $HgH(X^2\Sigma^+)$ according to

$$Hg(^3P_{1,0}) + RH \rightarrow HgH(X^2\Sigma^+) + R \quad . \qquad (15)$$

Similarly $Hg(^3P_{1,0})$ reactions with HCl[15] and CH_3Cl[17] produce $HgCl(X^2\Sigma^+)$. No electronically excited mercurous species are energetically accessible in these reactions. Absorption studies of the HgH and HgCl[18] following flash photolysis show no vibrational excitation in the diatomic product. The extent of vibrational relaxation occurring in these systems is unknown. Callear and McGurk[18] suggest that the formation of HgH proceeds by formation of a short lived intermediate of C_{2v} symmetry, and their view is supported by the larger yield for HgD they observed in the reactions of $Hg(^3P_{1,0})$ with HD. The fast quenching of $Hg(^3P_1)$ by electrophilic species[19] is also evidence for interaction of the mercury atom via partial delocalization of its p electron with the π system of the quenching gas. The reaction of $Hg(^3P_1)$ with Cl_2 could proceed by electron transfer while the reactants are widely separated on a potential hypersurface which leads them into a somewhat stabilized complex of C_{2v} symmetry which barely begins to distribute its energy into the available modes before dissociating to $HgCl(B^2\Sigma^+)$ and Cl. This could explain the smaller fraction of exothermicity channeled into vibration of $HgCl(B^2\Sigma^+)$ compared to the analogous reactions of the alkali and alkaline earth metals.

D. The Prospects of Chemical Laser Action from $Hg^* + Cl_2$.

Because the HgCl product is both electronically excited and vibrationally hot, the possibility of laser action exists in this system. The two basic requirements for laser emission between two energy levels of an atom or molecule[20] are that the higher level has

a larger population than the lower, and that there be a gain in emission intensity as the laser cavity is traversed. The gain equation can be written as

$$\frac{dI}{dx} = a\nu B(N^* - N) - b \qquad (14)$$

where a is a constant which is inversely proportional to the Doppler width of the transition at low pressures and b represents the rate of loss at mirrors and other non radiative processes. B is the Einstein coefficient for absorption, ν is the transition frequency, and N* and N are concentrations of the upper and lower energy levels. Two types of laser emission are possible for the $Hg^* + Cl_2$ reaction. If the reaction to produce ground state HgCl in level v" is slow compared to that producing $HgCl(B^2\Sigma^+)$ in v',

$$Hg(^3P_1) + Cl_2 \rightarrow HgCl(X^2\Sigma^+, v'') + Cl(^2P) \qquad (15)$$

Stimulated emission could occur between v' and v". Since the lifetime of $HgCl(B^2\Sigma^+)$ is probably $\sim 10^{-7}$ sec, and its emission will, of course, populate the ground state, electronic inversion will exist only at t=0. Because the electronic transition moment is larger for the blue shaded bands than for red shaded bands originating in the same v', and the population of very low v' is less than high v', the best prospects for observing stimulated emission would be the blue shaded bands, which occur for $v' \geq 15$. This kind of experiment could be done in a reaction vessel with Brewster angle windows. Flash photolytic generation of

$Hg(^3P_1)$ in an apparatus similar to that used by Callear et al.[18] with oscilloscope monitoring of the stimulated emission can be envisaged. Chemical laser action could also occur in the infrared spectral region, due to stimulated emission between $HgCl(B^2\Sigma^+,v'J')$ and $HgCl(B^2\Sigma^+,v''J'')$, but because the infrared emission occurs on a longer time scale than electronic emission this would be difficult to observe, even if rotational analysis of the HgCl(B→X) were on hand so that the emission frequencies were known. The prospects of an infrared chemical laser would be better for studying the high levels of ground state HgCl, $39 \leqslant v'' \leqslant 41$, since these will be populated preferentially by the fast decay of $HgCl(B^2\Sigma^+)$, $15 \leqslant v' \leqslant 27$. Infrared stimulated emission involving the ground state of HgCl might be interesting in its own right, especially if the gain of the system were higher than that known for other infrared chemical lasers,[21] but information on the relative rates of formation of the vibrational manifold of $HgCl(B^2\Sigma^+)$ could only be obtained from the electronic emission. This information has been obtained here admittedly crudely, by simply monitoring the chemiluminescent emission due to $HgCl(B^2\Sigma^+,v') \rightarrow HgCl(X^2\Sigma^+,v'') + h\nu$. Chemical laser emission from the reaction of $Hg(^3P_1)$ with Cl_2 and possibly other halogens might be useful, if the power output were high enough, as a tunable laser source between 4800 and 5300Å, for other types of spectroscopic or kinetic studies. Again, this prospect would depend on the rate of formation of ground state HgCl in reaction (15), and continuous dye lasers are available for spectroscopic and kinetic studies.

CHAPTER VI REFERENCES

1. R. Grice and P.B. Empedocles, J. Chem. Phys. 48, 5352 (1968).
2. J.H. Birely, R.R. Herm, K.R. Wilson, and D.R. Herschbach, J. Chem. Phys. 47, 993 (1967).
3. S.M. Lin, C.A. Mims, and R.R. Herm, J. Chem. Phys. 58, 327 (1973).
4. J.L. McGee, J. Chem. Phys. 8, 867 (1940).
5. a) C.D. Jonah and R.N. Zare, Chem. Phys. Lett. 9, 65 (1971).
   b) M. Menzinger and D.J. Wren, Chem. Phys. Lett. 18 431 (1973).
6. S.J. Riley and D.R. Herschbach, J. Chem. Phys. 58, 27 (1973).
7. S. Freund, G.A. Fisk, D.R. Herschbach, and W. Klemperer, J. Chem. Phys. 54, 2510 (1971).
8. P.B. Foreman, G.M. Kendall, and R. Grice, Mol. Phys. 23, 127 (1972).
9. G. Herzberg, Electronic Spectra and Electronic Structure of Polyatomic Molecules, Van Nostrand, New York, 1966, p. 287.
10. W.A. Chupka and J. Berkowitz, J. Chem. Phys. 54, 1885 (1971).
11. A. Ben-Shaul, R.D. Levine, and R.B. Bernstein, J. Chem. Phys. 57, 5427 (1972).
12. K.T. Gillen, A.M. Rulis, and R.B. Bernstein, J. Chem. Phys. 54, 2831 (1971).
13. R. Grice, J.E. Mosch, S.A. Saffron, and J.P. Toennies, J. Chem. Phys. 53, 3376 (1970).
14. J.C. Polanyi, MTP International Review of Science, Physical Chemistry Series 1, Volume 9, Butterworths, London, 1972, Table 5.1.
15. A.B. Callear and R.E.M. Hedges, Trans, Far. Soc. 66, 605 (1970).
16. A.C. Vikis and D.J. LeRoy, Can. J. Chem. 51, 1207 (1973).

17. A.C. Vikis and D.J. LeRoy, Chem. Phys. Lett. 21, 103 (1973).

18. A.B. Callear and J.C. McGurk, Far. Trans. II, 68, 289 (1972).

19. H.E. Gunning and O.P. Strausz, Adv. in Photochem. 1, 209 (1963).

20. J.C. Polanyi, J. Appl. Optics, Suppl., 2, 109 (1965).

21. C.B. Moore, Ann. Rev. Phys. Chem. 22, 389 (1971).

Table A-1. Axial variation of HgCl* emission intensity with ground state mercury and chlorine concentrations.[a]

a)	$(Hg)_o$, (Cl_2) Code	$(Hg)_o$ atoms/$cm^3 \times 10^{-13}$	(Cl_2) Torr	τ_{Cl_2} sec
	1	1.31	0.043	3.40
	2	0.921	0.085	2.40
	3	0.702	0.129	1.83
	4	0.637	0.170	1.66
	5	0.575	0.211	1.35

b)	Monitoring Position[b] cm	I_e[c] Arbitrary Units	$v\int_o^t Idt'$[c] Arbitrary Units	1-(HgCl*)[d] Arbitrary Units	2-(HgCl*)	3-(HgCl*)	4-(HgCl*)	5-(HgCl*)
	3.86	0.567	0.77	0.70	1.34	1.76	2.60	2.64
	7.15	0.700	7.20	1.07	1.74	2.19	2.57	2.70
	8.34	0.600	8.88	0.98	1.44	1.80	2.62	2.81
	11.13	0.715	10.5	0.88	1.61	2.47	2.77	2.95
	19.08	0.740	25.0	0.63	1.28	1.77	2.31	2.39
	22.28	0.703	29.6	0.96	1.46	1.69	1.90	2.18
	24.43	0.684	32.6	0.66	0.93	1.01	1.46	1.30
	26.43	0.648	34.8	0.55	0.69	0.81	1.07	1.35

a) Experimental parameters are listed in Table IV-3.

b) Distance from the upstream end of the irradiated zone of the reaction vessel.

c) These experimental radiant flux parameters are plotted in Figs. IV-2 and IV-3.

d) Time normalized data. 1-(HgCl*) means $(Hg)_o$ and (Cl_2) are given by $(Hg)_o$, (Cl_2). Code = 1 in part a) of this table.

Table A-2. Axial Variation of $HgCl^*$ Emission Intensity with Ground State Mercury and Chlorine Concentration[a]

a) Experimental Variables

Mercury source temperature	508°K
Mercury flow rate	2.78×10^{16} atoms/sec
Incident intensity	10 lamps

$(Hg)_o$, (Cl_2) Code	$(Hg)_o$ atoms/sec$\times10^{-13}$	(Cl_2) Torr	τ_{Cl_2} sec
1	8.65	0.10	2.20
2	5.85	0.19	1.58
3	4.96	0.26	1.36
4	4.63	0.36	1.12
5	3.10	0.60	0.835

b) Experimental Data

Monitoring Position[b] cm	I^c. Arbitrary Units	$v\int_0^t I_c dt$,[c] Arbitrary Units	1-($HgCl^*$)	2-($HgCl^*$)	3-($HgCl^*$)	4-($HgCl^*$)	5-($HgCl^*$)
			Arbitrary Units				
0	.506	0	0.83	1.31	1.62	2.49	3.18
1.8	.818	1.8	0.65	1.33	2.12	3.16	3.26
3.6	.902	5.9	1.11	1.26	1.87	2.69	4.49
5.1	0.941	5.9	0.79	1.15	1.68	2.40	3.42
6.4	0.940	7.8	0.87	1.44	1.45	2.28	2.96
7.7	0.957	9.7	0.94	0.99	1.31	1.77	3.05
9.1	0.996	11.8	0.92	1.09	1.94	2.16	2.48
15.8	0.980	22.4	0.71	0.72	0.63	1.37	1.90
17.1	0.943	24.3	-	-	0.54	1.23	1.66

a) This data has a mercury flow rate such that imprisonment lifetimes fall in the region of $\tau/\tau_o = 30$. This data has not been treated in Chapter IV because of its high imprisonment and extensive absorption of incident resonance radiation. It is included here for future reference and analysis.

b) Distance from the upstream end of the irradiated zone of the reaction vessel

c) These radiant flux functions are shown in Figs. IV-2 and IV-3.

ACKNOWLEDGEMENTS

Many people have contributed to the complex trajectory which began with the initial research ideas for this project and which undergoes a curve crossing with the completion of this thesis. For inspiration, critical analysis, and for suggesting this project I acknowledge the input of Ron Herm, who has endeavoured to communicate to me some of his physical insight into molecular dynamics. Peter Frosch also gave me useful assistance in idea development and in sharing his spectroscopic experience with me.

Thanks are due to Charlotte Sholeen for her patience in introducing me to molecular beam experimentation, and to my other colleagues as well for many stimulating discussions. For fine technical and financial assistance I acknowledge the input of people and services of the UCB Department of Chemistry, the Inorganic Materials Division of Lawrence Berkeley Laboratory, and of the Atomic Energy Commission. Particular thanks to Alice Ramirez for typing and special handling of this document.

For essential non-scientific aid and encouragement I acknowledge the benefits of interaction with the women's caucus of the Chemistry department, and especially the warmth and support of Lois Rosenthal and Aubrey Lindgren. Special notes of appreciation are added for the understanding, encouragement and assistance given me by Leslie Gundel and Steve Brewer.

TECHNICAL INFORMATION DIVISION
LAWRENCE BERKELEY LABORATORY
UNIVERSITY OF CALIFORNIA
BERKELEY, CALIFORNIA 94720